ANALOGUE MODELLING OF SALT TECTONIC PROCESSES BENEATH THE SHELF AND DEEPWATER SLOPE OF THE EASTERN NOVA SCOTIAN MARGIN

by

Jonathan W. A. Cribb

Submitted in partial fulfillment of the requirements
for the degree of Master of Science

at

Dalhousie University
Halifax, Nova Scotia
November 2009

DALHOUSIE UNIVERSITY

DEPARTMENT OF EARTH SCIENCES

The undersigned hereby certify that they have read and recommend to the Faculty of Graduate Studies for acceptance a thesis entitled "ANALOGUE MODELLING OF SALT TECTONIC PROCESSES BENEATH THE SHELF AND DEEPWATER SLOPE OF THE EASTERN NOVA SCOTIAN MARGIN" by Jonathan W. A. Cribb in partial fulfilment of the requirements for the degree of Master of Science.

Dated: July 24, 2009

Supervisor:

Readers:

DALHOUSIE UNIVERSITY

DATE: November 1, 2009

AUTHOR Jonathan W. A. Cribb

:

TITLE: Analogue modelling of salt tectonic processes beneath the shelf and deepwater slope of the eastern Nova Scotian margin.

DEPARTMENT OR SCHOOL: Earth Sciences

DEGREE: M.Sc. CONVOCATION: May YEAR: 2010

Permission is herewith granted to Dalhousie University to circulate and to have copied for non-commercial purposes, at its discretion, the above title upon the request of individuals or institutions.

_____

Signature of Author

TABLE OF CONTENTS

LIST OF FIGURES

LIST OF TABLES

ABSTRACT

The Scotian Basin is situated on the Atlantic continental margin offshore Nova Scotia and is composed of a series of interconnected Mesozoic rift basins. Thick clastic syn-rift sediments and late syn-rift salt deposits floor these interconnected sub-basins. Along the margin, complex salt basin morphologies and variable post-rift sedimentation patterns during Jurassic and Cretaceous times have resulted in a laterally variable and diachroneous evolution of salt and sedimentary overburden structures. These characteristic salt features have been used to divide the Scotian margin into five distinctive salt subprovinces (Shimeld, 2004). However, detailed understanding of the link between early post-rift salt mobilization, late-post-rift formation of allochthonous salt bodies, and their relation to depocenter migration within individual sub-basins and salt subprovinces of the Scotian margin is yet to be gained. This gap in understanding is underscored by the unsatisfactory results from the recent round of hydrocarbon exploration in the deepwater slope.

For this project, analogue experiments constrained by regional seismic data are used to study evolution of the eastern Scotian margin (Subprovince IV), an area dominated by salt tectonics. Regional GXT NovaSpan seismic line 2000 and GSC seismic line 89-1, spanning the continental shelf to the deep basin (abyssal plain) within Subprovince IV, and the interest of the petroleum industry in this area make this study particularly attractive. The study area is comprised of a characteristic extensive allochthonous salt nappe and detachment system with distinctive rotated strata referred to as the Banquereau Syn-kinematic Wedge (BSW). The eastern boundary of Subprovince IV, imaged by Line 2000, displays several wide (~10 km) extensional passive diapirs within the autochthonous basin and a widespread (~65 km wide) climbing salt nappe outboard of the rift basin. Within the western Subprovince IV line 89-1 displays a lack of significant autochthonous salt structures but a similar (~70 km) allochthonous salt detachement system.

New velocity profiles coincident with line 89-1 (Funck et al., 2004) and Seismic interpretation of line 2000 have indicated that the seaward limit of the autochthonous salt basin is uniform within Subprovince IV. The width of the salt basin (~ 90 km) is also comparable to those of surrounding salt subprovinces (III and V). The seismic interpretation of line 2000 has yielded key features of the salt system, implemented in analogue modeling. The salt basin floor (syn-rift sediments covering rifted basment blocks) consists of two seaward thinning half graben wedges filled with thick (~ 3 km maximum) late syn-rift Argo Salt. Sedimentation rates driving salt mobilization have an overall decreasing trend from the Middle Jurassic to the Late Cretaceous with a maximum of 200m/Ma during the Late Jurassic.

Scaled 4-D physical analogue models have successfully simulated the evolution of characteristic salt tectonic features imaged within line 2000, giving insight into the development of this portion of the Scotina margin. High-resolution optical strain monitoring (DIC – Digital Image Correlation) techniques used to quantify model surface

deformation indicate that the model can be divided into 4 kinematic salt tectonic domains from the shelf to deep water: (1) salt weld and pillow, (2) extensional diapir, (3) contractional salt massif and canopy, (4) allochthonous nappe and minibasin. Experiments suggest that early post-rift sediment input (Middle Jurassic) on a salt basin comprised of two proportional seaward thinning half graben wedges with thick salt deposits led to early widespread mid-basin inflation of salt. Experiment strain monitoring data indicate that early (Middle Jurassic) salt ridges developed in response to extension of an overriding sedimentary wedge. Salt ridges widened to form passive diapirs while significantly translating basinward. High sedimentation rates during the Late Jurassic resulted in the seaward extrusion of salt and the basinward translation of an inflated salt massif along a seaward thinning salt basin. This massif was arrested at the salt basin seaward edge during the Early Cretaceous. Overriding sedimentation loading the inflated salt complex during this time is responsible for development and extrusion of the climbing nappe. Early Cretaceous minibasins translated seaward through the extrusion of an open toe salt nappe and the development of passive diapirs.

Analogue experimentation indicated that complex sediment fairway patterns throughout the Cretaceous (model time) were controlled mostly by the topography of allochthonous salt (nappe) and secondary canopy development at the salt basin edge. Here, localized channels (turbidites) transporting sediments seaward form adjacent to salt canopies where subsidence is active. These small potentially sandy deposits beyond the slope of the eastern Scotian margin are the most likely source for untapped reservoir accumulation.

LIST OF ABBREVIATIONS USED

ASW – Autochthonous Salt Wall
B – Basement
BSW – Banquereau Syn-kinematic Wedge
CCF – Cobequid – Chedabucto Fault
COB – Continent Ocean Boundary
DC – Dawson Canyon
DIC – Digital Image Correlation
ECMA – East Coast Magnetic Anomaly
GSC – Geological Survey of Canada
ISM – Inflated Salt Massif
LC – Logan Canyon
Mc – Mic Mac
Mi – Missisauga
O – O Marker
OCT – Ocean Continent Transition
PM – Petrel Member
Sc – Scatarie
SC – Salt Canopy
SR – Syn-Rift
Sw – Salt withdrawal basin
tJ – top Jurassic
Wy – Wyandot

ACKNOWLEDGEMENTS

I wish to extend sincere thanks to my supervisors Dr. Juergen Adam (Royal Holloway, University of London) and Dr. Mladen Nedimovic (Dalhousie University) for organizing this project and keeping everything on track for these last few years. I appreciate the many long discussions, quick feedback and encouragement from across the pond throughout the project. Thanks for your time and patience.

Thanks to the "guys" of the Salt Dynamics Group. Due to our many discussions, collaborations and your thoughtful answers to my questions my best work was achieved for this project. It was great being part of the team. Thanks for doing all those 2, 4, and 6am sieving shifts.

The support and encouragement of my wonderful wife, caring family and great friends gave me the motivation necessary for such a project. Ashley, your role was more important than you'll ever know. Thanks Mom and Dad for providing such a relaxing haven for stress-free weekends.

Finally, the following research would not have been possible without the generous donation of the 2-D NovaSpan dataset by ION GX Technology (Menno Dinkelmann) and financial contributions from the Pengrowth-Nova Scotia Petroleum Innovation Grant, ACOA/AIF (Atlantic Canada Opportunities Agency and Atlantic Innovation Fund), CFI (Canada Innovation Fund), NSERC (Natural Sciences and Engineering Research Council) and PRAC (Petroleum Research Atlantic Canada). Thanks to the C-NSOPB (Canadian-Nova Scotia Offshore Petroleum Board) for the use of their facilities and seismic database. Seismic interpretation was made possible through the use of Kingdom suite (Seismic Micro Technology (SMT)) academic license software.

Chapter 1: Introduction

The structural style and evolution of salt basins along passive continental margins is highly variable. The style and mechanics of salt mobilization and the formation of characteristic salt and sedimentary structures throughout basin history is known to be a response to several factors:

1. Variable sedimentation patterns and rates of migrating depocenters on top of salt.
2. Initial thickness of salt deposits during the early phases of basin formation.
3. The original salt basin shape often influenced by basement and syn-rift topography.

What is not known is what individual effect these factors have and how they interplay jointly in the evolution of salt basins.

Along the Scotian margin offshore Eastern Canada, thick deposits of late syn-rift Argo Salt coupled with a complex rift basin geometry and post-rift sedimentation patterns have resulted in a complex and laterally variable basin evolution. Unsatisfactory results from the recent round of hydrocarbon exploration in the deepwater slope demonstrate that a better understanding of basin-scale salt tectonic processes is necessary. With improved kinematic and mechanical concepts of the basin-scale salt tectonic processes, a link can be made between early post-rift salt mobilization, late-post-rift formation of allochthonous salt bodies, and their relation to depocenter migration throughout basin

evolution. Therefore, a better understanding of the structural and tectono-stratigraphic evolution of the margin can be applied to thermal evolution, hydrocarbon migration and reservoir characterization.

This study investigates the formation of an extensive allochthonous salt detachment system and related autochthonous salt structures of the eastern Scotian margin salt basin offshore Nova Scotia (eastern portion of salt Subprovince IV, Shimeld, 2004) (Figure 1.1). This salt detachment is the result of an early and efficient extrusion of salt from the autochthonous basin of Subprovince IV. However, salt structures characterizing the surrounding salt Subprovinces (III, V) vary drastically in both timing and structural style. This study examines the reasons for such a distinct structural evolution along this portion of the margin.

1.1 Study area

The Scotian Basin is situated on the Atlantic continental margin offshore Nova Scotia (Scotian margin) and is composed of a series of interconnected Mesozoic sub-basins resulting from the break-up of Pangaea. The study area spans the Sable, Abenaki, and Laurentian Sub-basins incorporated within the eastern salt Subprovinces IV and V (Shimeld, 2004) (Figure 1.1). The focus of this study includes basement and Triassic – Cretaceous sediments within these basins below the continental shelf, slope and deepwater regions of the margin where salt deformation has affected sedimentary overburden.

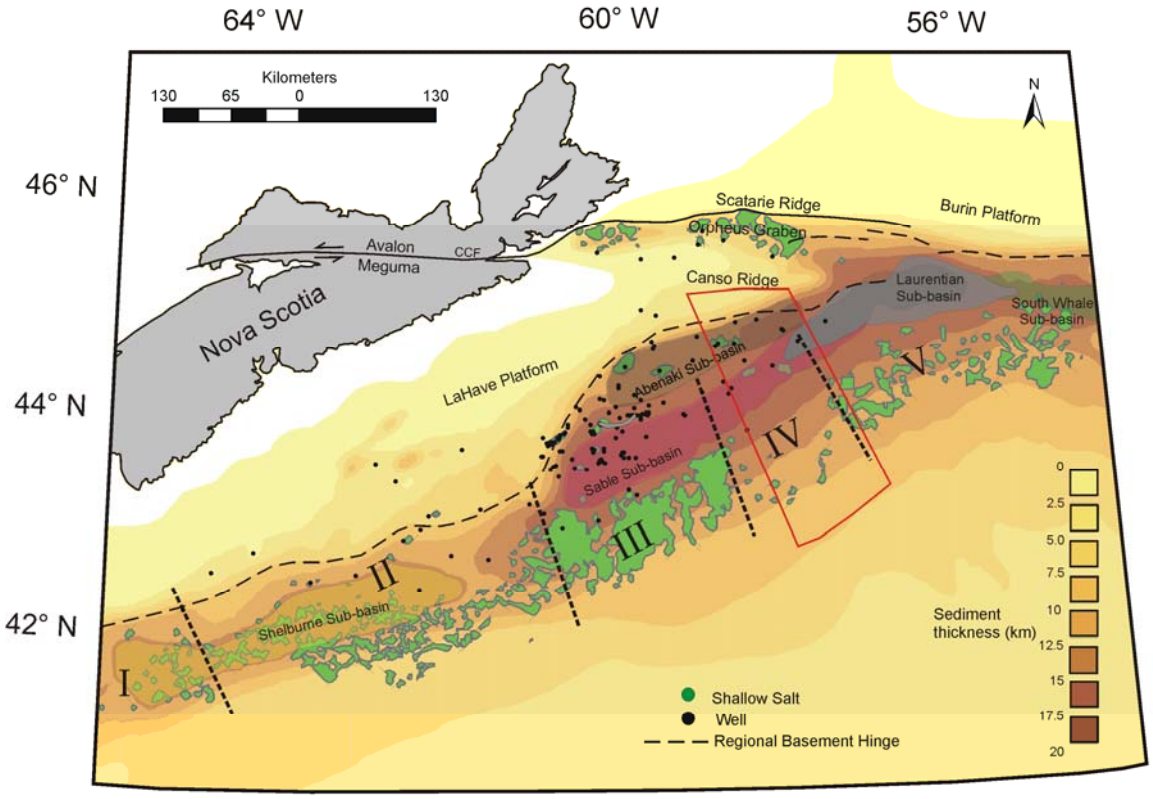

Figure 1.1. Location of the study area on the continental shelf and slope of the Scotian Margin, offshore Nova Scotia. Sediment thickness shown as colour background. Sub-basins of the Scotian Basin shown as colour overlay. Salt subprovinces (I-V) and shallow salt diapirs (green) after Shimeld (2004). CCF = Cobequid-Chedabucto Fault.

1.2 Hypotheses

The two hypotheses being tested for this study are:

1. An overall seaward thinning salt basin wedge is responsible for the early mid-basin inflation and continuous extrusion of salt from the autochthonous basin.

2. Initial thick (~ 3 km) syn-rift salt deposits within the basin of the eastern Scotian margin resulted in dominant passive downbuilding of depocenters, driving seaward salt mobilization through salt basin history.
3. High sedimentation rates during the Late Jurassic and Early Cretaceous evacuated salt from the autochthonous basin to produce an extensive salt nappe/detachment system throughout salt Subprovince IV.

1.3 Objectives

The purpose of this study is to analyze the structural and tectono-stratigraphic evolution of the eastern Scotian margin (Subprovince IV) salt basin by interpretation of basin-scale seismic data and derived 4-D scaled analogue experiments.

From the seismic interpretation the major controlling factors of basin evolution (sedimentation patterns and rates, salt thickness, basin architecture) were derived. Scaled analogue experiments were used to better understand the interplay between these major factors and salt tectonic processes through the post-rift salt basin evolution of the study area. This study focuses on the analysis of the basin structure of the eastern salt Subprovince IV, simulating the development of key structural features, e.g. autochthonous salt diapirs, salt withdrawal and mini basins, canopies in the original basin, and an extensive allochthonous nappe/salt detachment system.

Results of the study are used to link salt mobilization mechanisms and patterns along the Scotian margin, and better constrain the timing and relationship of salt interflow between salt subprovinces.

The objectives of the presented study are to:

1. Identify the location, depositional history and formation mechanism of the major Jurassic –Cretaceous depocenters within the eastern Scotian margin (eastern Subprovince IV) and associated deepwater slope.
2. Constrain the late syn-rift/early post-rift salt basin architecture and original salt thickness for the eastern Scotian margin through the interpretation of modern day basement and syn-rift features
3. Use the regional geologic constraints interpreted from seismic profiles to conduct a 4-D scaled physical analogue experiment of the eastern Scotian margin salt system to monitor the interplay between salt mobilization and sedimentation patterns.
4. Apply concepts concerning the mechanics, kinematics, and timing of salt structures derived from the analogue experiments to better understand the salt tectonics and basin evolution of the eastern Scotian margin and improve seismic interpretations in the region.

Chapter 2: Salt Tectonics

2.1 Formation of Salt Basins

Although present worldwide, salt basins are primarily found along rifted continental margins due to available accommodation space and marine conditions conducive to evaporite deposition. Salt basins at these "passive" margins can form during the prerift, synrift or interrift, and early postrift stages of basin evolution (Figure 2.1.) (Jackson and Vendeville, 1994). Many sedimentary basins around the South Atlantic margins (e.g. offshore Brazil and offshore West Africa), as well as those offshore of the U.S. Gulf Coast and from the Red Sea area contain postrift salt deposits that accumulated shortly after basement-related (thick-skinned) extension ceased with the onset of the tectonic drift stage. Similarly common are salt basins formed during synrift or interrift stages where salt was deposited either during rifting or between episodes of active rifting. Good examples of salt basins with this intermediate timing of salt deposition are found along the North Atlantic conjugate margins. Less common are salt accumulations that appear to have been deposited in a cratonic sag basin before rifting was initiated. Such basins include those of the North Sea and Persian Gulf.

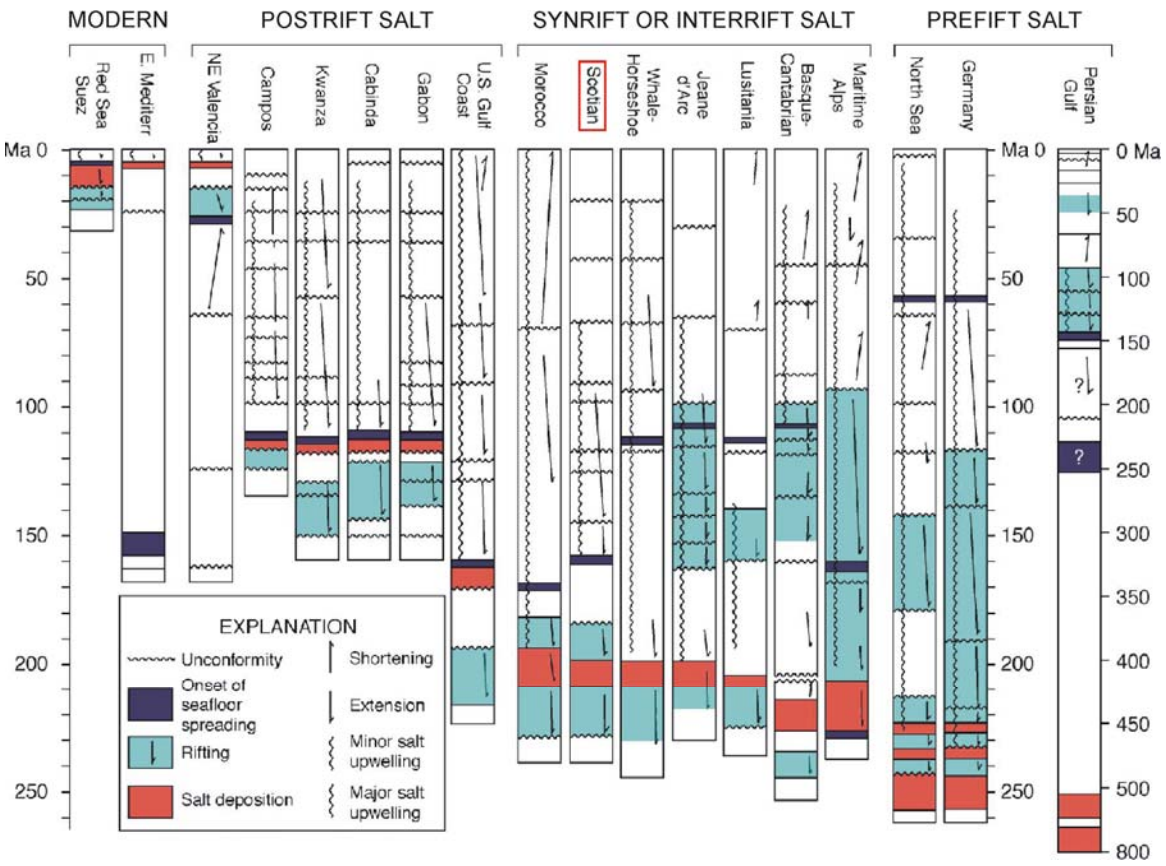

Figure 2.1 Timing of salt deposition in various salt basins worldwide. Note that salt deposition can, occur prerift, synrift or interrift, and postrift. As annotated, salt within the Scotian Basin is synrift in origin. (modified from Jackson and Vendeville, 1994).

However different the timing of salt emplacement, rift basins share a similar early depositional history conducive to evaporites. Most commonly through the rift process, extension of continental crust forms grabens and half grabens that are initially filled with non-marine clastic sediments from eroding rift shoulders uplifted due to high heat flow. Subsidence during continued rifting or more commonly postrift thermal and loading subsidence eventually leads to episodic or subsequent marine incursions. During the transition from non-marine to restricted marine environment, with warm and arid climatic conditions, evaporites are deposited. Deposition is often episodical as a result of relative seal level changes and the transition from open to closed marine conditions, with

cumulative deposits reaching up to thicknesses of several kilometers (Rowan, 2005). Contrary to clastic or even carbonate deposition, evaporite deposition can be very rapid; with significant accumulation occurring several orders of magnitude less time than clastics or carbonates.

The areal extent and thickness of the original evaporite basin is generally constrained by distinct basement geometry along with sedimentation rates and timing of evaporite formation (Rowan, 2005), or in other words by the tectonic stage of the rifting process (Fort et al., 2004). The effect of rift basement geometry on salt deposited during the postrift stage is often subdued or even negligible as a consequence of synrift and early postrift sediments filling once available accommodation space of grabens and half grabens (e.g., basins of the West Africa margin; Figure 2.2). In contrast, synrift and interrift salt deposits can be strongly influenced by rift basin geometries. These deposits frequently fill the remaining accommodation space of rift grabens and half grabens allowing for laterally extensive accumulations with large variations in thickness (e.g., basins onshore northern Gulf of Mexico; Figure 2.3) (Rowan, 2005). Initial salt basin geometry, thickness and variations of these are major first order control factors for thin-skinned suprasalt deformation and basin evolution as a whole.

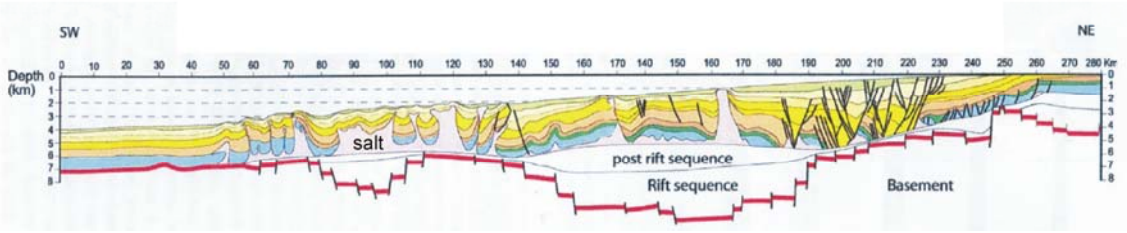

Figure 2.2. Schematic cross-section profile of the West African margin showing original rifted basement accommodation space completely filled by synrift and early postrift sequences (modified from Calassou and Moretti, 2003). Therefore salt deposition and thickness of deposits was not affected by the rift basin geometry. Coloured layers indicate stratigraphy from the Early Cretaceous through Tertiary.

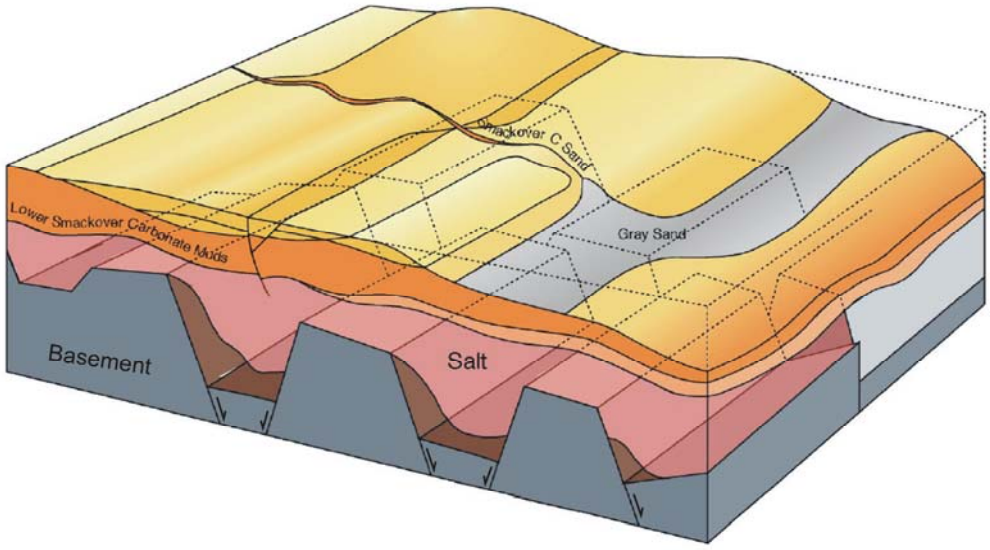

Figure 2.3. Schematic basin architecture for onshore northern Gulf of Mexico displaying highly variable salt thickness, geometry and distribution due to filling of rifted basement blocks (modified from Adams, 1989).

2.2 Mechanics of Salt Deformation

The mechanics of viscous salt deformation differs widely from that of brittle sedimentary strata. The two main factors that dictate the behavior of salt sediments are low strength and low density.

2.2.1 Strength

As shown in Figure 2.4, salt is significantly weaker in both tension and compression than nearly all the surrounding brittle sedimentary rocks. The viscous nature of salt is reflected by the constant weak strength displayed with increasing depth. In contrast, the strength of brittle sedimentary layers increases linearly with depth (Figure 2.4). Therefore, salt being the weakest component of the basin; it often accommodates strain through thin-skinned salt tectonic deformation.

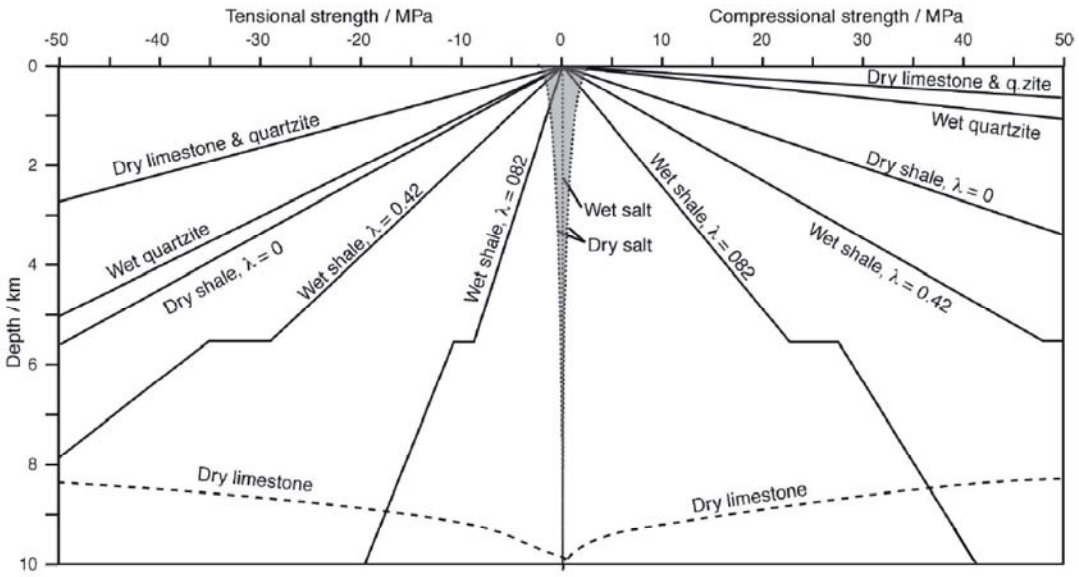

Figure 2.4. The strength of various lithologies in both tension and compression (modified from Jackson and Vendeville, 1994). Note that salt is by far the weakest of these rock types (grey) and wet salt is effectively a viscous material due to its strength curve lying on the zero axis.

Natural samples of rock salt contain at least traces of water. This "wet" salt deforms by solution-transfer creep under geological conditions and is considered to act as a Newtonian viscous fluid (Wawersik and Zeuch, 1986; Urai et al., 1986, 1987; Spiers et al., 1986; Weijermars, 1993) in most cases with strength of effectively zero. In the rare cases of no water content, "dry" salt sediments are hundreds of times stronger than wet

salt. However, this dry salt is still significantly weaker than surrounding rocks with the exception of very shallow shale lithologies (Figure 2.4).

The low strength of salt is displayed through the effective viscous flow of the material under differential pressure. Salt effectively flows as a viscous material through a combination of channel flow and shear flow. Channel flow (Poiseuille flow) is generated by differential loading of salt and leads to passive downbuilding (subsidence) of overburden sediments. Shear flow (Couette flow) is also a result of differential loading but results in extension and overburden translation (Figure 2.5) (Rowan, 2005; Vendeville and Jackson, 1992a, b; Gemmer et al., 2004). During Poiseuille flow differential pressure from overburden loading drives the lateral flow of viscous material while thinning the viscous layer in the process. Flow velocities during this channel flow are greatest in the center of the channel and reduced to virtually zero along boundaries as a result of viscous drag (Figure 2.5). The rate of overburden vertical subsidence (thinning of the source layer) is proportional to (1) the lithostatic pressure at the base of the overburden (therefore, overburden density and thickness) and (2) salt layer thickness cubed (Vendeville et al., 1993).

During Couette flow however, overburden is sheared by lateral basinward translation on top of the salt detachment. Here shear flow results in an increase of the flow velocity from zero at the basal boundary to the maximum along the upper interface of the viscous material (Figure 2.5). The salt layer neither thins nor thickens as the salt layer experiences layer-parallel simple shear. This shear flow is proportional to (1) the

thickness of the salt layer and (2) the applied shear stress through the slope parallel component of the lithostatic pressure in the case of margin tilt and gravity spreading down slope. Different flow types are considered endmembers, with some combination of flow occurring in nature. These topics will be discussed fully in section 2.3.

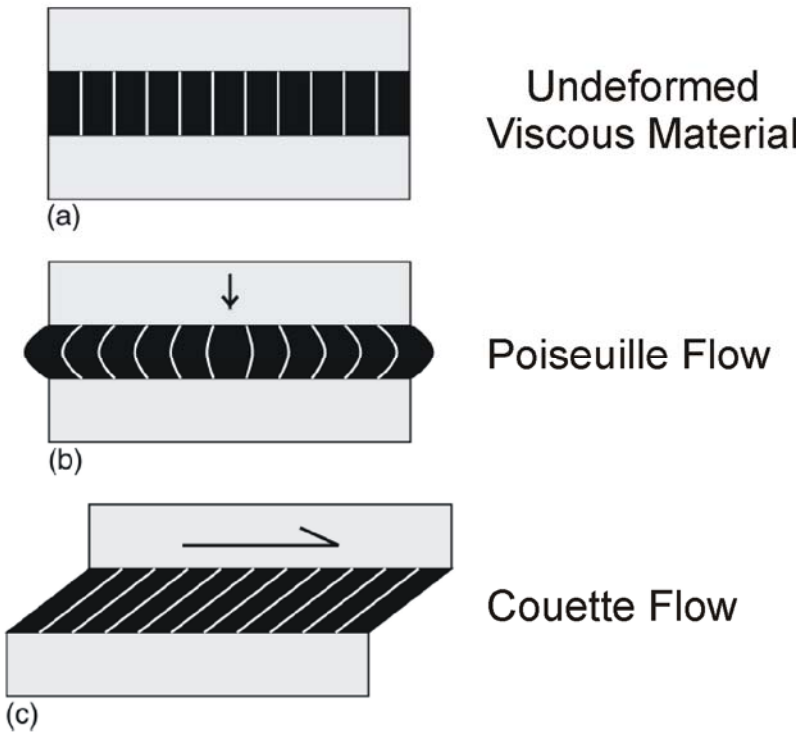

Figure 2.5. Different types of flows induced in an undeformed viscous material (Modified from Rowan, 2005). (a) Undeformed viscous material. (b) Poiseuille or channel flow, during which overburden loading drives lateral flow with the highest velocity of flow in the center of the viscous layer. (c) Couette flow, during which overburden is sheared through the lateral translation of overburden, with the highest velocities along the shearing boundary.

2.2.2 Density

The second main attribute that determines the behavior of salt is density. The density of salt is approximately 2.2g/cm^3, which slightly decreases with depth due to thermal expansion (Figure 2.6). This also is in contrast to the density variations of sedimentary rocks such as shales and sandstones, which increase in density with depth due to

compaction. Therefore, although more dense on the Earth's surface salt becomes less dense than the surrounding sedimentary strata between depths of 1000-1500 m. Where density contrasts and subsequent buoyancy forces once were believed to be the driving force of salt deformation, they are now considered to have only a second order effect with regard to salt tectonics. This is due to the brittle deformation behaviour and significant strength of the sedimentary overburden. Previous concepts modeled salt and sedimentary overburden both as fluids. Differential density between salt and overburden was theorized to drive salt to rise and pierce through overburden until neutral buoyancy was reached. Modern concepts consider salt as a fluid material when regarded to in geological processes and sedimentary overburden as brittle (Rowan, 2005; Vendeville, 2005; Jackson and Vendeville, 1994; and Vendeville and Jackson, 1992b). The association of faulting and diapirism (Vendeville and Jackson, 1992b), initiation of diapirism within the brittle regime above the brittle-ductile transition zone, and common high strain rates of salt tectonic processes encouraging brittle deformation all suggest that a model of brittle overburden is justifiable.

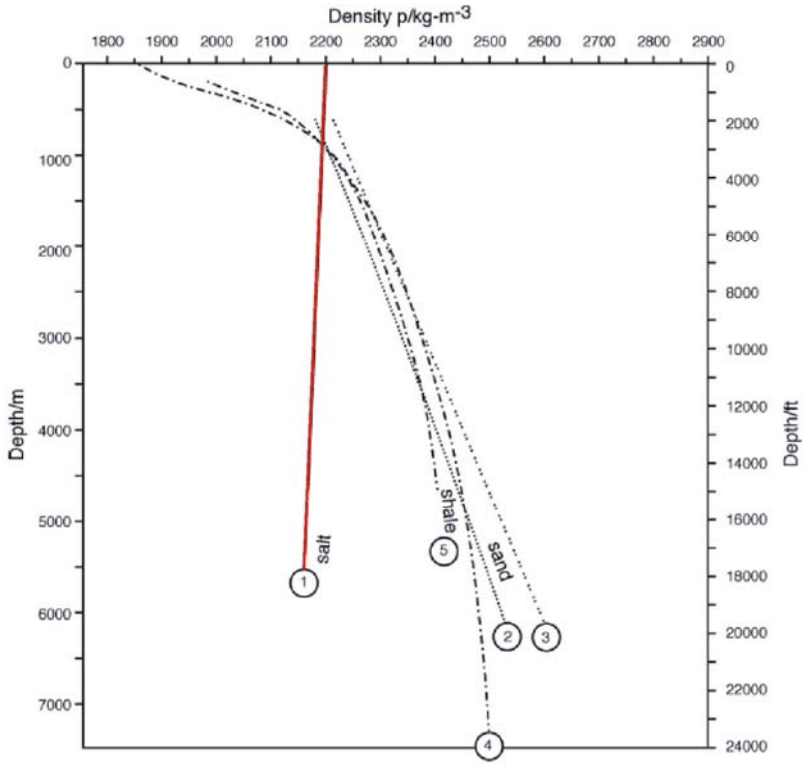

Figure 2.6. Density as a function of depth for salt (1) (red), sand (2-3), and shale (4-5) (modified from Jackson and Talbot, 1986). Note that density increases with depth for sand and shale, and slightly decreases for salt. This density relationship is a main controlling factor for the rheological behaviour of salt at depth.

Figure 2.7 displays how strong brittle overburden minimizes the effects of density contrast and impedes salt from rising and piercing it. From this schematic Vendeville and Jackson (1992b) discuss salt as a pressurized fluid, with pressure originating from its own weight and the weight of the overburden regardless of respective densities. P_2 is the pressure at the viscous-brittle interface and is generated by the weight of the overburden through $P_2 = \rho_0 g(z_0 - z_2)$. The pressure at the base of the viscous layer is $P_3 = P_2 + (\rho_s g z_2)$.

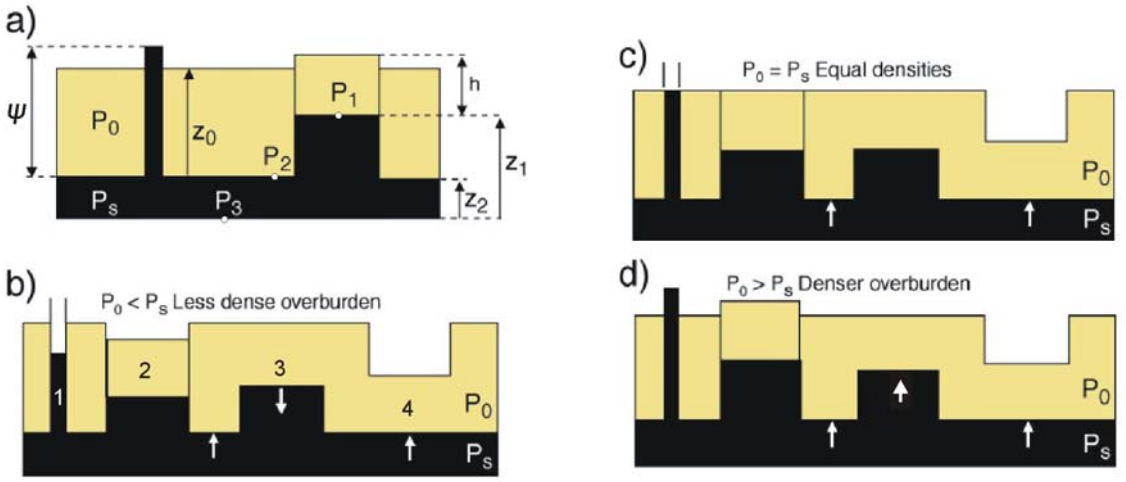

Figure 2.7. Model of salt represented by a pressurized fluid (black) covered by a rigid, brittle overburden (yellow) (Modified from Vendeville and Jackson, 1992b). (a) Symbols ρ_o and ρ_s are overburden and fluid (salt) densities; z values are elevations above a pressure datum at the base of the fluid layer, *h* is the reduced (to 50%) thickness of the overburden above the fluid; *P* values are fluid pressures at points indicated; Ψ is the pressure head of the fluid layer; white arrows show the relative movement of overburden if there is faulting. (b, c, d) Pressures and equilibrium levels for less dense, equally dense, and more dense overburden respectively. Structures 1 – 4 discussed in text are labelled accordingly in (b). It is important to note that regardless of equal, lesser, or greater density of overburden with respect to fluid, this density contrast is a secondary factor for diapir development. With these scenarios (b-d) a differential load will drive fluid into an open conduit (left side "diapir") and a "diapir" will not forcefully pierce its way through the brittle, strong overburden (center).

Figure 2.7 b-d shows a series of schematics illustrating the implications for a pressurized viscous layer below (b) less dense, (c) equally dense, and (d) denser brittle overburden. For all diagrams there is (1) an open column of fluid with the height being equal to the pressure head, Ψ; (2) a thin roof block with frictionless movement allowing vertical displacement corresponding to the underlying fluid pressure; (3) a fluid column covered by a thin, rigid roof block with frictional boundaries; (4) a thin, rigid overburden trough over tabular fluid (Figure 2.7b). The pressure at the top of the viscous layer covered by a frictionless block is $P_1 = \rho_0 gh$. The open columns or pressure heads simulating passive diapiric structures illustrate why pressurized fluid will rise regardless of the density ratio

if the fluid remains unbounded by overburden. It also shows how a differential pressure applied to a viscous material will cause flow despite these differences in density. Vendeville and Jackson (1992b) concluded that regardless of density ratios a freely slipping, thin, overburden block (structure 2) will reach equilibrium at a position with an underlying column of fluid representing a diapir and that frictional and shear strength of overburden create a vertical constraint whereby not all fluid ridges can rise or thin floors above tabular fluid be pierced.

Perhaps the most important conclusion of Vendeville and Jackson (1992b) suggests that regardless of density ratio overburden troughs above tabular fluid are relatively unstable due to the pressure forces below troughs (P_2) being greater than those above a fluid column (P_1). Geologically, these troughs can be produced through differential deposition or loading, erosional unroofing, or extensional faulting and therefore act as conduits for salt flow and diapirs (Figure 2.8).

A differential fluid pressure will only cause salt flow if:

1. there is an open path to a near-surface salt body,
2. the overburden is thin, faulted or weak enough for pressure to overcome overburden strength,
3. or some other process (e.g. regional tectonic deformation) creates accommodation space (Rowan, 2005).

In contrast to previous views salt tectonics is now considered relatively non-intrusive; not driving salt tectonics, but simply reacting to and sometimes assisting external forces. Due

to salt generally being the weakest element of passive margin settings, thin-skinned regional deformation patterns and overall structural styles are common (Jackson and Talbot, 1991).

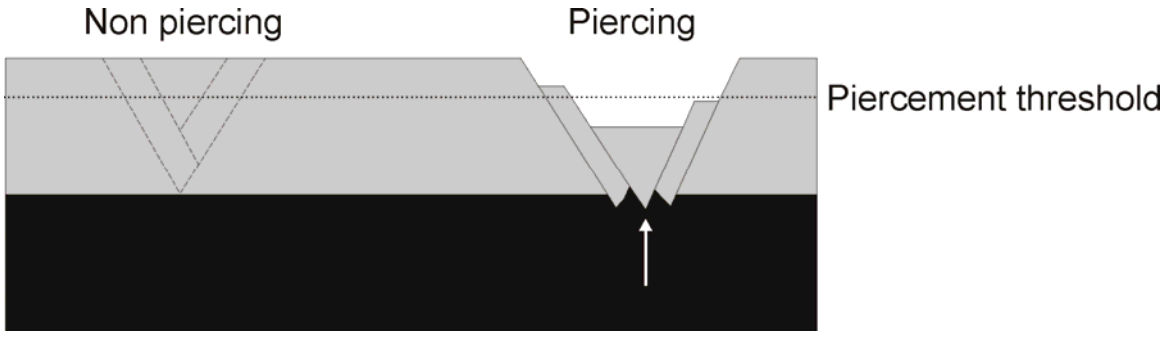

Figure 2.8. Schematic condition for active salt piercement of extensional structures (modified from Vendeville and Jackson, 1991). For a diapir to pierce overburden a "salt" ridge has to be taller than the piercement threshold, or a trough has to be deeper than the piercement threshold. Non-extended overburden is too thick and strong to be pierced (left), whereas thinned overburden through extensional normal faulting causes overburden to fall below the piercement threshold and therefore piercement (diapir) (right).

2.3 Salt Tectonics on Passive Margins

An important characteristic of all continental margins bearing salt structures is a seaward-thinning wedge of sediments derived from onshore and deposited onto initially horizontal salt within a basin (Last, 1988; Vendeville and and Jackson, 1992a,b; Poliakov et al. 1993; Jackson and Vaudeville, 1994; Ge et al., 1997; and Vendeville, 2005). A close correlation exists between the timing of major depositional events and that of phases of salt mobilization. The link between these occurrences as discussed previously is the differential loading of sediments onto a viscous sub-stratum of salt, driving salt flow (Figure 2.9).

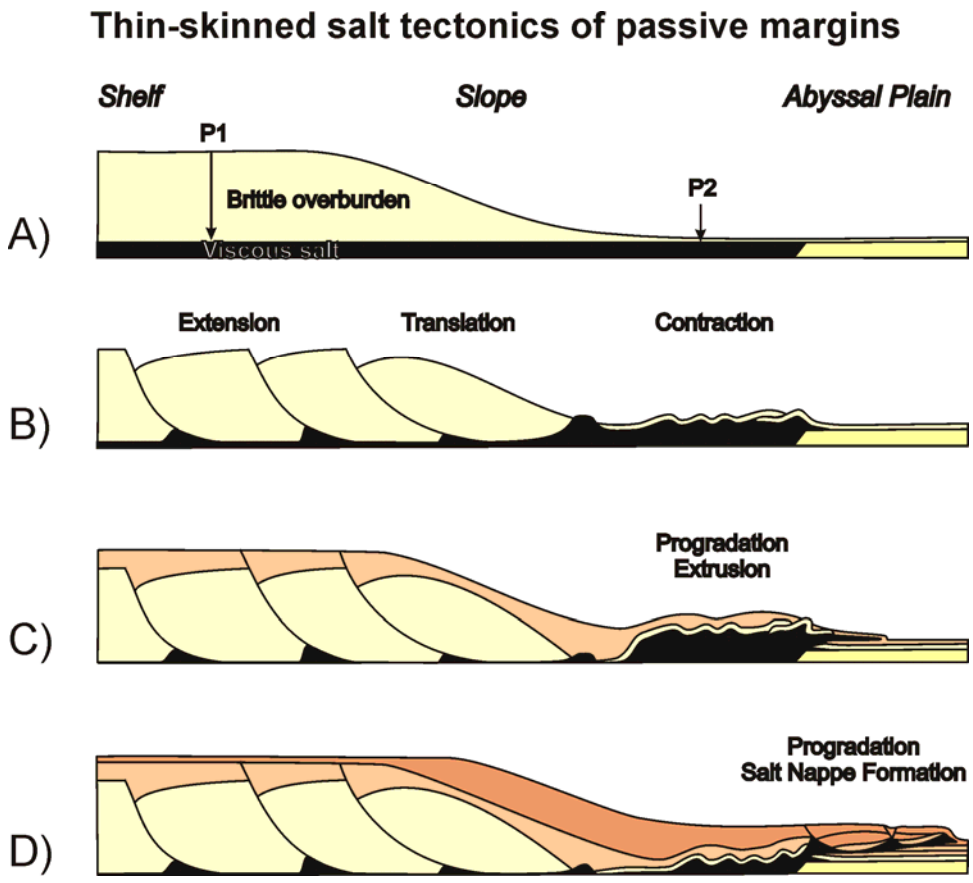

Figure 2.9. A) Schematic of a passive margin with a sedimentary wedge of brittle overburden covering a viscous salt layer. Pressures P1 and P2 are derived from the differential load of the sedimentary wedge. B) First stage of deformation includes kinematic segmentation of the margin into landward extension, central translation and distal contraction over salt. C) Next stage includes distal inflation of salt driven by the next progradational pulse and initial extrusion of salt out of the autochthonous salt basin. D) The last stage includes the formation of an allochthonous salt nappe driven by the last pulse of progradational sedimentation. In this stage initially compressional features such as buckle folding, can be overprinted by extensional structures on the salt nappe.

Gravitational failure of sedimentary overburden at passive margins occurs through a combination of gravity gliding (translation of a rock mass down a sloping detachment) and gravity spreading (vertical collapse and lateral spreading of a rock mass under its own weight due to differential loading as a result of a sloped upper surface) (Vendeville, 2005; Rowan *et al.*, 2004) (Figure 2.10). A spreading wedge along a passive margin is considered to be comprised of three deformational domains: (1) a proximal (upper slope

and part of the shelf) extensional region; (2) a central translational region; and (3) a distal (on and in front of the lower slope) compressional region (Figure 2.9). In these scenarios up-dip extension is balanced by down-dip shortening and salt inflation in the early stages of salt mobilization. As loading continues salt is extruded from the original or autochthonous basin and flows out of the initial basin and into the distal or allochthonous region.

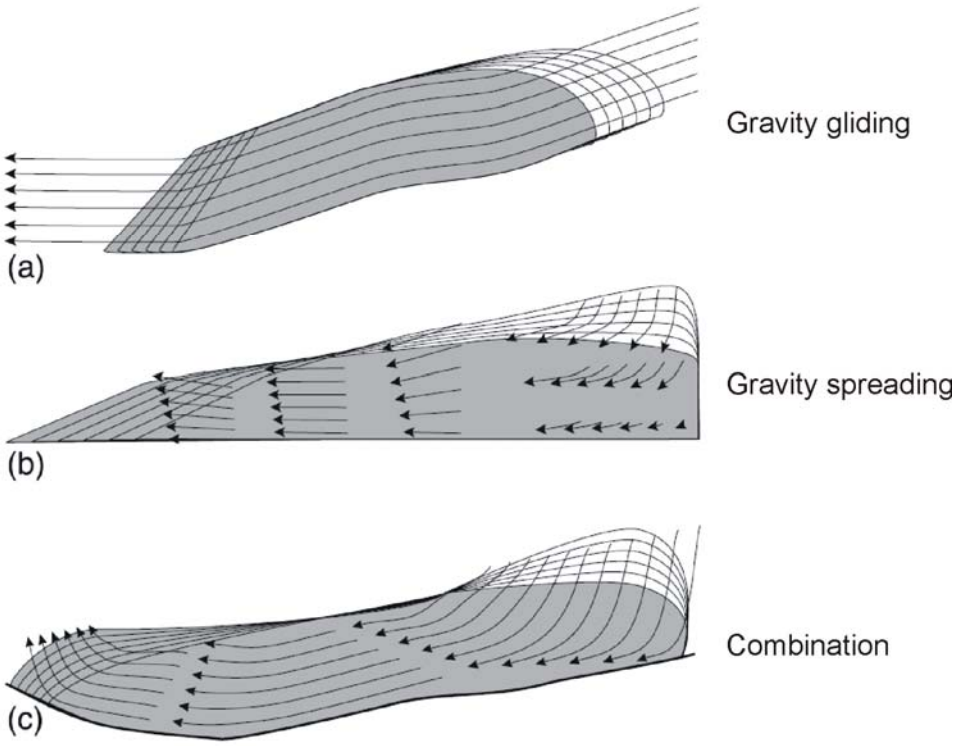

Figure 2.10. Schematic of gravity driven deformation of salt (modified from Rowan et al., 2004): (a) gravity gliding, in which a rigid block slides down a sloped detachment; (b) gravity spreading, in which a rock mass distorts under its own weight by vertical collapse and lateral spreading; (c) A combination of both styles of deformation. Shaded areas represent the final stage of deformation with arrows indicating vectors of material deformation.

Taking into account only gravity spreading Gemmer *et al.* (2004) considers three different salt flow regimes for a viscous (salt) substratum overlain by a brittle overburden

sedimentary wedge (Figure 2.11). Differential loading produces a channel (Poiseuille) flow within the salt layer (Figure 2.11a) where there is no horizontal movement of the overburden. Overburden stresses may exceed its yield strength and failure occurs due to either an increased overburden thickness differential or a reduction in overburden strength. In this case a component of shear (Couette) flow is initiated, along with channel (Poiseuille) flow, caused by the seaward translation of the overburden (Figure 2.11b). The other end member includes dominant Couette flow as a result of higher overburden instabilities and further translation (Figure 2.11c). The relationship between these forces determines deformation within the transition region of passive margin settings (Figure 2.12). The horizontal force balance can be described by the following equation:

Eq. 1) $F_1 + F_2 + F_p + F_c = 0$

F_1 and F_2 represent vertically integrated horizontal stresses that are derived from the differential load of the seaward thinning sedimentary wedge. F_1 denotes landward horizontal tensional stresses while F_2 corresponds to the distal compressional stresses in the yielding plastic overburden. The Poiseuille flow of the viscous salt layer creates a traction force on the base of overburden resulting in F_p. Conversely the Couette flow produces a basal traction force, F_c, as the brittle overburden fails and is translated horizontally. When equation 1 is equal to zero forces are balanced and overburden is considered at yield with no deformation, although Poiseuille flow continues (Gemmer et al., 2005). If F_1 and F_p increase due to continued differential loading or weakened overburden such that:

Eq. 2) $F_1 + F_p > F_2 + F_c$

deformation is initiated with landward extension and distal contraction associated with an increase in Couette flow.

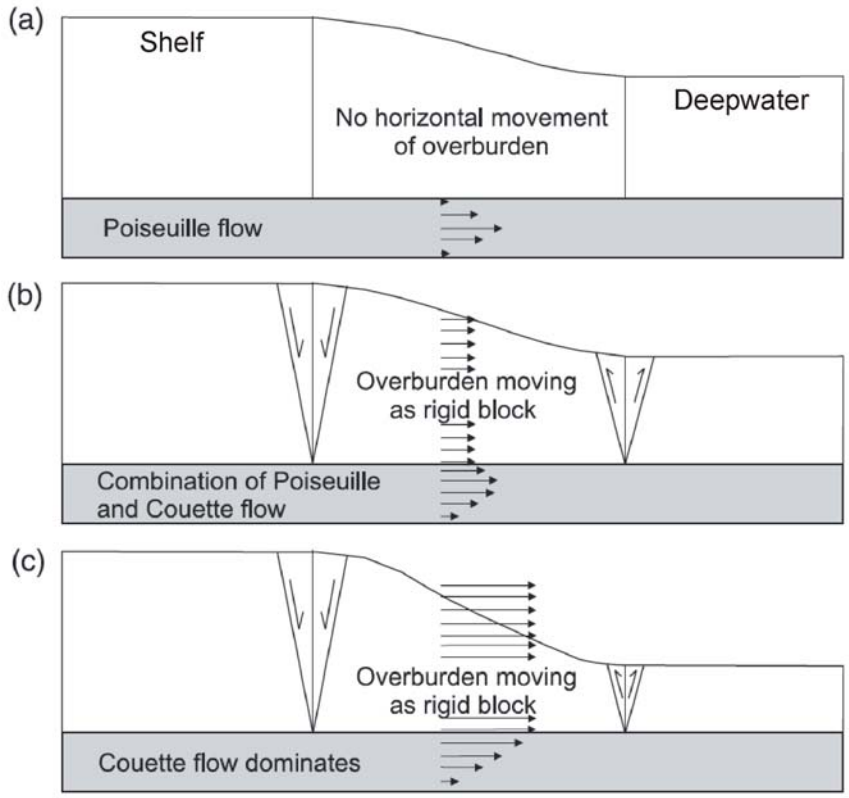

Figure 2.11. Differing deformation styles of a frictional-plastic overburden wedge (white) covering a viscous substratum (grey) (modified from Gemmer et al. 2004). (a) Stable overburden with a load driven Poiseuille flow in the viscous channel dominating deformation. (b) Unstable overburden with a combination of Poiseuille and Couette flow. Couette flow velocities induced from overburden translation are less than maximum Poiseuille flow within viscous channel. (c) Unstable overburden with dominant Couette flow in the viscous channel.

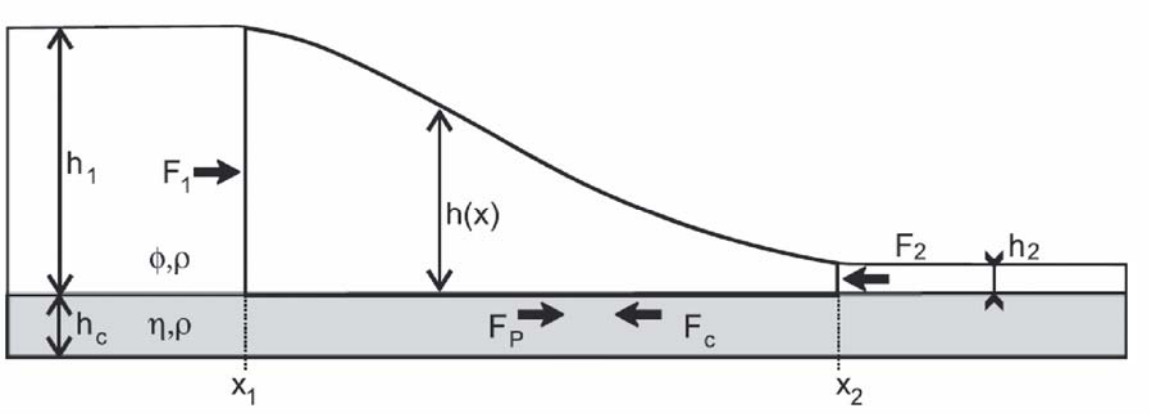

Figure 2.12. Horizontal forces acting on overburden transition zone (modified from Gemmer et al. 2005). Overburden is white and underlying viscous salt is grey. F_1 and F_2 represent horizontal forces resulting from differential load of overburden wedge. F_p (Poiseuille) and F_c (Couette) represent resultant Poiseuille forces from differential loading and Couette force from basal traction.

Further control factors of gravity spreading along passive margins affected by salt tectonics include: seafloor slope dip, basal salt detachment dip along with its coefficient of friction, and the internal strength of the overburden. Of these controlling parameters, the surface slope of the seabed is considered the most prominent (Rowan *et al.*, 2004). The surface slope is mainly controlled by sedimentation. Sediment progradation onto the outer shelf and upper slope maintains or increases the slope angle, therefore driving gravity spreading through differential load. However, sediment bypass into more distal regions (basal slope, distal basin) will reduce the slope of the sediment wedge and increase the thickness of overburden, effectively reducing spreading (Rowan et al., 2004) (Figure 2.13).

In contrast, the dip of the basal detachment is the dominant factor controlling gravity gliding (Rowan et al., 2004). A steeper dip increases the load of the overburden down dip, making it easier to overcome the frictional forces acting on the detachment. Tectonic

processes can therefore affect this detachment dip and subsequent translation. Differential thermal subsidence common to oceanic crust and resulting cratonic tectonic uplift increases basal dip and therefore accelerates basinward translation of overburden. Differential loading subsidence resulting from deposition of proximal prograding deltaic lobes, however, decreases basal tilt therefore retarding or halting basinward translation.

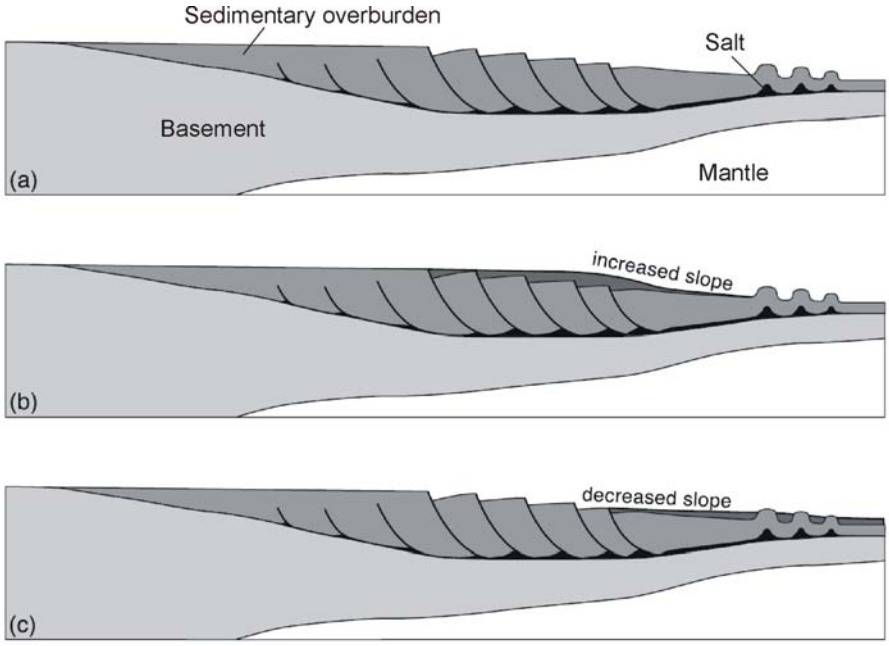

Figure 2.13. Schematic passive margin characterized by significant salt accumulation (black) with: (a) failure dominated by gravity spreading; (b) progradational deposition along the outer shelf and upper slope that increases the surficial slope and therefore drives further spreading; (c) sediment bypass on the shelf and upper slope resulting in distal sedimentation on the lower slope and abyssal plain that reduces the surficial slope and therefore slows or stops spreading (modified from Rowan et al., 2004).

Physical analogue models have been used to describe the structural consequences of distal shortening and contraction and proximal extension of a sedimentary wedge above a viscous substratum (Adam et al., 2008; Kresek et al., 2007; Vedeville, 2005; Fort et al., 2004; Ge et al., 1997). Extension in the upper slope is first accommodated by symmetric or asymmetric grabens detaching above the source layer. With initially thin salt layers

extension is often accommodated with normal faulting throughout the entire deformation history. With initial thick salt normal faulting thins graben floors allowing diapirs to form, rise reactively, and eventually pierce overburden creating a network of salt ridges and diapirs. These structures are the main consequence of early extension in the proximal region of the sediment wedge. Symmetric buckle folding or lateral shortening and vertical inflation of any preexisting salt diapirs or massifs located in the distal part of the wedge accommodate contraction on and in front of the lower slope. Deformation domains depend on the timing of basin evolution. With time younger extensional structures become superimposed on distal contractional structures, which are buried by ongoing sediment progradation on the slope and deepwater basin (Figure 2.9).

Passive margin sedimentary basins worldwide have undergone a combination of gravity gliding and spreading, although the structural styles of most of these margins often appear to be dominated by one of these processes (Figure 2.14). Salt mobilization along many of these margins (Eastern Canada, the Gulf of Mexico, and South Atlantic) began early during thermally or tectonically controlled subsidence and tilting of the crust. Therefore regional tilting may have partially triggered salt deformation through extension of overburden and seaward translation (Vendeville, 2005). Examples of this are observed throughout raft tectonic characteristics of south Atlantic basins (Figure 2.14).

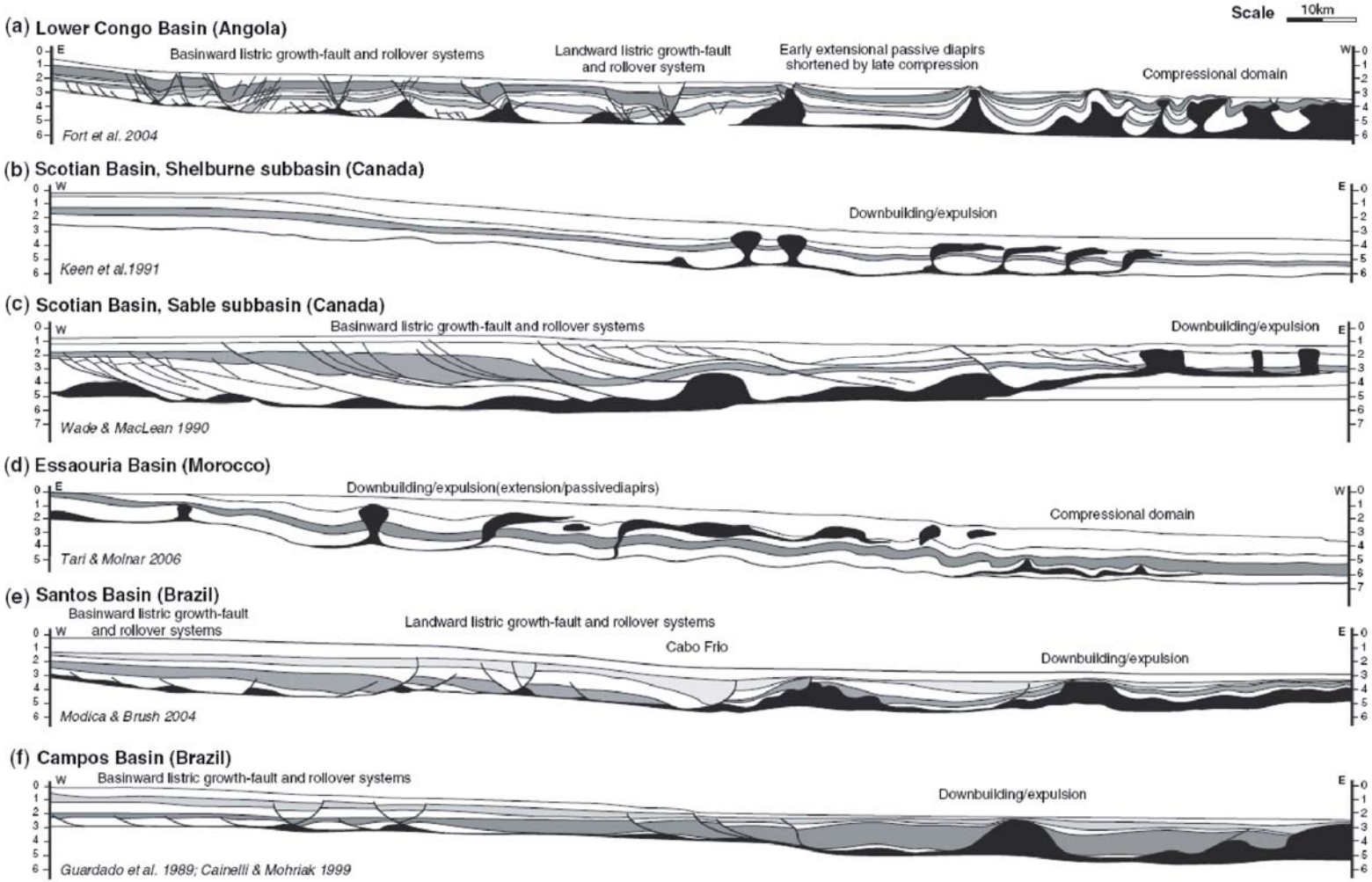

Figure 2.14. Kinematic domains and characteristic salt structures of passive margin basins detached on salt (Courtesy of Krezsek et al., 2007). Schematic line drawings of interpreted regional seismic profiles from (a) offshore Angola, (b, c) Atlantic Canada, (d) offshore Morocco, (e, f) offshore Brazil. Two way travel time is displayed along the vertical axis. Salt is shown as black with grey and white layering indicating stratigraphy of brittle overburden No pre-salt basement is shown.

However, long after thermal subsidence had ceased salt movement continued through the differential loading of sediments. In some cases passive margin buildup and related flexural loading has produced a landward dipping basin floor, therefore prohibiting basinward gravity gliding. In some cases (e.g., Mediteranean) evaporite deposition occurred some tens of millions of years after thermal subsidence ceased. For these reasons it is believed that sediment loading, instead of margin tilting and gravity gliding, is the main process driving long-lived salt tectonics. In passive margins settings the critical slope allowing salt flow through differential loading is built up externally (i.e. not tectonically) by the deposition of prograding sediments assuming no distal buttress obstructing salt flow. The Scotian margin is an example of significant salt mobilization and structure development more than 75 Ma post-rift and 60 Ma after the onset of seafloor spreading (Jackson and Vendeville, 1994, Wade and MacLean, 1990) (Figures 2.1, 2.14).

Two processes occur spontaneously with the deposition of a sedimentary wedge above a salt layer. First, differential overburden subsidence is triggered by differential loading (Figure 2.9). This loading triggers a large lateral movement of salt, through mostly vertical downbuilding in the proximal basin and often inflation of distal salt. Second, gravity spreading facilitates the seaward translation of overburden (Vendeville, 2005). In nature, deformation of overburden will be a combination of differential subsidence and lateral spreading. A thick salt layer or thick distal sediments favor differential subsidence,

while lateral spreading is favored by a thin source layer or distal sediments that are thin or absent.

The tectonic and sedimentary history of passive margins can be quite different, leading to variable histories of gravitational failure. The early stage of salt tectonics for most margins is characterized by landward extension accommodated by basinward shortening (mostly thickening of salt) (Krezsek et al., 2007). Early folding of deep-basin strata as a result of early contraction is only recorded on Angolan, Moroccan and Brazilian margins (Figure 2.14a, d – f). Within extensional domains basinward listric growth-fault and rollover systems are observed within the Congo (a), Scoian/Sable (c) and Campos (f) basins. In contrast landward listric growth-fault and rollover systems dominate the northern Santos Basin (e). In both the Scotian and Moroccan margins passive diapirs dominate (Krezsek et al., 2007).

2.4 Previous salt tectonic insights and results

The Salt Dynamics Group of Dalhousie University through the use of 4-D physical analogue models has had great success in studying thin-skinned deformation of salt influenced passive margin (Adam et al. 2008, Kresek et al. 2007, Campbell, 2007, MacDonald, 2007). Insight from previous analogue experiments suggests that first-order parameters influencing salt basin evolution are:

1. Salt basin geometry
2. Salt thickness

3. Basement configuration, and
4. Sedimentation patterns and rates

2.4.1 Salt basin geometry and initial salt thickness

Ge et al. (1997) first discuss the implications of non-uniform basement configurations on salt structures within basins, using scaled physical models. In experiments differential loading through the progradation of sedimentary wedges were considered the driving force behind salt diapirism. Experiments with basal salt (silicone) layers having a flat bottom efficiently extruded salt basinward through the formation of a broad expulsion rollover. However, no diapiric salt structures formed.

Experiments utilizing a basement configuration having two landward facing steps with similar progradational wedges, conversely, did form diapirs (Figure 2.15). Early model evolution was very similar to that of the flat based experiments including basinward extrusion of salt by the differential loading of a sedimentary wedge. However, basement steps impeded efficient basinward lateral flow of salt, concentrating salt above the step edge, especially where progradation was too rapid for salt to escape basinward. At this location salt first formed a salt-cored anticline and later passive diapir and salt sheet. As the salt mobilized basinward over step 1, salt was inflated on the distal flank of the diapir, generating the source for another diapir above step 2 through similar mechanisms. These scaled analogue experiments illustrate the importance of considering salt basin variability and its influence on salt structures.

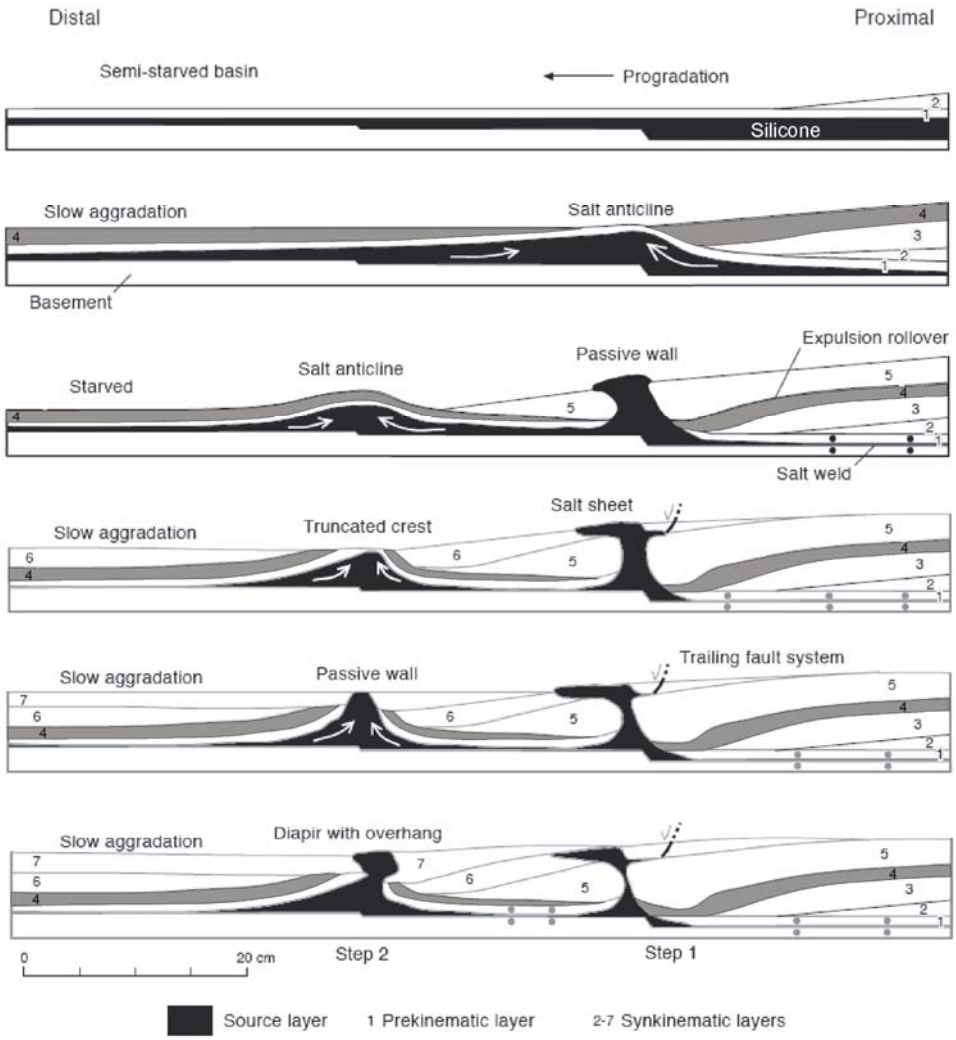

Figure 2.15. Cross-sections illustrating the schematic evolution of "salt" (silicone) structures of an analogue model simulating the progradation of a sediment wedge over a salt basin consisting of several basement steps (modified from Ge et al., 1997). Note that basement steps act as nucleation points for silicone inflation and later passive diapir and salt sheet development. Pairs of dots represent welding. For discussion see text.

Expanding on the work of Ge et al. (1997) previous analogue experiments of the Salt Dynamics Group suggest that syn-rift continental salt basin geometry and therefore salt thickness variations are a main factor in the formation of different salt subprovinces along the Scotian Margin. A series of pilot experiments, having constant sedimentation rates approximated for the Jurassic-Cretaceous and a simplified (2-D) sedimentation pattern from slope to deep basin, were conducted to test possible salt basin configurations for the

Scotian margin. These configurations include 1) Symmetric rift graben, 2) Half graben wedge, 3) Half graben with fault step, and 4) Symmetric graben with intermediate basement horst (Figure 2.16). A first order control factor for the structural evolution observed in models is the geometry of the salt basin. **Early**, **intermediate** and **late** stage model evolution is markedly different in models, with particular differences observed during early silicone mobilization within extensional and translational segments and very late stage allochthonous extrusion (Figure 2.17).

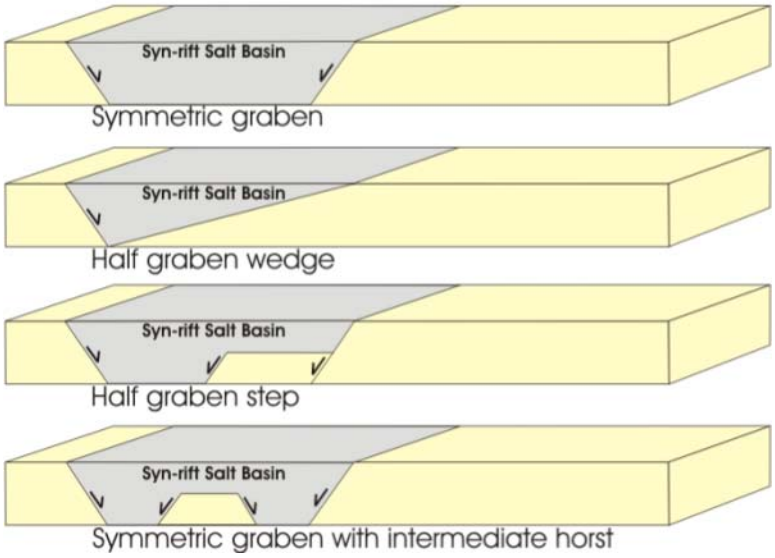

Figure 2.16. Various rift basin geometries represented by analogue models (Courtesy of Campbell, 2007, MacDonald, 2007). Total basin dimensions are modeled to represent 80 km x 30 km x 2 km. Land is to the left for experiments and sea is to the right.

The **Early** stage is defined by the initiation of salt mobilization and strong subsidence as a result of differential loading of early post-rift sediments on the autochthonous salt basin. Deformation begins with basinward dipping growth faults in the landward edge of the basin (Figure 2.18). Faults begin to cease as the "salt" source layer is depleted through passive downbuilding of a relatively undeformed overburden sedimentary

wedge. The basinward limit of this sedimentary package is marked by a passive diapir (D in Figure 2.18) or inflated silicone body (salt massif). The end of the early stage may incorporate expulsion rollover development along the basinward edge of the sediment packages flanking inflated salt. Contractional small-scale buckle folding and a small amount of silicone inflation characterize the seaward portion of the salt basin.

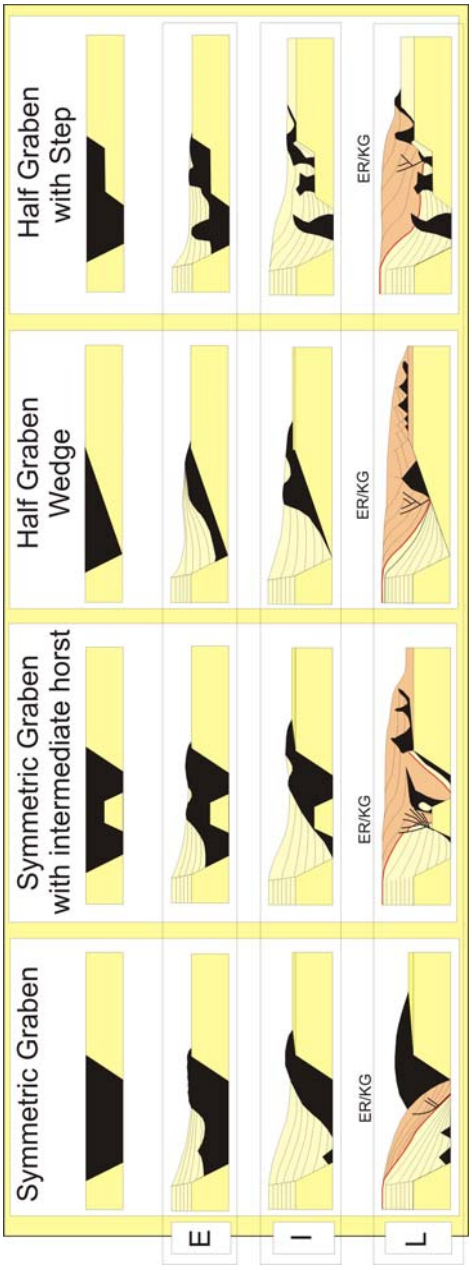

Figure 2.17. Schematic overview for the evolution of analogue experiments denoting the early (E), intermediate (I) and late (L) stage of model evolution (Courtesy of MacDonald, 2007; Campbell, 2007). Bright yellow indicates (sny-rift) salt basin geometry, with pale yellow and pale orange (divided by red line) illustrating shelf build-up and progradational phases of model sedimentation procedures. Black indicates silicone putty. For discussion see text.

The **intermediate** stage of model evolution is characterized by the seaward progradation of the sediment wedge and associated welding within the original salt basin(s). Within the half graben wedge and symmetric graben with horst experiments, a very efficient early and basinward evacuation of silicone from the original basins is observed. Near the seaward basin edge however, silicone is strongly inflated into complexes due to this edge acting as a buttress. Long-lived expulsion rollovers develop and begin to extrude silicone out of the autochthonous basin forming allochthonous canopies overlying older deep-water sediments (Figure 2.18). The symmetric graben and half graben with step experiments trapped more silicone within landward passive diapirs. Basement steps mainly control the distribution of these diapirs. Within all experiments diapirism and the formation of expulsion rollovers has rafted the stratigraphic section of early salt withdrawal basins.

The **late** stage of model evolution is focused on sedimentation and deformation within the deepwater basin and associated silicone nappe and canopy systems. Here silicone has flowed out of the initial salt basin onto older deepwater sediments (Figure 2.17, 2.18). Continued sedimentation and progradation on top of allochthonous silicone can produce new minibasin formation and growth fault rollovers. This deepwater extensional domain is observed best within the roho-like system of the half graben wedge experiment.

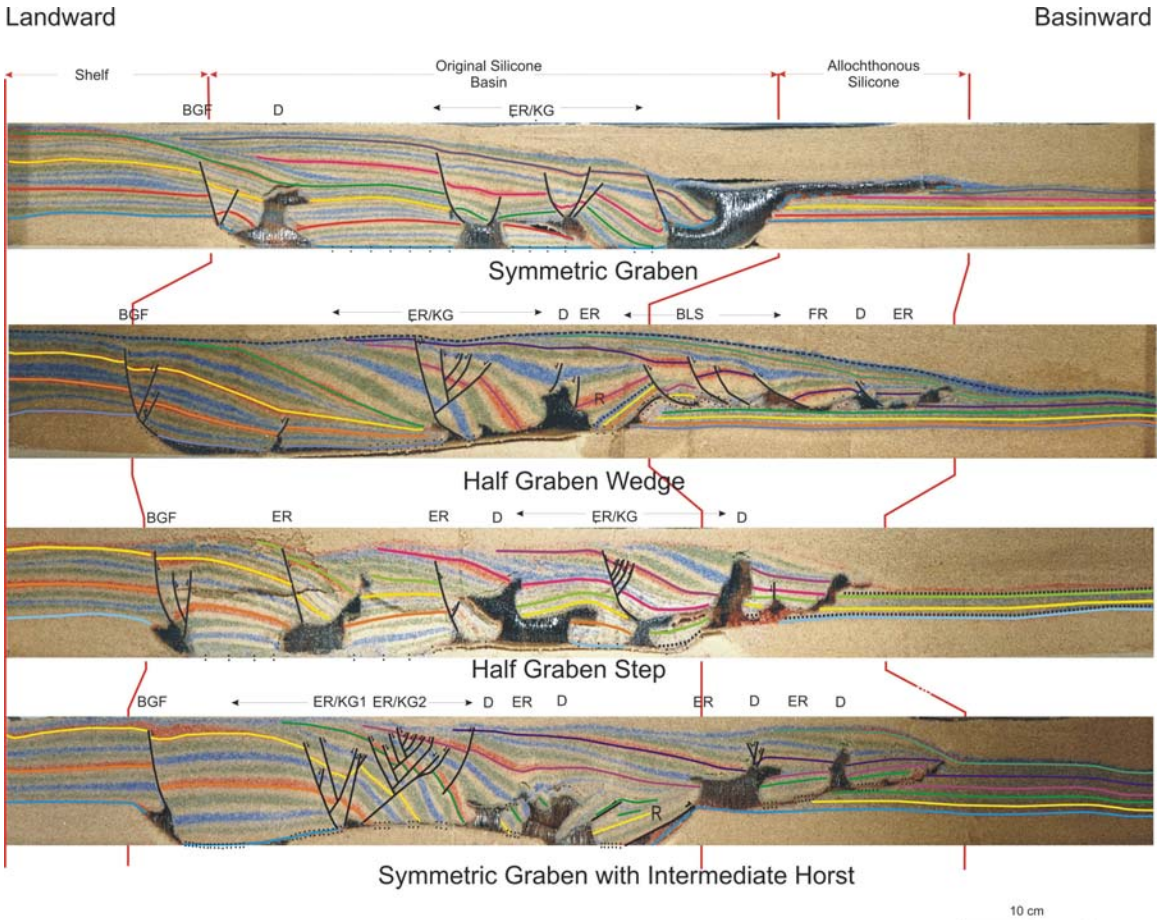

Figure 2.18. Characteristic cross-sections of analogue pilot experiments investigating the effect of salt basin geometry and salt thickness on basin evolution (Courtesy of MacDonald, 2007). Silicone appears as black structures in between coloured sand layers. Coloured marker horizons represent every 8th sieving interval and black lines represent faults within the model. BGF – basinward listric growth fault, D – diapir, ER – expulsion rollover, KG – keystone graben.

The main conclusions of the variable salt basin geometry experiments are (Campbell, 2007 and MacDonald, 2007):

1. The dominant mechanism for early salt mobilization in salt basins containing thick (> 2 km) salt deposits is channel (Poiseuille) flow resulting from sedimentary loading and passive downbuilding of early salt withdrawal basins. This mechanism is observed to favour passive

diapirism and associated expulsion rollover structures as opposed to extensive basinward listric growth faulting.

2. Initial landward salt withdrawal and the location of seaward inflated salt depend mainly on salt thickness controlled by basin floor geometry. This is contrary to previous study suggesting that the geometry or angle of the basinward rift shoulder determines its efficiency as a buttress.
3. The timing and extent of allochthonous salt nappe advancement are dependent on the efficiency of early salt evacuation of the landward original salt basin and continued sedimentation and progradation on top of the inflated salt.

2.4.2 Sedimentation patterns and rates

Krezsek et al. (2007), using similar analogue experiments, considers the effect of varied sedimentation rates on the structural evolution of gravity driven salt tectonics. High sedimentation models had a 5 mm thick sand layers sieved onto the initial salt basin every hour (equivalent to 1600 m/Ma.) simulating aggradation and later progradation of sediments onto salt basins of passive margins. Low sedimentation models had 2.5 mm thick sand layers sieved every 2 hours, equivalent to 420 m/ma in nature. Stagnation experiments received early high sedimentation rates during shelf build up and then sedimentation was ceased to observe model evolution with no sedimentation. Experiments generated complex salt-related structures similar to those observed along passive margins worldwide (Figure 2.19). Structures include salt withdrawal minibasins,

landward and seaward dipping growth fault and rollover structures, expulsion rollovers, triangular-shaped reactive, passive and active dipairs, turtle structures, canopies, and folds, thrusts and allochthonous salt sheets (Figure 2.19). All experiments display a similar kinematic segmentation (e.g. extensional, transitional and contractional domains) comparable to that along passive margin settings with salt tectonic deformation resulting from gravity spreading (see Section 2.3).

For experiments varying sedimentation rates and coupled strain rates controlled the structural evolution of fault and "salt" structures. In low sedimentation experiments reactive diapirs beneath thinning grabens, pierce overburden and develop into passive diapirs and eventually extensive canopies. However, in high sedimentation experiments early forming grabens later transform into growth fault rollover systems. Figure 2.20 summarizes the temporal evolution of extensional structures and associated diapirs with relation to sedimentation rates derived from experiment results.

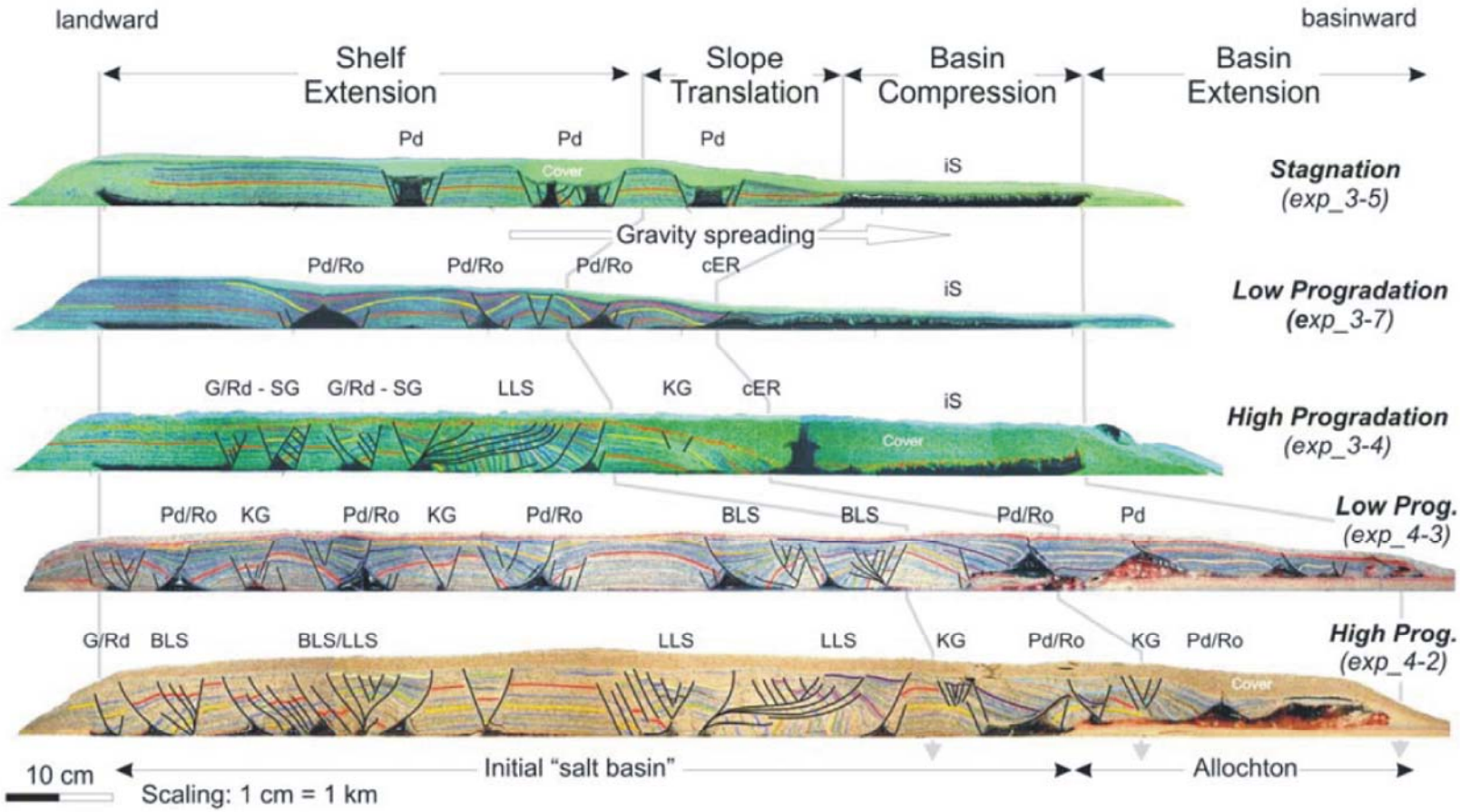
landward
basinward
Shelf Extension
Slope Translation
Basin Compression
Basin Extension
Pd
Pd
Pd
Cover
iS
Stagnation
(exp_3-5)
Gravity spreading
Pd/Ro
Pd/Ro
Pd/Ro
cER
iS
Low Progradation
(exp_3-7)
G/Rd - SG
G/Rd - SG
LLS
KG
cER
iS
Cover
High Progradation
(exp_3-4)
Pd/Ro
KG
Pd/Ro
KG
Pd/Ro
BLS
BLS
Pd/Ro
Pd
Low Prog.
(exp_4-3)
G/Rd
BLS
BLS/LLS
LLS
LLS
KG
Pd/Ro
KG
Pd/Ro
Cover
High Prog.
(exp_4-2)
10 cm
Scaling: 1 cm = 1 km
Initial "salt basin"
Allochton

Figure 2.19. "Salt" (silicone)-related structures (black polygons) observed in cross-sections of analogue experiments with varying sedimentation rates and basal slope (bottom two sections) (Modified from Krezsek et al., 2007). Coloured marker horizons are chosen to best illustrate stratigraphy (coloured sand layers) of models, with black lines indicating faults. Above coloured sand layers a post-experiment cover (illustrated) stops the deformation of models for sectioning. G/Rd - Graben systems and associated reactive diapirism, LLS / BLS - Landward / basinward dipping listric fault/rollover systems, Pd, Pd/Ro - Passive diapirism and associated symmetric rollovers, KG – keystone graben, iS – inflated silicone, cER – compressional expulsion rollover.

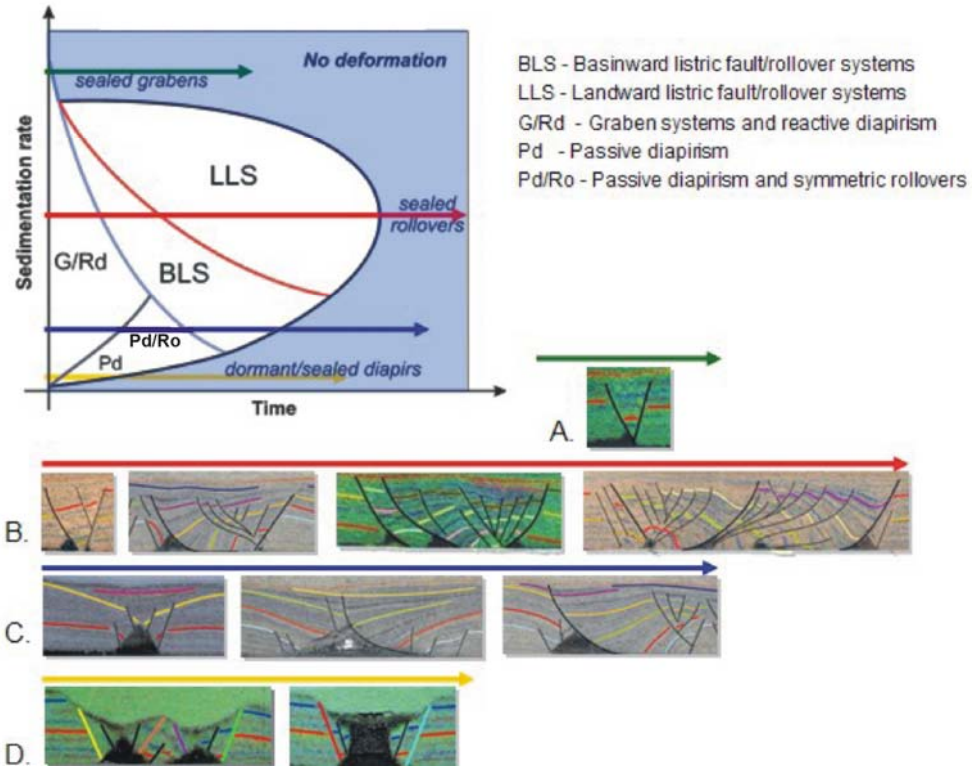

Figure 2.20. Temporal relationship between sedimentation (strain) rate and evolution of extensional salt-related structures and diapirs in scaled analogue experiments from Figure 25 (Modified from Kreszek et al., 2007). Ductile layer thickness 10 mm (= 1000 m in nature), x-axis total time 50 hours (= 15 my), sedimentation rates: high 5 mm/h (= 1600 m/my), low 1.25 mm/h (= 420 m/my). A – D: Characteristic succession of fault and diapir structures; A – very high, B – high, C – low, and D – stagnant sedimentation.

Characteristic successions of structural styles for different experiments reflect that differential load is the driving force behind stresses and individual strain histories of fault structures in the models. Very low or no sedimentation rates favour reactive diapir rise, forming passive diapirs and related canopies (Adam et al., 2008). These form along the

dynamically unstable shelf-slope transition and deepwater slope of the passive margin sedimentary wedge. Low sedimentation rates in models encourage long-living symmetric passive diapir/rollover systems and basinward growth fault/rollover systems (Figure 2.19, 2.20). High sedimentation systems in models evolve from symmetric grabens, early, mature, and late (collapsed) basinward growth fault/rollover systems into landward growth fault/rollover systems with asymmetric salt rollers. Very high sedimentation rates were observed to seal extensional structures.

In comparison with model results, even the highest calculated sedimentation rates observed within the Scotian Basin (Laurentian and Sable Sub-basins) are considered moderate in comparison with many passive margins known for salt tectonic development. These models produced many similar structures (expulsion rollovers, canopies, diapirs, etc.) when compared to the North Central Scotian margin.

Chapter 3: Regional Overview of the Scotian Margin

3.1 Scotian Margin evolution

The Scotian Basin is situated on the Atlantic continental margin (Figure 3.1), offshore Nova Scotia and is composed of a series of interconnected Mesozoic rift basins resulting from the formation of the present day Atlantic Ocean, as North America rifted from Africa during the Late Triassic to Early Jurassic (~230-190 Ma) (Jansa and Wade, 1975). The Scotian Basin spans over 1200 km along the Eastern Canada seaboard from the southwestern Yarmouth Arch to the Avalon Uplift of the western Grand Banks offshore Newfoundland, encompassing a total area of 300,000km^2, including the Shelburne, Sable, Abenaki, Laurentian, and South Whale Sub-basins (Wade and MacLean 1990) (Figure 3.1).

To the northwest of the Scotian Basin, the Lahave Platform and Canso ridge form a stable flank that contains an Early Jurassic (post-breakup) basement hinge zone. To the northeast, the Burin Platform acts as the basin margin. Across this northeasterly trending hinge zone the basement depth increases from approximately 4 km along the shelf to up to 18 km along the eastern margin (Laurentian sub-basin). Complex rifted basement structures (e.g. Orpheus and Mohican Grabens) are located south-east of this hinge zone, but are not always reliably observed on seismic reflection images due to the thickness of sediments. However, geometries of these structures are often inferred from deformation observed in brittle overburden or mobilized salt (Wade and MacLean 1990). The main structural elements typical of this and other passive continental margin basins include shallow basement platforms in the shelf area, hinge zone, structural high flanking deep

marginal sedimentary basins and, more distally (seaward of the continental shelf and slope), a deep water abyssal plain oceanic basin (MacLean and Wade, 1992).

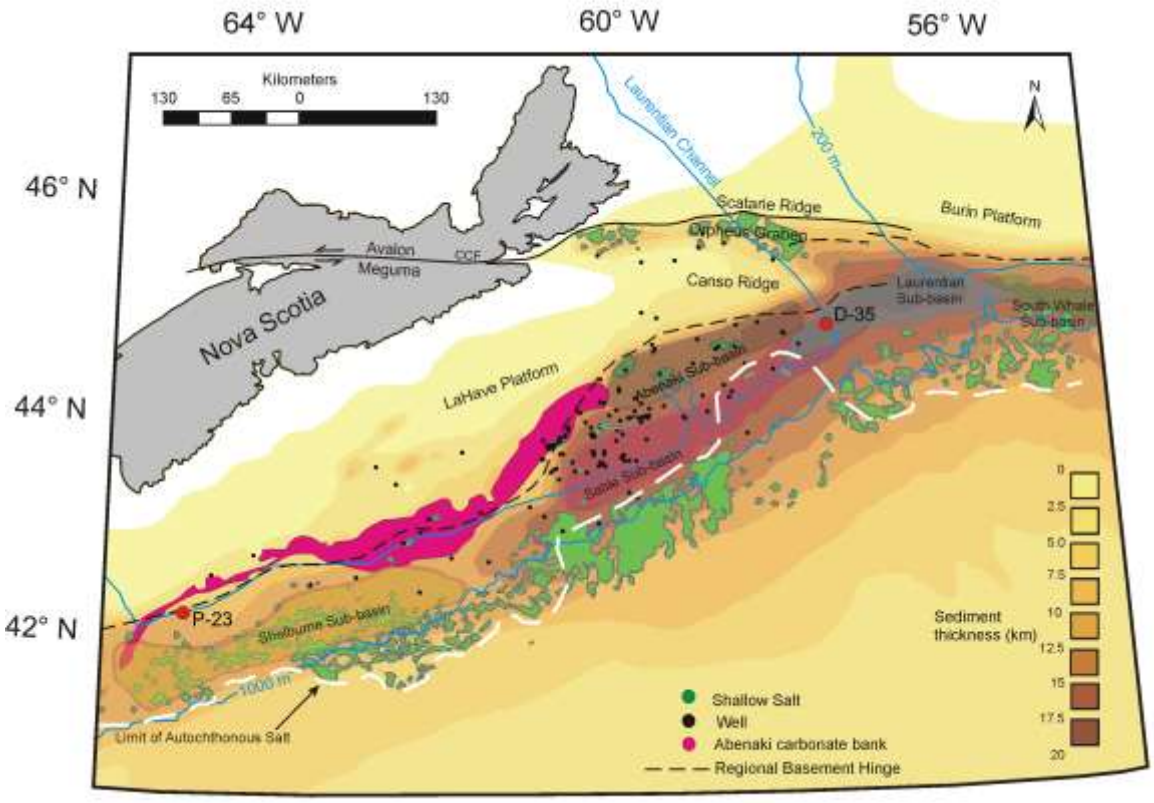

Figure 3.1. Continental shelf and slope of the Scotian Margin, offshore Nova Scotia with sediment thickness shown as colour background. Sub-basins of the Scotian Basin are shown using colour overlay. Salt provinces defined by Shimeld (2004) are labeled I-V with the limit of autochthonous salt indicated by a white dashed line. Salt diapirs, mainly of the Slope Diapiric Province are indicated by green. Bathymetry is labeled with blue lines indicating 200 and 1000m contours. The regional basement hinge is represented by a black dashed line. CCF = Cobequid-Chedabucto Fault. Present day location of Abenaki Formation carbonate bank (Baccaro Member) is indicated along the central and western margin. Wells mentioned in text are indicated by red.

3.1.1 Crustal structure

The Scotian margin and the Canadian East Coast formed during the past 200 million years as Pangea rifted apart in several stages (Figure 3.2) with North America separating

from Africa sometime before chron M29 (160 Ma) (Louden, 2002). The Scotian margin is located at a transition from volcanic margins in the south (e.g. southern Baltimore Canyon Troughs) (Talwani and Abreu, 2000) to non-volcanic margins to the north (e.g. Grand Banks and Newfoundland basins) (Funck et al. 2004). Regional magnetic data of the margin show a 300 nT linear northeast-southwest trending anomaly named East Coast Magnetic Anomaly (ECMA) that extends from Georges Bank to Sable Island (Figure 3.3). SDRs (seaward dipping reflectors), observed on several deep marine seismic reflection profiles (lines 89-3, 4, 5), coincide with high amplitude areas of the ECMA in the southern portion (Shelburne Basin) of the anomaly west of SMART (Scotian MARgin Transects) seismic refraction profile Line 3 (Keen and Potter, 1995) (Figure 3, 4). North-eastward weakening of ECMA amplitudes and its eventual disappearance east of the Sable Island suggest reduction or lack of igneous material emplacement in these areas.

Seismic reflection GSC Line 89-1 in the northern portion of the margin (Figure 3.3) is absent of SDRs and any significant associated magnetic anomaly suggesting a non-volcanic margin (Keen and Potter, 1995). Line 1 of the SMART refraction profiles is coincident with Line 89-1 and supports this conclusion through velocity modeling which shows highly thinned continental and oceanic crust at the OCT (ocean-continent transition) overlying serpentinized and exhumed mantle (Funck *et al*., 2004)(Figure 3.4). However, the ambiguous central margin still has a pronounced magnetic anomaly and yet no SDR observed in reflection Line 88-1A (Keen *et al*., 1991). Wide-angle SMART Line 2, coincident with line 88-1A, has an OCT zone characterized by partially serpentinized

mantle overlain by highly faulted continental crust to the northwest and thin oceanic crust in the southeast (Wu *et al*., 2006) (Figure 3.4).

The presence of exhumed and highly serpentinized mantle in the OCT of Line 1 indicates that no melt was created during break-up in the Northern margin while only limited magma was generated in the central margin as suggested by the inferred presence of partially serpentinized mantle within the OCT of Line 2. Thicker oceanic crust (~5-7 km compared to ~4 km) and lower percentages of serpentinized mantle inferred from Line 2 than from Line 1 also indicate a magma starved northern margin with increasing magma supply in the central Nova Scotia margin. Therefore both SMART Lines 1 and 2 suggest primarily non-volcanic rifting for both the central and northern Nova Scotian margin. No analyzed data from SMART Line 3 has been published to date.

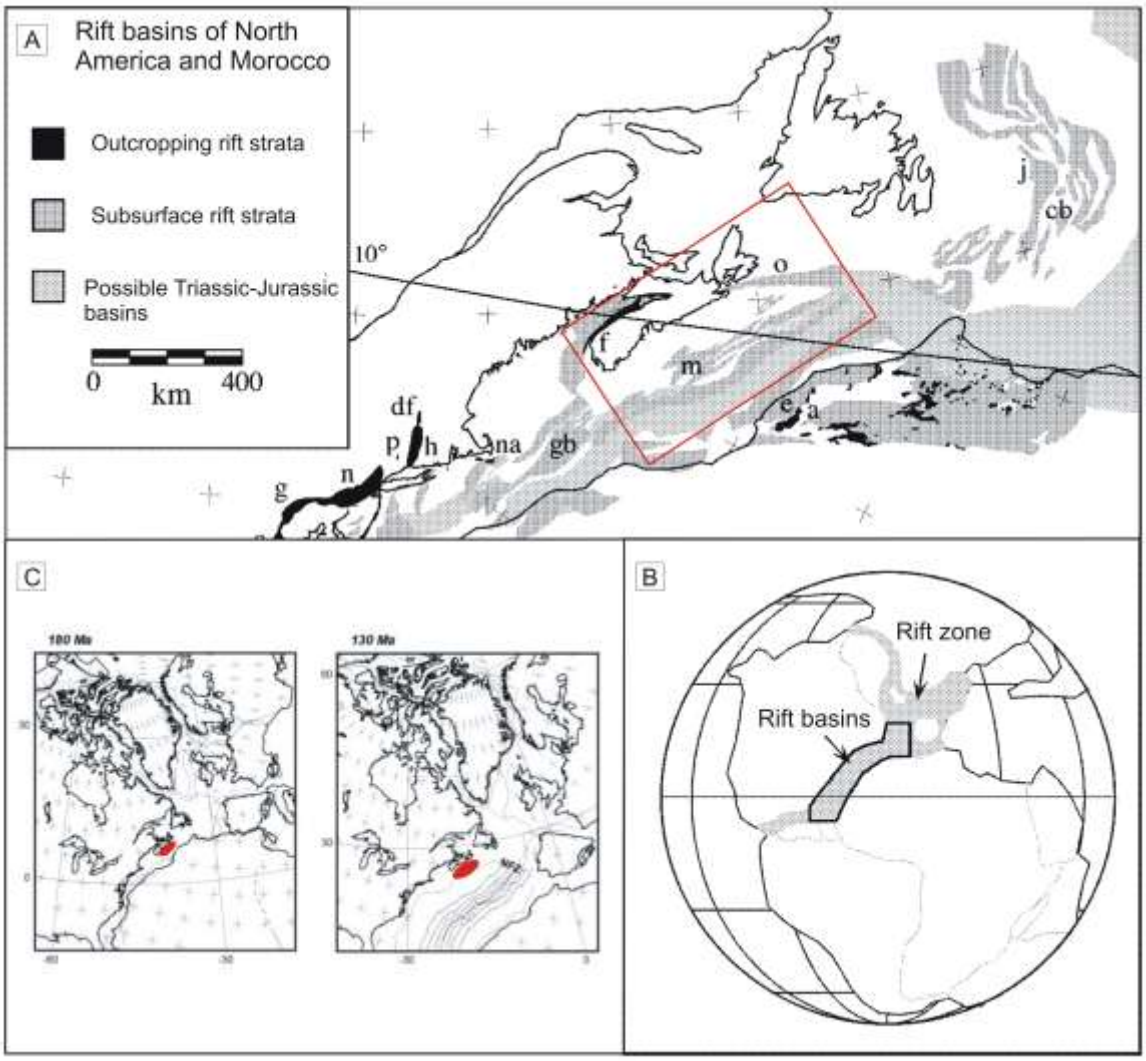

Figure 3.2. Rift basins of North Americain and Morocco and their paleogeographic position (paleolatatude lines) for the Late Triassic (Carnian ~225 Ma) (Kent et al., 1995). (A) Scotian margin (red box) basins: f, Fundy basin; m, Mohican basin; o, Orpheus basin; (B) Reconstruction of Pangea for the Late Triassic (Carnian), showing the rift zone (gray) and the Scotian margin rift basins detailed in (A). Modified from Olsen, 1997). C) North Atlantic rifting plate reconstruction at 180 Ma, 130 Ma. Dotted lines indicate anomalies associated with sea-spreading. Red indicates the approximate location of the paleo-Scotian margin at these times. The Nova Scotia margin was formed through the separation of North America and Africa sometime before chron M29 (160 Ma) (from Coffin *et al.*, 1992). a, Argana basin; cb, Carson basin; df, Deerfield basin; e, Essaouira basin; f, Fundy basin; g, Gettysburg basin; gb, Georges Bank basin; h, Hartford basin; j, Jeanne d'Arc basin; m, Mohican basin; n, Newark basin; na, Nantucket basin; o, Orpheus basin; p, Pomperaug basin.

Velocity models also suggest an interpretation that continental crustal thinning along SMART Line 2 was initially gradual (~5km) within the modern outer continental shelf, followed by a much faster thinning along the continental slope and into the ocean basin (Wu *et al*., 2006). Therefore, little accommodation space was created along the shelf edge because gradual thinning of the crust and the resulting deepening along the LaHave Platform was unable to counteract the thermal uplift from thinning mantle lithosphere as predicted through subsidence analysis (Keen and Beaumont, 1990). In the south – central portion of the margin (e.g. LaHave Platform, Shelburne Sub-basin; Line 2) only relatively thin sediments could be deposited as a result of this syn-rift crustal thinning. However, thick sediments did accumulate along the north – central margin (e.g. Sable, Abenaki, and Laurentian Sub-basins; Line 1) due to drastic thinning of continental crust from the initialization of rifting followed by gradual thinning to the ocean basin (Wu *et al*., 2006). This rapid thinning and resulting subsidence allowed accommodation space for the thick sediment deposits of the deep north – central Scotian Basin seaward of the basement hinge zone including much thicker syn-rift deposits than along the central margin.

3.1.2 Rift basin architecture

To the north, northwest, and northeast of the Scotian Basin, the Lahave Platform, Canso ridge and Burin Platform form a stable basin flank containing an Early Jurassic (post-breakup) basement hinge zone consisting of a series of faults or flexures. Basin depth increases greatly across this hinge zone with average depth to basement rising from ~ 4

km on the platforms to up to 18km within the sub-basins (Wade and MacLean, 1990). The hinge zone trending northeast-southwest across the margin is not one fault; instead, it is a series of interconnected and offset faults (Figure 3.5). The complex development of the hinge zone suggests a syn-rift origin with some development during a post-rift reactivation phase. Therefore independent crustal downwarp and subsidence as a result of

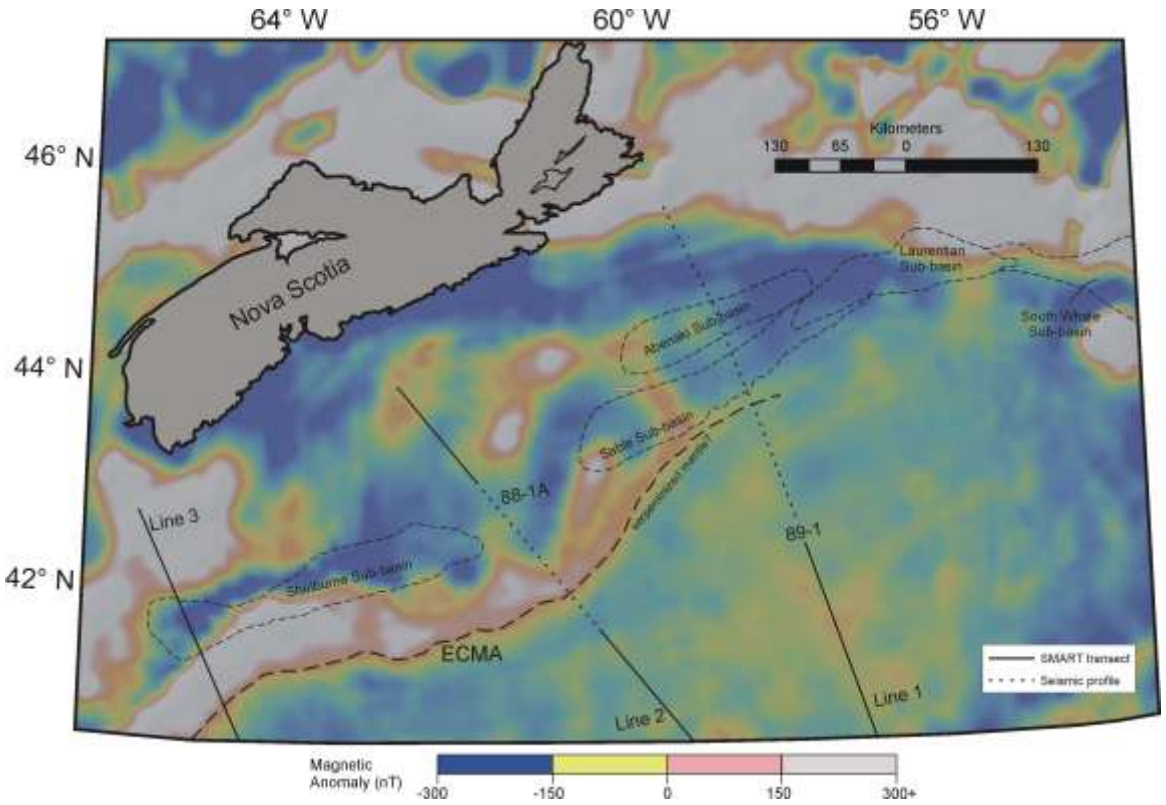

the early seafloor spreading processes is considered the origin of this feature.

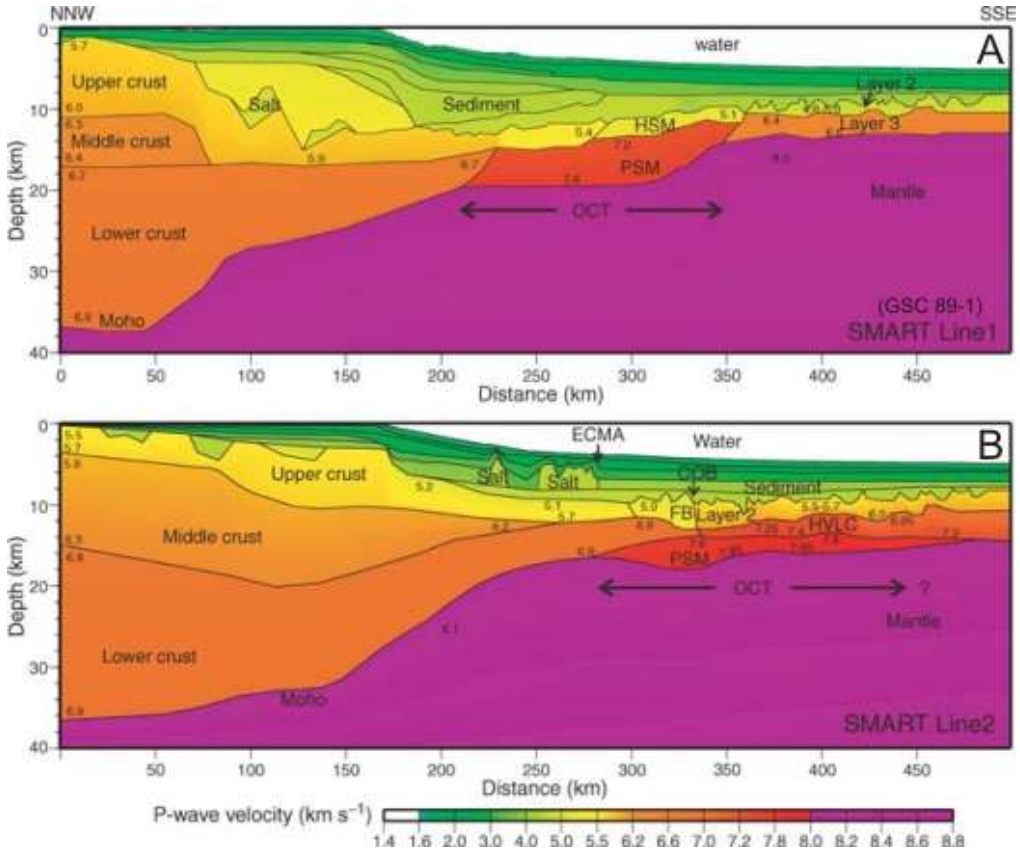

Figure 3.4. Comparison of velocity models along (A) Line 1 (coincident with GSC Line 89-1, Funck *et al.* 2004) and (B) Line 2 illustrating crustal structure of the central and eastern Scotian margin including the ocean-continent crust transition zone (OCT). Abbreviation: HSM, exhumed and highly serpentinized upper mantle; COB: continent–ocean boundary; ECMA: East Coast Magnetic Anomaly; FB: faulted blocks; HVLC: high-velocity lower crustal layer; PSM: partially serpentinized mantle. Line 3 (Figure 3.3) has not been analyzed to date.

The Early Scotian Basin is thought to consist of a northeast-trending complex of fault bounded rift basins, located southeast of the hinge zone (Figures 3.2 and 3.5). These rifted basement structures most likely initiated as a result of sinstral transtensional forces within a broad zone to the south of the Acadian suture (MacLean and Wade, 1992). Therefore the bounding extensional faults comprising the hinge zone of the Mesozoic

Scotian Basin is most likely reactivated Paleozoic faults (Ratcliffe *et al.*, 1986).

Rifted basement blocks are observed seaward of the Canso Ridge and LaHave Platform, consisting of Meguma basement. Along the stable flank, basement is generally less than 4 km deep and slightly tilted seaward with rifted grabens and half-graben blocks, bounded by northeast and east trending normal faults, located southeast of the hinge zone. Graben sizes vary from small (> 25 km) and shallow (> 5 km) to large, containing significant syn-rift (pre-breakup) red beds and associated salt. Along the northeast Scotian margin, below the Burin Platform and Scatarie Ridge (Figure 3.5), the Avalon Terrane acts as basement. In contrast to the Meguma Terrane, Avalon basement seems not to have been affected by early Mesozoic rifting, with very little deformation observed except along the Cobequid/Chedabucto fault (MacLean and Wade, 1992). Within the southern extension of the Syndney Basin (northeast of Cape Breton Island), Avalon Terrane basement is observed to be covered by Carboniferous and subsequently thin (1 – 2 km) Late Mesozoic and Cenozoic sediments. This relationship on the northern flank of the Scotian Basin confirms that Avalon basement was stable and left in tact during Meguma rifting allowing first undisturbed Carboniferous sedimentation and then later Mesozoic deposition (MacLean and Wade, 1992).

The Mohican and Naskapi Grabens are both southwest-plunging structural complexes, located within the LaHave Platform (Figure 3.5). The south boundaries of these structures are sub-parallel down-to-the-north dipping faults trending northeast-southwest. Sediment fill of the Mohican Graben based on well data and seismic control is comprised of ~ 2km

thick Jurassic southward dipping strata, partially capped by Early Jurassic basalt flows (MacLean and Wade, 1992).

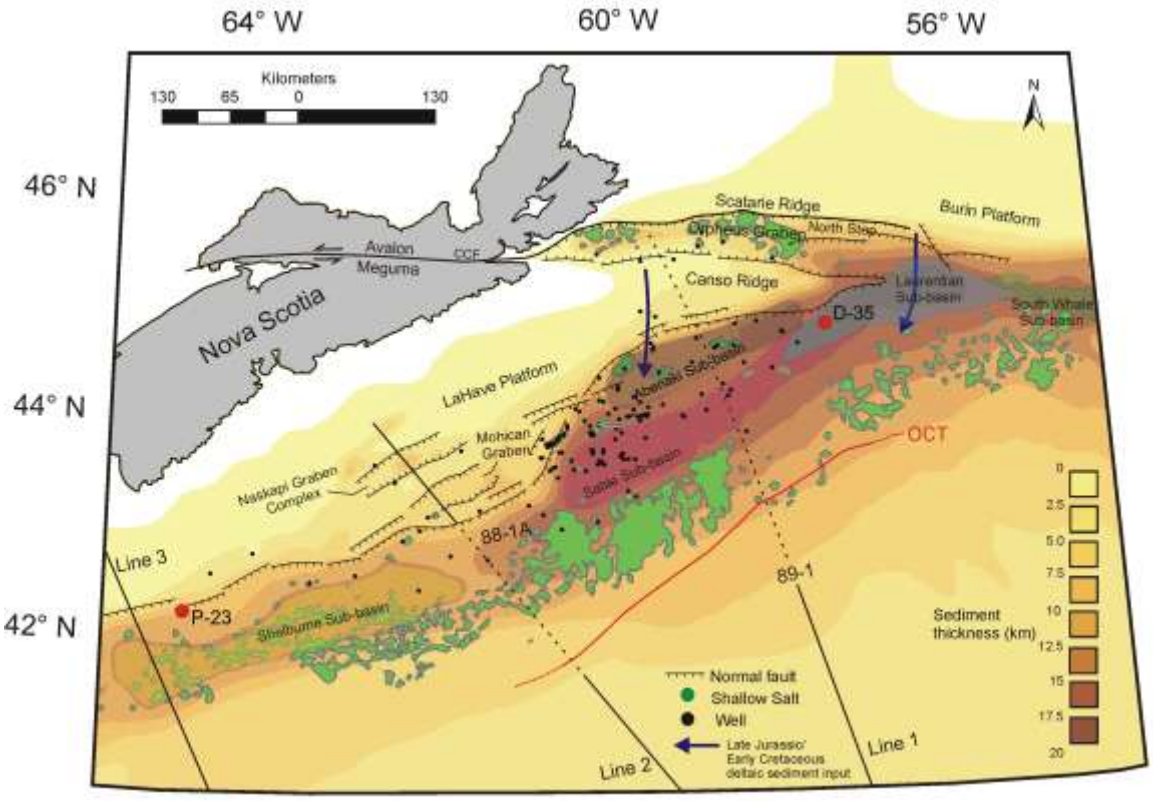

Figure 3.5. Structure of the regional Early Jurassic (post-breakup) basement hinge zone of the Scotian Margin, offshore Nova Scotia with sediment thickness shown as colour background. Sub-basins of the Scotian Basin are shown using colour overlay. Salt diapirs, mainly of the Slope Diapiric Province are indicated by green. SMART (Scotian MARgin Transects) seismic refraction seismic Lines (1 - 3) and GSC seismic reflection profiles (89-1 and 88-1) are labelled. The approximate landward extent of the oceanic-continent crust transition zone (OCT) bassed on velocity modelling (Funck et al., 2004; Wu et al., 2006) is labelled in red (Figure 3.4). Paleo-deltaic Late Jurassic/Early Cretaceous sources and approximate sedimentation directions are labelled. CCF = Cobequid-Chedabucto Fault. Wells mentioned in text are indicated by red.

The Orpheus Graben acts mostly as a half graben, with major basement throw along the northern boundary. This structure is located on the eastern Scotian Basin between the Canso and Scatarie Ridges, containing very thick syn-rift sedimentary fill (Figure 3.5). This structure is an important part of the eastern Scotian Basin as it forms the

northwestern interconnected extension of the Laurentian Sub-basin. Its northern flank is the Chedabucto fault zone, which was reactivated in the early Mesozoic with down-to-the-south normal fault movement, similar to the development of the Fundy Basin. The southern flank of the Orpheus Graben along the Canso Ridge experienced only minor fault reactivation (MacLean and Wade, 1992).

The northern portion of the Orpheus Graben is occupied by a shallow half graben called the North Step (Figure 3.5), extending east of the Laurentian Channel and bounded to the north by the offshore extension of the Chedabucto Fault Zone. The main segment of the Orpheus Graben is much larger than the North Step, and plunges east-southeast into the Laurentian Sub-basin through normal faulting, south of the Canso Ridge. Where the Orpheus Graben is present on the margin, the regional hinge zone is located on the southern flank of the North Step where basement is dropped down to the main graben. To the east of the Laurentian Sub-basin a east-west trending down-to-the-south fault acts as the hinge zone within Avalon basement. Close to the easterly edge of the Laurentian Channel the connection between these hinge faults is inferred to represent the suturing of Meguma and Avalon basement terranes.

3.1.3 Syn and Post-rift stage

Stratigraphic and regional data indicate that deposition within the Scotian Basin began in the Middle Triassic. With the possible exception of the Jeanne d'Arc Basin of the eastern Grand Banks, this is the earliest of any basin on the continental margin of Eastern

Canada. The early Scotian Basin is thought to consist of a northeast-trending complex of small fault bounded rift basins that later became the major locus of sedimentation (Orpheus and Mohican Graben, Shelburne, Sable, Abenaki, Laurentian, and South Whale Sub-basins, Figures 3.1, 3.2, and 3.5) Depocenters were initially floored with Late Triassic syn-rift continental red beds followed by halite rich evaporites. The location and distribution of salt within the sub-basins of the Scotian Basin demonstrates that these grabens and half grabens were the major centers of early deposition. Syn-rift sedimentation continued until the Early Jurassic marked by a breakup unconformity. Along the LaHave Platform and Canso Ridge and proximal Scotian Basin this unconformity is denoted by an easily mappable strong seismic marker horizon that separates areally restricted somewhat deformed Late Triassic-Early Jurassic strata (syn-rift) from relatively undeformed Early Jurassic (post-rift) strata (Wade and MacLean 1990). Within sub-basins of the Scotian Margin, due to extensive salt mobilization, the break-up unconformity is mostly unrecognizable; however, it is taken to occur at the top of salt.

Lens shaped prograding clastic packages comprised of mostly delta complexes constitute the majority of sedimentation from the Early Jurassic throughout the Cretaceous in the Scotian Basin (Figure 3.6). By the end of the Early Jurassic the edge of the rift zone, no longer under extension, began to cool and subside along with early rifted basins forming broad depocenters, incorporating the sub-basins of the Scotian Basin. At this time the major depositional systems consisted of river systems bringing sand and clay/silt from highland areas to the coast. Early sedimentation filled accommodation space within the

young Scotian Basin with thickest accumulations resulting from the development of delta systems forming at the mouths of drainage systems. Paleo-river interpretations and mapping of terrigineous sand dispersal patterns and envelopes suggests that by the Late Jurassic the paleo-St. Lawrence river and Sable delta were fully developed; comprising the major deltaic depositional systems of the Scotian margin (Figure 3.7A) (East Coast Basin Atlas Series, 1991). Paleo-sedimentation patterns for these systems imply that large amounts of sand were deposited in a south – southwest trend. Also, by this time reefs developed parallel to the paleo-shoreline along the warm waters of the shelf within carbonate banks (Abenaki Formation).

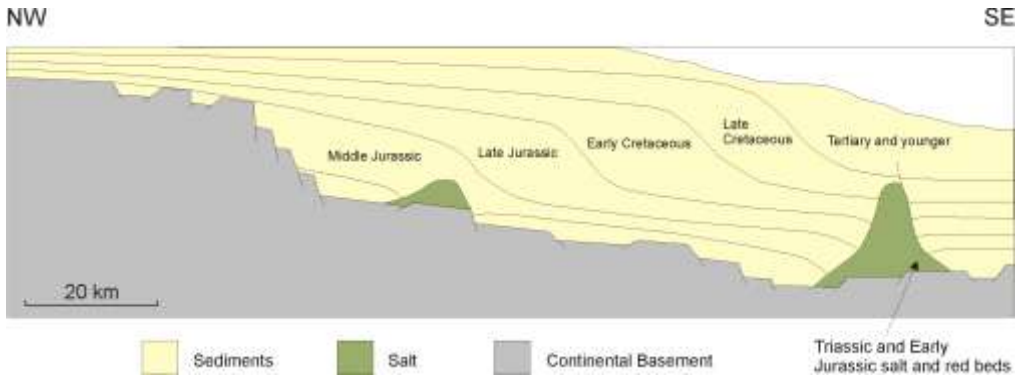

Figure 3.6. Generalized regional schematic cross-section across the Scotian Shelf (LaHave Platform) and Slope (located near Sable Island) illustrating location and geometry of prograding depositional units (modified from Wade and MacLean, 1990).

By the Early Cretaceous the Sable delta alone is the main deltaic system of the Scotian margin (Figure 3.7B) as sedimentation from the Laurentain Delta has slowed. As sea level rose sediments deposited offshore became finer, mostly silt and mud. Distributary channels branched out to the south covering a large portion of the north central margin while still maintaining an overall southwest sediment transportation direction. The Tertiary is marked by the fall of sea level and the deposition of coarser material offshore

as a result of erosion and incursion of land by channels and river systems, depositing sediments offshore on a broad continental shelf (Figure 3.7C).

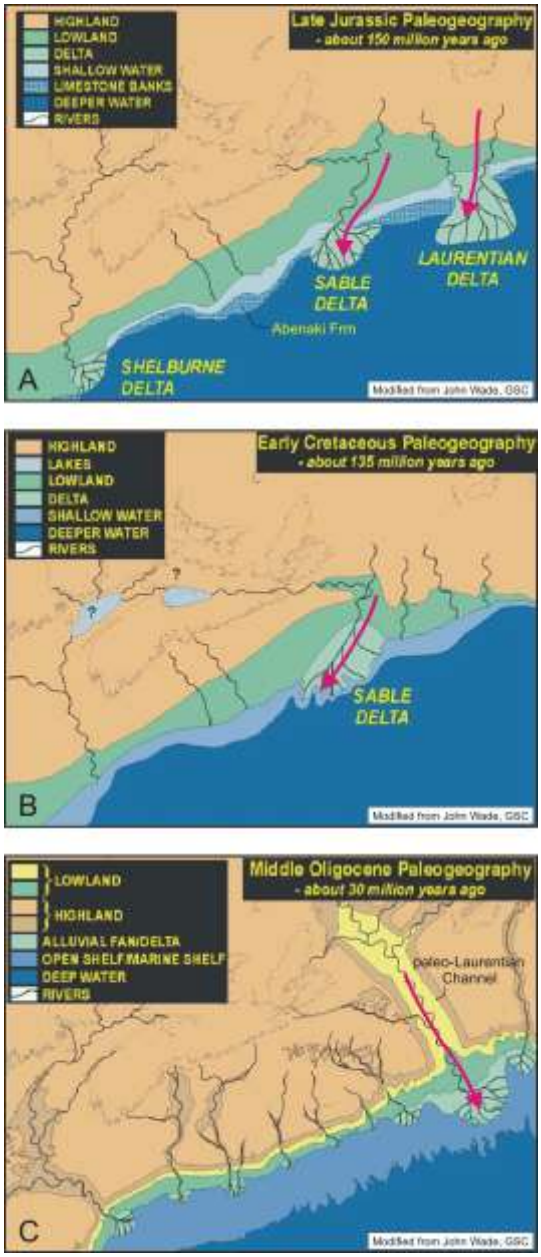

Figure 3.7. Paleogeography and paleo-delta sediment transport directions (pink arrows) along the Scotian margin for the Late Jurassic (A), Early Cretaceous (B), Tertiary (C). (Modified after John Wade, GSC).

Overall the thickest sediment accumulations are observed in the outer shelf to upper slope areas of the margin (Wade and MacLean 1990). The Slope Diapiric Province of the

Scotian Margin is defined as a zone of diapiric structures observed in a southwest-northeast trend in the deep-water slope (Figure 3.1) (see Chapter 3.3). Originally thought of as the Sedimentary Wedge Province, seismic data now clearly illustrate that these structures are salt related diapirs. Today the thickness of original deposited salt and present distribution of mobilized salt is not known precisely.

3.2 Tectono-stratigraphy of the eastern Scotian margin

3.2.1 Basement

The Scotian basin formed on top of a suite of Paleozoic terranes composed of metamorphic and igneous rocks assumed to be offshore extensions of analogous rocks found onshore Nova Scotia and Newfoundland and Labrador (MacLean and Wade, 1992). Basement rocks of southern and central Nova Scotia and offshore equivalents are low-grade metasedimentary strata of the Cambro-Ordivician Meguma Terrane. The northern Nova Scotia and southern Newfoundland basement consists of very thick late Precambrian and Cambrian metasedimentary and igneous rocks belonging to the Avalon Terrane. The Cobequid/Chedabucto Fault Zone and its offshore extension, along the northern boundary of the Orpheus Graben (Figure 3.5), act as a suture zone between these two terranes recording accretion during the Acadian Orogeny (Devonian) accompanied by the emplacement of a series of “suturing” granitic batholiths (MacLean and Wade, 1992; Williams and Hatcher, 1983; Keppie, 1989).

3.2.2 Syn-rift

The oldest syn-rift sediments of the Scotian Basin are thick sequences of red sandstones, siltstones and shales of the Eurydice Formation (Figure 3.8). Stratigraphic and regional data indicate that deposition within the Scotian Basin began in the Middle Triassic. At this time, early rift basins were floored with thick Eurydice continental redbeds. Seismic data indicate a total thickness of more than 3km along the northern flank of the Orpheus Graben (MacLean and Wade, 1990). Early grabens continued to be filled with coeval Eurydice sediments and Argo evaporites to the Early Jurassic. The Argo Formation is overlying and interfingering with the Eurydice Formation along basin margins in many of the deeper grabens. The Argo formation consists primarily of a series of massive salt beds that are coarsely crystalline, separated by minor red shale zones and anomalously low amounts of anhydrite. Indicative of many evaporite deposits, these shale intervals are interpreted to mark periods of little or no salt deposition (Wade, 1981). Deposition of syn-rift sediments continued until the Early Jurassic where a breakup unconformity along the LaHave Platform and Canso Ridge separates them from overlying strata.

3.2.3 Post-rift succession

Overlying the breakup unconformity is the locally developed dolomitic Iroquois Formation (Early Jurassic) and the thick clastic-rich Mohican Formation (Early – Middle Jurassic) (Figure 3.8). The Bonnet P-23 well on the Lahave Platform of the Scotian Shelf contains the thickest section of the Iroquois Formation at 800 m. The estimated total

thickness estimated from seismic data though is 1600 m, due to the bottom of the formation not being drilled. This dolostone is considered a facies unit coeval with the basal Mohican Formation and was deposited along the outer edge of the LaHave Platform where carbonate deposition had been favorable. To the east, in the transitional area where the hinge is mapped to significantly diverge northeasterly, environmental conditions for carbonate sedimentation were not favorable. Instead, a thick clastic wedge of Mohican Formation prograded over underlying red beds and evaporites.

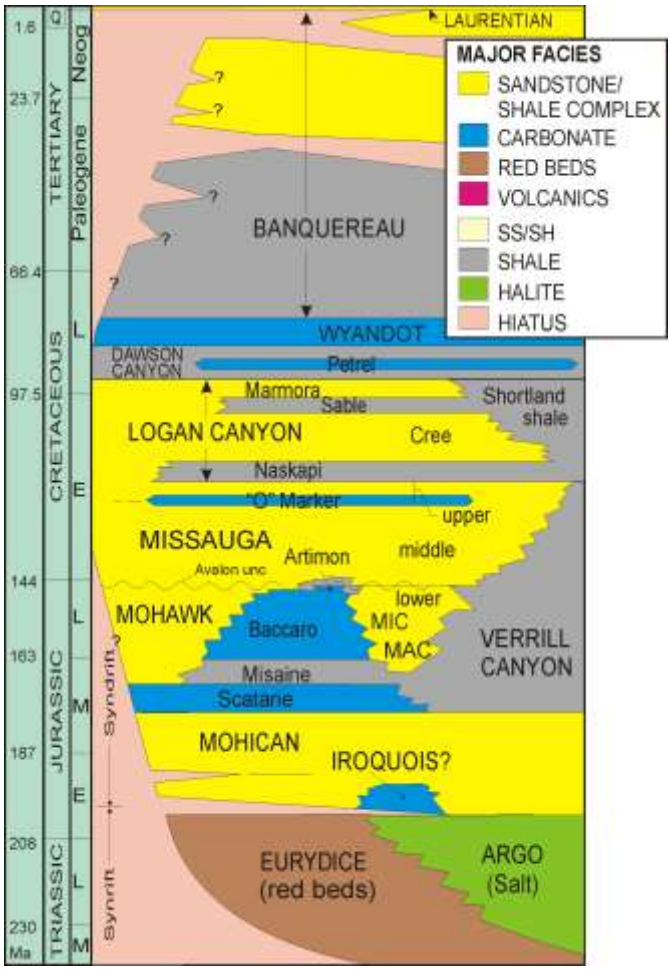

Figure 3.8. Generalized stratigrahpy for the Nova Scotia margin (modified from Wade and MacLean, 1990).

Early Jurassic sedimentation along the Scotian margin consists of mainly continental clastics sourced from continental break-up, interfingering with shallow marine dolomite carbonate facies and then grading southeast across the regional hinge zone into thick marine clastics (Wade and MacLean, 1990) (Figure 3.8). The Early to early Middle Jurassic dolomitic siltstones, fine grained sandstones and interbedded shales of the Mohican Formation overlay the Iroquois Formation and comprise a molasse sequence that filled early rift grabens, overlapping basement highs, as it was deposited into actively subsiding sub-basins seaward of the hinge zone along the Scotian Margin. The Mohican Formation varies greatly in thickness beneath the shelf and across the hinge zone. In the Abenaki Sub-basin (Figure 3.1) the formation is more than 4000 m thick while thinning to the northwest at the hinge zone; either eroded by the Jurassic-Cretaceous Avalon uplift or pinching out against the Avalon unconformity (Wade and MacLean 1990).

The Middle-Late Jurassic Abenaki Formation (Figure 3.1) forms a very distinctive lithologic complex of predominantly reef carbonates that overlies the Mohican Formation (Figure 3.8). It is mainly developed along the hinge zone between the Lahave Platform and Sable Basin. To the northeast of this it appears to interfinger with clastic and carbonate facies of the Mic Mac Formation until it pinches out. Only the lowermost Scatarie Member of the Abenaki Formation is laterally extensive and occupies parts of the eastern Scotian margin (Figure 3.8). This oolitic transgressive limestone forms a seaward thickening wedge (maximum thickness of 600 m) that rapidly shales out south of the Canso Ridge (Wade and MacLean 1990). Due to its lithology, the Scatarie Member

acts as an excellent seismic marker and is observed to overlie prograding clastics in the Mohican Formation.

From the late Middle to Late Jurassic, along the eastern Scotian margin, the thick dominantly clastic Mic Mac Formation was deposited in an alluvial plain setting. Time-equivalents to this formation are the Abenaki, Mohawk and Verrill Canyon Formations (Figure 3.8). The Mohawk Formation was deposited on the western Scotian Shelf and consists of continent-derived sandstones. The Verrill Canyon Formation is merely the basinal fine-grained facies (siltstone, shale) of the Mic Mac, Abenaki and Mississauga Formations. Deposition of the Verrill Canyon Formation continued post Mic Mac to the Early Cretaceous.

The interbedded sandstones, shales, and minor limestones of the Mic Mac Formation are interpreted to originate from a broad alluvial plain system including seaward strand plain or deltaic environments undergoing rapid subsidence with a transition into an outboard neritic facies. The Mic Mac Formation includes a series of thick clinoforms consisting of a shale-sandstone bottomset, sandstone-shale foreset, and a sandstone topset capped by progressively younger limestones (Wade and MacLean, 1990). Within the Scotian Basin the MicMac Formation is approximately 4000 – 5000 m thick with a maximum thickness of 6000 m within the Laurentian Sub-basin. The Avalon unconformity marks the approximate upper limit of the Mic Mac Formation and forms a boundary between underlying deformed Jurassic sediments and evaporites and overlying relatively undeformed Cretaceous sediments.

An important feature of the eastern Scotian Basin is the Avalon unconformity. Uplift, deformation and erosion related to this Late Jurassic – Early Cretaceous event resulted from initial seafloor spreading between the Grand Banks and Western Europe. This event is recorded in the area of the Grand Banks south of Newfoundland and Labrador where evidence of extensive uplift, deformation and large-scale erosion of Jurassic sediments is documented by the Avalon unconformity, marking uplift of the rift shoulder and subsequent erosion and sediment re-working during the Early Cretaceous. Reworked sediments were either deposited to the southwest into the Scotian Basin or east of the Avalon uplift into basins beneath the Grand Banks (e.g. Jeanne d'Arc Basin). Within the Scotian Basin the Avalon Unconformity is observed along the inner Canso Ridge, the Orpheus Graben, Burin Platform, and the western flank of the Laurentian Sub-basin; although having slightly less impact than its easterly counterpart (Wade and MacLean, 1990).

The Early Cretaceous Mississauga Formation is overlying the Mic Mac Formation and associated Avalon Unconformity (Figure 3.8) and contains a thick sequence of sandstones deposited in delta plain to inner neritic environments in an overall regressive prograding succession. Thick sandstones belong to "up dip" alluvial plain facies, whereas a succession of thinner sandstone and interbedded shales constitute "down dip" lower delta plain to inner neritic facies. The fluvial-deltaic environment of this formation causes significant thickness variations along the Scotian Margin. The "up dip" facies along the LaHave and Burin Platforms as well as the Canso Ridge is less than 500 m thick, whereas

in the depocenter of the Sable Sub-basin the formation is more than 2000 m thick. The Mic Mac and Mississauga Formations are conformable throughout the majority of the basin, except in proximal areas of the LaHave Platform. Here, the Early Cretaceous regression associated with the Avalon unconformity separates the two formations. Well data indicate that in some locations the Mississauga Formation overlies the Verril Canyon Formation, confirming that the Mississauga is a seaward thickening prograding wedge as observed in seismic data.

The O Marker is a laterally extensive minor transgressive sequence deposited in an overall regionally regressive episode (Mississauga) (Figure 3.8). The unit consists of a series of oolitic limestones and chalks in the upper succession of the Mississauga Formation (Hauterivian to Barremian) and is observable throughout much of the Scotian Shelf. Therefore the O marker makes a distinct mappable horizon that gently dips southeast on the shelf. Seaward beyond the hinge zone the horizon is more irregular as a result of salt mobilization and syndepositional extensional deformation. In some locations along the LaHave Platform the O Maker is observed to pinch out westerly in the deep water and downlap on Jurassic sediments indicating local sediment starvation during its deposition (Wade and MacLean, 1990).

The Early to early-Late Cretaceous Logan Canyon Formation overlies the Mississauga Formation and is composed of a series of thick shale and sandstone-shale units (Figure 3.8). These units are interpreted to belong to a broad coastal plain and shallow shelf environment with sand and shale deposited during periods of variable clastic sedimentary

input (Wade and MacLean 1990). Across the hinge zone, the Logan Canyon formation thickens seaward as a result of salt withdrawal and progradation beyond the Early Cretaceous shelf edge, with a contemporary increase in shale content. Many of the shale-rich units of the Logan Canyon Formation, such as the basal unit, represent transgressive episodes and therefore depositional transitions from a proximal to distal facies.

The Late Cretaceous Dawson Canyon Formation consists of mostly grey marine shale or mudstone units with less frequent thin beds of sandstone, siltstone and limestone (Wade and MacLean, 1990) (Figure 3.8). The thickness of this transgressive succession varies from more than 500 m in the South Whale Sub-basin to under 100 m in the outer portion of the Sable Sub-basin. Within the Dawson Canyon Formation the Petrel Member limestone regionally produces a strong reflector that can be mapped across most of the Scotian Shelf. The Petrel Member thickens regionally from southwest to northeast. The northern limit of the Petrel Member and therefore presumably for the Dawson Canyon Formation as well occurs where it crops out at seafloor. On the eastern Scotian Shelf Tertiary channels have eroded the Dawson Canyon Formation. To the south, the depositional limit occurs along the paleo shelf edge where the marker is truncated by either erosion associated with Wyandot downlap or large-scale Tertiary erosional events (Wade and MacLean, 1990).

The Late Cretaceous Wyandot Formation overlies the Dawson Canyon Formation and is perhaps the most seismically recognizable lithologic unit along the shelf (Figure 3.8). This distinction as a strong seismic reflector is due to a lithologic composition of chalks, chalky mudstones, marls and minor limestones. In the eastern shelf, chalks and marls

developed in the bottom set position of prograding sequences marking regression during the Late Cretaceous. These chalks grade landwards into calcareous shales and eventually mudstones. Similar to the Dawson Canyon Formation, Tertiary channels and erosion along the shelf-edge cut into the Wyandot Formation, restricting it to the shelf position of most sub-basins. The total thickness of the Wyandot Formation increases easterly along the shelf from an average of 50 m on the LaHave Platform to nearly 400m at the Dauntless D-35 well. Sedimentation rates during the deposition of the Wyandot Formation were some of the lowest throughout the Scotian Basin. Biostratigraphical data in several wells along the Scotian Basin indicate a hiatus occurred at the top of the Wyandot Formation (Doeven, 1983).

The younger post-Wyandot sediments of the Scotian Margin are incorporated into the latest Cretaceous to Neogene Banquereau Formation (Figure 3.8). The lithology of this formation is predominantly mudstone that grades upwards into sandstone and conglomerate, resulting from the latest Cretaceous and Paleogene transgression and subsequent Neogene regression. The Banquereau Formation ranges in thickness from zero along the middle part of the shelf to over 1500 m within the Sable Sub-basin.

3.3 Salt Provinces of the Scotian Margin

The thick post-salt sediment cover and the complexity of modern salt structures in deepwater locations of the Scotian Margin make seismic imaging and interpretations difficult. Areas within basins having very thick sediment fill, salt expulsion structures,

and deep-reaching listric faults are considered to originally have had substantial initial salt thickness (Wade and MacLean 1990).

The regional 2D seismic survey of the Scotian Slope (TGS-Nopec, Canada-Nova Scotia Offshore Petroleum Board programs NS24-G026-001P and NS24-G065-001P) along with an improved understanding of salt tectonic processes has allowed a regional study of the Slope Diapiric Province of the Scotian Margin (Shimeld 2004). From this study a complex 3D morphology of salt structures was observed along the Nova Scotian margin leading to the definition of five distinct salt subprovinces based on observed salt and sediment deformation styles (Shimeld, 2004; Figure 3.1). Characteristic styles of salt structures of each subprovince appear to be a direct result of differing sedimentation patterns and basement (salt basin) morphology. The salt deformation styles range from passive diapirs to extensive allochthonous bodies and canopy systems that are all sourced from initially deposited syn-rift salt within the evaporite basin (Shimeld, 2004). The regional coverage of the 34,000 km survey and the 8 km maximum spacing of both strike and dip lines allows for a constrained interpretation of the area. The Eastern Scotian Margin, the focus of this thesis, is comprised of subprovinces IV and V (Figure 3.1).

Subprovince I

Subprovince **I**, located on the western edge of the Scotian margin (Figure 3.1), is characterized by autochthonous salt walls and diapirs that record passive growth during the Jurassic and Cretaceous. No major salt movement was recorded during the Tertiary

most likely due to source depletion as observed from strata concordant with diapir crests above the Upper Cretaceous Wyandot Formation (Figure 3.8). Outboard of the initial salt basin, allochthonous salt in the form of a 15- 20 km wide salt canopy system is observed to overlie Middle Jurassic and older sediments (Shimeld, 2004).

Subprovince II

Elongate salt walls approximately parallel to the Abenaki Formation carbonate bank edge characterize subprovince **II** (Figure 3.1), incorporating most of the Shelburne Sub-basin (Shimeld, 2004). A transitional boundary is observed between subprovince **I** & **II** with diapirism of **II** varying from vertical diapirs in the west to seaward verging and finally highly squeezed and possibly detached diapirs in the east.

Subprovince III

Subprovince **III**, located on the central margin and partially containing the Sable and Abenaki sub-basins, consists of allochthonous tongue canopies overlying Lower Cretaceous and older sediments. The predominantly allochthonous salt structures of Subprovince **III** contrast rooted autochthonous salt diapirs and walls of subprovinces **I** and **II**. To the east, coalescence of canopies and the overall structural maturity of salt features increase. Deformation on top of canopies is restricted to latest Cretaceous sediments in the form of extensional syn-kinematic structures such as turtles and expulsion grabens (Shimeld, 2004). With little evidence for feeders in this area the

seaward edge of canopies is interpreted to be up to 100 km seaward of the autochthonous basin edge. This indicates significant and efficient salt withdrawal and seaward translation in this area, most likely driven by Middle Jurassic through Early Cretaceous Sable delta.

Subprovince IV

Subprovince **IV** is located on the eastern margin and is comprised of the Sable and Abenaki sub-basins and the west margin of the Laurentian Sub-basin (Figure 3.1). A particular phenomenon within subprovince **IV** is the lack of salt diapirs or related salt structures. Also a seaward and westward thinning package of mostly landward dipping reflectors, interpreted as Late Jurassic and older is observed within this subprovince. These reflective units thin towards the top of the package, which is estimated to be 3.5 km thick. The base of this feature, referred to as the Banquereau Syn-kinematic Wedge (BSW), is observed above the stratigraphic position of the Argo salt and is suggested to act as a salt detachment surface. The seaward portion of the wedge base climbs up stratigraphic horizons as it truncates them, forming a ramp geometry (Shimeld, 2004) (Figure 3.9A). Although sparse, isolated diapirs are present below the modern middle and lower slope and form an arcuate seaward rim geometry. Upper Jurassic and overlying Cretaceous strata also show signs of contraction, e.g. thrusts and seaward verging open folds. These salt-cored thrusts and folds follow the rim pattern exhibited by salt diapirs and contraction is interpreted as being concentrated in the Late Cretaceous.

Ings and Shimeld (2006) interpret using publically available seismic data and finite numerical modeling that the BSW is a result of seaward extension and translation of Middle-Upper Jurassic sediments along a salt detachment surface. Rapid progradation of the Mic Mac Formation during the Late Jurassic may have mobilized allochthonous salt

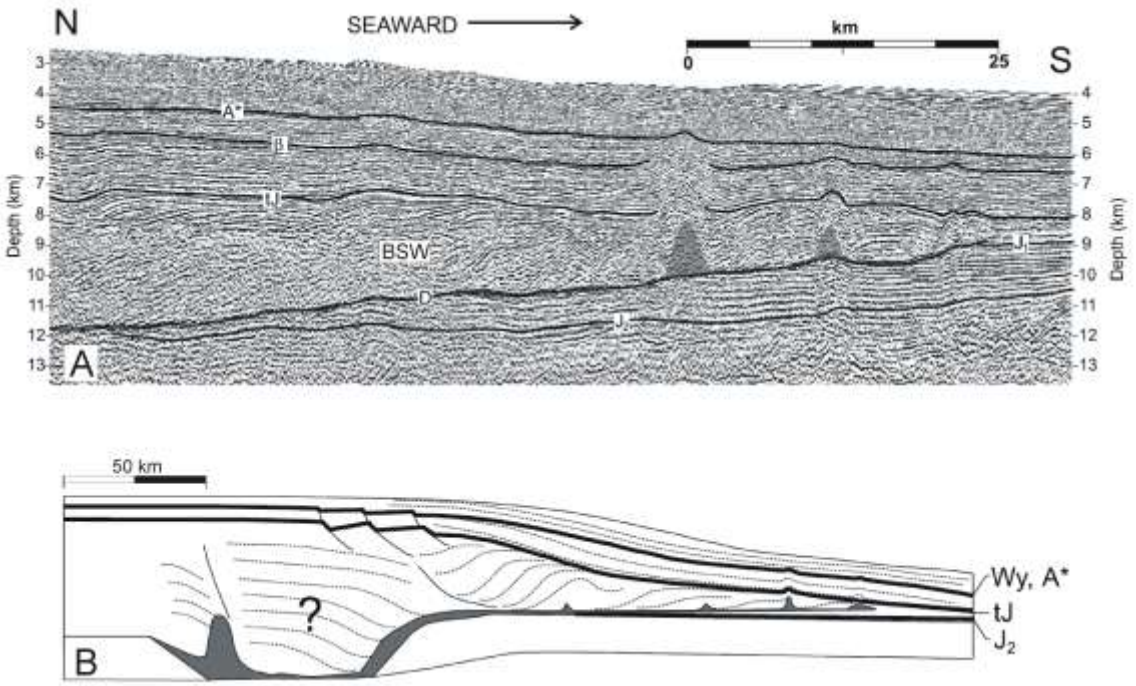

beyond the initial salt basin where, thermal subsidence tilted the margin seaward and created an efficient detachment system (Figure 3.9B).

Subprovince V

Subprovince **V** is located on the eastern most portion of the margin and mostly incorporates the Laurentian and South Whale sub-basins. Along the western portion of sub-province **V** the BSW is not easily visible and is interpreted to be obscured by a series of sutured allochthonous salt tongues sourced from deeper salt layers (Ings and Shimeld, 2006). Sub-province **V** is the most complex of the salt sub-provinces due to the variety of

salt structures; allochthonous salt tongues and thick post-Jurassic sedimentary accumulation (Shimeld 2004). Generally the overburden above diapirs in sub-province **V** is thinner than other regions of the Scotian Margin (< 100 m to the modern seafloor in some instances). Contraction similar to sub-province **IV** is focused in the uppermost Cretaceous to Neogene with extension focused in the underlying Cretaceous (Figure 3.10), leading to the assumption of a thick source layer for sub-province V. Contractional features are also seen at the seaward limit of the salt system. Questions still remain regarding whether this diapirism is from an initial primary salt basin filled after syn-rift sediments or allochthonous salt mobilized from the nearby Laurentian Sub-basin through a large amount of Jurassic sedimentation.

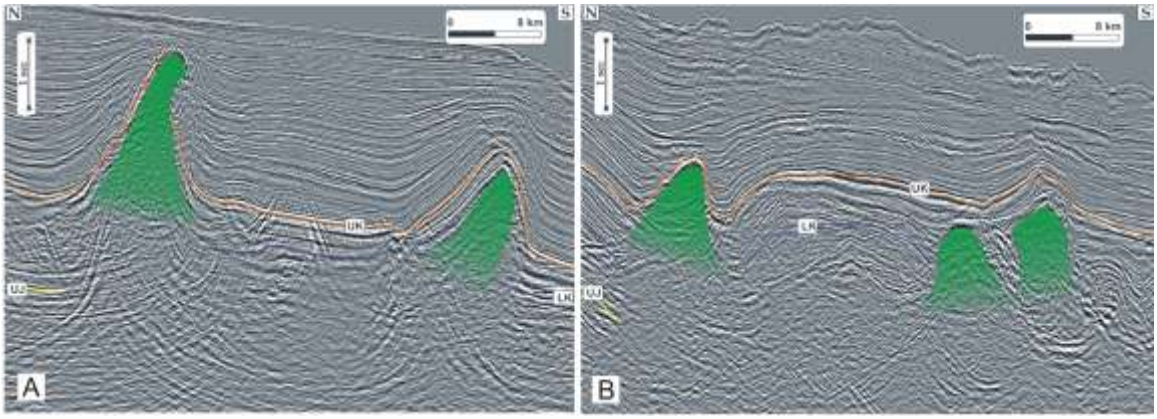

Figure 3.10. Characteristic salt structures along the slope of salt subprovince V. A) Reactivated asymmetric squeezed diapers with crestal faulting within subprovince V of the slope diapiric province, formed as a result of distal compression during the uppermost Cretaceous to Neogene. B) Highly deformed Cretaceous units of subprovince V. Note the downbuilding of reflectors on the flanks of allochthonous salt forming a turtle-like structure in the middle of the image. Green indicates interpreted salt. UK=Upper Cretaceous, LK=Lower Cretaceous, UJ=Upper Jurassic. (Modified from Shimeld, 2004).

Chapter 4: Seismic Data Interpretation

The following section discusses the seismic data base, seismic interpretation workflow, seismic stratigraphy, basement architecture and salt tectonic characteristics of the eastern Scotian margin mainly based on seismic interpretation of GXT line 2000. Correlations of GXT strike lines 5420 and 5100 and GSC Lithoprobe line 89-1 have been made to characterize basement, depocenter and salt structure variations along the margin. These major features of seismic profiles will be used to constrain analogue experiments of the eastern Scotian margin (see Chapter 5).

4.1 Seismic data base

The primary source of regional seismic interpretation of the eastern Scotian margin is the basin-scale 2D GX Technology Nova Span seismic survey (Figure 4.1).that includes 3400 km of recently acquired depth-migrated reflexion seismic profiles with very long offset (9000 m). The design of the GXT program paied particular attention to improve imaging of deep source rock, reservoir, sub-salt, and basement structures to better understand the regional tectono-stratigraphic evolution of the Scotian margin.

The following features make the GXT seismic survey the ideal data base for the in-depth interpretation of salt structures, rift architecture, and depositional history of the western Laurentian Sub-basin in the regional context of the eastern Scotian Margin:,

1. High quality of the seismic data

2. Advanced processing techniques (e.g., free surface multiple elimination and Kirchhoff pre-stack depth migration) enabled
3. Length of seismic lines (280 km Line 2000)
4. Depth of seismic imaging (~ 20 km)

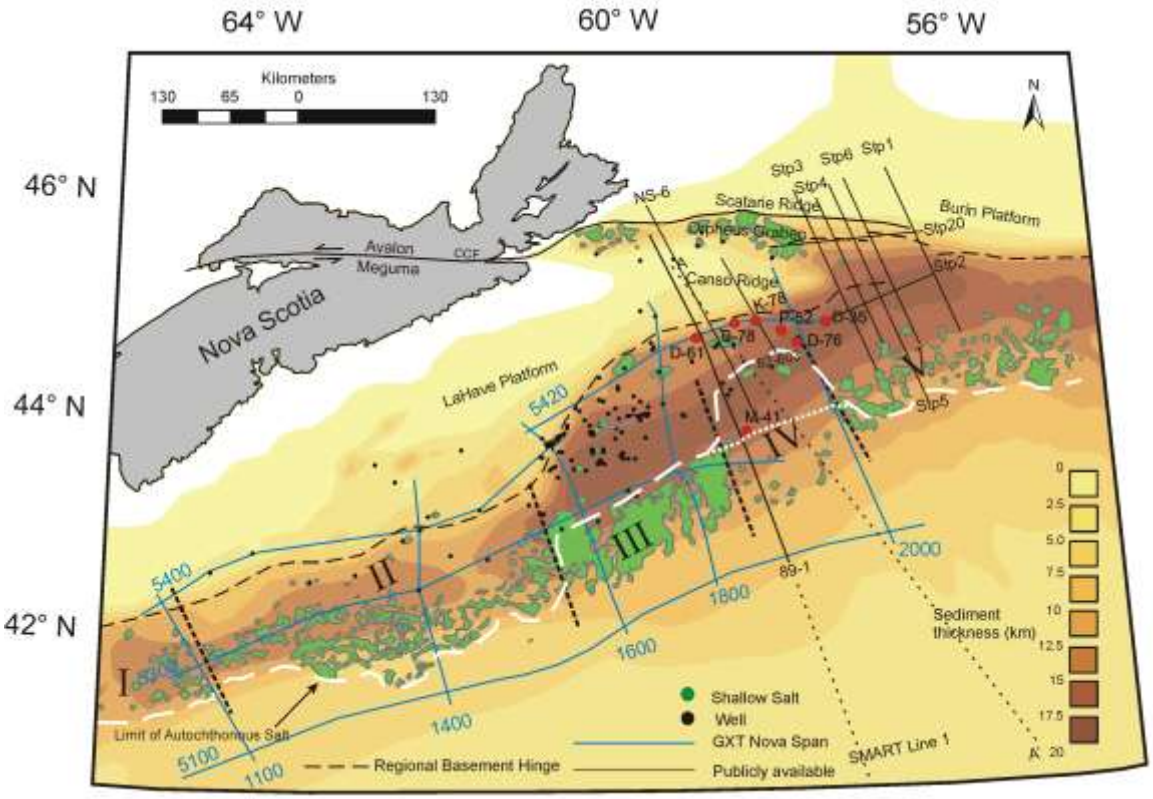

Figure 4.1. Location of GXT NovaSpan reflection seismic survey indicated by blue lines with profile 2000 the focus of this regional study. Other publicly available seismic profiles used in regional interpretation have been outlined in black and labelled (further information can be found in table 4.1), of particular importance is profile 89-1, located nearly parallel to and west of 2000. Background; continental shelf and slope of the Scotian Margin, offshore Nova Scotia with sediment thickness shown as colour background. Shallow salt structures, mainly of the Slope Diapiric Province are indicated by green. Red dots indicate well locations used for lithostratigraphic picks and correlations from the shelf to the slope (Hesper P-52, Sachem D-76, West Esperanto B-78, Tuscarora D-61, Tantallon M-41, Figure 4.2). Fine dashed white line near well M-41 indicates new interpretation of the limit of autochthonous salt within sup-province IV. Wide-angle refraction SMART Line 1 (coincident with MCS reflection line 89-1) and A – A' indicate the location of crustal profiles derived from velocity and gravity models (Figure 4.5).

The position of lines within the survey were selected on the basis of proximity to well locations and the sampling all of the salt subprovinces and associated deep, salt and

structural characteristics. The specific rationale for line 2000 in the western Laurentian Sub-basin was the imaging of:

1. Very deep basin fill (~17 km) and underlying rift structures below the modern shelf
2. Extensive seaward salt detachment and salt nappe system, beneath the slope of the eastern Scotian margin.

To analyse the basin architecture, depositional history, and salt tectonic styles of the eastern Scotian margin in this thesis, GXT line 2000, located on the eastern edge of Subprovince IV along with strike lines 5420 and 5100 on the shelf and abyssal plain respectively (Figure. 4.1) were interpreted.

However, the spacing of Nova Span dip lines is sparse (> 100 km). Additional publicly available industry and academic seismic reflection data (digital SEGY data and scanned paper copies) were included to study the structural and stratigraphic variation along the margin. The data includes a complete 3720km 2D seismic survey (Geological Survey of Canada, 1984-1987) within the St. Pierre Moratorium Block, of the Orpheus Graben and the Laurentian Sub-basin. Although the public seismic data are time-migrated, they enable the regional correlations of basement, depositional and salt tectonic features observed in line 2000 and along the eastern Nova Scotia margin. All seismic data used for this study are summarized in Table 4.1.

Line	Area	Project	Company	Year
82-603	Scotian shelf	8624-B011-003E	Bow Valley	1982
NS-6	Scotian shelf	8624-C055-003E	Canterra Energy	1982
STP-2	Scotian Shelf/Slope/St. Pierre Bank	St. Pierre Survey	Western Geophysical	1983
STP-20	Scotian Shelf/Slope/St. Pierre Bank	St. Pierre Survey	Western Geophysical	1983
STP-21	Scotian Shelf/Slope/St. Pierre Bank	St. Pierre Survey	Western Geophysical	1983
STP-3	Scotian Shelf/Slope/St. Pierre Bank	St. Pierre Survey	Western Geophysical	1983
STP-4	Scotian Shelf/Slope/St. Pierre Bank	St. Pierre Survey	Western Geophysical	1983
STP-5	Scotian Shelf/Slope/St. Pierre Bank	St. Pierre Survey	Western Geophysical	1983
STP-6	Scotian Shelf/Slope/St. Pierre Bank	St. Pierre Survey	Western Geophysical	1983
STP-7	Scotian Shelf/Slope/St. Pierre Bank	St. Pierre Survey	Western Geophysical	1983
STP-1	Scotian Shelf/Slope/St. Pierre Bank	St. Pierre Survey	Western Geophysical	1983
89-1	Scotian Shelf/Slope	LITHOPROBE	GSC (Atlantic)	1989

Table 4.1. Publicly available seismic reflection profiles used for interpretation and correlation of salt structures and major depositional phases of the eastern Scotian margin. Table indicates project numbers or names of surveys that profiles were a part of, the company responsible for shooting the surveys and the year of data acquisition.

4.2 Interpretation workflow

Along the eastern Scotian margin well control in the shelf is adequate and lithostratigraphic data from five nearby wells (Sachem D-76, Dauntless D-35, Esperanto K-78, West Esperanto B-78, and Hesper P-52) on the shelf allow the correlation of formation tops with seismic horizons picked in line 2000 and line 5420 (Figure 4.1). Well data were derived from the BASIN database of the GSC (Atlantic) (http://basin.gsca.nrcan.gc.ca/index_e.php). Stratigraphic picks for interpretations were based on availability of well data and were chosen to represent major depositional events in the Jurassic and Cretaceous (Figure 4.2). Nomenclature used for shelf lithostratigraphy was adopted from Wade and MacLean (1990) and the East Coast Basin Atlas Series: Seismic markers and stratigraphic picks in the Scotian Basin wells (MacLean and Wade, 1993). For the additional seismic reflection profiles various proximal wells in the shelf were used and lithostratigraphic picks were based on the correlation of published seismic markers given in time at well locations.

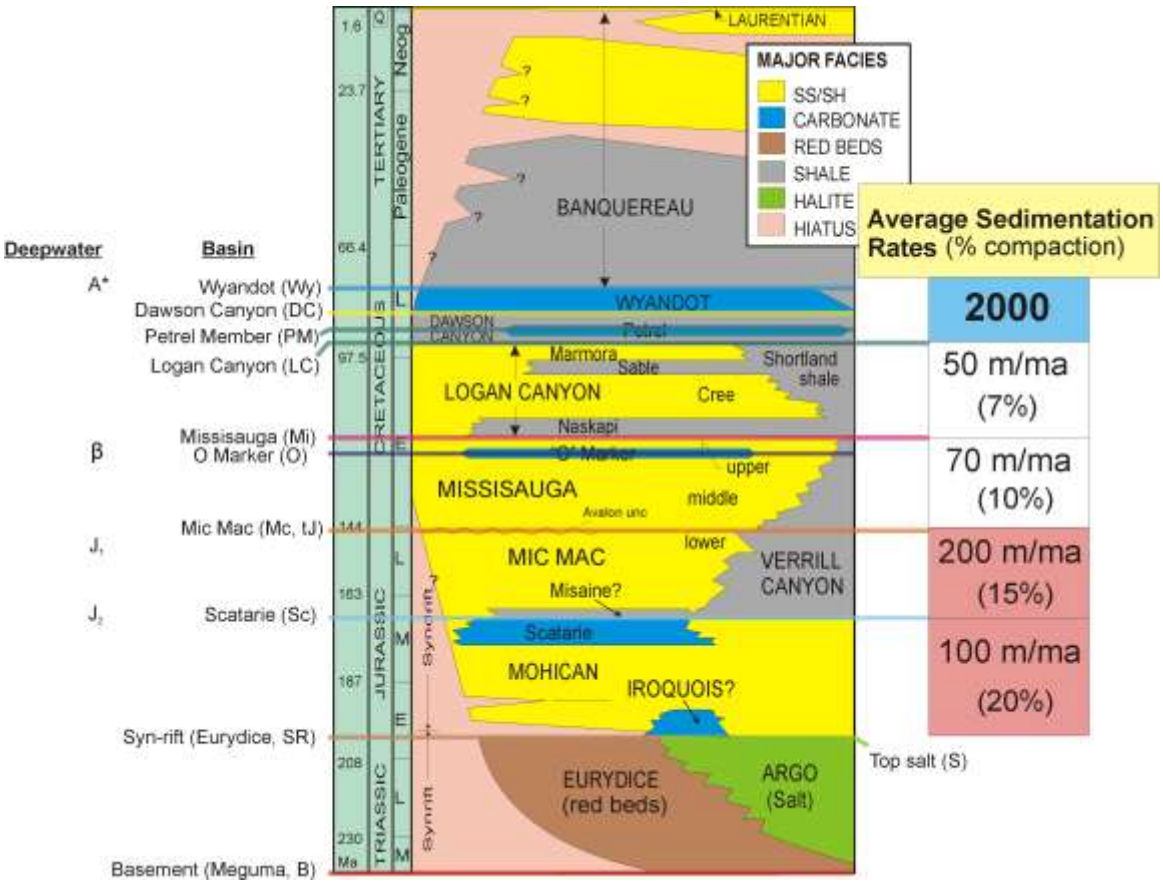

Figure 4.2. Generalized stratigraphy for the Nova Scotian margin (modified from Wade and MacLean, 1990). Stratigraphic seismic horizons (shelf and slope) used for interpretation and age constraint of profile 2000 are shown as coloured lines. Approximate sedimentation rates are shown (with estimated compaction percentages illustrated) for the eastern Scotian margin based on seismic interpretation of NovaSpan line 2000. Note that lithostratigraphic picks in time for the top Logan Canyon are not available for wells proximal to profile 89-1. Instead, the near stratigraphically equivalent Petrel Member horizon is used as the closest approximation from available well data.

However, well control in the deepwater slope is inadequate, with the nearest deep-water well being Tantallon M-41, some 90km west of line 2000 (Figure 4.1). As a consequence the accurate lithostratigraphic correlation in the slope and deep-water is dependant on:

1. Concepts of seismic stratigraphy
2. Correlation of seismic horizons and regional erosional events across the shelf (see Chapter 4.2.4)

3. Published seismic reflectors from slope into deep-water (Wade, 1978, Ewing and Rabinowitz, 1984, Swift, 1985, Ebinger and Tucholke, 1988).
4. Tectonostratigraphic concepts and salt tectonic models developed as part of this project

Interpretations of seismic horizons across the shelf break and slope are particularly difficult not only due to the lack of well constraint, but also due to facies changes from shelf to deepwater across the paleo-slope (see Chapter 3.2.3, Figure 3.8), strong dipping multiples, complex salt structures of the Slope Diapiric Province, deep erosive events of the Tertiary, and extensive faulting (Wade and MacLean, 1990).

4.3 Seismic Stratigraphy

For the stratigraphic correlation and further interpretation of the basin history and structural evolution of the basin fill in the shelf and slope, nine characteristic stratigraphic horizons (Figure 4.2) were picked using well data and seismically correlated. Due to the lack of well penetration, top basement (Megum), top syn-rift (Eurydice Formation), and Argo Salt stratigraphic horizons were determined through strictly observable seismic signature.

Basement

Along the eastern Scotian margin basement consists of the Meguma Terrane. Unlike exclusively crystalline basement, dominant Meguma slates often results in somewhat

coherent seismic reflections. Therefore basement cannot be solely determined on distinct boundaries between coherent stratified reflectors and incoherent non-reflective noise, indicative of crystalline basement.

Along the shelf and within the basin the discontinuous top basement surface is interpreted by a transition from stratified high amplitude reflectors to a concordant weaker reflective zone (Figure 4.3a), most likely resulting from a small impedance contrast at the basement sediment interface at these depths. Within the basin basement consists of rotated fault blocks. In the distal basin and abyssal plain transitional continental basement is determined by a change in seismic signature. The transitional crust is characterised by strong irregular and non-parallel reflectors overlain by strongly stratified reflectors indicating deepwater sediments starting approximately at SP 3000 (Figure 4.4a, in pocket).

Eurydice (Syn-rift – Late Triassic)

Syn – rift (Eurydice) sediments well imaged within the basin are characterized by high amplitude stratified and rotated reflectors directly above the top basement (Figure 4.3a). Strong reflectivity is likely due to stratified continental red sandstones, siltstones and shales characteristic of the Eurydice Formation. Syn – rift strata displays growth along rift related normal faults bounding basement blocks. A transition from strongly reflective rotated reflectors up to a more transparent zone determines the top of syn – rift packages.

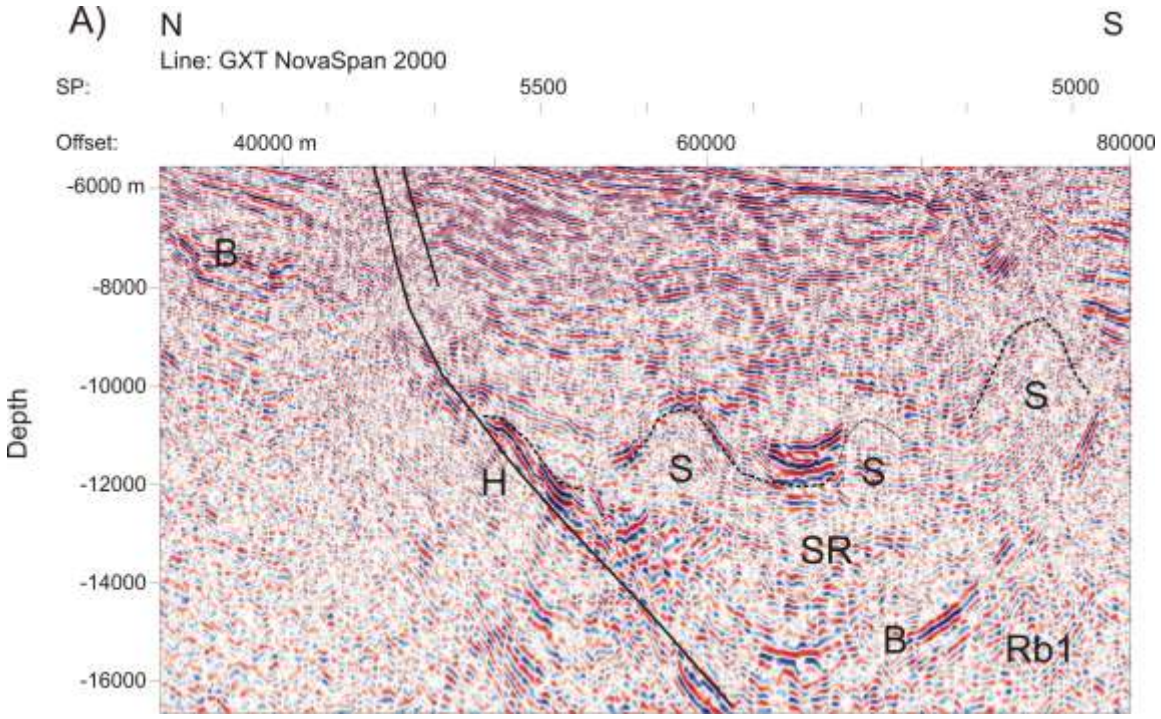

Figure 4.3A) Seismic stratigraphy near the hinge zone (H) of NovaSpan Line 2000. Stratigraphic picks for salt (S), basement (B), and syn-rift sediments (SR) (Eurydice Formation) are based on recognizable seismic signatures (refer to text).

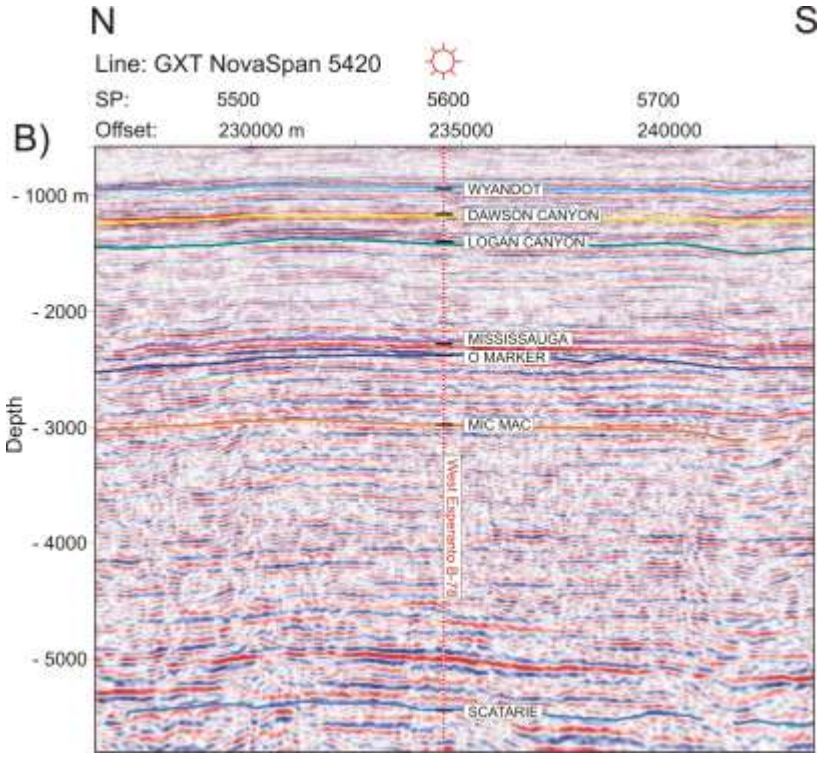

Figure 4.3B) Seismic stratigraphy along the shelf of NovaSpan line 5420. Lithostratigraphic picks used for correlation and interpretation of formation tops on profile 2000 are shown for well West Esperanto B-78 (Figure 4.1). This well is the only tie of the top Scatarie to profile 2000. Refer to text for characteristic seismic signatures of formation tops.

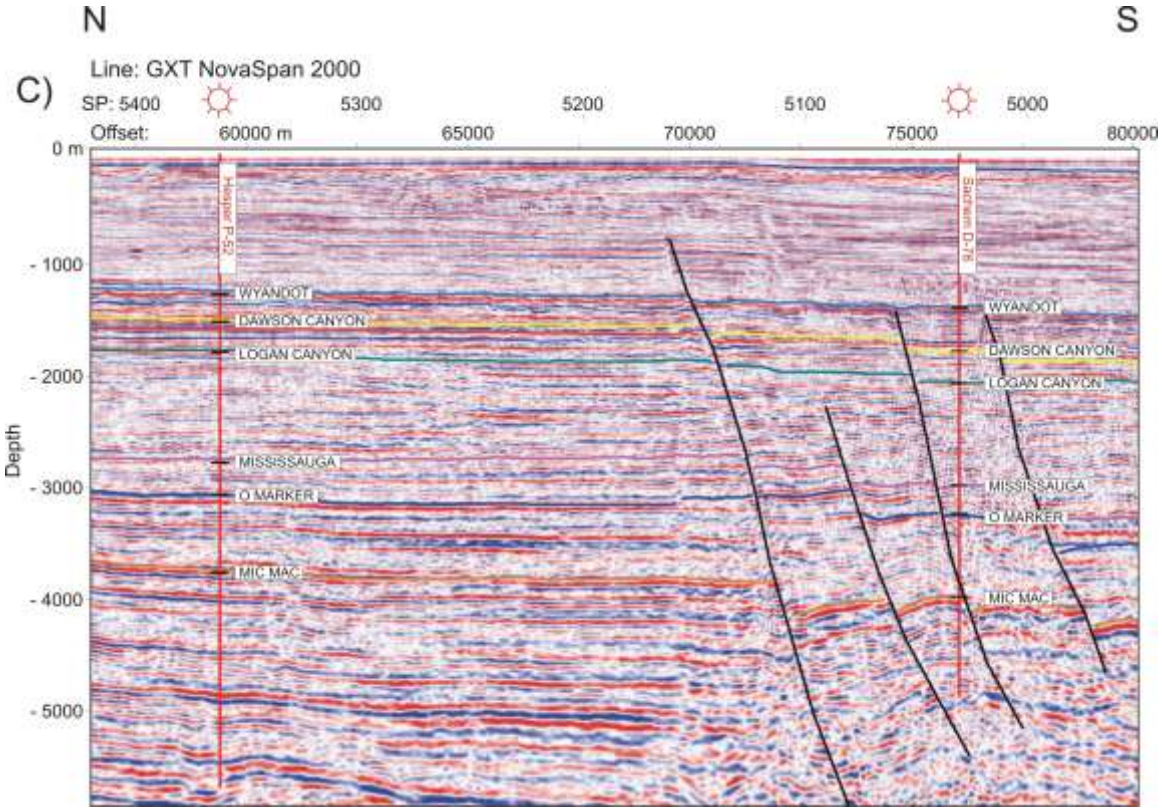

Figure 4.3C) Seisimc stratigraphy along the shelf of NovaSpan line 2000. Lithostratigraphic picks used for correlation and interpretation of formation tops along profile 2000 are shown for wells Hesper P-52 and Sachem D-76 (Figure 4.1). Refer to text for characteristic seismic signatures of formation tops.

Argo Salt (Triassic – Early Jurassic)

Due to complex structural relations and the thick post-salt sediment fill salt sediments pose challenges to interpretations within NovaSpan line 2000. However, when compared to public domain seismic data of the last two decades, seismic imaging of salt structures in the GXT data has significantly improved. Because no wells near line 2000 penetrate the Argo Formation, the salt has been inferred from different seismic indicators:

- Chaotic and transparent seismic signature
- Strong amplitude reflectors at the top of salt caused by significant impedance contrast (Figure 4.3a, e.g. minibasins SP 5300 Figure 4.4a)

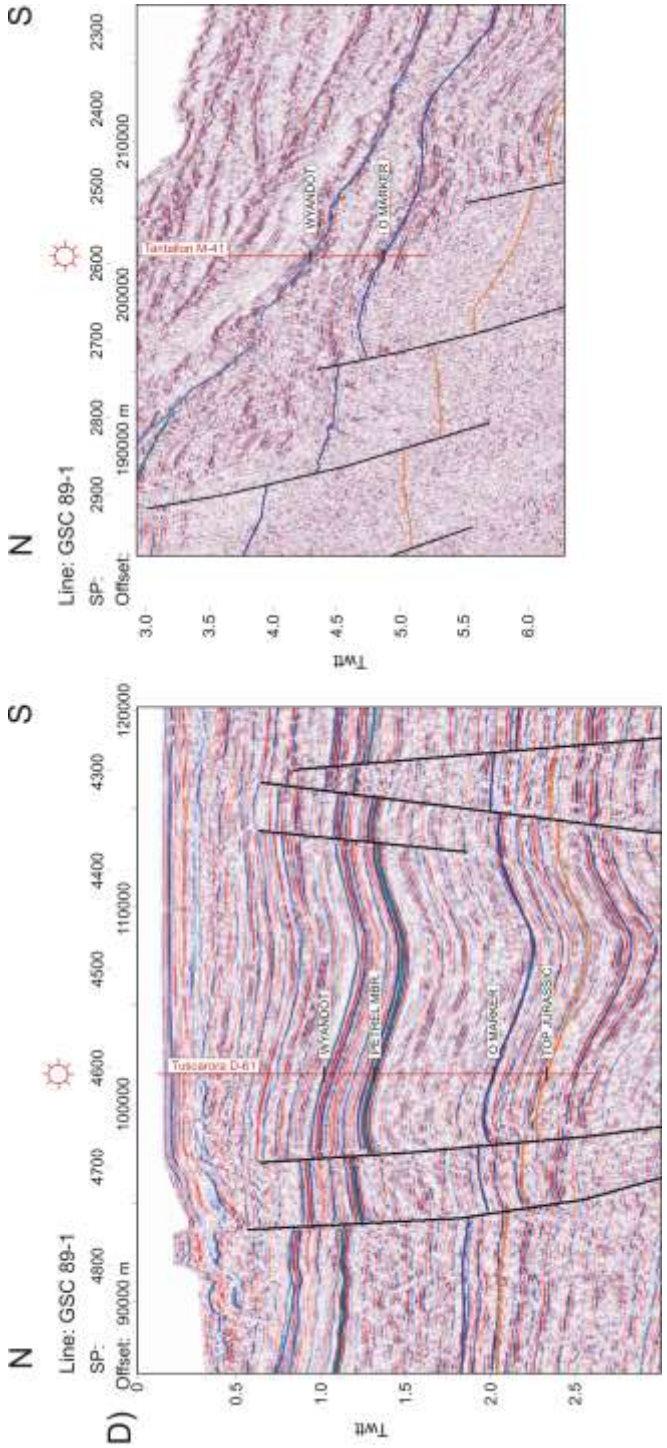

Figure 4.3D) Seismic stratigraphy of GSC Line 89-1: Shelf (left): Relevant formation picks of well Tuscarora D-61 (Figure 4.1). Slope (Right) Relevant formation picks of deepwater well Tantallon M-41 (Figure 4.1).

Diapir flanks and especially crests were interpreted based on surrounding reflectors because here a clear boundary was not observable. Instead, a broad transition zone from a chaotic transparent signature to more reflective and coherent reflectors exists. Crests are interpreted below continuous reflectors (SP 3550) frequently associated with crestal faulting and domal geometry (Figure 4.3a, SP 4500 in Figure 4.4a). Along diapir flanks adjacent reflectors inbasin sediments appear to sheath diapirs as reflectors are deflected upwards towards and tangential to salt bodies (SP 4500) Figure 4.4a).

Scatarie Member/Mohican Formation – J_2 (Early – Middle Jurassic)

In the western Laurentian Basin area (eastern Scotian margin), the Scatarie Member is the oldest correlated stratigraphic unit penetrated by a well (Figure 4.2, West Esperanto (B-78) well in Figure 4.3b). High amplitudes for the carbonate (limestone) Scatarie Member are derived from the high impedance of surrounding clastic strata. The underlying Mohican Formation above the shelf (Line 2000, Figure 4.4a) and beyond the hinge zone (Line 2000, 89-1, Figures 4.3 and 4.4) is comprised of mostly strongly stratified high amplitude reflectors, likely signifying the continental sandstone and shale complexes of early clastic basin fill. Deep reflectors (> 9 km, Line 2000) become more transparent, likely due to deformation related to salt. Seismic transparency beyond the hinge zone (along the landward flank of D1 in Line 2000) is conducive to the shaling out of the Scatarie Member. Seaward of this highly stratified reflectors represent mostly shale/silty strata of the Mohican Formation.

In GXT strike line 5420, the Scatarie reflector can be correlated easily from well B-78 along the shelf to profile 2000 (Figure 4.3c) as it obliquely crosses the regional hinge zone and deepens significantly to the east. Beneath the shelf in profile 2000 the continuous Scatarie horizon and underlying reflectors dip gently southward towards the hinge (Figures 4.3c, 4.4a). At the hinge the horizon is downthrown about ~ 1 km through a series of normal faults parallel to the regional hinge. Within the basin the reflectors continue to dip gently seaward nearly covering a landward salt diapir (D1 in Figure 4.4a). Beyond SP 4850 reflectivity is poor and the deepwater equivalent of the Scatarie reflector is expected to follow the dip trend of underlying strata and terminate along the northern boundary of a salt structure (D2 in Figure 4.4a), beyond which a reasonable interpretation cannot be made.

In profile 89-1 the Scatarie horizon was picked based on the Crow (F-52) well (Figure 4.3d, 4.4b). At this location this strong amplitude reflector is lying nearly directly over Meguma basement. Basinward along the shelf the horizon dips gently seaward while underlying reflectors of the Mohican Formation fill basement grabens. Beyond the regional hinge the Scatarie horizon and underlying strata is folded presumably above a basement high and salt, with normal faulting above the basinward rifted basement block. Similar to line 2000 this reflector dips seaward with reflectivity weakening just landward of the modern shelf break where it appears to cease.

Deepwater (abyssal) marker horizon J_2 (Swift et al., 1986; Ebinger and Tucholke, 1988), nearly equivalent to the top Scatarie marker, consist of a strong amplitude reflector above

transparent reflectors that lie on transitional crust in profile 89-1. The transparent seismic signature of underlying sediments in line 89-1 is a result of sediment accumulation being mostly pelagic fines with little impedance between successive strata. Landward of SP 1600 this marker cannot be followed due to interference from overlying salt detachment surface.

Mic Mac, tJ – J_1 (Late Jurassic)

Sachem (D-76) and Hesper (I-52) wells along the shelf proximal to line 2000 supply projected lithostratigraphic tops for the Mic Mac Formation (Figures 4.2, 4.3c). Similarly projections of lithostratigraphic picks along the shelf of profile 89-1 for the equivalent top Jurassic (tJ) horizon are derived from the Tuscarora (D-61) and Sauk (A-57) wells (Figure 4.3d).

The Mic Mac formation top is a high amplitude reflector along the shelf and proximal basin that denotes the top of a strongly stratified and reflective package of the Mic Mac Formation. Stratified reflectors are likely due to layered sandstone/siltstone or shale successions characteristic proximal alluvial plain and deltaic deposits of the Mic Mac Formation. Under the shelf break seismic reflectivity is significantly weaker possibly as a result of lateral velocity contrasts within long – offset seismic profiles (lines 2000, 89-1). However this seismic transparency may also be attributed to a transition into outboard more uniform neritic and deepwater shale facies.

The top Mic Mac reflector along the modern shelf dips gently seaward and is slightly offset by several normal faults (Figures 4.3c, 4.4a). Along the shelf, the top Mic Mac may also be coincident with the Avalon Unconformity, separating Jurassic and Cretaceous stratigraphy through a erosional unconformity (Figure 4.2). Reflectivity of the strata directly above the Mic Mac package is lower. This characteristic has been used to correlate this horizon seaward into the slope where there is little well data.

Within Line 2000 the top Mic Mac is offset (~ 1 km) by normal faulting at SP 4600 (Figure 4.4a). Beyond SP 4450 the top reflector of a similar, although less distinguishable seismic package is interpreted as top Mic Mac equivalent. Seaward of SP 4100 seismic reflectivity is decreasing and reflectors have an overall seaward dipping trend.

Beneath the slope of Line 89-1 the equivalent top Mic Mac (tJ) horizon has been correlated to profile 89-1 (Shimeld, 2004; Ings and Shimeld, 2006) and is observed to act as a transition from planar reflectors above to dipping reflectors of the BSW below (Figure 4.4b). Seaward of the shelf break this surface is easily recognizable as it constitutes an angular unconformity. Landward dipping Late Jurassic reflectors (Mic Mac time) may have a high reflectivity due to the combination of sand/silt and shale complexes of Mic Mac time and thinner overburden beyond the shelf break.

For the correlation with time-equivalent deepwater reflectors, abyssal seismic marker horizons defined by Swift et al. (1986) and Ebinger and Tucholke (1988) were correlated to profile 2000 (Figures 4.2, 4.4a) The Late Jurassic J_1 horizon is nearly stratigraphically

equivalent to the top Mic Mac within the shelf. This high amplitude reflector in both lines 2000 and 89-1 is subhorizontal and displays very little topographic relief. Often it is observed to act as the top of a strongly stratified and reflective package (Figure 4.4a) likely comprised of prodelta sand/siltstone and shale sequences. In both profiles the J_1 horizon is truncated by salt detachment surfaces (Figure 4.4).

Mississauga (Early Cretaceous)

Wells P-52 and D-76 proximal to line 2000 both contain lithostratigraphic picks for top Mississauga and younger formation tops (Figures 4.2, 4.3c). Along the shelf the Mississauga top displays strong amplitudes as a result of a strong impedance contrast with overlying transgressive Naskapi shales. Underlying reflectors comprising the Mississauga Formation consist of a strongly stratified and reflective package, indicative of prograding delta plain to inner neritic sandstones and siltstones/shales.

Along the shelf Mississauga reflectors truncate the top Mic Mac horizon (Figure 4.4a,b). Here, onlap of prograding Early Cretaceous sediments onto the Avalon Unconformity is clear. Just landward of the shelf break in Line 2000 (SP 4800 – 4650, Figure 4.4a) the top Mississauga horizon is present above several distinct parallel strong amplitude reflectors. At the shelf break (SP 4400), this characteristic feature is used to correlate the horizon into deepwater and above a salt canopy (SP 3750). Along the seaward portion of the line seismic characteristics do change frequently as a result of facies changes, but a correlation is possible above a transparent zone. Seaward of SP 3650 to approximately SP

2500 the correlation is solely based on expected stratigraphic position of the horizon and placement above a strong amplitude reflector similar to that at approximately SP 3950.

Lithostratigraphic picks in time for the top Mississauga are not available for wells proximal to profile 89-1. Instead the O Marker horizon is used as the closest approximation from available well data.

O Marker – β (Early Cretaceous)

In line 89-1 the close-by wells Tuscarora D-61 and Sauk A-57, constrain the lithostratigraphic picks of the O Marker (Figures 4.1, 4.2, 4.3d). This limestone unit has a large impedance contrast with surrounding clastic strata and, therefore, is easily recognizable through high amplitude reflectivity. This seismic signature makes the interpretation of the horizon beneath the shelf straightforward. Beneath the modern shelf break, similar to profile 2000, the O Marker reflector (β) is poorly imaged, likely due to facies changes as limestone shales out seaward and seismic imaging problems due to the shelf break (Figure 4.4b).

Along profile 2000, the wells Sachem D-76 and Hesper P-52 serve as the source for O Marker lithostratigraphic picks (Figures 4.1, 4.2, 4.3c). The O-marker is offset by normal faults near the Sachem well but due to high reflectivity the correlation is not difficult. Beyond SP 4500 reflectivity of this unit and chronostratigraphic equivalents is poor (Figures 4.2, 4.4a). Seaward of this position, interpretations cannot be reliable made.

Oceanic marker horizon β (Swift et al., 1986; Ebinger and Tucholke, 1988), nearly a time equivalent of the O Marker horizon on the shelf, has been correlated to deepwater reflectors of profile 2000 and 89-1. The β reflector is a weak amplitude subhorizontal reflector surrounded by well stratified weak amplitude deepwater reflectors, implying pelagic and prodelta fine sedimentation of similar deposits. (Figure 4.4a, b).

Logan Canyon – Petrel Member (Early – Late Cretaceous)

Within profile 2000 beneath most of the shelf the top Logan Canyon is distinguished by a mapable high amplitude reflector above a package of significantly weaker reflectors (Figures 4.2, 4.3c, 4.4a). Seismic transparency is likely due to uniform sand/shale deposits along a broad coastal plain and shallow shelf environment during the Early – Late Cretaceous. Seaward of SP 5300 underlying reflectors become stronger in amplitude, signifying more diverse sedimentation with the Logan Canyon top capping this package landward of the shelf break. At the shelf break the seismic reflectors are chaotic and difficult to interpret. Beyond SP 4400 the top Logan Canyon is identified below a strong amplitude reflector with discordant and irregular characteristics (Figure 4.4a). This reflector most likely is an erosional discordance due to Tertiary uplift (Wade and MacLean, 1990; MacLean and Wade, 1992; Grist and Zentili, 2003; Ravenhurst and Zentilli, 1995). Assuming that erosion of the Logan Canyon Formation is insignificant the time equivalent of the top Logan Canyon has been interpreted to follow this strong reflector.

Time-converted lithostratigraphic picks of the top Logan Canyon are not available for wells near profile 89-1. Instead the closest stratigraphically equivalent Petrel Member horizon is used as the closest approximation from available well data (Figures 4.2, 4.3d, 4.4b). This high amplitude reflector follows much the same trend as the top Logan Canyon in profile 2000 and is easily correlated through closely spaced faulting below the shelf break. The prominent reflectivity of the Petrel Member is due to its carbonate (limestone) lithology being embedded in predominantly shales. This seismic marker appears to be cut by the Tertiary(?) unconformity directly beneath the shelf break as evidenced by the absence of the Petrel Member in the Tantallon M-41 slope well (Figures 4.3d, 4.4b).

Dawson Canyon (Late Cretaceous)

Below the shelf of profile 2000 the top Dawson Canyon horizon is denoted by a very planar and strong amplitude reflector, below which there is similar yet weaker reflectivity (Figures 4.2, 4.3c, 4.4a). Homogeneous reflectivity within this unit is most likely the result of the Dawson Canyon Formation being comprised of shale lithologies. This reflectivity is easily recognizable up to the shelf break. Beyond the shelf break a younger irregular strong amplitude reflector (Tertiary unconformity?) appears to truncate the top Dawson Canyon horizon. Interpretations into deepwater are therefore not correlated.

Lithostratigraphic picks in time for the top Dawson Canyon are not available for wells proximal to profile 89-1. Instead the Wyandot horizon is used as the closest approximation from available well data.

Wyandot – A* (Late Cretaceous)

Within line 2000 the top Wyandot is a very recognizable strong amplitude reflector that can be easily correlated across the shelf (Figures 4.2, 4.3c). The Wyandot Formation consists of mostly chalks (limestone) and is surrounded by mostly shales. This strong impedance contrast is the reason for such strong reflectivity. Beyond the shelf break (SP 4500) the irregular strong amplitude reflector (Tertiary unconformity?) also appears to cut the top Wyandot horizon (Figure 4.4a). Interpretations into deepwater are therefore not correlated.

Lithostratigraphic picks for the top Wyandot are available for all wells proximal to profile 89-1, including the only deepwater well Tantallon (M-41) on the slope (Figures 4.1, 4.3d). Similar to line 2000, the top Wyandot horizon displays strong amplitudes along the shelf. Well data from M-41 proof that the top Wyandot (deepwater equivalent A*) is present beyond the shelf break in this location (Figures 4.3d, 4.4b). Therefore imaging is either poor along the shelf break and slope of line 2000 and the Wyandot is present, or erosion was not nearly as severe along profile 89-1. Correlations across the shelf break and slope are based on similar characteristics to that along the shelf, with reflectivity

decreasing seaward as a result of increasing shale content, evident from the weak reflectivity of the A^* horizon and surrounding strata (Figure 4.4b).

4.4 Rift architecture (basement and syn-rift fill)

The following is an overview of the regional rifted basement structure along the eastern Scotian margin as imaged by seismic reflection profiles 2000 and 89-1 and the SMART Line 1 velocity profile (Figure 4.1). Both GXT line 2000 and GSC line 89-1 (coincident with SMART Line 1) share a common rift style and processes. The lack of seaward dipping reflectors (SDRs) in either profile and the abundance of serpentinized mantle and thinned oceanic crust within profile 89-1 (SMART Line 1) (Funck et. al, 2004) illustrate a easterly trend to a progressively more non-volcanic margin. Similar rifting styles observed between these lines display significant continental thinning below the north-central Scotian Basin through listric rift faults causing half graben formation and rotation of basement blocks (Keen and Potter, 1995). Profile 2000, similar to SMART Line 1, may also contain a transitional crust zone comprised of underlying serpentinized mantle and overlying continental crust or perhaps highly serpentinized mantle in the continent-oceanic transition.

The rift shoulder (shelf) is defined as the stable landward platform of the passive margin, with the seaward boundary marked by the regional hinge zone. The hinge is denoted by the often sharp transition through both flexure and faulting from the shallow shelf to the deep basin in the south (Figure 4.4). Within the basin (Scotian Basin) the proximal basin

is defined as the loci of major deposition on salt throughout basin evolution. This region is also coincident with the boundary between continental basement and seaward transitional crust. The distal basin is defined by deepwater sedimentation above transitional crust.

4.4.1 Rift shoulder (shelf)

Below the shelf of profile 2000 basement increases in depth from 4 km in the northwest up to 9.5 km to the southeast landward of the hinge zone (SP 5650) (Figure 4.4a). Along the stable basement platform (Canso Ridge) basement is not completely undeformed, instead small (700 m – 200 m wide, ~ 1.5 km deep) fault bounded grabens are present (Figure 4.5). Similar reflectivity and basement features are interpreted beneath the shelf of profile 89-1 with comparable dimensions of graben structures ranging from 800 ms to 250 ms in depth (Figure 4.4b).

4.4.2 Rift margin (hinge)

The hinge zone of the eastern Scotian margin is imaged as a series of sub-parallel synthetic listric faults (Figure 4.4a) or a series of faulted basement steps into the basin (Figure 4.4b). The hinge zone and accompanying synthetic faults are well imaged in GXT line 2000 at shot point (SP) 5700. A set of parallel and very strong high angle reflectors at approximately 10 km and deeper represent the major and associated synthetic faults of the hinge zone. Depth to basement across this hinge zone increases from approximately 9

km on the shelf to over 16 km within the Scotian Basin (western Laurentian Sub-basin) (Figure 4.4a).

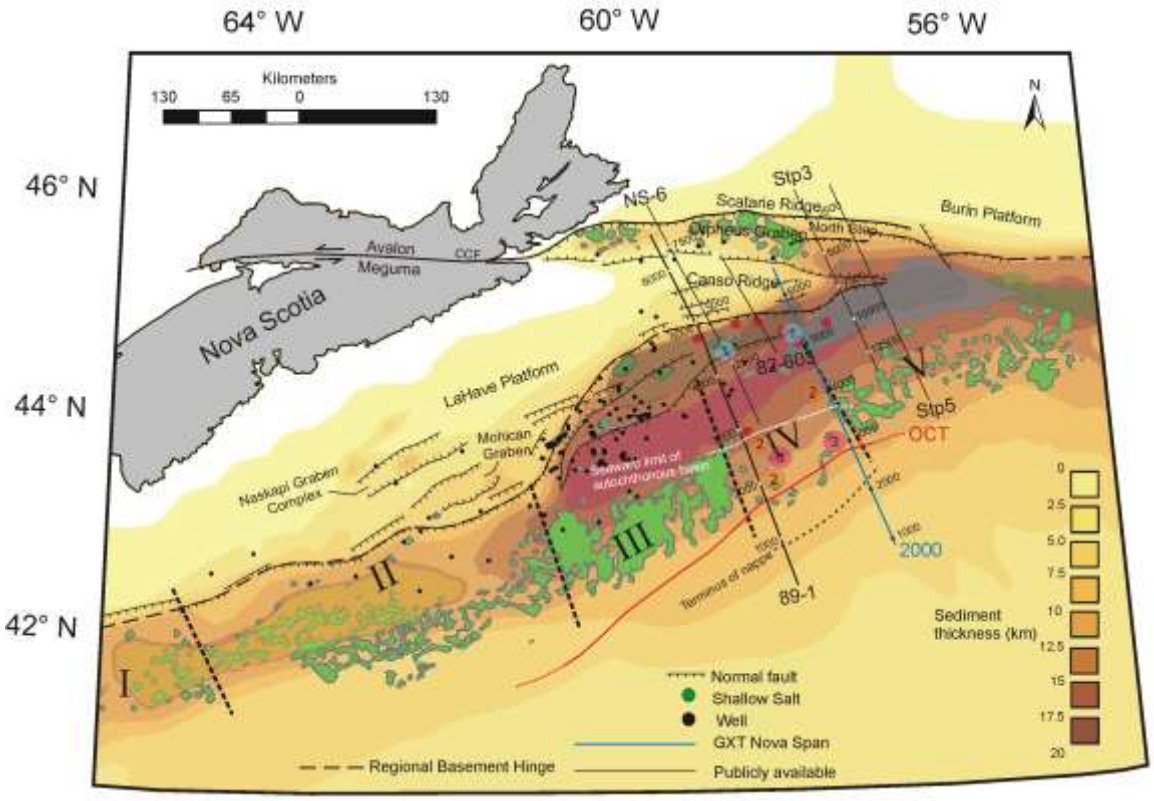

Figure 4.5. Hinge, depocenter, and salt features of Subprovince IV as interpreted from seismic profiles 2000, 89-1, 82-603, NS-6, and STP 3. Shot points of seismic profiles (Figures 4.?) are labelled. The location of major progradational depositional units are identified for lines 2000 and 89-1: 1 – Scararie/Mohican (Middle Jurassic), 2 – Mic Mac (Late Jurassic), 3 – Mississauga (Early Cretaceous). Red line indicates the approximate boundary between continental crust in the northwest and transitional crust in the southeast (OCT – ocean- continent transition).

GSC line 89-1, located 90 km west of GXT Line 2000, is the only publically available seismic profile with sufficient depth-penetration to image the basement across this transition from shelf to deep basin. Here the hinge is comprised of several large (8 – 10 km wide) normal fault block steps (Figure 4.5), with a less pronounced hinge zone than profile 2000 displaying a more flexural transition. The depth of the basement increases from 3.5 s on the shelf to approximately 7.5 s in the deepest portion of the basin (Figure

4.4b). In both profiles (2000, 89-1) normal faulting observed within sedimentary overburden is subparallel to and overlying the hinge. This faulting is related to salt evacuation and flexing of the margin in the proximal basin, adjacent to the hinge zone; not the reactivation of basement faults.

4.4.3 Proximal basin

The basement of the Scotian Basin deepens to the southeast (>16 km) and is completely imaged only in few seismic profiles (NovaSpan line 2000, 5420, and GSC line 89-1). Based on landward dipping reflector sets in profile 2000, the basement structures have been interpreted as rotated fault-bounded crustal blocks (Figure 4.4a). Although reflections at these great depths are noisy, the major basement blocks (RB1 – 7 in Figure 4.4a) can be outlined with sufficient confidence. In most cases these rotated crustal blocks are observable immediately beneath clastic syn-rift sediments imaged as wedge-shaped, strongly reflective and stratified growth packages bounded by basement faults. The basal reflector of these packages is interpreted as the top of basement and appears to be mostly dipping northwest from rotation along bounding faults that dip to the south.

Rift block 1 (Rb1) has a strong reflector associated with the top of basement (SP 5050) and appears to be offset by secondary faults. The southern portion of the block is dipping very steeply. Alternatively, the steeply inclined strong reflector could be a remnant stratigraphic unit that has been encapsulated in salt. However, this strong reflector does appear to continue well below interpreted salt therefore suggesting a basement feature.

Whether this reflector is indeed basement or has some other origin, it appears to have little effect on salt deformation and sedimentation patterns above.

Rb1, Rb3 and Rb4 are well constrained basement structures within line 2000. Clearly stratified growth sediments overlay a much less reflective unit illustrating a sharp basement transition . Although separate basement blocks, Rb3 and Rb4 may be draped by the same syn-rift growth package as continuous reflectors over these blocks suggest. Further seaward basement blocks (Rb5 – 7) display weaker contrasts and more gradual shifts in seismic signature making interpretations of top basement more difficult. Poor imaging is most likely due to seismic interference associated with overlying allochthonous salt bodies. In general, weaker reflective units follow similar trends as the well imaged landward crustal blocks forming rotated rift blocks with northwest dipping reflectors along north bounding and southeast dipping listric faults (Figure 4.4a).

The basement structures in GSC line 89-1 show a comparable style (Figure 4.4) as observed in GXT line 2000. South of the hinge zone in line 89-1 rifted and rotated basement blocks also form half grabens that constitute the majority of basement structures. However, although reflection data regarding sediments is of very good quality, along the shelf break and slope reflection data is very poor below 6 s. To better constrain the basement interpretation (Figures 4.6, 4.7) published crustal velocity models (Funck et al., 2004) and gravity models (Keen and Potter, 1995; Zheng and Arkani-Hamed, 2002) have been used.

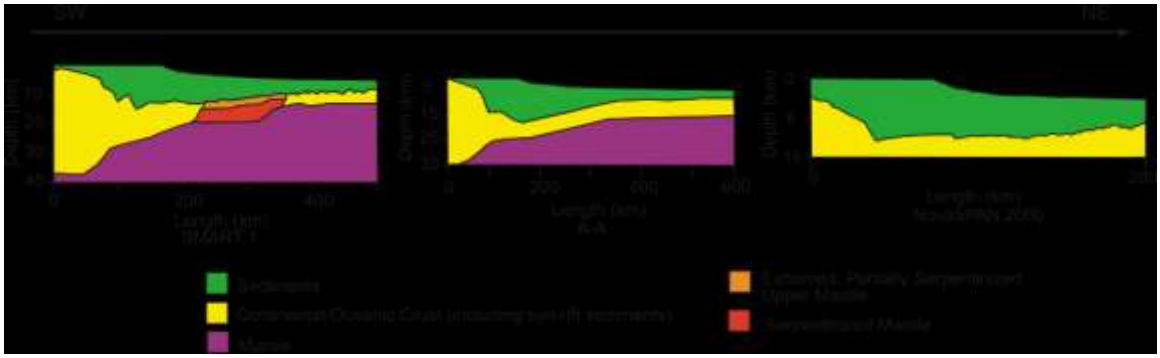

Figure 4.6. Crustal profiles of P-wave velocity (SMART 1, Funck et al., 2004), gravity (A - A', Zheng & Arkani-Hamed, 2002), and seismic reflection (NovaSpan 2000) along the eastern Scotian margin (see Figure 4.1 for locations). Profiles indicate a wedged basin floor with an overall trend of thinning seawards, suggesting that proximal locations have thickest salt accumulation.

Fault-bounded crustal blocks of 89-1 have the same orientation as those in line 2000, but with a deepening trend from the hinge to SP 4100 and an average width of 13 km (Figures 4.4b, 4.7). Although time-migrated seismic data of this line suggest a relative basement high (approximately shot point 3550), depth-converted velocity models (Figure 4.5) indicate this to partly be a relict of low seismic velocities of the water column. In both velocity and gravity models the basement climbs a seaward ramp outboard of a small basement high (SP 2500), forming a similar configuration as observed in profile 2000 (Figure 4.6).

4.4.4 Distal basin

Transitional crust initiates at approximately SP 2750 (Figures 4.4a, 4.5) of Line 2000. The surface of this crust much more variable than that of the continental basement. Faults are interpreted based on discontinuous reflectors and are much more closely spaced (~6 km) with less rotation of the hangingwall and fault displacements. In general the

basement displays a shallowing trend from the hinge to the seaward extent of the profile to the south.

In profile 89-1 the transitional basement within the distal basin displays a similar trend. Faulting is difficult to interpret due to the low quality of seismic reflectivity. Interpreted highly-serpentinized mantle (Funck et al., 2004) occupies the last 80 km of line 89-1 (SP 1800 - 200) delineating a transition zone from continental crust to oceanic crust (Continent Ocean Boundary – COB) (Funck et. al, 2004) (Figures 4.5, 4.6, 4.7). True oceanic crust begins 25 km south of line 89-1.

4.4.5 Variation along the margin

The rift shoulder (shelf) and regional hinge zone along the Canso Ridge shows a uniform architecture across much of the eastern Scotian margin. Public seismic data image other small (~ 2 s deep) ~4 km wide steeply walled grabens along the shelf (Line NS-6) of the margin (Figures 4.5, 4.8). However, to the east (line 82-603) these structures are absent, suggesting limited lateral extent (Figure 4.5). These shallow grabens common along the shelf likely resulted from large scale rifting processes associated with the opening of the Atlantic. In particular the failed rifting of the nearby Triassic Orpheus Graben may also be related. Steep and deep rooted bounding faults for these grabens suggest a possible transtensional component of deformation. It's possible that reactivation (Triassic?) along the seaward extension of the strike-slip Cobequid-Chedabucto Fault bounding the Orpheus Graben may be associated with these structures (Figure 4.5).

North of the Canso Ridge the Orpheus Graben changes the architecture of the Scotian shelf from a stable platform in the south to a complex of grabens and half-grabens in the north. STP seismic profiles (Figures 4.1, 4.5) image the hinge zone changing drastically east of line 2000 as it shifts from the southern bounding fault of the Canso Ridge to approximately 75 km north, at the southern bounding fault of the North Step (Figure 4.5, SP 3600 in Figure 4.9). This portion of the hinge zone has similar features to that of the Canso Ridge including closely spaced stepping faults often synthetic to the main hinge. Within the Orpheus graben south of the hinge, basement is reported to be at an average two-way travel time (twtt) of 7 s (MacLean and Wade, 1992), but none of the STP seismic profiles collected for this study record beyond 7 s twtt. Therefore most basement structures within the main Orpheus Graben are not recorded. However, at the edge of the graben the extension of the Canso Ridge is imaged within STP-5 (Figure 4.5). This basement high marks the basinward edge of the graben, with basement deepening significantly to the southeast (Laurentian Sub-basin) (Figure 4.9).

4.5 Salt structures

4.5.1 Early passive extensional structures

Line 2000

In line 2000 extensional passive salt structures consists primarily of autochthonous broad triangular shaped diapirs; the most prominent are diapers D1 – 3 (Figures 4.4a, 4.10a). Salt structures are separated by thick, mostly welded salt withdrawal basins comprised of Middle – Late Jurassic depocenters (Figure 4.10a). A clear progradational trend is observed from depocenters, with major accumulation (~ 4 km) of Middle Jurassic (Mohican) sediments landward of D2 and Late Jurassic (Mic Mac) seaward of D2 (~ 5 km). Diapir initiation is a result of seaward extension of overburden from the differential load of prograding sediments on salt, driving seaward salt extrusion. Normal faulting is therefore common above the seaward flanks of diapirs, where salt was once passive. During diapir development through continuing downbuilding of sediments and salt withdraw, faulting accommodates differential subsidence.

Thick Middle Jurassic deposits seaward of the hinge zone have accumulated in proximal salt withdrawal basins landward of D1 and D2 as a result of passive downbuilding into originally thick salt sediments as diapirs formed. Smaller (~ 5 km wide) minibasins within salt are recognized by u-shaped reflector packages above salt (SP 5300 in Figure 4.10a). Subhorizontal reflectors between D1 and D2 support an interpretation of a broad expulsion rollover, perhaps intersected by a basinward listric fault (Figure 4.10a). The weak internal deformation and gently inclined strata suggest that passive downbuilding into underlying salt and its subsequent seaward extrusion was the dominant process of basin formation in the Early and Middle Jurassic.

Along the north-eastern flank of D2 Late Jurassic (Mic Mac) reflectors are rotated along southeast dipping faults, interpreted to be downthrown up to 800 m. It is likely that normal faulting is due to extension and rotation of strata along a secondary salt detachment surface. A landward salt overhang may have formed in the late Middle Jurassic. Profile NS-6, west of line 2000 (Figure 4.1), images a significant salt structure within the autochthonous basin, ~25 km south of the hinge zone (Figure 4.8). Interestingly this structure appears to also have a landward overhang, similar to that discussed for D2 of profile 2000. However, the timing of landward salt flow is quite different with that of profile NS-6 being of latest Jurassic with vertical passive diapirism continuing into the Tertiary (Figure 4.8).

Alternatively, the D2 salt body may be much smaller than the first interpretation. A smaller salt roller type structure would simply continue the regional trend of this area, having southward dipping normal faulting located above the south flank of diapirs, accommodating extension and rotation of this reflective package (Figure 4.4a, 4.10a). The steeply inclined reflectors at approximately 6.3 km depth near SP 4450 show characteristic sheathing or tangential reflectors along the flank of D2 with overlying conformable domed reflectors. These observations imply that the interpretation of a large diapir with a landward salt overhang is most probable.

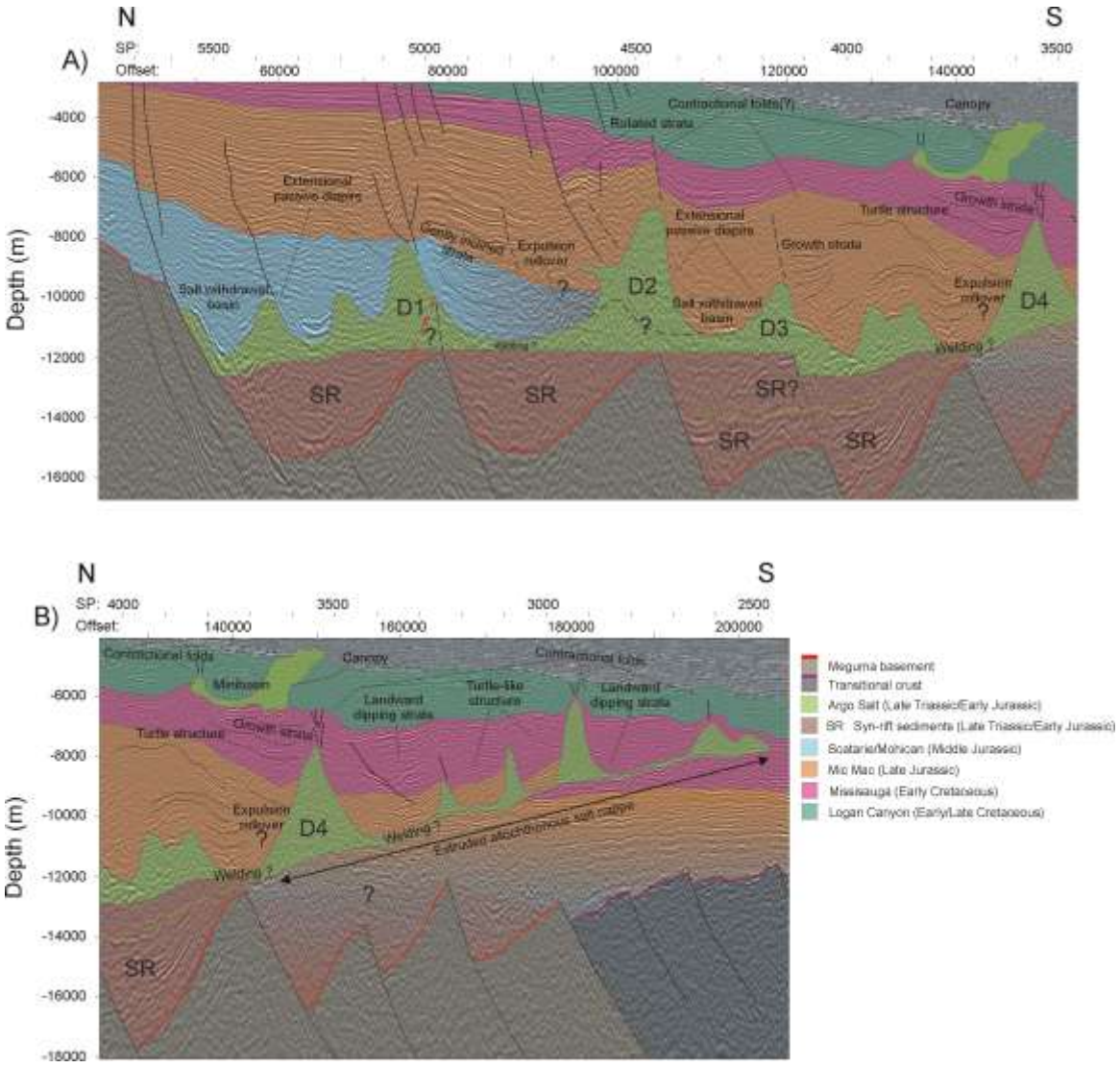

Figure 4.10. Interpreted salt structures and characteristic features of NovaSpan Line 2000. A) Extensional passive salt diapirs (D1 – 4) formed as a response to the extension of a sedimentary wedge above salt. Passive downbuilding structures such as salt withdrawal basins, expulsion rollovers and turtle structures dominate Jurassic and Cretaceous strata. B) Extrusion salt structures (allochthonous salt nappe) formed through the loading of Early Cretaceous (Mississauga) sediments on top of an inflated salt complex at the basinward edge of the salt basin (D4). Late stage contractional structures include concentric folding above diapirs. Secondary canopy development is likely sourced from salt bodies at the basinward margin of the salt basin (D4).

Along the distal portion of the autochthonous salt basin, seaward of D2, two smaller salt bodies are located along the edge (D3) and seaward of a syn-rift fault. Major Late Jurassic depocenters are located above this salt and consist of a thick (> 5 km) turtle-like structure with both north and south dipping reflectors surrounding a salt-cored anticline

(Figure 4.10a). Within the turtle structure, a smaller one exists on the south side of a normal fault that lies above the south flank of D3. The main depocenter of the Mic Mac Formation terminates along the landward flank of D4, similar to that of the Early and Middle Jurassic depocenter (Figure 4.10a), and is denoted by a narrow salt weld. Rolling Late Jurassic strata on both flanks of the turtle structure again suggest; passive downbuilding, diapir formation, and mostly basinward expulsion of thick salt through flank collapse, as the main salt tectonic process during the Late Jurassic.

The landward flank of D4 is overlaying the seaward margin of the autochthonous salt basin, suggesting that loading by thick Late Jurassic sediments sourced from the extension of the Laurentian Delta were a major cause of basinward salt inflation and subsequent allochthonous salt extrusion. This indicates that basinward salt inflation is controlling the location of major depocenters, limiting seaward sedimentation as observed for Middle Jurassic (Mohican) depocenters. This causes a positive feedback between focused sedimentation and higher rates of basinward salt mobilisation and salt inflation. At the end of the Late Jurassic an inflated salt complex is postulated to have been located at the seaward margin of the rift basin.

Widespread salt welding is not interpreted to be a characteristic feature of profile 2000. Welding is localized underneath mostly thick salt withdrawal basins between large autochthonous diapirs. The most likely of these being located between D1 and D2 near shot point 4900 (Figure 4.4a, 4.10a). This feature indicates that although salt was

mobilized seaward throughout Jurassic basin evolution, it was not extremely efficient with plenty of remnant salt trapped within the autochthonous basin.

Line 89-1

As mentioned in section 3.1.2 Subprovince IV, including profile 89-1, is considered absent of significant salt structures. However, with the aid of velocity models (Funck et al., 2004) it is possible to interpret small remnant salt within the lows of landward half-grabens and possibly inflated salt influenced by the high between the two blocks. This inflated salt likely attributed to the folding of overlying strata observed between shot points 4200 and 4700 (Figure 4.4b, 4.11b). However, basement influenced and trapped salt of Line 89-1 formed differently than the extensional diapirs of Line 2000.

Within profile 89-1 similar wedge shaped Middle Jurassic depocenters are observed with maximum thickness (> 2 s) just seaward of the hinge zone within landward half grabens above salt (Figures 4.4b, 4.11b). The basement configuration derived from velocity models (Funck et al., 2004) indicate that Middle Jurassic depocenters thin significantly beyond SP 3800 (Figures 4.4b, 4.11b), similar to profile 2000. The lack of salt structures within the autochthonous basin is likely a result of an extremely efficient and rapid basinward extrusion of salt from the basin. Middle – Late Jurassic sediments (Mohican) likely extruded salt to the seaward portion of the basin, leaving little remnant salt behind through mostly welding.

4.5.2 Intermediate extrusion structures

A characteristic feature of Line 2000 is an extensive (~ 70 km) allochthonous Early Cretaceous salt nappe system outboard of the original salt basin (Figures 4.4a, 4.10b). Similarly Line 89-1 displays a similar yet older (Late Jurassic) salt detachment surface (D) with distinctive landward dipping reflectors and remnant salt along the toe (figures 4.4b, 4.11b). Although the timing of these features is slightly different, the mechanism for their development are believed to be the same. The loading of prograding sediments on inflated salt complexes at the basinward margin forced salt to climb out of the basin, with extension along the salt detachment accommodated by the landward rotation of strata and normal faulting above small salt pillows.

Line 2000

Allochthonous salt within line 2000 is more easily recognized and imaged than that of autochthonous salt. A well defined transparent seismic signature is likely due to thin and less deformed overburden and a lack of seismic interference from the shelf break and slope. The salt nappe initiated during the Late Jurassic as observed from salt truncating the J_1 deepwater and underlying horizons. The nappe initiates where the base of salt is interpreted to begin climbing (SP 3750) and extends to shot point 2500 (Figure 4.10b). Along this nappe several salt diapirs are present having a similar symmetric geometry to those interpreted within the autochthonous basin but are significantly smaller in size. The largest of these allochthonous diapirs is D4, located at the landward margin of the nappe.

Normal faults are limited, but appear above the southern flanks and crests of some diapirs. Welding along the salt nappe in Line 2000 is debatable, although near welding and thin salt is interpreted between allochthonous diapirs (Figures 4.4a, 4.10b).

Major depocenters above the nappe are Early Cretaceous (Mississauga). Sediment thickness increases to > 3 km on the basinward flank of D4 while depocenters thin near the toe of allochthonous salt. Depocenters consist of passive downbuilding strata displaying growth along the basinward flank of diapir D4. Reflectors dip mostly landward while forming in some cases turtle-like structures between diapirs (Figure 4.10b). The loading of Early Cretaceous (Mississauga) depocenters on an inflated (allochthonous?) salt complex at the basinward edge of the rift basin is proposed to be the main factor responsible for extensive nappe development and basinward salt extrusion. D4 is interpreted to represent a remnant of the inflated salt complex.

Beneath the ramp Early Cretaceous (β) stratified reflectors suggest significant accumulations of deepwater and prodelta sediments during Mississauga time, illustrating significant basinward salt climbing during this time (Figure 4.4b, 4.10b).

Line 89-1

To the west in profile 89-1 thickest accumulation of Late Jurassic (Mic Mac) sediments occur in the landward part of the seaward climbing basement wedge (~ 3 s, SP 2700, Figure 4.11b). However, significant accumulations constitute a roho-like structure (BSW

– Banquereau Syn-kinematic Wedge) above a climbing salt detachment (D), similar to that of Line 2000. The defining characteristic of the salt detachment (D) is rotated landward dipping reflectors of the BSW along a series of normal faults that sole out into the salt detachment, with low angle salt rollers below footwalls. From the correlation with deepwater horizons, this salt detachment was initiated in the Middle Jurassic (J_2) while terminating at the end of the Late Jurassic (J_1) (Figures 4.4b, 4.11b). Small triangular diapirs along the seaward extent of the detachment surface are similar to those of Line 2000. However, the amount of salt is significantly less in profile 89-1 than 2000, as evidenced from extensive welding along the majority of the salt detachment surface (D) (Figure 4.11b).

Post-rift evolution of Salt Nappe in Subprovince IV (eastern Scotian margin)

The geometry and features of the salt nappe imaged in Line 2000 are conducive to a history of early and continuous salt expulsion from the autochthonous salt basin. Interpreted seaward equivalent horizons and regional oceanic marker horizons suggest that allochthonous salt began to extrude by the Late Jurassic (J_1) and continued at a steady pace through the Early Cretaceous (β), as evidenced by the overall uniform ramp angle (~1°) and consistent truncation of underlying reflectors as the salt climbed up section (Figures 4.4a, 4.11a). The toe of the tongue appears to level out and constitute a flat in an otherwise ramp system that formed during the middle Early Cretaceous as interpreted from the β stratigraphic horizon. This time denotes the end of seaward extrusion and a short lived reduction in sedimentation, allowing the passive glacier-style

flow of salt along the sea floor. Shortly after this the shut down of salt movement and burial of the front of the salt-ramp system is achieved.

A similar ramp geometry, length (~ 70 km), and angle (~1°) is observed along a salt detachment (D) within Subprovince IV through profile 89-1 (Figures 4.4b, 4.11b) and interpretations of other nearby publically available seismic profiles (Ings and Shimeld, 2006). Within profile 89-1 the structure is interpreted to begin at approximately shot point 2800 and stratigraphically climb up section truncating oceanic markers (J_2, J_1,). The location of ramp initiation is slightly landward when compared to that of line 2000 (< 20 km), but considerably adjusted seaward (~35 - 40 km) compared to previous interpretations of Subprovince IV (Ings and Shimeld, 2006). However, at its terminus (SP 750 in Figures 4.4b, 4.11b) the base of the ramp is conformable with oceanic marker J_1 of Late Jurassic time. The related nappe of line 2000, however, terminates much later in the Early Cretaceous (Figures 4.4, 4.11).

The rapid extrusion in the western profile 89-1 when compared to its eastern counterpart line 2000 is debatable. The depth of the original salt basin (autochthonous) within profile 89-1 from velocity models (Funck et al., 2004) suggests only a slightly shallower (~ 1 – 2 km) salt basin than that of line 2000, with similar basin geometries (seaward thinning wedge). Such a contrast in volume of salt in each profile is quite surprising. But similarities in ramp geometry, salt structures, overburden geometry and locations of initiation and termination of this feature suggest a similar mechanism of salt mobilization. The base of the BSW in cross-section (NE-SW) is concave. Profile 89-1 is located near

the center of the BSW with profile 2000 located on its eastern flank (Figures 4.1, 4.5). Perhaps the center of this feature (BSW) received higher early sediment influx mobilizing salt to the flanks where sediment accumulation was slightly less.

Another key difference is the highly rotated and faulted strata of line 89-1 (Figures 4.4b, 4.11b) with little salt present compared to the abundant salt and broader reflector configuration of profile 2000 (Figure 4.11a). Abundance of salt may be a major factor affecting these differences. Thin salt facilitate shear flow induced from brittle extension of overburden displaying domino style faulting or roho systems (Campbell, 2007; MacDonald, 2007; Kreszek et al., 2007). The abundance of landward dipping reflectors above the salt detachment (D) of profile 89-1 would therefore be a result of extensive faulting that sole into D, forming a roho system. In comparison, the thicker inflated allochthonous salt of line 2000 may have better facilitated extension through passive downbuilding driving salt extrusion and growth along diapir flanks, forming more broad packages.

Initially thin (< 1 km) salt deposits within profile 89-1 linked with higher sedimentation rates in the Jurassic than easterly line 2000 may account for the different timing of depocenters above the salt detachment/nappe. Higher sedimentation rates on relatively thin salt may have led to a more rapid and efficient evacuation of salt. Therefore salt may have been inflated at the autochthonous basin edge during the Middle Jurassic with subsequent development and termination (Late Jurassic) of the BSW in profile 89-1 much earlier than the salt nappe (Early Cretaceous) of line 2000.

4.5.3 Secondary canopy development

Line 2000 images a small (~ 10 km wide) canopy (SP 3650 in Figure 4.10) just landward of D4, with the feeder located nearby out of section. This salt body is easily distinguished by transparent and incoherent reflectors surrounded by high amplitude and highly stratified reflectors. The canopy diverges seaward with a minibasin located on its landward portion. The canopy appears to have formed during passive salt mobilization during the Early Cretaceous with continued seaward movement during the Late Cretaceous (Logan Canyon) due to differential loading of sediments.

Similarly salt bodies on higher secondary salt levels (canopies?) are interpreted beyond the shelf break of line STP-3 (SP 13500) (Figure 4.9) and perhaps line STP-6, outboard of the Orpheus Graben within Subprovince V (Laurentian Sub-basin) as mapped from Shimeld (2004) (Figures 4.1, 4.5). In both cases canopies have been passive during the Late Cretaceous (above Wyandot stratigraphic marker) and are associated with an erosional unconformity (Teritary?) (Figure 4.9). Shimeld (2004) portrays Subprovince V containing coalesced salt canopies as observed from mapped shallow salt structures related to the shallow secondary salt structures observed within STP-3 (Figure 4.5). Canopies are suggested to be fed by allochthonous salt along an outboard detachment surface (Shimeld, 2004), such as the allochthonous nappe and diapirs observed in line 2000. However, from interpretations of GXT line 2000 and the apparent location of the canopy overlying the boundary of autochthonous salt, it may be possible that canopies are

fed by autochthonous salt, or more likely large salt bodies riding the seaward salt basin border (D4) (Figure 4.10b).

4.5.4 Late stage contractional structures

Late stage contraction is evident across the eastern Scotian margin affecting both autochthonous and allochthonous salt. Above several salt diapiric structures (D2, D4 of Line 2000, Figure 4.10a) and small salt bodies along the salt nappe/detachment (lines 2000 and 89-1) domed and folded reflectors and sharply curving tangential reflectors occur in Cretaceous strata (Figures 4.4, 4.10). Crestal normal faulting in Cretaceous sediments above allochthonous salt in Line 2000 (SP 3550, 2800, and 2650 of Figure 4.10b) suggests compression of salt and reactivation of diapirs. Folded strata of Line 2000 are mostly Late Jurassic – earliest Late Cretaceous. However, similar folding within Line 89-1 is concentrated within Early – Late Cretaceous strata, including the Wyandot stratigraphic marker and younger sediments. Contractional structures such as folding are interpreted to affect sediments as young as Neogene age in Subprovince V (Shimeld, 2004). Due to extensive Tertiary erosion observed in line 2000 these features may have been eroded and overprinted with younger sediments (Figures 4.4a, 4.11a).

4.5.5 Orpheus Graben

The salt tectonic evolution of the Orpheus graben has been significantly different from the outboard passive Scotian margin. The variations of salt tectonic structures and

inferred evolutionary processes within the Orpheus Graben distinguish it from the rest of the Scotian margin. Therefore when considering the evolution of salt structures and basin evolution along the eastern margin south of the Canso Ridge, the Orpheus Graben is considered detached.

The Orpheus Graben formed as a result of reactivation along the Cobequid-Chedabucto fault zone during early Mesozoic rifting (see Chapter 3.1.2). Salt structures in the graben consist mostly of narrow vertical (Figure 4.9) diapirs that show occasionally late contractional deformation. Early – Middle Jurassic symmetrical expulsion rollover structures are indicated by broad seaward and landward dipping reflectors on both sides of mid-graben diapirs (Figure 4.9) suggesting that gravity driven salt tectonic processes (loading of sediments) within a restricted basement is responsible for vertical diapir growth.

Alternatively partial basement involved deformation (reactivation of faults) has recently been suggested as a source of salt mobilization (Durcanin et al., 2008). Frequent crestal faulting and folding of Middle Jurassic through Late Cretaceous sediments above diapirs suggests a late stage contractional event, similar to much of the margin. This reactivation of diapirs also affected the modern day configuration of salt structures within the graben.

4.6 Original salt basin geometry and salt thickness

The high amount of crustal extension and therefore subsidence (Funck et al., 2004; Keen and Beaumont, 1990) created a large accommodation space and thick syn-rift

sedimentary infill along the eastern Scotian margin in the earliest Jurassic. NovaSpan line 2000 shows thick stratified packages on top of interpreted basement, displaying growth along bounding syn-rift faults (Figure 4.4a). The seaward extent of syn-rift sediments is not completely known. Rifted blocks beyond Rb4 are assumed to have related syn-rift packages, but appear to be covered with deep-water equivalents originating from the abyssal plain (Sohm Basin) (Ebinger and Tucholke, 1988; Keen and Potter, 1995). For further discussion only those syn-rift packages of the autochthonous salt basin overlying basement of Rb1 – 4 are considered (Figure 4.4a).

As with basement structures the confidence with which syn-rift sediment packages are identified varies. In the east (Laurentian Sub-basin) syn-rift fill (above Rb1 – Rb4) is the thickest along the margin with a maximum of over 4 km (Wade and MacLean, 1990). Syn-rift packages on top of Rb3 and Rb4 appear to have the highest reflectivity and display rotated growth strata along northern bounding faults. Possibly another interior basement fault existed and then ceased to allow overriding sediments to be continuous over the two basement blocks (Figure 4.4a). Reflection signal at the top of Rb1 and Rb2 is chaotic and characterized by high amplitude noise. This noise may in part be due to multiples or migration as it appears in some locations (Rb2) to be conformable with overlying reflectors. Syn-rift fill above Rb1 and Rb2 is interpreted to have similar geometry and characteristics to that over Rb3 and Rb4.

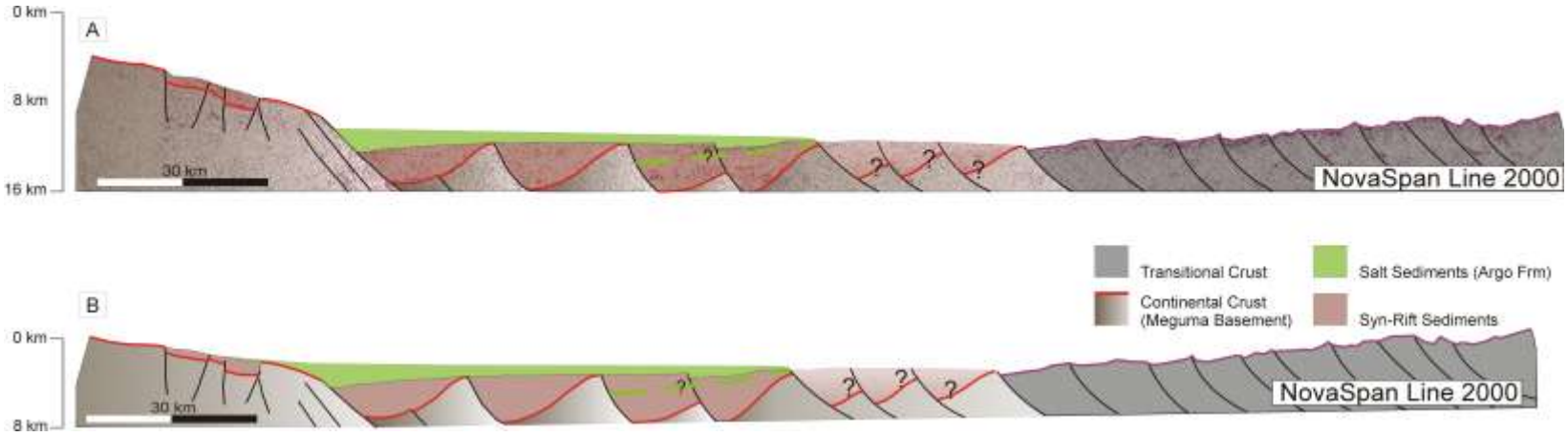

Figure 4.12. Schematic interpretation of NovaSpan line 2000 displaying original salt basin geometry (above syn-rift sediments) with overlying sediments stripped away (A) and restoration of basin flexure from loading illustrating the approximate late syn-rift/early post-rift configuration during salt deposition. Maximum salt thickness along the basin hinge is approximated at 3 km. The preferred interpretation of the original salt basin floor from preliminary seismic interpretation for modeling purposes is comprised of two (large landward / small seaward) asymmetric half graben seaward thinning wedges. Another interpretation (dashed green line) suggests that the basin floor consisted of two similar sized half graben wedges formed as a result of sediments draping over both autochthonous seaward rift blocks.

Argo salt is interpreted to directly overly the syn-rift strata. Although the top of salt has changed significantly throughout the post-rift basin evolution, the stationary base of salt is a reliable proxy for salt basin geometry (Figure 4.12). From the nature of interpreted salt, syn-rift and basement features, the autochthonous salt basin within line 2000 is considered from the hinge zone seaward to Rb4 near shotpoint 3750 (Figure 4.4a). Salt sediments further south are interpreted as allochthonous salt expelled from the original basin.

Generally, the base of salt has no easily distinguishable seismic signature, instead the base of salt is considered conformable with the top of syn-rift packages, mostly having a relatively low topographic profile. This interpretation coincides with the observation of thick syn-rift sediments infilling and levelling the rift topography of the basement. In some cases it is difficult to interpret a distinct base of salt, e.g. top of syn-rift package, above Rb3 and Rb4 where above syn-rift reflectors a seismic transparent zone exists. At this location (SP 4500 – 4000 in Figure 4.10a) the base of salt may consist of a small half graben wedge a maximum of 1 km deep and approximately 20 km wide (Figures 4.4a, 4.10a) based on high amplitude chaotic reflectors. Alternatively transparent seismic characteristics may signify a much broader (~ 40 km) and deeper (up to 3 km) half graben wedge geometry formed by sediment draping two rifted blocks after faulting between them ceased. Overall from the hinge to SP 4150 the base of salt is interpreted as a relatively conformable interface showing a wedge geometry thickening towards the hinge zone (Figure 4.12).

From both the interpretation of base of salt and approximated top of salt along the hinge of profile 2000 an estimated thickness of deposited salt is considered 2.5 - 3 km. Also considered is the mechanics of salt mobilization and related salt structures (eg., diapirs, salt withdrawal basins). These observations can be used as a proxy for initial salt thickness (Krezsek et al., 2007). This is discussed in section 4.3.1.

Interpretation of salt distribution and thickness display similar challenges in the seismic reflection data of profile 89-1. However velocity model data (Funck et al., 2004) provide further constraints for salt interpretation (Figure 4.7). In Subprovince IV salt structures in general are rare (Wade and MacLean, 1990; Ings and Shimeld, 2006). Velocity models suggest small trapped salt bodies above landward rifted basement blocks (Figures 4.4b, 4.7). Due to the limited resolution of crustal-scale velocity models the detailed interpretation of syn-rift features is not possible. However, it is evident that basement features have played a more important role in line 89-1 then in line 2000 farther to the east. Basement of Line 89-1 similar to Line 2000 forms an overall seaward thinning half graben wedge with a smaller half graben along the hinge zone (Figure 4.7).

In line 89-1 also a salt detachment (D in Figures 4.4b, 4.7) is imaged beneath the modern slope. This salt detachment has a similar ramp geometry and angle (~ 1°) as observed in profile 2000. The landward termination of this horizon near basement (Figures 4.4b, 4.7) represents the new seaward limit of the autochthonous salt basin suggesting that the salt basin extends over 40 km farther seaward than in previous interpretations (Wade and

MacLean, 1990; Shimeld, 2004; MacLean and Wade, 1992; Ings and Shimeld, 2006) (Figures 4.1, 4.5).

4.7 Depocenter characteristics and migration

Overall the major depocenters of the eastern Scotian margin (Line 2000) prograde seaward through time (Wade and MacLean, 1990) (Figure 4.11). Early – Middle Jurassic depocenters of the Mohican and Scatarie Formations are thickest along the shelf and proximal basin just beyond the hinge zone. Late Jurassic thick (up to 5 km) Mic Mac Formation and deepwater equivalent deposits are focused within the seaward portion of the autochthonous basin. The major depocenters of the Early Cretaceous Mississauga Formation and deepwater equivalents are located on top of allochthonous salt, with Late Cretaceous and younger sediments being thin on the modern shelf and mostly blanketing the deep basin.

Mohican/Scatarie (Middle Jurassic)

Beneath the shelf in profile 2000 the Scatarie Member and Mohican Formation show a maximum thickness of 2.5 km immediately northwest of the hinge (Figure 4.11a). However, a maximum thickness (~ 4 km) of this unit is reached between the hinge zone and D1, with seaward dipping reflectors seaward of D1 suggesting thinning of the sedimentary wedge. Seismic transparency of strata seaward of D2 make seaward

correlation of this unit difficult. Significant accumulation of the Scatarie and underlying units are not expected south of D2.

To the west in profile 89-1 a similar Middle Jurassic (Scatarie Member and Mohican Formation) seaward thinning sediment wedge is observed. A maximum thickness (> 2 s (twtt)) is reached just seaward of the hinge zone within landward half grabens and a the wedge thins significantly at approximately the same seaward position compared along strike to Line 2000 (Figure 4.11b).

Regionally the geometry of the Scatarie and underlying sedimentary reflectors suggests that Early and Middle Jurassic continental clastics were restricted in seaward extent. Major depocenters end near the modern shelf break, with thickest sediment accumulations just south of the hinge (~ 20 km).

Mic Mac (Late Jurassic)

Along NovaSpan line 2000 the Mic Mac Formation beneath the shelf reaches a maximum thickness of ~ 2.5 km. Deepwater equivalents increase in thickness rapidly south across the hinge to a maximum of over 5 km beyond D3 within the major depocenter of the Late Jurassic (Figure 4.11a) as a result of Laurentian Delta sedimentation. The average thickness of this entire unit is ~ 3 km, with a distinctive seaward shift (~ 60 km) in the location of major depocenters during this time.

It is difficult to determine the extent of Late Jurassic deposits beyond D4 due to the discontinuity of reflectors. From the downbuilding of seaward sediments above the allochthonous salt (nappe) and the orientation of reflectors landward of D4, significant depocenter accumulation is not likely.

To the west in profile 89-1 significant Late Jurassic (Mic Mac) sediment accumulations are more extensive outboard of the rift basin than in Line 2000, likely as a result of Sable Delta prodelta sediment input. Depocenters imaged above the salt detachment (D) are located from SP 2500 – 1000. However, similar to Line 2000 the thickest accumulation of Late Jurassic sediments occur in the distal portion of the autochthonous salt basin (~ 3 s (twtt), SP 2700, Figure 4.11b), also approximately 60 km seaward from Middle Jurassic (Scatarie/Mohican) depocenters within this profile.

Mississauga (Early Cretaceous)

Early Cretaceous (Mississauga) sediments beneath the shelf of profile 2000 are a maximum of only 500 m thick. Basinward of the hinge zone this unit thickens significantly, reaching an average of 1.5 km landward of approximately SP 4000, just landward of the salt canopy. However, the major depocenter of this time is located seaward of the salt canopy, above the allochthonous salt nappe (Figure 4.11a), reaching a maximum thickness of ~ 2 km, approximately 30 km seaward of previous Late Jurassic major depocenters.

Within profile 89-1 broad Early Cretaceous depocenters drape and cover the BSW (Late Jurassic) and related salt structures (Figure 4.11b). Thickest sediment accumulations are located seaward of the shelf-break between SP 2900 - 2000 with a maximum thickness of 1.25 s (twtt) (Figure 4.11b). These major depocenters are only slightly seaward (~ 10 km) when compared to older Late Jurassic deposits. As in line 2000 many normal shallow late – stage faults are observed just landward and along the shelf-break and slope. Broad widespread depocenters of this time are likely a result of earlier salt evacuation and the shut down of salt withdrawal basins acting as the locus for sediment accumulation.

Logan Canyon (Early/Late Cretaceous)

Along the shelf of profile 2000 the Logan Canyon Formation is thin (~ 1 km). Broad depocenters do not thicken significantly across the hinge zone and throw is minor. Only a slight thickening is observed until approximately SP 4800 across a large normal fault. Here the Logan Canyon reaches a maximum of over 2.5 km directly under the shelf break (Figure 4.11a), likely due to continued salt withdrawal. A thick minibasin is imaged on the landward flank of the salt canopy (SP 3750). Major depocenters also include thick (< 2 km) deposits above the landward edge of the nappe system, where sediments cover and seal small allochthonous diapirs. Broad sediment packages are the result of a broad coastal plain depositional environment as the Sable Delta had a diminished sediment supply during this time.

The location of major Logan Canyon deposits within line 2000 is notably landward (~ 35 km) than that of the underlying Mississauga depocenters. However, along the onset of the slope a widespread and highly erosive Tertiary unconformity (MacLean and Wade, 1990) truncates Late Cretaceous reflectors and the top Logan Canyon stratigraphic marker horizon. The unconformity becomes nearly tangential to the top Logan Canyon near SP 4100 (Figure 4.11a). Therefore the true thickness of the Logan Canyon Formation is not known beyond the erosional surface.

Within profile 89-1 a similar yet less variable trend in thickness is observed from the analogous Petrel Member seismic marker (Figure 4.11b) This stratigraphic horizon is nearly equivalent to the Logan Canyon top and displays a maximum thickness (~ 1 s (twtt)) under the shelf break. A Tertiary erosional unconformity is also present here, appearing to erode a significant portion of the Petrel Member and underlying Logan Canyon. Therefore the A^* deepwater horizon is used to correlate the top of this stratigraphic unit into the deep basin.

Late Cretaceous stratigraphy

Interpreted stratigraphy of the Late Cretaceous include the Dawson Canyon and Wyandot formations. These deposits are significantly lesser than older formations, with a cumulative thickness of approximately 700 m above the shelf in profile 2000 (Figure 4.11a). Basinward of the regional hinge zone this thickness does not significantly increase until immediately landward of the shelf break to a thickness of nearly 1 km.

Beyond the shelf break the same Tertiary erosional unconformity affecting the Logan Canyon Formation is interpreted to completely truncate the Dawson Canyon and Wyandot formations (Figure 4.11a). Seaward of this truncation no proximal deepwater wells are available and therefore interpretations are limited. However, the Tantallon M-41 well (Figure 4.1) is stratigraphically tied to profile 89-1 (Figure 4.11b). At this location the Late Cretaceous Wyandot Formation is present in well M-41. Here erosion is interpreted to consist of a maximum of 10 – 15 km beyond the shelf break with Late Cretaceous sediments (A^*) present seaward of well M-41. Due to their late timing regarding major salt mobilization, these stratigraphic units play only a very minor role in the salt tectonic history of this region.

Deepwater sediments

Correlations of Jurassic and Cretaceous deepwater (abyssal) marker horizons (J_2, J_1, and β) (Swift et al., 1986; Ebinger and Tucholke, 1988) equivalent to equivalent stratigraphic markers on the shelf, illustrate the continuous interaction between deepwater sedimentation and salt movement. Anomalous thick sediment accumulation outboard of the salt basin observed along the eastern Scotian margin suggests that sediments are derived from a combination of pelagic deepwater and significant prograding pro-delta (Sable Delta: Late Jurassic – Early Cretaceous; Laurentian Delta: Late Jurassic) sources (see Chapter 3.1.3). Considerable sedimentation outboard (basinward) of salt from the Jurassic (J_2, J_1, Line 89-1) through Early Cretaceous (J_1, β, Line 2000) is responsible for

the climbing ramp geometry of the extensive salt nappe/detachment system of salt Subprovince IV (Figure 4.11).

4.8 Derived analogue model constraints

Interpreted seismic features of the eastern Scotian margin are simplified and scaled for the purpose of including these constraints in analogue model experiments. 3D analogue experiments are dynamically scaled such that geometries, kinematics and stresses observed in the models are quantitatively comparable to natural prototypes (Costa and Vendeville 2002, Weijermars et al. 1993) (see Chapter 5.3). With a geometric scaling factor ($L^* = 10^{-5}$) applied, 1 cm in analogue experiments is equivalent to 1 km in nature. The time scaling factor, $t^* = 4.3 \times 10^{-10}$, deduced from the viscosity of salt and silicone, density of overburden, and load of the water column equates to one hour in models being equivalent to ~300,000 years of the geologic record.

The first order controlling factors believed to influence salt tectonic evolution and therefore the major constraints used in models are:

1. Initial salt basin geometry
2. Salt thickness
3. Sedimentation rates

4.8.1 Initial salt basin geometry and salt thickness

Detailed interpretation of the salt base or top of syn-rift deposits is challenging because of the limited quality of seismic reflection images at these great depths. However, high-quality regional scale interpretations that are required for constraining analogue modeling can be made. From seismic interpretation of profile 2000, the autochthonous salt basin is interpreted to exist between the regional hinge zone and the landward flank of D4, a distance of ~ 90 km (Figures 4.4a, 4.10a, 4.12). The overall geometry of the salt basin appears to be a seaward thinning wedge, with the deepest part of the basin along the hinge (Figure 4.12). Strong reflectors between shot points 4400 – 3900 located above stratified syn-rift fill and below basin stratigraphy, are taken to suggest salt emplacement (Figures 4.4a, 4.10a, 4.11a). At this position there is a step in the salt basement of approximately 500 – 1000 m (Figure 4.12). This step forms a second seaward dipping wedge that is approximately 20 – 25 km wide, the seaward tip of which marks the terminus of the autochthonous salt basin. For analogue modelling purposes, this base of salt interpretation in the RB3 and RB4 area is favoured over a wider (~ 40 km) and deeper (> 2 km) half graben wedge (Figure 4.10a). This interpretation is based on the apparent efficiency of allochthonous salt extrusion from the original salt basin.

Previous model results (MacDonald, 2007; Campbell, 2007; Kreszek et al., 2007) suggest that an overall single wedge shaped salt basin is extremely conducive for proficient allochthonous silicone mobilization. Seismic data indicates a prominent and extensive allochthonous nappe system in NovaSpan Line 2000. To produce an analogous salt structure through modelling, a wedge shaped salt basin with only a small offset half graben wedge is considered the best match (Figure 4.12). Thick syn-rift packages filling

basement rifted blocks of the eastern Scotian margin determine for the most part the geometry that salt was initially deposited in. However, the trend of rifted continental basement within the basin determines the overall form of the initial salt basin. In particular basement involvement is evident along the second basinward half-graben wedge, as it was lowered along reactivated basement faults (Figure 4.12).

Although the initial salt thickness within the western Laurentian Sub-basin is not known precisely, some assumptions can be made. The deepest interpreted salt deposits occur just seaward along the regional hinge zone (Figures 4.11a, 4.12). Here from an interpreted salt roller along the hinge fault zone and thick salt withdrawal basins, relatively thick (> 2 km) salt deposits are expected. The vast amount of salt withdrawal basins between diapirs and numerous passive downbuilding structures compared with previous analogue modelling results suggest the same (MacDonald, 2007; Campbell, 2007; Kreszek et al., 2007). Due to the thickness of these depocenters an approximate maximum salt thickness at the deepest portion of the landward wedge is taken to be 3 km (3 cm in the model). This landward wedge thins toward the seaward wedge reaching an estimated minimum thickness of 1.5 km (1.5 cm for model purposes) at the offset in the basement. The seaward wedge is thickest (~2 km; 2 cm in the model) at this step in the basement and thins out seaward (Figure 4.12). The available modelling apparatus cannot accommodate a ~ 90 cm (km) initial salt basin configuration, therefore a 70 cm wide salt basin was used with the wedges scaled to keep the width ratio between them as interpreted.

4.8.2. Sedimentation patterns and rates

Sedimentation rates of profile 2000 were calculated based on average formation (geological unit) thickness and duration (age) of major stratigraphic successions. Formation thickness for the previously described units (neglecting Late Cretaceous units) was measured every 10 km above the shelf, within the basin and above allochthonous salt. Sediments below the allochthonous salt nappe (ramp) seaward of the initial salt basin were neglected and assumed a result of mostly deepwater sedimentation, not directly linked with the progradation system driving salt tectonics in this region. Considering the duration of deposition for a stratigraphic unit and the calculated average thickness, an average sedimentation rate can be calculated (m/Ma).

Estimated sedimentation rates are therefore computed assuming no compaction due to loading and burial of originally deposited sediments. In reality sedimentation rates would therefore be higher. To compensate for this an approximation of compaction percentage can be calculated through approximating densities of stratigraphic units based on burial depth. From average density curves for sedimentary units with increasing depths (Jackson and Talbot, 1986) an approximated density for each formation can be calculated (Table 4.2). This is done in much the same way as the average thickness calculations. The average depth of each unit is calculated every 10 km within the boundaries previously stated. The average of these depths is then compared with the density curves to approximate a unit density. When compared to the density of sediments at the surface a percentage difference can be calculated. For simplification these percentage differences can be rounded and then added as a function of unit thickness to approximate an initial

depositional thickness and hence a new simplified decompacted sedimentation rate (Figure 4.3).

Although simplified, this method approximates natural sedimentation rates for the major four depositional units defined for this study (Scatarie/Mohican, Mic Mac, Mississauga, and Logan Canyon) (Figure 4.2). The assumption that each stratigraphic unit is a disconnected depositional episode is unrealistic. Units are averaged without the consideration of realistic transitions and fluctuations between the lithologic formations of the Scotian margin. However, sedimentation rates are only considered for the purpose of a regional modeling study of the depositional system of the eastern Scotian margin. Of importance is the effect of different sedimentation rates on salt tectonic evolution in this location. Therefore assumptions concerning complicated sedimentation input on the margin are acceptable.

NovaSpan line 2000

	Scatarie/Mohican	Mic Mac	Mississauga	Logan Canyon
Duration	25Ma	16.4Ma	23Ma	28.4Ma
Avg thickness	2076m	2956m	1427m	1343m
Avg sedimentation rate	83.04m/Ma	180m/Ma	62.04m/Ma	47.3m/Ma
Avg depth	7000 m	5800 m	4200 m	2500 m
Avg Density	2600kg*m-3	2500kg*m-3	2400kg*m-3	2300kg*m-3
Surface Density	2150kg*m-3	2150kg*m-3	2150kg*m-3	2150kg*m-3
% Avg (delta) density	20%	15%	10%	7%
Sed. Rate	100m/Ma	200m/Ma	70m/Ma	50m/Ma

Table 4.2. Estimated sedimentation rates and corresponding data for NovaSpan line 2000. Of particular interest is the difference between calculated average sedimentation rates and recalculated decompacted rates (red). See discussion for explanation of data calculations.

The calculated decompacted sedimentation rates of profile 2000 illustrate an overall trend of high sedimentation rates early in basin evolution (late syn-rift, early post-rift) that in

general diminish through time (Figure 4.2, Table 4.2). High sedimentation rates in the study area of 100 m/Ma within the Early – Mid Jurassic (Mohican and Scatarie) are the highest for these units along the Scotian margin (MacLean and Wade, 1990, Wade and MacLean, 1992). The eastern margin was a major depositional element during early development of the Scotian Basin, however the Mohican and overlying Scatarie formations do not vastly extend seaward. The localization of these units is most likely due to associated salt inflation and is considered instrumental in early seaward salt mobilization.

The peak of sediment influx along the eastern margin is within the Mid – Late Jurassic Mic Mac Formation and deepwater equivalents. With a decompacted sedimentation rate double (200 m/Ma) that of the Mohican and Scatarie formations, this episode accumulated very thick sediments within depocenters along the seaward half of the initial salt basin (Figures 4.3 and 4.11a). From preliminary seismic interpretation it is believed that this sedimentation period is responsible for such an efficient seaward extrusion of salt from the basin and inflation at the seaward terminus leading to the formation of the characteristic allochthonous salt nappe system. The climbing of the nappe system is interpreted to begin at this time and it occurred as a result of an upward movement of salt over the sediments accumulating in the deepwater.

Sedimentation rates in the Cretaceous are significantly reduced when compared to those of the Jurassic. During the Early Cretaceous (Mississauga) a decompacted sedimentation rate of 70 m/Ma has been calculated (Figure 4.2). However, the majority of sedimentation

during this period is concentrated in thick (up to 3 km) depocenters on top of allochthonous salt (Figure 4.11a). This distinctive sedimentary succession is expected to have driven allochthonous salt nappe formation and seaward expulsion through differential loading. The ramp geometry at the base of allochthonous salt persists as deepwater sediment accumulation keeps pace with salt and overburden translation.

Sedimentation rates during the Early – Late Cretaceous (Logan Canyon) is the least of the measured intervals at 50 m/Ma (decompacted) (Figure 4.2). During this period sediments cap the allochthonous salt nappe and nearly cover the mid-basin canopy, effectively shutting major salt movement down. Although some salt mobilization is still active, apparent from the salt withdrawal basin beneath the shelf break (SP 4600 – 4300, Figure 4.10a), it is very minimal and the majority of key features have developed.

4.8.3. Basin tilt

Although the differential load of a sedimentary wedge is considered the major factor driving salt tectonics along passive margin basins, basin tilt assisting seaward gravity gliding of overburden on a salt detachment will have significant implications (Rowan et al., 2004, Fort et al., 2004). Considerations have been made regarding the landward uplift of the eastern Scotian margin from seismic interpretation of the Avalon unconformity. This unconformable surface, a result of the Avalon Uplift, is often coincident with the top Mic Mac seismic marker horizon along the shelf (Figure 4.2). Truncating inclined reflectors onlapping onto top Mic Mac seismic marker horizons defining this feature are

easily mappable across the eastern margin (Figure 4.4). The most prevalent effects of the Avalon unconformity are observed on the Newfoundland margin with diminishing erosion to the west offshore Nova Scotia.

The truncation of underlying dipping reflectors within profiles 2000 (SP 6400 – 5700) and 89-1 (SP 6200 – 5700) (Figure 4.4), prevalent along the shelf, as well as prominent erosive surfaces within the Orpheus Graben (Figure 4.9) suggests that this event has strongly affected the entire of the eastern Scotian margin. Observations from seismic data suggest thermal inversion and mainland uplift conducive to a significant basinward tilt. Seismic interpretation of NovaSpan 2000 suggests that a major phase of seaward salt mobilization and inflated salt build up along the eastern margin responsible for allochthonous nappe development may correspond roughly to Avalon unconformity/top Mic Mac time and therefore basin tilt.

Chapter 5: Analogue modeling of the eastern Scotian basin

5.1 Analogue modeling overview

Analogue modeling of passive margin salt basins has improved greatly in the last two decades through the advancement of sedimentation procedures and scaling factors, development of regional scale studies, and more recently monitoring and visualization of models (Jackson and Talbot, 1986; Koyi et al., 1995; Talbot 1992, Vendeville and Jackson, 1992a; Vendeville and Jackson, 1992b; Ge et al., 1997; Vendeville, 2005, Krezsek et al. 2007, Adam et al. 2008).

New insights into the structural evolution of salt controlled sedimentary basins including extensional salt tectonics (Mauduit et al., 1997), formation of diapirs (Vendeville and Jackson, 1992b), and rollover anticlines (Mauduit and Brun, 1998; Vendeville and Jackson, 1992a; Ge et al., 1997) has gained attention from the petroleum industry focusing on reservoirs or traps related to salt structures (e.g., diapirs). However, few studies have focused on the regional evolution of syn-sedimentary structures within a passive margin sedimentary wedge, extending from the proximal extensional through distal (deep-basin) compressional domains (Fort et al., 2004; Vendeville, 2005). Other experiments have failed to employ realistic model timescales or sedimentation procedures simulating natural thin-skinned extension on salt at passive margins due to sediment loading.

The Salt Dynamics Group of Dalhousie University applies dynamically scaled 3D physical analogue experiments to investigate the evolution of passive margin salt basins, with emphasis on the interaction of salt tectonics processes from early salt mobilization in the rift basin to the late post-rift evolution of allochthonous salt. Experiments incorporate state-of-the-art 3D optical deformation analysis monitoring (DIC – Digital Image Correlation) (Adam et al. 2005; Adam et al., 2008; Krezsek et al., 2007) and geologic constraints (e.g., sedimentation patterns, salt thickness, salt basin floor geometry) deduced from seismic data.

This new generation of physical experiments incorporates regional geological data and seismic interpretation into model parameters and includes quantification of experimental deformation processes such as the kinematic coupling between extension in the shelf and slope and contraction in the deep-water basin.

5.2 Analogue modeling objectives

The main objective of the presented analogue experiments is to gain an insight into the post-rift basin evolution and salt tectonics history of the eastern Scotian Basin. The main 3-D scaled experiment represents the first order characteristics of the eastern Scotian margin:

1. basin architecture (salt basin geometry and basement morphology)
2. sediment input (volumes and sedimentation rates)

Experiment results were used to provide mechanically constrained concepts and structural templates for:

1. Kinematical modeling and regional correlations of salt features in the eastern Scotian margin
2. Paleogeographic reconstructions and tectono-stratigraphic framework for the development of salt province IV and western section of salt subprovince V.

These templates can be utilized to better understand and minimize uncertainty of salt-basin evolution with applications to petroleum exploration within the study area and potentially within similar salt provinces worldwide.

Specifically, experiment results will be used to solve questions generated by interpretation of regional seismic data from the eastern Scotian margin (NovaSpan line 2000, GSC line 89-1):

1. What is the geometry and seaward extent of the top Scatarie seismic marker horizon and older poorly imaged Mohican Formation?
2. How far do the top Mic Mac seismic horizon and its deepwater equivalents extend above allochthonous salt (seaward of D4)?
3. What are the geometry and kinematics of individual salt structures (D2, D4, allochthonous nappe)?

5.3 Materials and scaling

Sifted silica sand (grain size: 0.02-0.45 mm; angle of internal friction: 34°; density: 1.6 g/cm^3) is used in analogue models to simulate the non-linear frictional-plastic deformation behavior of brittle sedimentary rocks (Lohrmann et al., 2003; Adam et al., 2005; Krezsek et al. 2007; Adam et al., 2008). PDMS silicone polymer (Wacker Elastomer NA US; viscosity: 6×10^4 PaS at 20˚Celsius; density: 0.99 g/cm^3) displays linear viscous behavior under experimental strain rates and simulates the viscous flow of salt sediments under gravitational loading (Wejiermas, et al., 1993).

The 3D analogue experiments are dynamically scaled such that geometries, kinematics and stresses observed in the models are quantitatively comparable to natural prototypes allowing the study of basin structural evolution (Costa and Vendeville, 2002; Hubbert, 1937; Weijermars et al., 1993).

The geometric scaling factor is $L^* = 10^{-5}$ (eq. 1). When applied, 1 cm in analogue experiments is equivalent to 1 km in nature.

Eq 1: $L^* = \ell_m / \ell_p$; (ℓ is length, subscripts m / p refer to model / prototype)

The time scaling factor is $t^* = 1.4\times10^9$ (eq. 2). One hour in the model is equivalent to ~150,000 years of the geologic record. This time scale does not incorporate the effect of water load.

Eq. 2: $t^* = (\eta_m.\rho_p.\ell_p) / (\eta_p.\rho_m.\ell_m)$; where η is viscosity of salt or silicone and ρ is density of overburden.

Recent significant improvement of the time scale has been made using numerical model results to reflect the effect of water loading on passive margin salt systems (S. Ings, personal communication). Our re-calculated time scale t^*_{water} is 2.8×10^9 (1 hour in model ~ 300,000 years in nature). The new model time scale t^*_{water} has been successfully verified in experiments simulating Scotian margin settings.

5.4 Main 3-D experiment setup and procedure

3D analogue experiments were performed on a horizontal rigid base plate (120 cm length × 90 cm width) (Figure 5.1). The basin margins and floor of the post-rift salt basin were built with sand. Silicone putty was placed in the accommodation space and allowed to spread into a flat layer over a couple of days forming the salt basin. Basin geometry and original salt thickness were constrained from seismic interpretation.

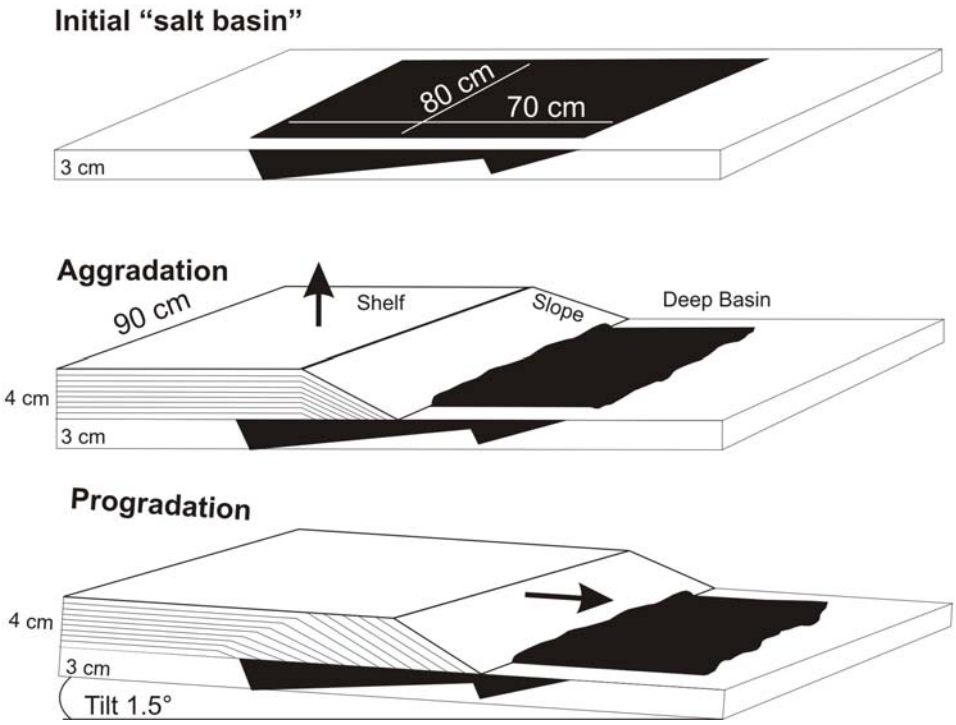

Figure 5.1. Initial experiment ("salt basin") setup and sedimentation procedures for eastern Scotian margin 3D analogue model. Salt thickness and salt basin (black) geometry interpreted from GXT NovaSpan line 2000 consists of two asymmetric half-graben wedges. Aggradation phase of models simulates shelf build up. Progradation phase simulates sediment bypass onto the slope. White and black signify sand and silicone respectively.

Sand volumes and sedimentation rates of models were also deduced from seismic data. Incremental sieving of sand onto the shelf and slope of the model basin using a predefined constant volume of white and coloured sand per time interval has been used to simulate river and delta discharge (Figure 5.2) during aggradation and progradation phases of the post-rift basin.

During the initial aggradation stage the shelf wedge was built incrementally to a predetermined total thickness (4 cm) using a height – adjustable guide and rail system. Incremental sieving of sand layers every 4 – 8 hours for the duration of 3 days simulate

shelf build up during an early post rift relative sea level rise (Figures 5.1, 5.2a). Following shelf build-up, progradation onto the slope area begins and continues for the experiment duration (9 days) simulating the subsequent basinward migration of depocenters with little or no sedimentation on the shelf (Figures 5.1, 5.2a).

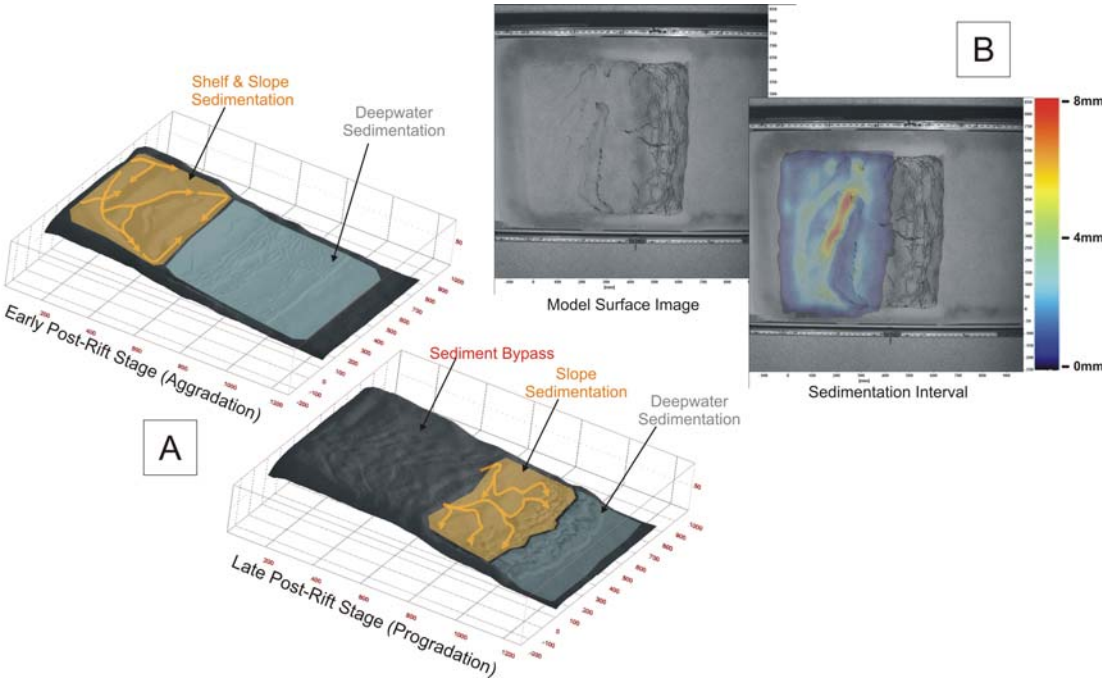

Figure 5.2. Detailed look at sedimentation procedures of 4D analogue model. A) Aggradation phase: sediments are built up on the shelf to a height of 4 cm (4km). Progradation phase: sediment bypass shelf and prograde onto the slope. Orange overlays: highest sediment input. Arrows- sediment fairways defined by model surface topography. Grey overlays: small amounts of deepwater sediment deposition. B) Sediment budget for one sedimentation interval during the aggradation stage with constant sand volume. Colour overlay shows variations in thickness variation of deposited sand illustrating increased sediment input into actively subsiding depocenters landward of diapir ridges blocking sediment transfer into basin.

The sieving procedure provides homogeneous mechanical conditions in the sand layer and allows specific sedimentation patterns in response to the morpho-structural evolution of the experiment surface (Adam et al., 2005; Adam et al., 2008). As in nature topographic features control sediment transport from shelf to slope. Subsiding grabens and withdrawal basins receive increased sediment input as in natural depositional systems

(Figure 5.2b). Positive surface elements such as diapir heads and canopies control the location of these sediment fairways along the slope and deep basin.

The completed experiment was sectioned in dip-direction (shelf-to-slope) in 5 cm intervals. Sections were photographed and individual photographs are visually optimized and stitched together using image processing software to produce cross-sections of the model.

These sections were structurally interpreted to analyse the (shelf-to-slope and along-strike) variations of silicone, fault, and related depositional structures. Interpreted model cross-sections formed the basis for sequential balanced restorations that demonstrated the structural evolution of the model. Knowledge gained from model evolution was applied to better understand the development of salt structures within the eastern Scotian margin.

5.5 Optical strain monitoring

DIC – Digital Image Correlation is an optical deformation monitoring technique adapted for the quantification of 2D/3D surface flow and deformation in analogue experiments (Adam et al. 2005). Time-series digital images of the model surface are taken from two high-resolution digital cameras in stereoscopic configuration (Figure 5.3). Surface evolution, subsidence and fault kinematics of the experiments are analyzed from 3D displacement field data and computed strain derivates allowing quantification of small and large-scale model deformation with sub-millimeter accuracy. Such deformation includes incremental and finite values for: horizontal displacement (v_x), subsidence (v_z),

and horizontal strain (e_{xx}). This quantitative time-series deformation and surface data allows accurate structural restorations of model sections and invaluable insights into the 3D basin scale evolution, timing and mechanics of salt related structures.

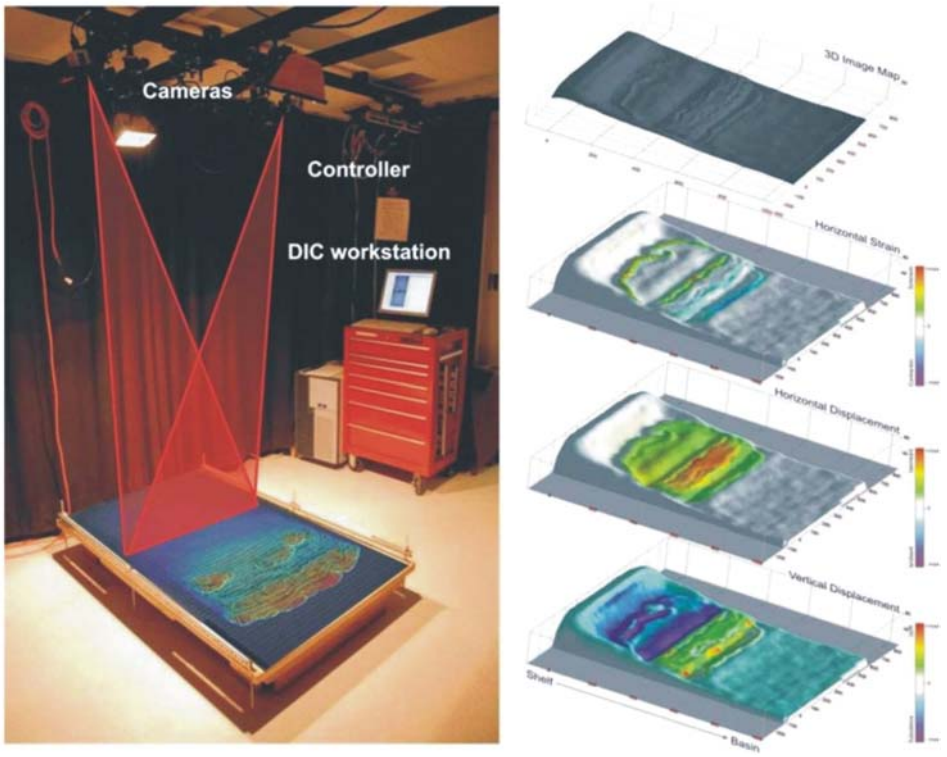

Figure 5.3. Overview of the strain monitoring system used for analogue modeling. (Left) Experiment setup with stereoscopic DIC monitoring system with two high resolution CCD cameras. Derived displacement data shown as vector grid on experiment surface. (Right) Example 3D DIC experiment data from top to bottom: 3D surface image, horizontal strain, horizontal displacement, and vertical displacement data of early experiment stage (Adam et al., 2009 *in press*).

5.6 Implications for main 3-D experiment setup deduced from previous pilot experiments and parameter study

Previous results of analogue experiments and sensitivity analyses of generic passive margin salt tectonics of the Salt Dynamics Group have been implemented in the setup of

the main analogue model of the eastern Scotian margin. Concepts derived from the previous studies were included in the development of the experiment deduced from the seismic interpretation of NovaSpan line 2000, particularly regarding (1) salt basin geometry, (2) initial salt thickness and (3) sedimentation rates.

(1) Salt basin geometry

An overall wedge shaped salt basin geometry was considered the best approximation for the eastern Scotian margin (line 2000) from previous pilot experiments due to the efficient and continuous extrusion of silicone forming an allochthonous nappe. Silicone was gradually and effectively extruded from the half graben wedge original basin. This characteristic was considered a function of flow vectors within the silicone. As silicone was mobilized basinward along the half graben, thinning of the wedge produced mid-basin inflation. This is due to a concentration and subsequent slowing of flow vectors along the thinnest portion of the wedge. The delayed silicone extrusion of inflated silicone led to the formation of a basinward massif at the autochthonous basin edge. The flow of silicone increased as the salt massif formed an allochthonous nappe through near horizontal flow and overriding sedimentation.

Although an overall half-graben wedge geometry is considered appropriate from a modeling standpoint, seismic signatures within line 2000 suggest a two half graben salt basin configuration. However, interpretational constraints are limited and allow for two end members: 1) the basinward wedge may have a small offset and originate above rift-

block 4 (Rb4); 2) the basinward wedge may be large and be present above Rb 3 and 4 (see Figure 4.4 of Chapter 4).

(2) Initial salt thickness

The abundance of large salt-withdrawal basins with very thick Jurassic to early Cretaceous sediment infill, broad expulsion rollover structures, lack of extensive deep-seated fault structures and abundance of salt within seismic data of the eastern margin (line 2000) indicate a very thick original salt layer deposited during late syn-rift to early post-rift periods of the eastern Scotian margin. An approximate maximum salt thickness at the deepest portion of the landward wedge is estimated to be 3 km (3 cm in the model) (see Section 4.8.1).

(3) Sedimentation rates

Previous modeling suggests that very high sedimentation rates (up to 5mm/h or 1500 m/Ma) evolve from extensive early, mature and collapsed basinward growth fault/rollover systems into landward listric fault/rollover systems (only in experiments with thin salt >1.5 cm), in some cases sealing all extensional structures. However, lower sedimentation rates favour the development of long-lived diapir/rollover systems with the formation of basinward growth fault/rollover systems. Such characteristics are similar to those of the eastern margin as imaged by line 2000.

These extremely high sedimentation rates used in prior experimentation are not reached during any time across the Scotian margin, with highest sedimentation rates occurring during the Jurassic to Cretaceous at <300 Ma. However, some global salt provinces (e.g. Santos Basin, Campos Basin, Angola Basin or Golf of Lyons) have seen episodes of very high sedimentation leading to the formation of specific structures similar to modeling results (e.g., Capo–Frio fault zone, Santos Basin).

5.7 Pilot experiments performed for this study

Two pilot experiments consisting of end-member initial salt basin geometries, including a half graben wedge (experiment 1) and a two half graben wedge (experiment 2) setup (Figure 5.4, Appendix B), were conducted to compare the structural and temporal evolution of the models. Results were then integrated to support interpretations of the eastern Scotian margin salt basin morphology. Results from pilot experiments were utilized to develop the setup of the large-scale 3-D strain monitored experiment.

5.7.1 Objectives and setup

Both pilot experiments test the role of very thick silicone layer (max. 3 cm) simulating thick initial salt deposits (3 km along the hinge zone). The half graben experiment consisted of a 35 cm long wedge and the two half graben experiment was formed by two 20 cm long wedges, while both experiments were performed in a 30 cm × 80 cm box (Figure 5.4, Table 5.1).

Experiment	Basin Geometry	Shelf buildup	Sedimentation Rate	Duration
Pilot exp 1	Half graben wedge: 35 cm length, 3 cm max silicone	4 cm	0.25 cm/4 hours	222 h
Pilot exp 2	Two half graben wedges: 20 cm length (each), 3 cm max silicone	4 cm	0.25 cm/2 hours (day time/12 hours) and no sedimentation (night time/12 hours)	170 h
Main 3D exp	Two half graben wedges: 55 cm length, 3 cm max silicone - 15 cm length, 2 cm max silicone	4 cm	Simulating important chrono-stratigraphic intervals of the Scotian margin (see Table 5.2)	296 h

Table 5.1. Experiment parameters for all analogue experiments completed for this study.

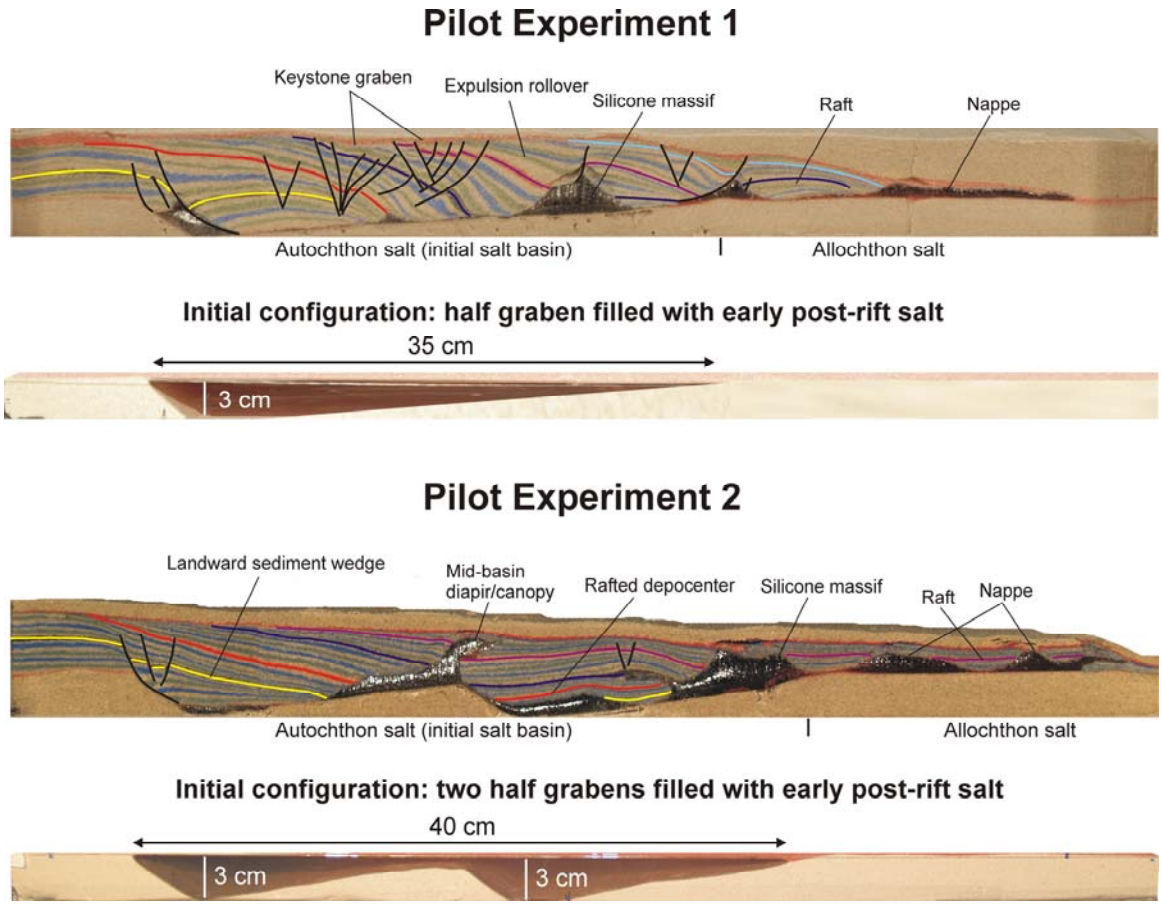

Figure 5.4. Salt basin experiment setup and representative cross-sections (12.5 cm Appendix B) of pilot experiments 1 and 2 (Table 5.1). Coloured horizons represent equivalent stratigraphic markers.

Identical scaled sedimentation rates were implemented for both experiments simulating high Jurassic sediment input of 200 m/Ma. For the half graben experiment (exp. 1) sieving intervals were 2.5 mm/4 hours. However the two half graben experiment (exp. 2) sieving schedule consisted of 2.5 mm/2 hours during the day time (for a total of 12 hours) followed by a sedimentation break during the night time (12 hours). Therefore through the course of one day (24 hours) sedimentation amounts were constant. Models with

prolonged sedimentation breaks show more extensive silicone canopies forming at the experiment surface. However, these breaks in experiment sedimentation give insight into salt tectonic behavior under natural stagnant conditions, such as transgressive periods or local basin areas with stagnant sediment input.

5.7.2 Temporal evolution

Overall the aggradation phase of model evolution between the two pilot experiments was very similar. Salt withdrawal basins start down building into the landward portions of asymmetric silicone basins, with differential subsidence being accommodated by normal faulting along the landward silicone basin edge. Silicone extrusion in the proximal basin caused by rapid subsidence of depocenters led to contemporaneous inflation of silicone in the distal basin and formation of a silicone massif in the basinward portion of the initial silicone basin.

During the progradation phase of experiment 1 (Table 5.1), sediments onlap on the landward flank of the silicone massif (Figure 5.4). With further sedimentation onlapping strata are rotated downwards due to the basinward evacuation of silicone, forming an expulsion rollover. This downward rotation of subsiding sediments causes the formation of an extensive rollover anticline with laterally extensive keystone grabens and welding along the landward base of silicone. With weld formation progradation of clinoform packages continued seaward producing a series of progressively younger keystone grabens in the basinward segment of the half graben wedge (Figure 5.4).

Within experiment 2 however, extensive rollover and associated keystone graben (faulting) structures are nearly absent (Figure 5.4). Instead as strata onlapped onto the silicone massif diapirs formed and were trapped in the first half graben as younger depocenters migrated seaward. Decoupling at the landward border of the second wedge led to the downbuilding of depocenters into silicone within the second half graben wedge. Subsidence of these sediments led to rafting of early depocenters forming a laterally extensive mid – basin diapir (Figure 5.4) and basinward canopy. As in experiment 1 a salt massif forms along the basinward margin (ramp) of the initial silicone basin.

In both experiments the advancement of the allochthonous nappe system was linked closely to the final stage of basinward evacuation of the silicone massif on the basin margin and overriding sedimentation, further driving silicone extrusion through differential loading. As depocenters migrated basinward on top of the allochthoneous silicone nappe, passive diapirs and intervening minibasins developed.

5.7.3 Structural cross-sections

Interpreted cross sections for both models are shown in Appendix A. Overall structures observed in both models are similar. The proximal portion of both initial silicone basins show a welded sedimentary wedge, as most of the silicone has been extruded basinward (Figure 5.4).

In experiment 1 the major diapir, forming the remnant of the silicone massif, is located at the basinward margin of the silicone basin (Figure 5.4). Some smaller diapirs remain trapped as well, such as the diapir located in sections 22.5 – 30 cm along the landward portion of the silicone basin (Appendix B). The most prominent features of experiment 1 are the extensive mid-basin expulsion rollovers and keystone grabens (Figure 5.4), demonstrating long-lived and very efficient basinward expulsion of silicone out of the initial basin.

Experiment 2 however, displays a somewhat different configuration of structures. Although a major salt body is also located at the basinward edge of the silicone basin, major diapirs are located on the intervening high dividing the half grabens (Figure 5.4), and to a lesser extent midway within the landward half graben. Remnant diapirs are found within the bottom of the second half graben wedge. Two distinctive depocenters (Figure 5.4) are located within the two half graben wedges through decoupling as the mid basin diapir formed. Although extension is apparent from the rafting and translation of early depocenters through this decoupling, faulting is very limited suggesting passive downbuilding as the main mechanism of basinward extrusion of silicone.

Basinward of autochthonous silicone, both models developed similar allochthonous nappe systems (Figure 5.4). On the allochthonous salt nappe level minibasins and intervening small diapirs formed in the late stage with sediment overburden consisting of rafts and rolled strata.

5.7.4 Conclusions

Pilot experiment results demonstrate that thick salt effectively reduces the mechanical coupling between the ductile layer (silicone) and sedimentary overburden. This low mechanical coupling favours channel flow in the ductile layer and passive diapirism and downbuilding of sediments instead of listric faulting and salt roller formation characteristic for thin salt and strong mechanical coupling. The experiment structures are consistent with the observed structures in the seismic data.

For experiment 1, a long-lived sedimentary wedge developed into expulsion rollovers and associated keystone grabens due to prolonged expulsion of silicone out of the initial basin as the wedge continually thins seaward. This interplay of continual and prolonged expulsion of silicone from the initial basin formed an extensive allochthonous nappe with overriding sediments keeping pace with silicone extrusion displayed through some fault rollover development.

However the sedimentary wedge in the proximal silicone basin of experiment 2 did not display significant rotation and expulsion rollovers. As silicone was expelled from the first half graben wedge it was able to merge with silicone of the second wedge. While depocenters migrated on top of the inflated silicone, sediments again subsided into silicone through passive downbuilding similar to the first wedge. In contrast to experiment 1 with continual expulsion of a single salt massif throughout the majority of

model evolution, the two – stage inflation of silicone in the individual half grabens, delays salt nappe extrusion in experiment 2.

Although the mid basin development of structures was different for the two models, salt massif development on the distal margin of silicone basins and extruded allochthonous silicone was quite similar. This is likely due to the characteristic salt tectonic behavior of a basinward-thinning wedge, slowing silicone extrusion through inflation of a silicone massif at the margin. Sediment loading over the basinward salt massif was key in developing the allochthonous nappe and was similar for both models.

5.7.5 Lessons learned: constraints for main 3-D experiment

Geologic constraints deduced from regional seismic data and salt tectonic concepts derived from previous analogue experiments have produced a clear view of the first-order characteristics and control factors of the post-rift eastern Scotian margin salt basin. These constraints must be integrated into the main 3-D experiment. The characteristic features of the eastern Scotian margin salt tectonic systems as interpreted from NovaSpan line 200 are:

1. Initial salt basin morphology composed of two asymmetric half graben wedges.
2. Thin-skinned rather than thick-skinned salt system.

3. A several km thick Early Jurassic (Mohican/Scatarie) sedimentary wedge in the landward portion of the salt basin.
4. Broad triangular diapirs affecting mostly Jurassic strata distributed within the autochthonous salt basin. Diapirs are mostly buried and sealed during the Early Cretaceous.
5. Lack of significant normal faults or steeply rotated expulsion rollovers within the Jurassic and Early Cretaceous overburden.
6. Extensive allochthonus salt nappe system formed over a regional ramp with stratified deepwater sediments in the footwall. A canopy is imaged just landward of the basinward edge of the initial salt basin, within Early Cretaceous sediments.
7. During the Early Cretaceous, late-stage progradation of sediments on top of allochthonous salt formed minibasins separated by small diapirs.

In order to simulate these important characteristics of the eastern Scotian margin the main 3-D experiment will have the following constraints:

1. **Silicone basin geometry consisting of two half grabens –** Seismic reflection data is interpreted to suggest an initial salt basin composed of two asymmetric half graben wedges. The size ratio between half graben wedges is difficult to determine from seismic data. From a preferred seismic interpretation due to recognizable seismic signatures and the expected continuous extrusion of salt necessary for nappe development a smaller second wedge is implemented in the

main 3-D experiment (Figure 5.5). This geometry is composed of two half grabens, but overall the basin still tapers steadily seaward.

2. **Thick primary salt layer –** Channel flow within a salt layer is considered necessary to allow quick passive downbuilding of sediments. Channel flow is dominant in experiments with an initial silicone thickness of > 1.5 cm (~ 1.5 km). Thin silicone favours horizontal basinward translation and extension of overburden through extensive faulting.

3. **Late stage allochthonous nappe system –** Both pilot experiments 1 and 2 were capable of forming extensive allochthonous nappe systems through the continued expulsion of silicone. Effective extrusion of silicone seaward limited the formation of extensive diapirs or canopies in the landward basin.

5.8 Main 3-D experiment setup

5.8.1 Initial salt basin geometry and salt thickness

The "salt" basin configuration of the main 3-D analogue experiment is illustrated in figure 5.5. The major silicone basin is a seaward thinning half graben wedge, as discussed for NovaSpan profile 2000. A smaller half graben wedge constitutes the basinward terminus of the rift basin formed by the offset of syn-rift sediments along reactivated basement faults.

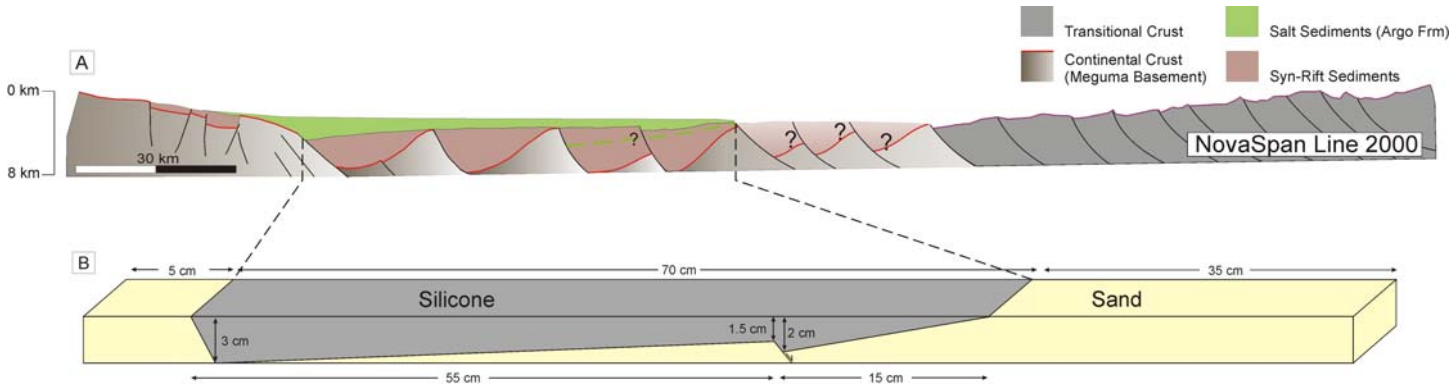

Figure 5.5. Salt basin geometry of the eastern Scotian margin (line 2000) and model setup of main 3-D experiment. A) Schematic interpretation of NovaSpan line 2000 displaying restored original post-rift salt basin geometry. Maximum salt thickness along the basin hinge is approximately 3 km.

The maximum silicone thickness along the hinge is 3 cm (equivalent to 3 km), with a maximum silicone thickness of the second wedge being 2 cm (Figure 5.5). Previous sensitivity analyses of silicone thickness (Campbell, 2007; MacDonald, 2007; Krezsek et al. 2007; Fort et al., 2004) showed that passive downbuilding is dominant with silicone thicknesses of over 1.5 cm. A 3 cm maximum thickness approximation is made from interpretations of remnant salt and thick salt withdrawal basins near the hinge zone of line 2000.

The initial salt basin geometry of the experiment was down-scaled slightly to a width of 70 cm (= 70 km in nature) from the interpreted 90 km autochthonous salt basin of line 2000 to meet experiment requirements. The experiment setup of the initial salt basin geometry and salt thickness together with interpretations from seismic profile 2000 are displayed in Figure 5.5.

5.8.2. Sedimentation patterns and rates

Model sedimentation rates were calculated to represent major depocenters observed in NovaSpan profile 2000 (Figure 5.6). High sedimentation rates (2.5 mm/8 and 4 hours for the Scatarie/Mohican (100 m/Ma) and Mic Mac (200 m/Ma) equivalents) (Table 5.2) characterize early basin evolution, respectively. Lower sedimentation rates constitute the remainder of model development during equivalent Cretaceous time (> 140 hours). A sedimentation rate of 1.7 mm/8h – 70 m/Ma and 1.5 mm/8h – 50 m/Ma characterize Mississauga and Logan Canyon time respectively (Table 5.2, Figure 5.6).

Table 5.2 presents the deduced sedimentation rates for the selected chrono-stratigraphic units and corresponding scaled experiment sedimentation rates. These data consist of volume sand and layer thickness for individual sieving intervals (hours). An experiment schedule provides a schematic comparison of model and corresponding geologic time intervals (Figure 5.6). The volume of sand needed for each sieving interval is calculated based on the dimensions of the model setup.

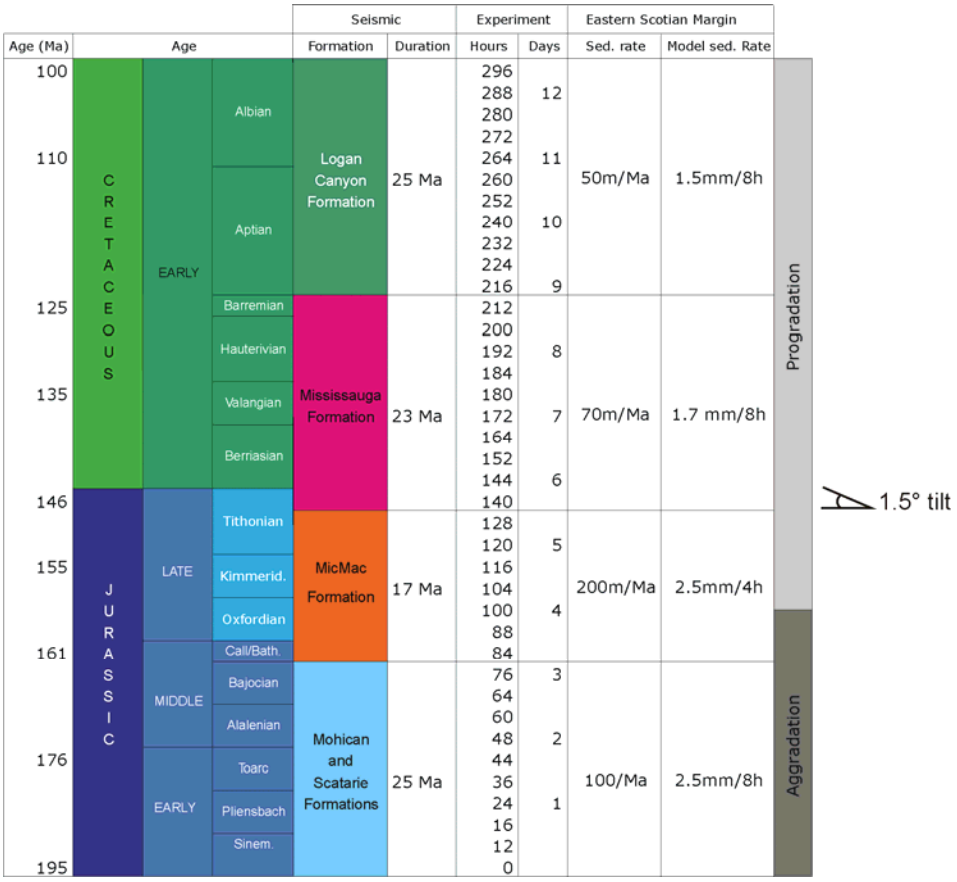

Figure 5.6. Main 3-D eastern Scotian Margin experiment schedule. Equivalent geological formation depositional phases, scaled sedimentation rates, model aggradation and progradation phases and model tilting are indicated.

Sieving intervals are considered in either 4 or 8 hour intervals to simulate continuous sediment input. Minimum thickness of a sand layer deposited in individual sieving intervals is approximately 1.5 mm.

Time	Formation	Duration	Sed Rate	Model Duration	Model Sed Rate (thickness)	Model Sed Rate (volume)	Sed Rate (vol) in nature
Early - Mid Jurassic	Scatarie/Mohican	25 Ma	100 m/ Ma	80 h	2.5 mm / 8 h	550 cm^3 / 8 h	228 km^3 / Ma
Mid - Late Jurassic	Mic Mac	16.4 Ma	200 m/ Ma	56 h	2.5 mm / 4 h	720 cm^3 / 4 h	600 km^3 / Ma
Early Cretaceous	Mississauga	23 Ma	70 m/ Ma	80 h	1.7 mm / 8 h	595 cm^3 / 8 h	248 km^3 / Ma
Early Cretaceous	Logan Canyon	28.4 Ma	50 m/ Ma	88 h	1.5 mm / 8 h	440 cm^3 / 8 h	183 km^3 / Ma

Table 5.2. Analogue modelling sedimentation constraints derived from NovaSpan seismic profile 2000.

5.8.3. Basin tilt

Although basin tilt along the eastern Scotian margin is evidenced by the Late Jurassic/Early Cretaceous Avalon Unconformity, the amount of uplift or tilt is very difficult to quantify. The extent of uplift is variable across the margin. In the study area, maximum uplift documented by extensive erosion was observed within the landward Orpheus Graben. Previous sensitivity analyses concerning experiment tilt suggest that a basinward tilt of < 1° does not notably affect model evolution. Considering this a gentle tilt of 1.5° was implemented for the main 3D experiment. Although margin uplift is a progressive event, based on the strong correlation between the timing of the Avalon unconformity and shortly after (Early Cretaceous) allochthonous salt mobilization observed in profile 2000, the tilt of the experiment base was carried out in one phase during the Late Jurassic (~ 155 Ma) or 128 h model time (Figure 5.6), simulating a moderately rapid basinward tilt.

5.9 Main 3-D experiment results

5.9.1 Overview

The results of the 3D main analogue experiment based on geologic constraints from seismic data (basin morphology, salt thickness, and sedimentation rates) provided insight into:

1. Timing and mechanics of salt mobilization
2. Salt-sediment interaction and depocenter history
3. Basin-scale structural evolution from early (Early Jurassic) salt mobilization in the landward post-rift basin to late allochthonous deformation of "salt" along the deep basin (Early Cretaceous).

The model ran for a total of 296 hours (~ 100 Ma) simulating basin evolution from the early post-rift stage in the Early Jurassic (Sinemurian) throughout the late post-rift stage in the Early Cretaceous (Albian) (Table 5.2). The shelf build-up phase ended at 100 hours followed by progradation for the remainder of the experiment. A 1.5° tilt was implemented at 128 hours simulating margin uplift as evidenced by the Avalon unconformity along the shelf of the eastern Scotian margin at Late Jurassic time.

3D displacement data were calculated by DIC from time-series images of the experiment surface. Derived displacement components and srain derivates in the form of incremental and finite values of horizontal displacement (v_x), subsidence (v_z), and horizontal strain (e_{xx}) allow insight into the salt tectonic evolution of the scaled model.

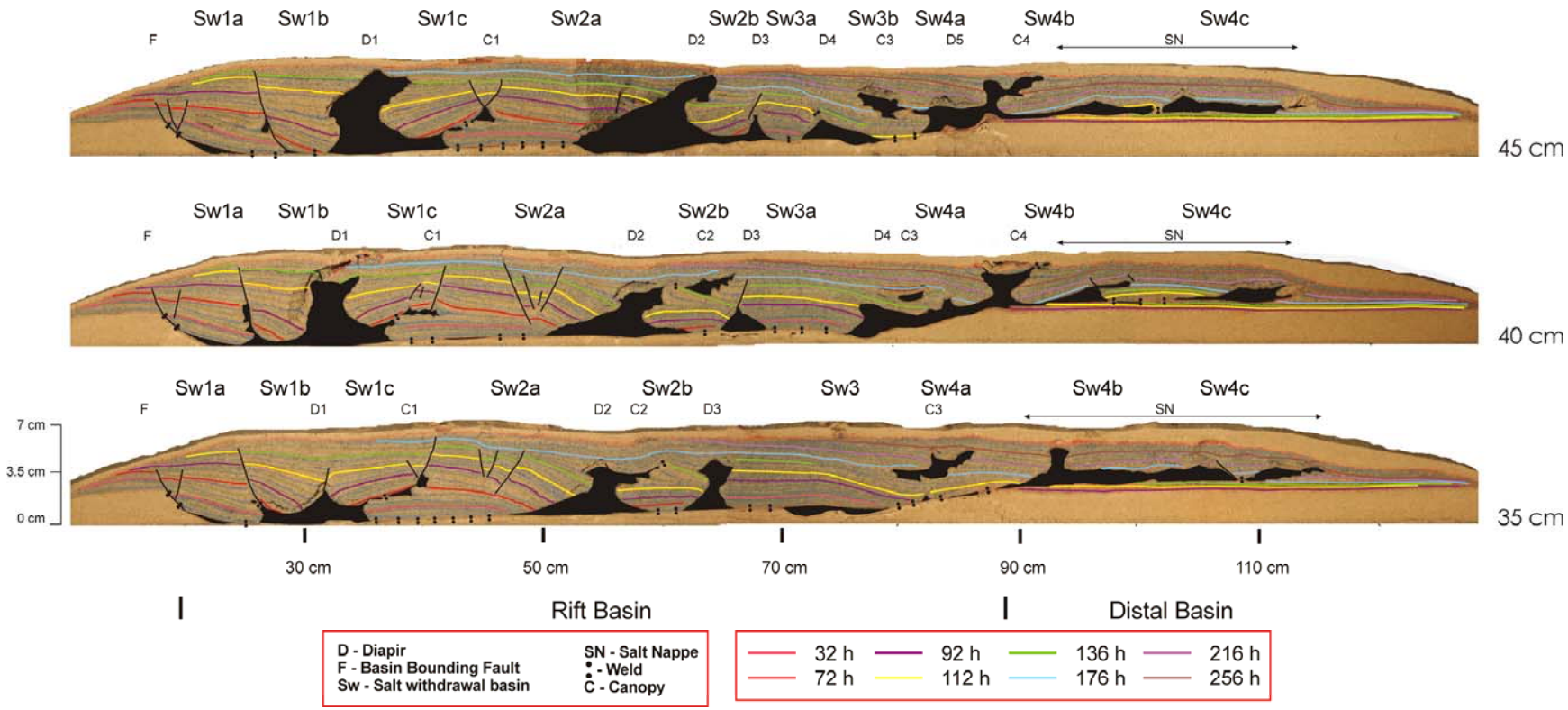

Figure 5.7. Central cross-sections of the main 3-D experiment simulating the eastern Scotian Margin. Coloured horizons illustrate the final placement of different timed sedimentation intervals (hours). Black overlays cover transparent silicone. Salt withdrawal basins are labelled for sections, but these depocenters were not active throughout basin evolution. For an illustration of when salt withdrawal basins were active or welded (shutdown) see Figure 5.8 or Appendix C. Silicone diapirs (D), canopies (C), and a nappe system (SN) correlatable across model sections are labeled.

5.9.2 3D structure

The 3D structure of the final experiment stage shown in figure 5.7 depicts three representative cross-sections located near the center of the concluded model (35 – 45 cm). The complete set of experiment sections is located in Appendix B. The overall structural characteristics of the experiment sections are similar as a consequence of the identical along-strike basin morphology and comparable sedimentation patterns. However, individual structures and depocenters demonstrate important 3-D variations from one section to another. These differences are linked to local variations in deposition, associated subsidence rates, and silicone flow.

Rift basin

A laterally continuous basinward listric growth fault (F in Figure 5.7) marks the landward (proximal) boundary of the silicone basin within model sections. Faulting was active during early salt extrusion of silicone from the proximal rift half graben and ceased between hours 72 – 92. Thickest sediment accumulation (up to 7cm) occurs within the landward portion of the silicone basin. Major salt withdrawal basins (Sw1-4 in Figure 5.7) are located between autochthonous silicone structures (D1- D4) and range in width from 5 – 15 cm. Subsidence through the expulsion of silicone led to the formation of extensive welds (Sw 1-3, Figure 5.7). Extensional structures within sediments of the silicone basin consist of expulsion rollovers (including minimal keystone grabens facilitating rolling) and rafts. Small normal faults are present, but not common suggesting

that the majority of salt mobilization was facilitated by passive downbuilding.

Final silicone structures within the rift grabens include trapped/sealed passive diapirs (D1 – D4, Figure 5.7) and associated second level canopies. Variations in structures are observed along strike, but first order characteristics of basinward leaning diapirs (5 – 10 cm wide, 2 – 6.5 cm high) having frequent silicone overhangs are continuous throughout the model. Welding along landward canopies (C1, C2, Figure 5.7) is common with canopy formation on the landward side of D1 acting as a major depocenter with subsidence accommodated by basinward normal faulting above the salt detachment. Along strike D1 appears to change from a bulbous vertical diapir in some sections (45 cm, Figure 5.7) to a series of landward and basinward verging expulsion rollovers (35 cm, Figure 5.7). A basinward canopy (C2) is present along much of the D2 axis, remaining passive through most of the basin evolution.

Landward diapirs (D1, D2 Figure 5.7) remain active through the majority of model evolution. The initiation of D2 was symmetric, similar to D1, which later transitioned into a basinward leaning asymmetric diapir. D3 consists of trapped silicone that is related to the formation of D2. The two diapiric structures are separated by a narrow salt withdrawal basin (Sw2b, Figure 5.7) and often a landward dipping normal fault. D4 and D5 are similar and also consist of trapped and sealed silicone. At the end of the experiment D4 is located at the landward border of the second rift half-graben with D5 at its basinward termination. These structures vary quite significantly along strike, and are not present in some sections (Figure 5.7).

Distal basin

Allochthonous silicone within model sections consists of a nappe system composed of extruded silicone mobilized from the initial rift graben "salt" basin. Most basinward silicone extrusion occurred rapidly after hour 112 as evidenced by the rolling of strata at salt basin margin (35 cm, Figure 5.7). Silicone extruded over 20 cm basinward from the salt basin. Depocenters above allochthonous silicone (nappe) were developed as minibasins (Sw 4); some of which have rafted on silicone. A passive canopy (C4), at the distal edge of the initial silicone basin, appears to have evolved from D5 (Figure 5.7). An expulsion rollover formed on the flanks of this passive canopy. Small diapiric and even canopy structures are present within allochthonous silicone, but most structures are broad.

5.9.3 4D Basin evolution (DIC time series data)

DIC incremental displacement and strain data were used to analyze the structural evolution of analogue experiments. The complex experiment evolution is visualized with the help of a time-space diagram (Figure 5.8) derived from the image and strain data (Figure 5.9). DIC displacement and strain maps for 24 hour periods of the entire experiment are shown in Appendix C.

The time-space diagram (Figure 5.8) is a synoptic presentation of the structural evolution and basin history of a characteristic experiment section in a coordinate system defined by a space and a time axis. Diagrams are derived from model surface time-series images and DIC strain data in 24 and 48 hour intervals.

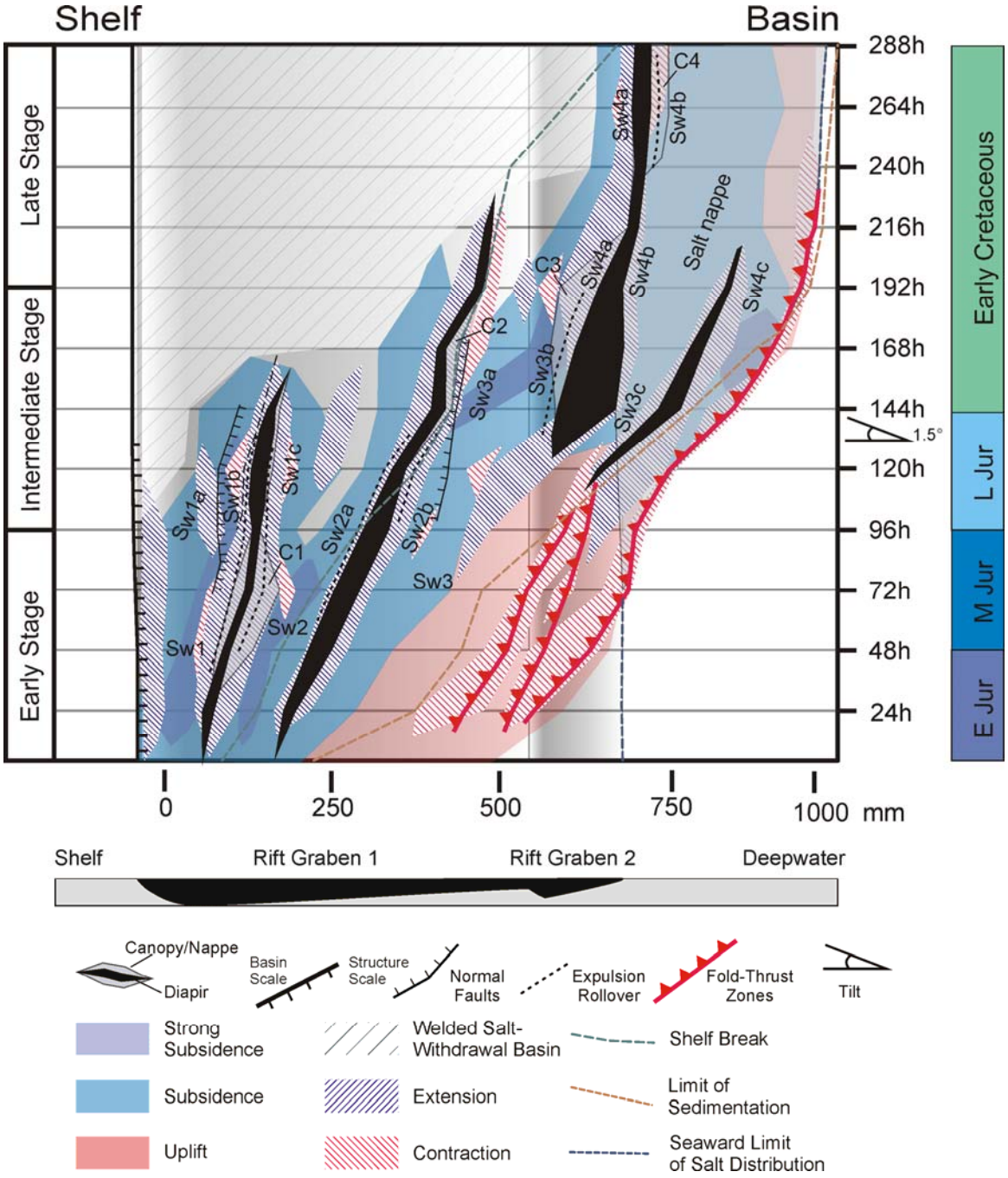

Figure 5.8A. Spatial and temporal diagram of the central cross-section (45 cm) of the main 3-D experiment (eastern Scotian Margin) illustrating the vertical displacement and horizontal strain during evolution of salt tectonics structures and associated depositional systems (salt withdrawal basins-Sw) deduced from time-series images and DIC strain analysis. The position of structural and depositional elements in a shelf-to-deep basin transect are plotted along the x-axis. The variation in the x position of elements was in 24 hour intervals, shown on the y-axis.

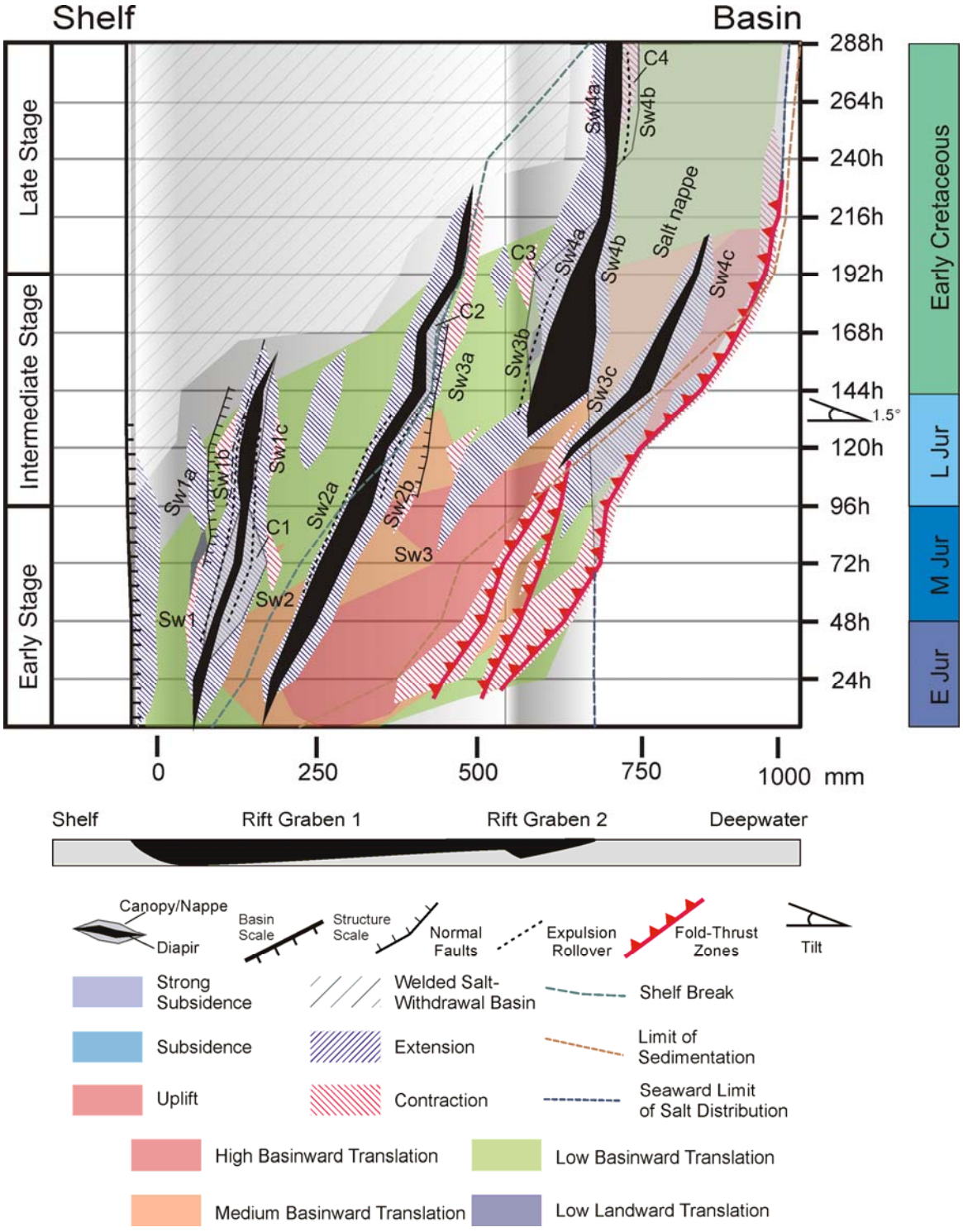

Figure 5.8B. Spatial and temporal diagram of the central cross-section (45 cm) of the main 3-D experiment (eastern Scotian Margin) illustrating the horizontal translation and horizontal strain during evolution of salt tectonics structures and associated depositional systems (salt withdrawal basins-Sw) deduced from time-series images and DIC strain analysis. The position of structural and depositional elements in a shelf-to-deep basin transect are plotted along the x-axis. The variation in the x position of elements was in 24 hour intervals, shown on the y-axis.

The x-axis refers to the position (shelf-slope) of respective structures and depositional elements for a center section (45 cm) of the model. The y-axis displays the temporal evolution and position of structural and depositional features.

Using the time-space diagram, 3D model time-series images and DIC strain analysis model evolution will be discussed in three proposed evolutionary stages: early, intermediate and late (Figure 5.8, 5.9).

- The **early stage (0 – 96 hours)** is dominated by "salt" withdrawal basins within the landward portion of the rift basin. Accommodation space is generated through the seaward expulsion of silicone. Extension and rafting of the sedimentary overburden in the proximal basin is balanced through inflation, contraction and buckle folding in the distal basin.

- The **intermediate stage (96 – 192 hours)** is characterized by the formation of welds beneath proximal withdrawal basins, shutting down landward expulsion rollovers and extensional rafting. This process leads to the seaward progradation of depocenters as early sediment input is increased. This progradation initiates inflated basinward silicone and extrusion from the initial silicone basin to eventually form an allochthonous nappe.

- The **late stage (192 – 288 hours)** starts with the conclusion of extension, translation and subsidence within the initial silicone basin. With autochthonous

salt tectonics shut down deposition progrades onto allochthonous silicone driving late stage canopy and mini-basin formation in the deepwater basin.

Early stage (0 – 96 hours)

Landward extensional and basinward contractional domains initiate very early in the experiment. The boundary between the two zones is located in the center of the initial silicone rift basin and propagates basinward with time (Figures 5.8, 5.9a). At the end of the early stage the transition zone reaches the distal small rift graben.

The extensional domain is characterized in the landward rift graben by sediment down-building and passive diapirism (D1 and D2 in Figures 5.7, 5.8, 5.9a, Appendix C). Extension is almost entirely localized in silicone and the diapir walls are accommodating nearly all strain (Figure 5.8, 5.9a).

A regional listric normal fault (F) initiated immediately with the onset of sedimentation (Figures 5.8, 5.9a) and accommodates mostly differential subsidence, not major extension. At the same time the sediment wedge spread/rafted above silicone. Passive diapirs were initiated through the spreading of the sedimentary wedge in the landward portion of the rift basin. The diapir heads form topographic highs that segment the proximal basin separating the major early salt withdrawal basins (Sw 1 – 2) (Figure5.9a). As sediments subsided between silicone ridges, these passive diapirs translate extensively (6 – 12 cm) basinward (Figure 5.8).

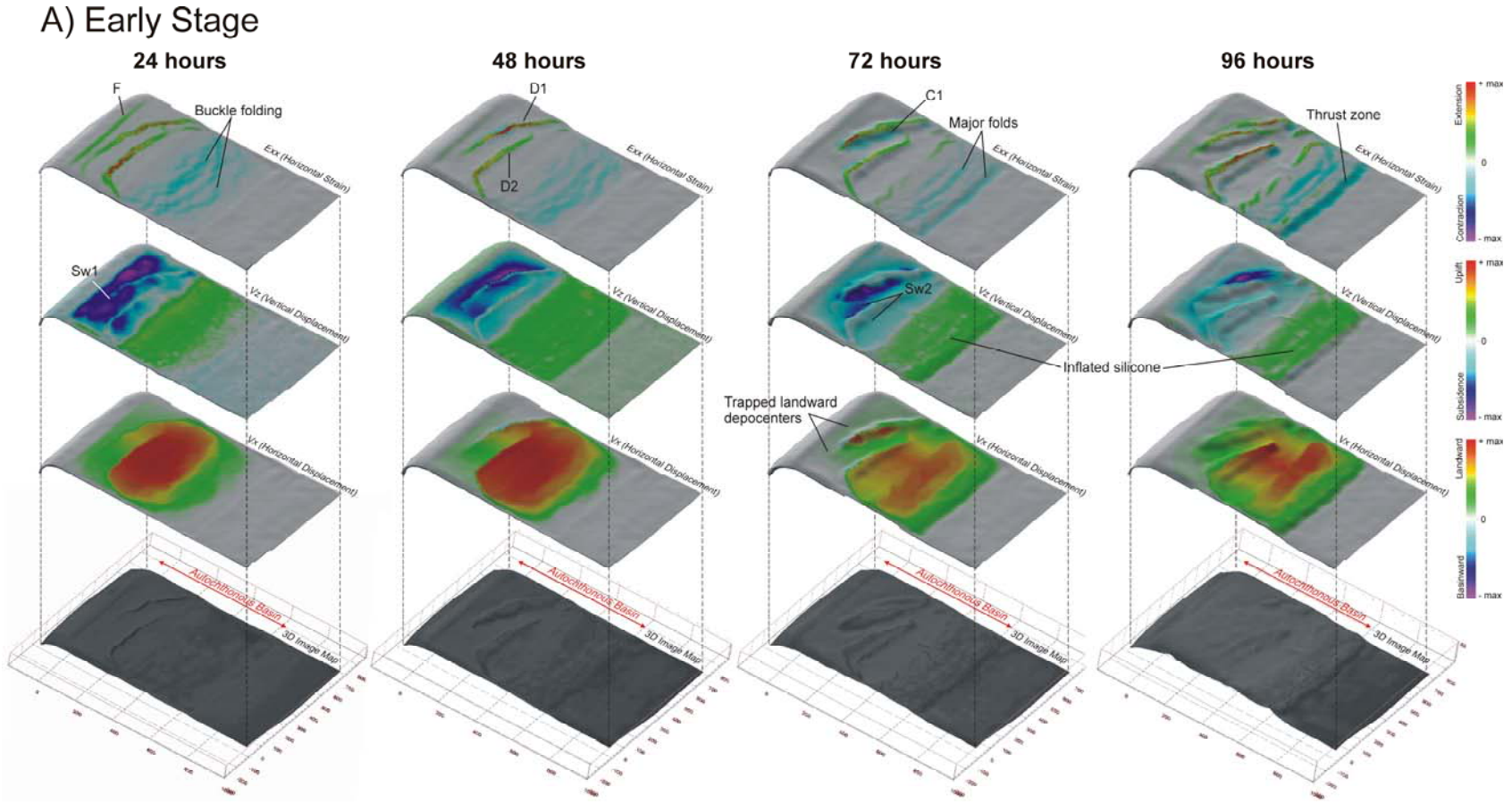

Figure 5.9. Temporal evolution of the 3D main analogue experiment simulating the eastern Scotian Margin salt basin evolution (A: Early Stage 0-96 hours; B: Intermediate Stage 96-192 hours; C: Late Stage 192-288 hours). Experiment evolution is mostly visualized in 24 hour intervals, with 48 hour intervals for the end of model development (Late Stage), through illuminated artificial 3D surface surfaces having overlays of horizontal strain (Exx), horizontal displacement (Vx), vertical displacement data (Vz), and experiment surface image (from top to bottom). Incremental strain and displacement components obtained by 3D DIC monitoring are summarized for the previous 24/48 hour interval and overlain on the ensuing model surface to visualize deformation trends for the individual intervals. For a discussion of deformation trends see text (Chapter 5.9). Sw – salt withdrawal basin, D – diapir, F – basin bounding fault, C – canopy.

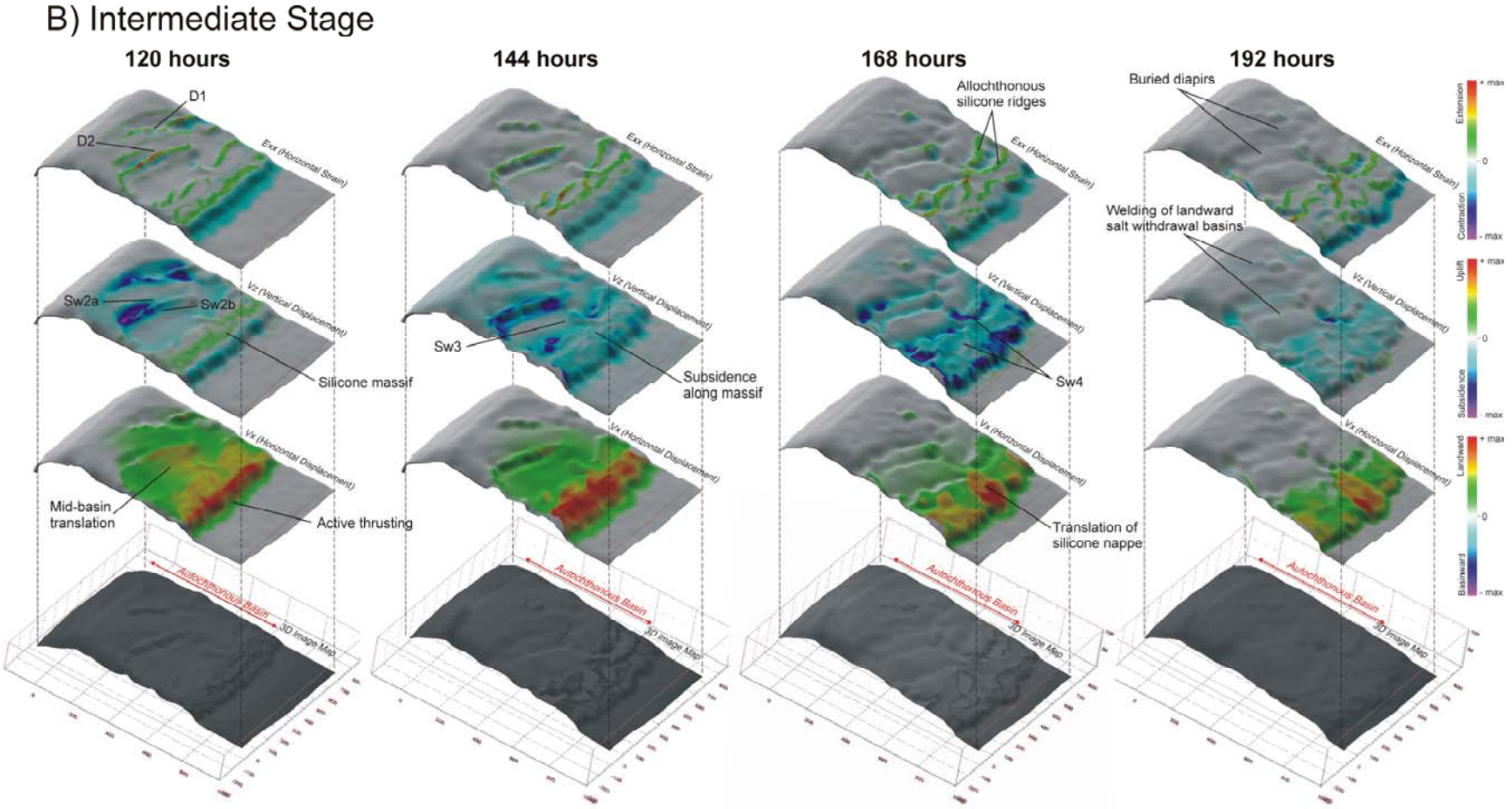
B) Intermediate Stage
120 hours
144 hours
168 hours
192 hours
D1
D2
Exx (Horizontal Strain)
Vz (Vertical Displacement)
Sw2a
Sw2b
Silicone massif
Vx (Horizontal Displacement)
Mid-basin translation
Active thrusting
Autochthonous Basin
3D Image Map
Sw3
Subsidence along massif
Allochthonous silicone ridges
Sw4
Translation of silicone nappe
Buried diapirs
Welding of landward salt withdrawal basins
Extension
Contraction
Uplift
Subsidence
Landward
Basinward
+ max
- max
0

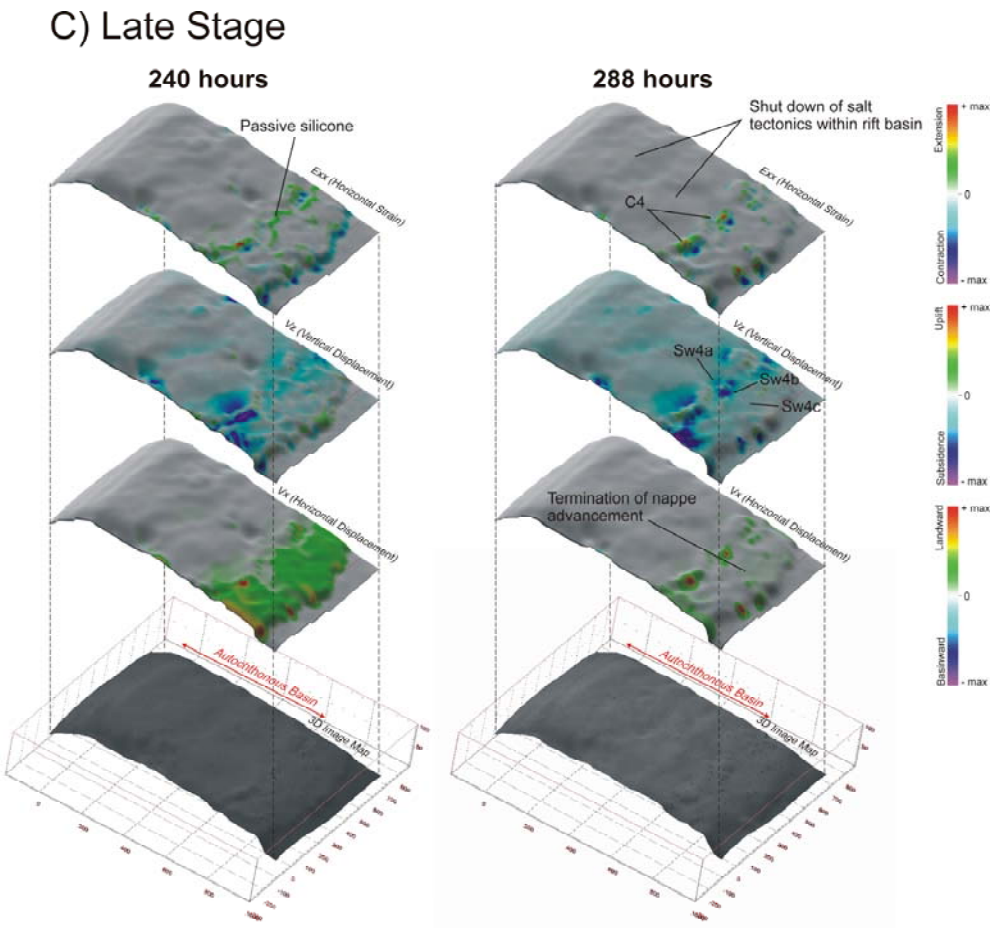

At the end of the early stage canopies (C1) form and salt overhangs develop seaward of D1 (Figure 5.8, 5.9a) as a result of passive silicone flow along the topographic gradient. Landward overhangs of D1 were later major depocenters (Sw 1b), with silicone acting as a detachment surface (Figure 5.7).

The contractional domain is characterized by regional uplift through silicone inflation, folding and minor thrusting. Contractional folding of silicone is a response to basinward mobilization and inflation of silicone as it is expelled from the proximal rift basin. Folding occurs on two different scales. Small scale (minor) folds have wavelengths of > 1 cm, being mostly non-cylindrical. Large scale (major) folds have wavelengths up to 10 –

15 cm becoming progressively closer spaced with model evolution. As major folds become adjacent/stacked, small thrusts develop with the major regional thrust forming at the distal rift basin edge. Overall the contractional domain and folds propagate > 25 cm within the silicone basin (Figure 5.8, 5.9a) during the early stage.

Intermediate stage (96 – 192 hours)

Regional welding of subsiding sediments to the proximal basin limiting newly created accommodation space initiating large scale progradation characterizes the intermediate stage of model evolution.

As welding occurs within the proximal rift basin subsidence progressively migrates basinward with major depocenters being located mostly beyond D1, in the autochthonous basin (Sw 2a,b, 3a,b) and later on top of extruded allochthonous silicone (Sw 3c, 4a,b) of the nappe system (Figure 5.7, 5.8, 5.9b). A large (15 cm wide) silicone massive formed at the silicone basin margin by 144 hours Small diapir ridges and canopies bound allochthonous minibasins (Figure 5.9b). By the end of this stage sedimentation advances and covers the toe of basinward-mobilized silicone.

The early intermediate stage is marked by a transition from silicone inflation and contraction in the distal basin to silicone extrusion out of the initial rift basin initiating the formation of an extensive allochthonous silicone canopy/nappe system in the deepwater basin (Figure 5.9b). The increase in sediment input during this time simulating Late

Jurassic sedimentation (Mic Mac) and tilting of the experiment coupled with the initiation of the progradation phase of model evolution facilitated in the efficient welding of the proximal rift basin and extrusion of silicone from the basin.

Whereas distal silicone contraction dominated the early stage, these structures were later buried under prograding sediments and subsequently overprinted by passive diapirs and extension in the overburden (Figure 5.8, 5.9b). Extension continued to be accommodated along diapirs (D1 and D2, Figure 5.9b) and to limited extent crestal grabens until they are buried under prograding sediments. Later (176 – 192 h) only canopies remained at the surface. By the end of the intermediate stage (192 h, Figure 5.8, 5.9b) the area of active extension is shifted from the diapirs in the rift basin to the allochthonous silicone nappe. Here, sediment depocenter moving on top of the silicone nappe initiate the formation of piggy-back minibasins and passive diapirs (Sw 4a, b, c) (Figure 5.8, 5.9b).

Overall there is a transition from silicone inflation and related uplift to dominantly subsidence over the entire experiment, including mini basin formation in the area of the allochthonous silicone nappe.

Thrusting is limited to the early frontal thrust of silicone as it is expelled out of the initial rift basin. As sediment loading continues to prograde the thrust shear zone is breached and silicone is rapidly extruded along with translating depocenters on the experiment surface to form an extensive (> 25 cm) allochthonous silicone nappe. Basinward

translation of sediments changes focus from the distal portion of the rift basin (96 – 144 h) to along the allochthonous silicone nappe (144 – 192 h) (Figures 5.8, 5.9b).

Late stage (192 – 288 hours)

The late stage is marked by the gradual cessation of extension and subsidence within the original rift basin as welding and the burial of diapirs effectively concludes deformation throughout the autochthonous basin (Figure 5.9c).

Silicone-related deformation is limited to late stage canopy formation (C4) (Figures 5.8, 5.9c). Late stage canopy formation is accompanied by only minor subsidence (Figure 5.9c). The new depocenters were established in minibasins along the flanks of canopies (Sw 4a,b) or within rafts above allochthonous silicone (Sw4c).

Although DIC deformation analysis records extension along allochthonous diapir ridges of the silicone nappe (Figure 5.9c), these measurements are deceptive. In actuality some of these data are derived from shifting sand particles on flowing passive salt. Early (92 – 240 h) in the late stage, rafted depocenters riding on allochthonous silicone between silicone ridges do extend basinward by small amounts (< 5 cm) as indicated by horizontal displacement measurements (v_x) (Figure 5.9c). However, for the remainder of this stage (244 – 288 h) of model evolution extension along the nappe system has generally ceased. This is mostly due to sedimentation completely covering and overriding the nappe system.

5.9.4 – 4D Kinematic evolution

Surface profiles, displacement and strain data derived from 3D DIC analyses enabled the sequential restoration of a central experiment section giving insight into the kinematic evolution of the experiment and the mechanics of "salt" structures and their role on depocenter migration. The 45 cm model section was chosen for restoration because its central location limits boundary effects and it is a representative section for discussion of the experiment evolution.

Early experiment stages were restored in 24 hour intervals to study the importance of early silicone structures and depocenter segmentation. Later experiment stages were restored for 48 hour intervals (Figure 5.10).

Balancing is performed with the assumption of plain strain deformation and is done manually using standard graphics software. The constant area vertical and inclined shear methods are implemented for structural restorations (Hossack, 1995; Rowan and Klingfield, 1989). Topographic surface profiles for each restoration time interval were used as regional reference horizons for model sections. Surface profiles were deduced from 3D DIC experiment surfaces, horizontal strain data (exx) and subsidence (Vz) were derived from 3D DIC displacement measurements. Time-series surface strain and subsidence/uplift data derived from 3D DIC data were used to correlate fault and salt structures as well as better understand their mechanics.

The restoration and associated structural evolution of model section 45 cm is shown in figure 5.10 and will be discussed in detail in the following section:

Early Stage: 0 – 24 hours

Early sediment input controlled the locations of proximal depocenters Sw1, 2, and 3. Salt withdrawal basins are separated by active grabens and reactive and passive diapir ridges (Figure 5.10). Depocenters closest to the growth fault F show the maximum subsidence (< 1 cm). The bounding basinward listric fault (F) also accommodates small amounts of extension. Extension in the proximal basin is matched by contraction of distal silicone through buckle folding near the 70 cm mark, with a small amount of silicone inflation seaward of Sw3. The majority of basinward overburden translation is restricted to depocenters Sw2 and 3 and within silicone landward of folding.

Early Stage: 24 – 48 hours

Extensional strain is mostly accommodated through the widening of silicone diapirs facilitating depocenter translation (rafting) (~ 7 cm) (Figure 5.10). Contractional silicone folding migrates to the distal edge of the initial rift basin. During this period depocenters Sw1, 2, and 3 continue to subside and raft as diapirs D1 and D2 rise and widen (Figure 5.10). D1 developed basinward and landward "salt" wings as silicone flowed passively on the adjacent experiment surface. Sieved sediments quickly covered "salt" wings. Maximum subsidence is observed along the landward basin margin in Sw1 (~ 1 cm) with

growth fault F accommodating differential vertical displacement and a small amount of extension. Distal inflation of silicone basinward of Sw3 accommodates silicone extrusion beneath the salt withdrawal basins.

Early Stage: 48 – 96 hours

Significant depocenter changes occur during this period, as subsidence of depocenters Sw1, 2 and 3 continue with a segmentation of Sw1 and 2 (Figure 5.10). Movement along F begins to cease. Sw1 is now differentiated into three segments.

Sw1a is the most landward basin and subsidence rates decrease as the underlying silicone layer is nearly depleted. Sw1b is bounded by a fault detached along a previous landward "salt" wing. Sw1b is located on top of the landward portion of D1, which has significantly (~ 5 cm) widened during this time interval accommodating extension and seaward rafting sediments (Sw2) (Figure 5.10). Part of Sw1c is located on a basinward canopy of D1 (C1). During this time interval "salt" wings of D1 form a passive canopy (C1) that was subsequently covered by sediments on its basinward flank.

Sw2 was divided by the quickly growing silicone diapir D2 into two adjacent depocenters located on the flanks of D2. Sw2a constitutes the earlier depocenter of Sw2. Sw2 developed into a raft that was significantly translated seaward with D2 (~ 10 cm) driven by the widening of D1 (> 5 cm) (Figure 5.10). The landward base of Sw2 is close to

welding underneath C1. The younger depocenter Sw2b is located on top of inflated silicone basinward of D2.

A narrow salt ridge separates sediments of Sw2b and Sw3. This inflated silicone structure later developed into a small diapir (D3). The older depocenter Sw3 has accumulated thicker sediments (~ 3 cm) than Sw2b and has rafted basinward a significant amount (~ 20 cm) from its original position at a rate of ~ 4 mm/h while subsiding over 1 cm (Figure 5.10).

Contractional silicone folds amalgamate within a 20 cm wide belt of the inflated silicone massif (~ 2cm above the original silicone height), forming minor thrusts. Thrusting (2 cm) occurs at the basinward margin of the initial rift basin as silicone begins to be evacuated from the basin (Figure 5.10). Basinward translation is focused seaward of D1 as overburden sediments are rafting seaward on mobilizing silicone.

Intermediate Stage: 96 – 144 hours

Ongoing subsidence of Sw1a and Sw2a result in welding and the end of subsidence for these depocenters (Figure 5.10). After welding Sw1b was transformed into an expulsion rollover along the landward flank of D1 receiving a very high sediment input. This depocenter initially formed on a salt detachment surface, e.g. a "salt" wing and was separated by a normal fault from the landward older part of the depocenter. Sw1c developed on top of the basinward canopy of D1. As the sediments of Sw2a welded in

front of D1 the diapir was forced to grow vertically. As sediment input increased around the diapir near welding of the canopy and rollover of sediment into D1 resulted in a bulbous shape. Extension associated with D1 has nearly ceased by 144 hours as the diapir is mostly buried and sealed.

Continuing progradation within Sw2a and Sw2b coupled with experiment tilting (128 h) results in the formation of the seaward verging D2 and related narrow salt canopy C2 near the seaward terminus of the landward half graben wedge (Figure 5.10). Sediments of Sw2b are situated in much the same way as those of Sw1c, with strata rolling downwards on the basinward flank of D2 with normal faulting accommodating differential subsidence. During this period extension is still being accommodated by D2 and D3 through basinward translation (~ 5 cm) and downbuilding of Sw2b and Sw3.

The spreading of an inflated silicone complex (massif) (D5) (Figure 5.10) at the seaward salt basin half graben wedge divides Sw3. With prograding sedimentation Sw3a is translated basinward (~ 5 cm) and downbuilds into silicone until welding occurs at the basin high of the landward wedge (Figure 5.10) essentially trapping landward salt structures. Basinward of this, Sw3b and Sw3c are deposited on the inflated silicone massif. Sediment loading on the landward flank of the inflated silicone further drives basinward mobilization of silicone into the allochthonous nappe system with an open toe acting as a major thrust. The extensive thrusting of the silicone nappe (> 10 cm, Figure 5.10) is also facilitated by the tilting of the experiment. Extension is accommodated as

silicone spreads below thin depocenters, causing rafting (Sw3c) above allochthonous silicone.

A shift is made during this stage from early inflated and uplifted silicone at the basinward margin (Figure 5.9b) of the salt basin to subsidence along the extruded allochthonous silicone, as it spreads basinward. Horizontal translation is focused at the basinward edge of the initial rift basin and allochthonous nappe (D4, D5 and SN, Figures 5.9b, 5.10) because silicone is rapidly evacuated out of the original basin.

Intermediate Stage: 144 – 192 hours

The beginning of this stage is marked by the ceasing of subsidence in all landward depocenters (Sw1 and Sw2) as extensive regional welds completely formed in this area and subsequently the intervening diapirs D1 and D2 became sealed (Figure 5.10). Although Sw3a has welded by this time, continued deposition causing subsidence (~ 2 cm) within Sw3b, also to the point of welding, drives further seaward mobilization of silicone into the allochthonous nappe (Figures 5.9b, 5.10). By hour 192, rolling of this salt withdrawal basin (Sw3b) has formed the basinward flank of D4. A landward canopy formed on top of the rapidly subsiding Sw3b basin sourced by D5, but is nearly buried by hour 192.

Prograding sediments cause further passive downbuilding on the allochthonous nappe driving seaward silicone mobilization and the development of minibasins (Sw4a, b, and

c). Subsidence is localized along the basinward edge of the rift basin and allochthonous nappe within depocenters Sw3b, Sw4a, Sw4b and Sw4c.

Salt withdrawal basins (minibasins) Sw4b and Sw4c developed due to extension and rapid spreading of allochthonous silicone leading to the formation of D5. Most basinward extension of rafted sediments had ceased by hour 192, with the thrust front stopping approximately 25 cm basinward of the salt basin (Figure 5.10). Similarly, basinward translation is localized in the distal portion of the initial rift basin and the allochthonous nappe.

Late Stage: 192 – 240 hours

Major basinward translation has ended by this time with most of the silicone nappe being covered by prograding sediments. Silicone at the experiment surface along the basinward edge of the rift basin displays extensional strain (Figure 5.9c). Most of this deformation is accommodated by the spreading of silicone in canopy C4 (Figure 5.10), not extension related to basinward translation of sediments on silicone. Extension during this stage is mostly localized in these late stage canopies.

Subsidence is related to the late stage canopy formation with depocenters Sw4a and Sw4b starting to form expulsion rollover structures adjacent to diapir D5 and the feeder of canopy C4, driving vertical salt flow (Figure 5.10). Sediments deposited basinward along

the allochthonous silicone nappe are starting to drape over sealed silicone structures rather than actively subsiding into it.

Late Stage: 240 – 288 hours

The structural evolution of this period is much the same as the previous interval. Subsidence is restricted to the continued development of expulsion rollovers on the feeder of canopy C4, sourced by diapir D5. Expulsion and spreading of canopy C4, facilitated by adjacent rollovers, during this stage increases with overriding sediment sealing it by hour 288 (Figure 5.10). Extension therefore is limited to canopy spreading. Minor uplift was observed along the covered toe of the allochthonous silicone nappe demonstrating the tendency for silicone to mobilize under differential load even when nearly sealed.

5.9.5 – Tectono-stratigraphic implications for eastern Scotian margin evolution

Final experiment sections (Figure 5.7) show very similar characteristics when compared to regional seismic data of the eastern Scotian margin. Silicone structures and salt structures are comparable including the development of allochthonous nappe systems outboard of the initial rift basin. Even more significant is the correlation of the relative timing of silicone mobilization and formation of major silicone ("salt") structures and the generation and migration of depocenters, in both models and regional seismic profiles. As

consequence, the experiment results can be effectively used to better understand the post-rift basin evolution and salt tectonics history of the eastern Scotian margin.

For a better comparison of evolutionary stages of the experiment with the basin history of the eastern Scotian margin as deduced from seismic studies (see results in Chapter 4) the experiment evolution is summarized and discussed for major time intervals that are equivalent to the major important chono-stratigraphic intervals of the study area (Figure 5.11).

Cumulative deformation (strain (e_{xx}), vertical displacement (v_z), and horizontal translation (v_x)) for experiment time intervals equivalent to the duration of deposition of the main stratigraphic formations visualize the active deformation, basin-scale structural evolution and location of related depocenters (Figure 5.11).

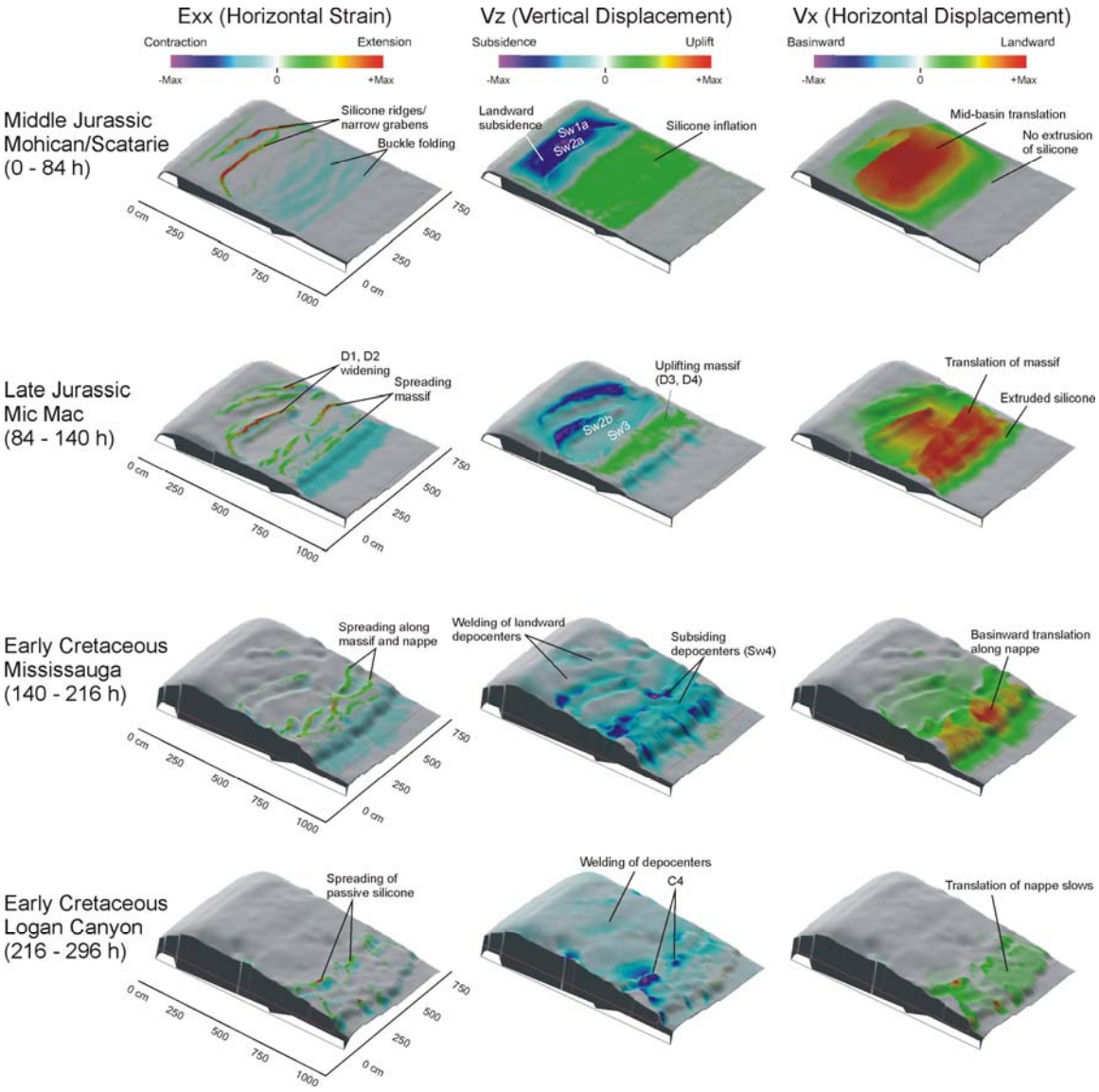

Figure 5.11. Summary of experiment evolution for major time intervals equivalent to chono- stratigraphic intervals (Mohican/Scatarie, Mic Mac, Mississauga, and Logan Canyon) of the eastern Scotian margin. Basin history is visualized by 3-D DIC displacement and strain maps (horizontal strain (Exx), horizontal displacement (Vx), vertical displacement data (Vz)). Sw – salt withdrawal basin, D – diapir, C – canopy. Salt basin geometry is illustrated along the side of 3-D maps.

Middle Jurassic Mohican/Scatarie chrono-stratigraphic time

During Mohican/Scatarie chrono-stratigraphic model time deposition is limited to mostly landward salt withdrawal basins (Sw1a, 2a) with smaller amounts of sediments deposited

basinward of D2 and on top of D1 (Figure 5.11). Due to localized sediment input within the proximal rift basin subsidence rates are very high with > 2 cm of subsidence generated. Counteracting proximal subsidence, regional uplift and silicone inflation (~ 1 cm) is dominant above the thin portion of the landward wedge and the basinward smaller wedge.

Extension is limited to proximal narrow grabens within the sedimentary overburden initiating reactive and passive diapirs. Silicone ridges segment sediments deposited on silicone as depocenters translate basinward. Highest amounts of translation are focused within rafted depocenters above the central rift basin (Sw2, 3), with maximum values up to 15 cm. Major buckle-folds formed on top of the distal inflated silicone massif above the thinnest portion of the landward wedge and the smaller basinward wedge to accommodate landward extension. Besides basinward inflation of autochthonous silicone, no major extrusion out of the salt basin has occurred yet (Figure 5.11).

Late Jurassic Mic Mac chrono-stratigraphic time

During Late Jurassic time of experiment evolution sediments continue to subside (~ 0.5 cm) within landward salt withdrawal basins (Sw1, 2a). As landward depocenters weld progradation is initiated producing new basinward salt withdrawal basins (Sw2b, 3a) (Figures 5.7, 5.11). Subsidence in the center of the basin (~ 1 cm) is concentrated in front of the still uplifting (~ 1.5 cm) salt massif (D4 and D5) above the small basinward half graben wedge. This silicone inflation is a function of slower silicone flow up the

basinward – thinning ramp beyond the massif. Extension is accommodated within the landward diapirs (D1 and D2) and the massif (D3 and D4). During this time passive salt diapirs control sediment distribution increasing sedimentation within Sw1 and 2 until welding occurs and diapirs begin to be sealed. Beyond D2, new depocenters begin to receive high sediment input (Sw3a, b, c) along the landward flank and above the silicone massif (Figures 5.7, 5.11).

The focus of major basinward translation (~ 13 cm) has progressively shifted towards the basinward edge of the rift basin as silicone started to extrude out of the autochthonous silicone basin (Figure 5.11). The initial formation of an allochthonous silicone nappe and associated depocenters was observed at the end of Mic Mac time. This is the consequence of high sediment input and prograding depocenters in the rift basin itself, which have strongly driven silicone expulsion of the inflated silicone massif and has finally initiated silicone flow into an allochthonous canopy/nappe.

Early Cretaceous Mississauga chrono-stratigraphic time

The formation of regional welds in the proximal basin has shutdown deposition in landward salt withdrawal basins. Sediment progradation and the development of basinward depocenters in the distal rift basin edge and the allochthonous silicone nappe characterize model evolution during Mississauga time. The majority of subsidence (~ 1 cm) is located within migrating depocenters (minibasins) above the silicone nappe (Sw4a, b, c) (Figures 5.7, 5.11). Gravitational loading of silicone caused by these depocenters

further drives the seaward mobilization of silicone into the allochthoneous nappe complex. Uplift has virtually ceased as once inflated silicone has now evacuated the rift basin and is flowing seaward while forming subsiding depocenters (Figure 5.11).

Extension also has shifted focus from landward diapirs to the rift basin edge and allochthonous nappe. Landward diapirs were mostly sealed during Mississauga time. The basinward translation (maximum of 15 cm) of rafting depocenters on the allochthonous nappe is accommodated through the extension of salt ridges located along the basinward edge of the rift basin (massif) and small diapirs throughout allochthonous silicone (Figure 5.11). However basinward translation slows near the end of Mississauga time.

During this time there is a transition from regional diapir traces and along – strike depocenters within the silicone basin towards irregular and smaller diapirs and depocenters developing in the inflated massif complex and on secondary silicone levels (nappe). This shift corresponds with model evolution becoming independent of basin floor geometry, as active depocenters are migrating beyond the basin.

Early Cretaceous Logan Canyon chrono-stratigraphic time

Active subsidence through Logan Canyon time is localized along the flanks of late stage canopies (C4) near the basinward edge of the rift basin (Figure 5.11), driving vertical expulsion of silicone (Figure 5.7). All landward salt withdrawal basins have welded by this time. Through this stage most extension and therefore basinward translation ends

through the covering and sealing of the allochthonous nappe by prograding deposition. Extensional deformation measurements are related to passive flow of silicone canopies (Figure 5.11), not translation of depocenters.

Chapter 6: Discussion – Implications for Scotian Margin geology

Final experiment model sections of the main 3-D model demonstrate very similar structural and depositional characteristics with the regional seismic data of the eastern Scotian margin (NovaSpan line 2000) (Figure 6.1). Silicone and salt structures are comparable including mid-basin diapirs and canopies, trapped salt/silicone at the basinward edge of the autochthonous salt basin (e.g. later salt massif), and the development of an extensive allochthonus nappe systems outboard of the rift basin.

There is a significant correlation between the relative timing of depocenter migration and major silicone ("salt") mobilization within the experiment compared to stratigraphic time constraints identified from the regional seismic interpretations. Therefore experiment results can be effectively used to make inferences regarding the temporal evolution of the eastern Scotian margin.

In this chapter, experiment results will be used to discuss the tectono-stratigraphic and salt tectonic evolution of the eastern Scotian margin and its role on the regional basin history of this region.

6.1 Kinematic segmentation of the eastern Scotian margin

The kinematic segmentation of experiment and seismic section can be used to organize and discuss the salt and silicone structures in similar kinematic domains and

developmental settings. The salt tectonic domains between the two are very similar and comprise 4 domains from the landward margin to the deepwater basin (Figure 6.1):

1. salt weld and pillow domain
2. extensional diapir domain
3. contractional salt massif and canopy domain
4. allochthonous nappe and minibasin domain

(1) Salt weld and pillow domain

The salt weld and pillow domain stretches from the shelf into a narrow (~ 30 km) region basinward of the hinge zone within profile 2000. Small trapped salt pillows within small syn-rift basins beneath the shelf, trapped salt beneath the hangingwall sediments of the hinge zone, and nearly welded saltwithdrawal basins landward of D1 characterize this domain (Figure 6.2). In the main 3-D experiment this zone is also quite narrow (~ 15 cm) consisting of the simulated basement shelf, small amounts of silicone trapped under the basin bounding fault, and the nearly welded depocenters along the flank of landward diapirs (D1) (Figures 6.1 and 6.2). This domain developed as a result of early landward sediment input and high rates of subsidence favouring rapid downbuilding of sediments (Sw1a,b) into thick landward salt/silicone. Subsidence as a result of early salt extrusion nearly welded depocenters within the “salt” basin as remnant salt/silicone remains in the form of pillows and small diapirs.

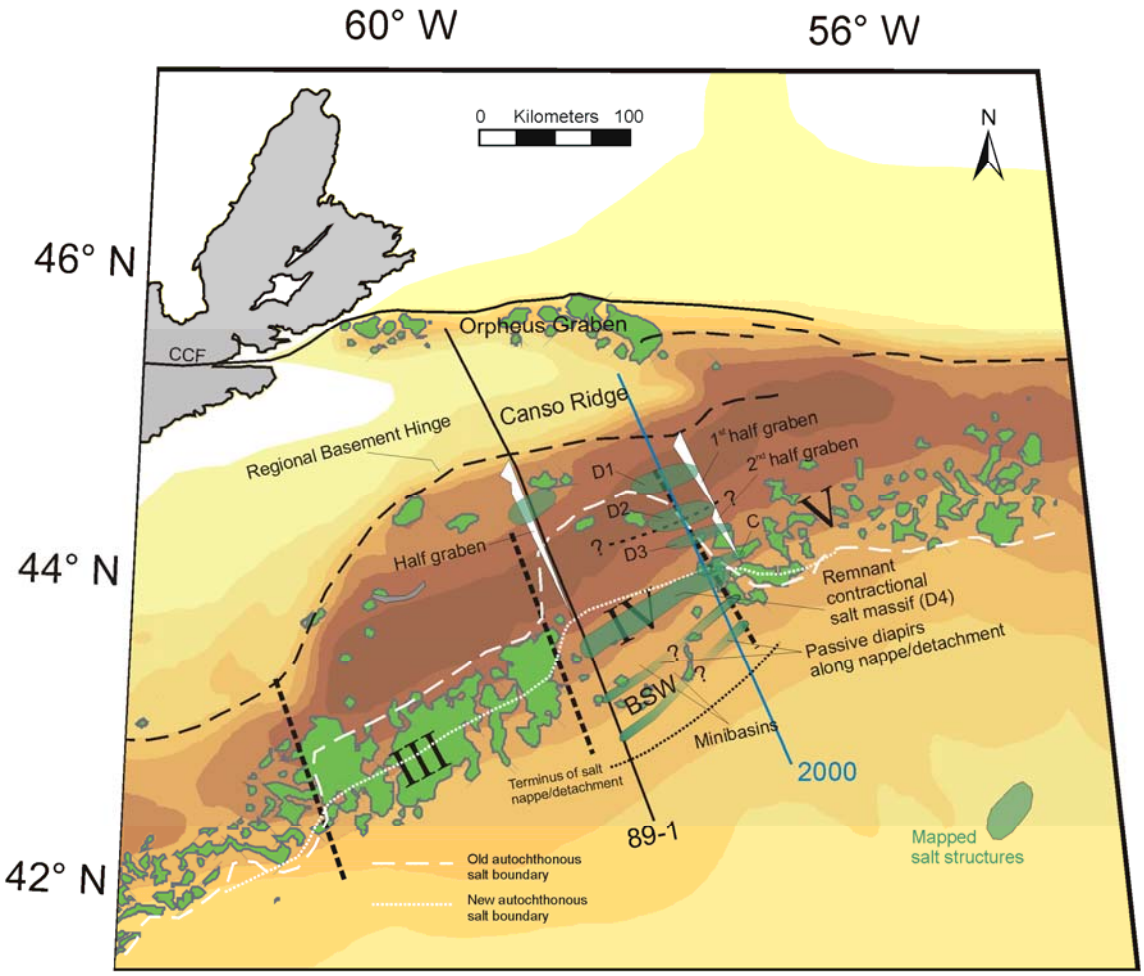

Figure 6.2. Modern day configuration of major salt structures within Subprovince IV mapped for this study (based on lines 2000 and 89-1). Shallow salt structures (green polygons) and salt subprovinces (III – V) mapped by Shimeld (2004). Note the location of salt basin floor with regards to salt structures.

(2) Extensional Diapir Domain

In profile 2000 the extensional diapir domain consists of several broad (5 – 10 km), triangular, evenly spaced (~ 20 km) diapirs (D1 – D3, Figures 6.1, 6.2) separated by thick and weakly deformed and nearly welded depocenters (Sw1c, Sw2a-b, Sw3a-b) (Figure 6.1). Above diapirs D1 and D2 strata have rotated landward in the hanging wall of basinward listric faults along detachments of landward canopies. The main 3-D

experiment also displays several broad diapirs. Narrow canopies are observed along both the landward and basinward flanks of mid-basin diapirs. Thick depocenters located between diapirs are mostly undeformed and have welded on the basin floor in the mid experiment stage (see Section 5.9).

In this domain diapir ridges begin to form passively in response to the basinward translation of the sedimentary wedge as a result of differential loading. Diapirs accommodate further extension as diapir ridges broaden, and their positive topographic relief restricts sedimentation into adjacent main depocenters. Experiment results indicate that rafting of early sediments is quite extensive (20 cm, ~ 20 km, Figure 6.1) (see Section 5.9).

The original location of passive diapirs controls the location of major long-term depocenters. The positive relief of the diapir ridges in addition increases sediment transport in the adjacent depocenters forming a positive feedback with further diapir growth. As consequence the localization of early diapirs control the development of diapirs and depocenters in the autochthonous salt basin for most of the basin history.

However, it is very important to note that significant basinward translation of diapirs and related early depocenters occurred through experiment evolution and their final position is not identical with the position of their formation (see Section 5.9, Figure 6.3). This has important implications for the tectono-stratigraphic analysis and seismic interpretation.

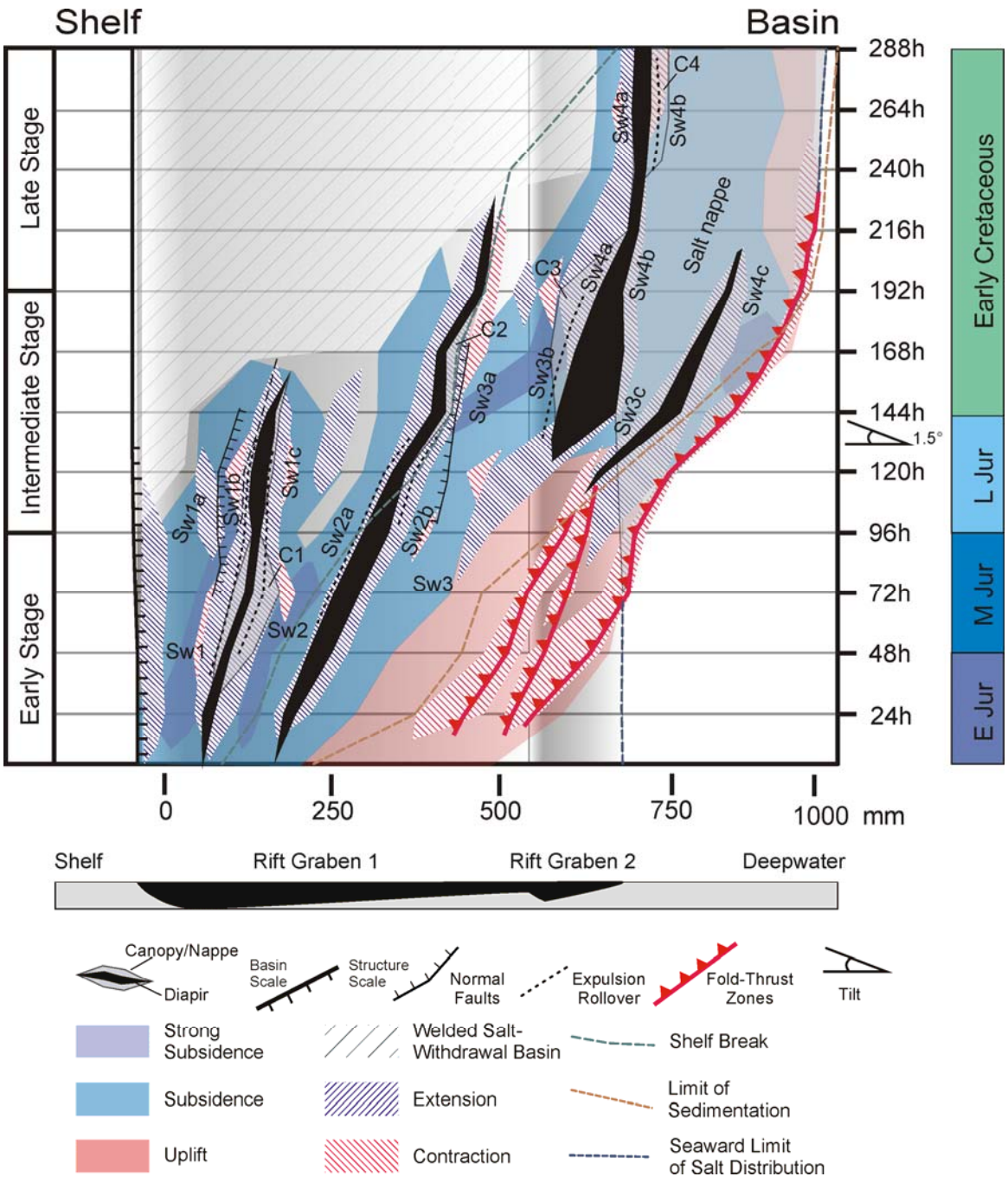

Figure 6.3. Spatial and temporal diagram of the central cross-section (45 cm) of the main 3-D experiment (eastern Scotian Margin) illustrating the vertical displacement and horizontal strain of salt tectonics structures and associated depositional systems (salt withdrawal basins-Sw) deduced from time-series images and DIC strain analysis (from Chapter 5). The position of structural and depositional elements in a shelf-to-deep basin transect are plotted along the x-axis. The variation in the x position of elements was in 24 hour intervals, shown on the y-axis.

(3) Contractional Salt Massif and Canopy Domain

The contractional salt massif and canopy domain is a result of salt/silicone contraction forming an inflated massif in the distal rift basin (Figure 6.2). In seismic line 2000 this domain consists of a broad trapped salt body (pillow), a triangular diapir along the basinward edge of the salt basin (D4, Figure 6.2), and an isolated canopy in overlying Early Cretaceous sediments (Figure 6.1). In the model this domain displays significant variations with depocenters and silicone structures along strike. In most sections a salt body has developed along-strike and is trapped along the basinward margin of the silicone basin. In some sections this silicone body has been segmented into two, and landward canopies have developed (Figure 6.1). In many model cross-sections late stage basinward verging canopies at the autochthonous basin edge (C4, Figure 6.3) are associated with inflated silicone complexes.

Modeling suggests that a concentration of flow vectors up a seaward thinning wedge at the basin limit is responsible for extensive mid-basin inflation of silicone. As inflated silicone/salt was extruded basinward by downbuilding and prograding depocenters (Sw 3a-b) it became arrested at the distal edge of the rift basin through the contraction of silicone/salt. The high amount of inflation and mobilization allowed for landward canopy formation above Sw 3b and Sw 4a within the model (Figures 6.1, 6.3). With prograding sediments overriding the inflated complex, silicone/salt was trapped at the basin edge. However, in the main 3-D experiment loading of this structure lead to the vertical mobilization of silicone and late stage canopy formation (C4).

(4) Allochthonous Salt Nappe and Minibasin Domain

The allochthonous salt nappe and minibasin domain in both seismic profile and model cross-section consists of an extensive salt nappe system (BSW, Figure 6.2). Late stage sediment progradation on this secondary salt level has led to the formation of numerous minibasins (Sw4, Figure 6.1, Figure 6.2) that are separated by small passive diapirs (Figures 6.1, 6.2). Within profile 2000 the base of the salt nappe climbs out of the salt basin at an average angle of 1° overlying deepwater sediments (Figure 6.1). Late-stage narrow diapirs on the nappe have accommodated seaward extension and formation of minibasins (salt withdrawal basins Sw 4b-c). In the experiment the silicone nappe did not truncate deepwater strata as prominently as in the seismic section. This is partially a result of a conscious effort to limit deepwater sedimentation allowing the uninhibited seaward flow of silicone, displayed through the basinward extent of the nappe.

The development of the salt nappe is a result of sediment loading onto the inflated salt/silicone complex at the distal margin of the salt/silicone basin (D4, Figures 6.1, 6.2). Gravitational loading of the massif by prograding sediments initiated major allochthonous salt flow; however continued sediment progradation keeping pace with salt/silicone mobilization is the key behind long-lived salt nappe formation through effective salt extrusion. In addition, experiment and seismic data suggest that the salt nappe formed with an open toe allowing the continual seaward mobilization of salt/silicone while minibasins were translated basinward.

6.2 Seismic interpretation modifications based on experiment results

Results of both pilot experiments and the main 3-D experiment have given insight into the tectono-stratigraphic evolution of the eastern Scotian margin. Experiment results and derived concepts were used to tackle open problems in the interpretation of the NovaSpan 2000 seismic profile discussed in Section 5.2.

In particular a better-constrained interpretation can be made regarding the ambiguous seismic characterization of the initial salt basin geometry and form of deep-seated salt structures in the deep part of the mid-basin section.

Salt basin geometry

Previous interpretations were conflicted regarding the basinward salt basin floor above rift-blocks 3 and 4 (Rb 3 – 4) (Figure 6.1). For the main 3-D experiment, from preferred seismic interpretations, a small basinward half graben wedge was implemented. Overall this setup generated the characteristic features observed in profile 2000. However, previous pilot experiments suggest that a slightly larger seaward wedge in proportion to the salt basin (as discussed in Section 4.6) may better approximate that of line 2000. The larger basinward wedge in experiments allowed remnant salt within the graben to form "salt" pillows and diapirs similar to D3 and a salt pillow located between D3 and D4 within line 2000 (Figure 6.1). Also pilot experiments suggest that this larger distal wedge

attributed to the large salt massif at the basin edge that subsequently developed an extensive silicone nappe system.

Deep mid basin salt structures (D2)

The most difficult areas for seismic interpretations within NovaSpan line 2000 are related to deep, mid-basin salt structures, in particular in the area of diapir D2. Preliminary seismic interpretations indicated two possibilities; a small salt roller beneath basinward listric normal faults or a large diapir with a landward salt detachment accommodating rotation of strata from sedimentation on a secondary canopy. In the pilot experiments and the main 3-D model, mid-basin diapirs form both landward and basinward canopies (Figure 6.3) (see Sections 5.7, 5.9, Figures 5.4, 5.7).

Similar to profile 2000, pilot experiment 2 (Appendix B, Figure 5.4) produced a major silicone diapir along the distal part of the landward half graben wedge. This diapir formed as a result of silicone inflation at the thin wedge tip. Overriding sediments trapped this diapir as sediments downbuilt into thick silicone of the adjacent second half graben. This diapir developed a basinward silicone canopy. The preference for mid-basin diapirs to form canopies in models suggests that a significant and similar salt body may be present in NovaSpan line 2000. The direction of canopy flow is a result of the topography of the model surface/sediment water interface. This topography is a product of subsidence due to salt withdrawal and sediment input and patterns. As models show, surface topography varies greatly across regional trends.

Based on this and anticlinal Late – Jurassic seismic reflectors observed at SP 4500 (~ 7000 m), the improved interpretation of this salt structure includes a large diapir with a thin landward secondary salt detachment formed earlier as a canopy. Seismic reflectors appear to be rotated along a major normal fault located below SP 4750 of line 2000 (Figure 6.1). Here Early Cretaceous (Mississauga) strata thicken significantly through rotation on this interpreted secondary salt detachment. The passive flow of this canopy nearly correlates to the top Scatarie time (Middle Jurassic). Probably, the distal location of this diapir allowed passive flow due to limited deepwater sedimentation and subsidence of sediments. Faulting above the basinward flank of D2 (main 3-D experiment) is likely a response to differential subsidence of sediments downbuilding into thick salt of the second half graben wedge (Figure 6.1).

Seaward extent of depocenters

A dominant feature in pilot experiment 2 and the main 3-D experiment (see Section 5.7, 5.9) was significant rafting of early depocenters between mid-basin silicone diapir walls (Figure 6.3). As the early sediment wedge was extended and passive silicone diapirs divided the landward basins in individual depocenters, continued sediment input created salt withdrawal basins that were translated basinward during time.

Previous seismic correlation of early sediments (Middle Jurassic - Scatarie/Mohican Formations and deepwater equivalents) was difficult seaward of D2 due to inadequate

seismic reflection imaging and discontinuous seismic markers as a result of salt structures. The experiment results indicate that depocenters seaward of D2 may incorporate a significant amount of Scatarie/Mohican deepwater equivalents that were rafted seaward during the development of diapirs D2 and D3 (Figures 6.1, 6.3).

Although rafting of early sediment layers in experiments is extensive (> 20 cm, Figure 6.1), this is partially due to analogue material properties. Sensitivity analyses have shown that experiments accommodate slightly higher strain rates than their natural prototypes. This is attributed to the higher density contrast of silicone polymer and silica sand (0.99:1.6 g/cm^3 or ~0.62) when compared to that of rock salt (halite) and sedimentary overburden (2.2:2.6 g/cm^3 or ~0.92). Although perhaps exaggerated, the preference for depocenters to significantly raft in analogue experiments, especially during early model evolution (see Sections 5.7, 5.9), suggests the importance of this occurrence within the eastern Scotian Margin.

Similarly small rafted Late Jurassic (Mic Mac) depocenters have been interpreted on top of allochthonous salt in profile 2000 (Figure 6.1). Here faulting and rotation of Early Cretaceous (Mississauga) sediments indicate significant extension on the allochthonous salt level leading to passive diapir formation (Figure 6.1). Late Jurassic minibasins are expected to have translated seaward above allochthonous salt as it was extruded. The main 3-D experiment displays similar yet not as pronounced minibasins on the allochthonous silicone nappe system. DIC strain monitoring illustrates translation of depocenters on top of the silicone nappe (10 – 12 cm) and some sections (40, 25, 20 cm

for main 3-D experiment in Appendix B) display diapirs separating minibasins and the landward rotation of strata (Appendix B). However, experiment structures are quite gentle when compared to highly rotated strata above allochthonous salt within profile 2000 or 89-1 (BSW, see Section 4.5).

Source of late stage canopy formation

A mid-Early Cretaceous passive canopy is imaged near the basinward edge of the salt basin within profile 2000 (Figures 6.1, 6.2). No feeders are imaged in the section; therefore it is difficult to determine the salt migration path. Experiment results (see Chapter 5.7, 5.9, Appendix B, C) demonstrate that canopies are being fed by either laterally extensive passive diapirs over basement highs in the rift basin or allochthonous diapirs located just seaward of the salt basin (Figure 6.3) at the base of the nappe. Due to the stratigraphic position and proximity of the canopy to D4 of profile 2000, it is most likely that this diapir or a related structure along strike is feeding the canopy. Similarly landward canopies along the basin edge of the main 3-D experiment were sourced from silicone structures just outboard of the rift basin at a similar equivalent stratigraphic position when compared to profile 2000. The salt distribution maps of Shimeld (2004) also show extensive Cretaceous salt sheets and canopies to the east of profile 2000 in Subprovince V that may be related to the canopy imaged in profile 2000 (Figure 6.2). Line 2000 may only image the border of the canopy trend of Subprovince V.

6.3 Conceptual structural and tectono-stratigraphic evolution of the eastern Scotian margin

The chrono-stratigraphic salt tectonic evolution of the eastern Scotian Margin as interpreted from NovaSpan profile 2000 has been influenced by varied sedimentation rates of the Jurassic and Cretaceous, particularly high rates during the Middle – Late Jurassic, on initially thick salt (~3 km) within an overall wedge shaped salt basin comprised of two half grabens. (Figure 6.4A).

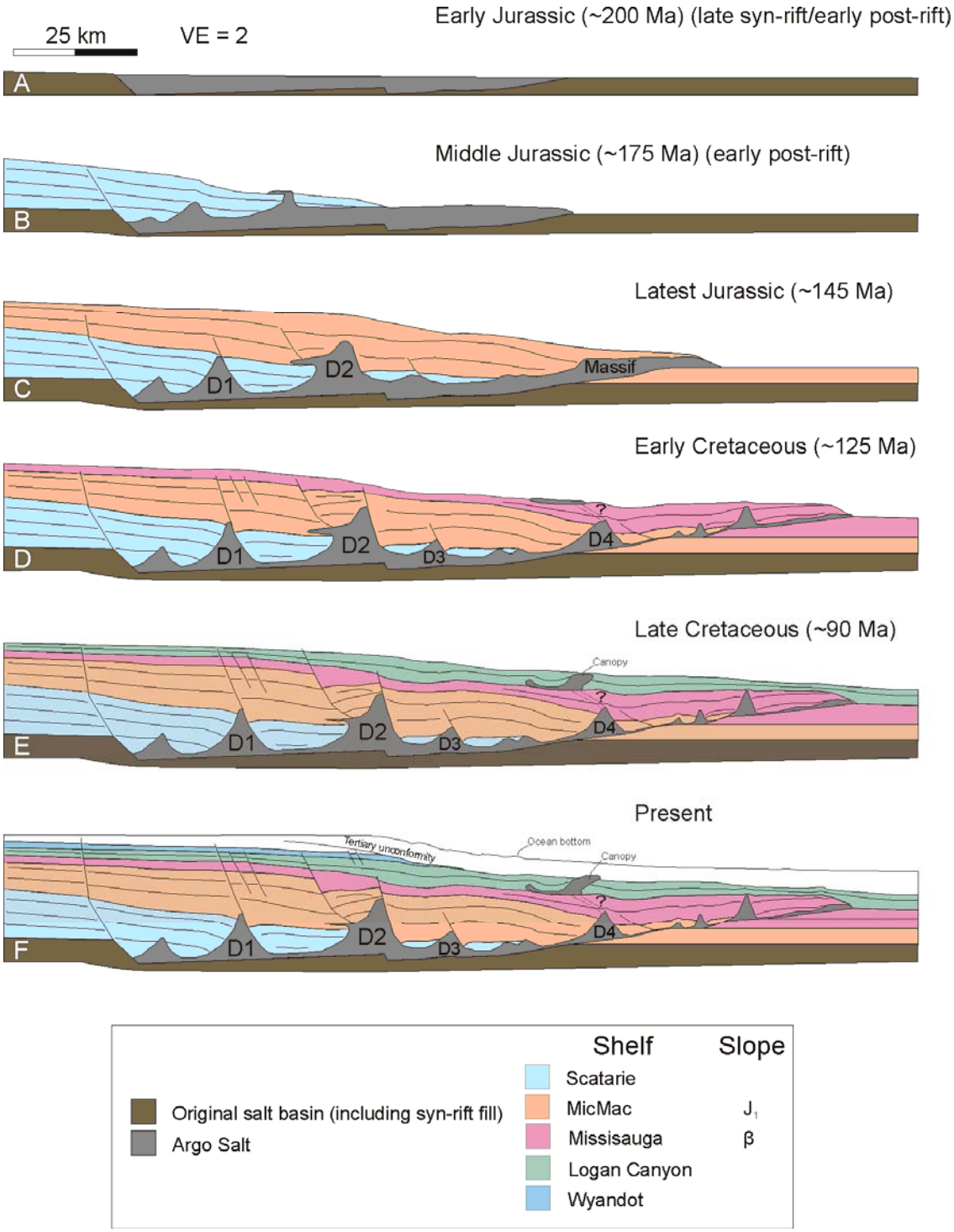

Figure 6.4. Basin-scale conceptual model for the structural evolution of the eastern Scotian margin based on NovaSpan Line 2000. A) Initial salt basin configuration of two seaward thinning half graben wedges (end of syn-rift). B) Middle Jurassic sedimentation of the Mohican Formation and Scatarie Member and deepwater equivalents . C) Late Jurassic sedimentation of the thick Mic Mac Formation and deepwater equivalents. D) Early Cretaceous sedimentation of the Mississauga Formation and deepwater equivalents. E) Late Cretaceous sedimentation of the Logan Canyon Formation and deepwater equivalents. F) Present day configuration of the eastern Scotian margin.

Early – Middle Jurassic**:** Initial depocenter formation and seaward salt inflation

Early – Middle Jurassic (Scatarie – Mohican) sediments formed a thick sediment wedge restricted to the landward salt basin. Related landward salt withdrawal initiated major seaward salt mobilization and basinward salt inflation (Figure 6.4B). Extension of the sedimentary wedge, initiates the formation of salt ridges. These topographic highs of passive diapir heads directed sediment supply to adjacent salt withdrawal basins leading to increased salt withdrawal and diapir development; a positive feedback cycle. The location of early diapirs for the most part determined the structural and depositional evolution of the eastern Scotian margin (Figure 6.1). At the end of the middle Jurassic landward canopies formed adjacent to distal diapirs. Most likely, high subsidence in landward salt withdrawal basins inhibited sediment transport in the distal basin allowing diapirs to extrude along the seafloor above landward subsiding salt withdrawal basins. Landward salt withdrawal basins began to weld to the salt basin floor trapping remnant salt pillows.

Late Jurassic: Inflation of the salt massif and onset of salt extrusion

Increased sediment input and sedimentation rates during the Late Jurassic (Mic Mac) initiated sediment progradation and passive downbuilding of sediments into basinward-inflated salt. Ongoing extension along the axes of passive diapirs caused rafting of underlying older (Scatarie – Mohican) sediments (Figure 6.4C). Diapir D2, initiated within the landward half graben wedge, is translated basinward and arrested at mid-basin

position along the thin basinward edge of the first half graben wedge. As depocenters on its basinward flank decoupled and passively downbuilt into thick salt of the second half graben wedge, D2 was trapped at this position. The slowing of flow vectors as silicone climbs the half graben wedge resulting in overriding sediments being deposited seaward of the diapir are responsible for the arrest of D2 on this basement high.

Efficient salt withdrawal and diapir formation led to near welding below mid-basin salt withdrawal basins. The initial salt basin geometry of a basinward seaward thinning wedge coupled with high sedimentation rates resulted in seaward salt mobilization and the development of a large inflated salt body or massif at the edge of the basin (Figure 6.4C). Broad and gently rolling Late Jurassic (Mic Mac) strata at the basinward edge of the rift basin indicate the expulsion of the salt massif. This salt body and its emplacement are key characteristic of this evolutionary stage necessary to produce the Early Cretaceous extensive allochthonous salt nappe outboard of the rift basin. Beyond the basin edge, deepwater and overriding sediments of this time equivalent accumulate and begin to form the base for the climbing allochthonous salt.

Early Cretaceous: Seaward extrusion and formation of extensive salt nappe

Deposition of Early Cretaceous (Mississauga) sediments drives the formation of the extensive salt nappe characteristic of NovaSpan profile 2000. Sediments of this time constitute the bulk of sediments directly overlying allochthonous salt (Figure 6.4D). Differential loading on the salt massif led to the continual seaward extrusion of salt with

extension being accommodated through the initiation of small passive diapirs. At the base of rafts, small amounts of Late Jurassic sediments are present. Minibasins were originally deposited on top of the salt massif then translated basinward on mobile salt. The deepwater stratigraphic controls indicate that allochthonous salt nappe formation occurred over a period of > 40 Ma. A combination of prograding sediments overriding the salt toe and deepwater pelagic sedimentation are subsequently overridden by extruding salt to form the base of the nappe. The constant angle of the ramp (~ 1°) indicates a continuous extrusion process. The experiments have demonstrated that the salt nappe did not evolve solely as a passive salt glacier but was most likely a result of interplay between loading sediments on inflated salt. Allochthonous salt was covered by translating sedimentary overburden with an open toe (Figure 6.4D) to allow seaward extension and a roho-style deformation of the overburden.

Mid – Early Cretaceous: Sedimentation on allochthonous salt and second level canopy

During the mid-Early Cretaceous (Logan Canyon) passive canopies formed near the basinward edge of the salt basin within profile 2000 (Figure 6.4E). The timing of passive salt flow at the ocean bottom corresponds to a transgressive episode of the early Cretaceous responsible for the widespread deposition of the Naskapi shale (Figure 6.5). The welding of earlier salt withdrawal basins and the capping of allochthonous salt by mid – Early Cretaceous sediments leads to the shut down of seaward salt mobilization. By this time the evolution of main salt tectonic structures in the eastern Scotian margin is complete.

Summary

In summary early (Jurassic) high sedimentation rates producing proximal salt withdrawal basins efficiently extruded and inflated salt seaward while forming mid-basin diapirs. Continued sedimentation (Cretaceous) on an inflated salt massif at the basinward margin of the rift basin drove seaward salt mobilization forming an allochthonous nappe. Allochthonous salt has undergone tremendous extension forming a detachment surface while stratigraphically climbing up-section. Late – Early Cretaceous sediments then covered and shut down basinward salt mobilization (Figure 6.4F).

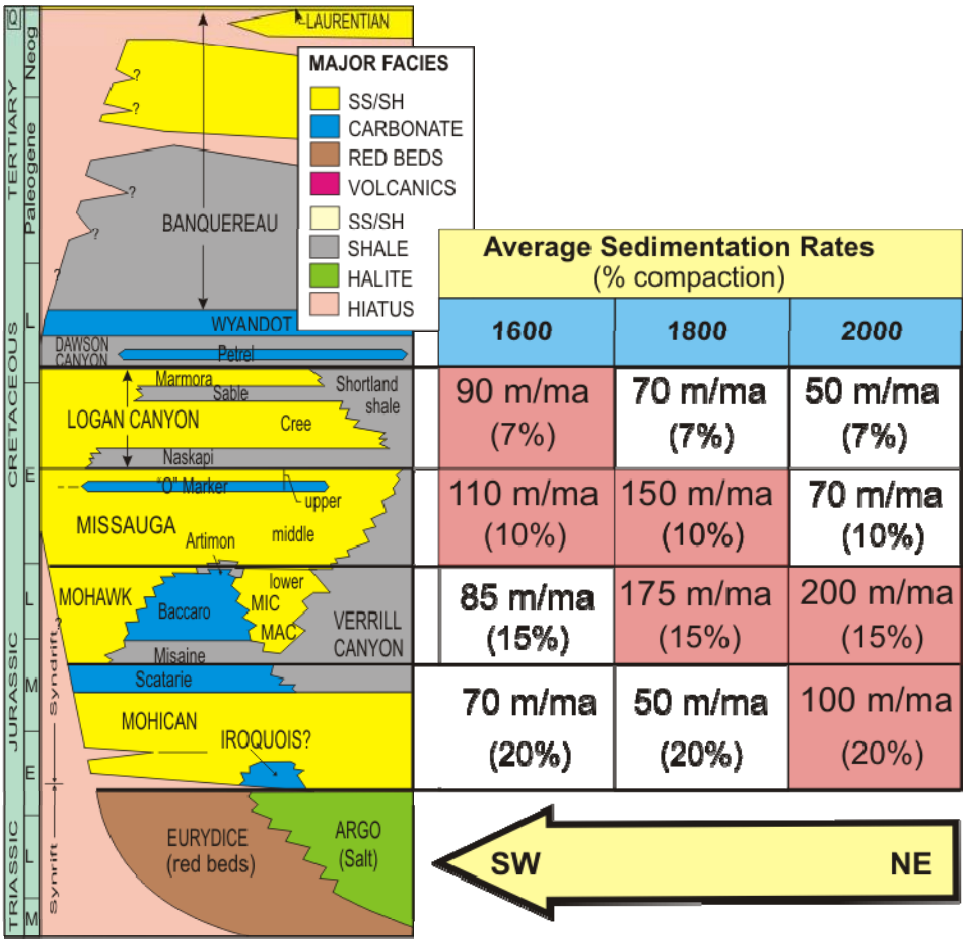

Figure 6.5. Generalized stratigraphy for the Scotian Margin with approximated sedimentation rates for stratigraphic intervals derived from NovaSpan seismic profiles 1600, 1800 and 2000. Note that the highest sedimentation rates occur during later stratigraphic periods across the margin in a southwest direction. This occurrence is suggested to be the main factor behind the apparent southwestern younging of major salt features observed across the North Central Scotian Margin.

6.4 Implications of new results for the evolution of salt Subprovince IV

The results of this study in combination with available public geophysical data and published geophysical work provide new insights in the regional salt tectonic evolution and basin history of the eastern Scotian margin (salt Sub-province IV). Additional data include velocity models of the SMART (Scotian MARgin Transects) seismic refraction Line 1 (Funck et al., 2004) (coincident with GSC Lithoprobe line 89-1), ~50 km west of profile 2000, seismic reflection data of Lithoprobe line 89-1, and gravity studies of Scotian Margin crustal profiles from Keen and Beaumont (1990), Keen and Potter (1995), and Zheng and Arkani-Hamed (2002).

Salt basin geometry

Basement and salt basin structures of GXT line 2000 are comparable to that imaged on GSC line 89-1 (Figures 6.1, 6.6). In line 89-1 rifted and rotated basement blocks are imaged immediately south of the hinge zone (Figure 6.6). Basement half grabens with syn-rift growth sediments constitute the salt basin floor. Depth converted crustal velocity models of SMART Line 1 image a broad 115 km wide seaward thinning basement wedge terminating near the Tanallon (M-41) well beyond the modern shelf break (Figure 6.6). Basement structures include an elevated landward half graben block (~20 km wide) adjacent to the hinge zone (Figures 6.2, 6.6) (see Section 3.1.1).

Previous studies of profile 89-1 suggested that the original salt basin in Subprovince V was much narrower than in surrounding subprovinces (Shimeld, 2004; Ings and Shimeld, 2006) (Figure 6.2). The seaward margin of the salt basin was interpreted just landward of the shelf break, limiting the width of the basin to ~90 km. From the NovaSpan profiles and the new interpretation presented in this study, the basinward limit of the autochthonous basin conforms much more to the regional trend in the adjacent salt sub-provinces, nearly aligned to that of profile 2000 (Figure 6.2). The crustal profile and seismic reflection data show clearly that seaward of the salt basin the inclined salt detachment surface D begins to climb and truncate deepwater strata. This position is interpreted as the new seaward margin of the autochthonous salt basin (Figure 6.6), which correlates along strike with the trend in profile 2000 (Figure 6.2).

Allochthonous salt systems

A link between the salt tectonic mechanisms of profiles 2000 and 89-1 is evident, most noticeably the formation of the allochthonous salt nappe system. The salt detachment D of line 89-1 and the base of the salt nappe in line 2000 correlate along strike of the margin and are characterized by similar width of allochthonous salt structures (89-1: Banquereau Syn-kinematic Wedge, ~ 70 km: GXT 2000 salt nappe ~ 65 km) and comparable ramp angles of the salt and detachment base (~ 1°). Similar formation mechanism for the allochthonous salt systems in both sections is inferred from the relationship between allochthonous salt and overburden. Landward dipping reflector packages and remnant salt diapirs of profile 89-1 (Figure 6.6) are analogous to that of the

nappe imaged in profile 2000 (Figure 6.1).

A major difference between allochthonous development between the two profiles is the timing of sedimentation pulses driving salt extrusion. In profile 89-1 the top Jurassic (tJ) horizon (equivalent to the top Mic Mac chrono-stratigraphic seismic marker) marks the upper boundary of the BSW and in the deepwater, the J_1 horizon denotes the end of climbing for the salt detachment (Figure 6.6). However, in profile 2000 the nappe formed later during the Late Jurassic (J_1) and ended in the Early Cretaceous (β). The sediment pulses driving allochthonous salt mobilization in profile 89-1 occurred earlier than in profile 2000 (see section 6.5) although the mechanisms and style of salt extrusion are very similar.

Another key difference is the roho-style deformation on the salt detachment with highly rotated and faulted strata of line 89-1 (Figure 6.6) with little salt present compared to the abundant salt and more broad reflector configuration of profile 2000. Abundance of initially deposited salt may be a major reason for the differences observed between profiles. Thin salt (< 1.5 km) better facilitates shear flow of salt and domino style faulting or roho formation (Campbell, 2007; MacDonald, 2007; Kreszek et al., 2007). In comparison, the abundant allochthonous salt of line 2000 better facilitated passively downbuilding minibasins and passive diapir formation driving salt extrusion.

Initially thin (< 1.5 km) salt deposits within profile 89-1 linked with higher sedimentation rates in the Jurassic, due to the location of the paleo-Sable delta, may account for the

different timing of the salt detachment and nappe. Higher sedimentation on thin salt most likely led to a more rapid and efficient evacuation of salt during the Middle Jurassic with subsequent development of the BSW in profile 89-1 much earlier than the salt nappe (Early Cretaceous) of line 2000. From the arcuate trend of mapped shallow salt bodies within Subprovince IV (Shimeld, 2004) higher sedimentation rates in the center of this region is a reasonable assumption. This geometry probably developed as a result of localized point sourced deltaic lobes deposited within the center of Subprovince IV, displacing salt in a radial pattern. Similarly the BSW is observed to have a concave base (Shimeld, 2004; Ings and Shimeld, 2006). These features suggest that the location of GSC line 89-1 in the central Subprovince IV is imaging earlier salt mobilization and related sedimentation than the salt system in NovaSpan line 2000, located on the easterly flank of the roho system (Figure 6.2).

Autochthonous salt structures

Autochthonous salt structures are very difficult to interpret in profile 89-1 due to poor imaging of deep structure. However, previous pilot experiment 1 (Chapter 5.7, Figure 5.4, Appendix B) provided insight into typical structures that develop under given basin characteristics. Experiments with half graben geometries and consequently wedge shaped salt basins often preferentially develop long-lived downbuilding of depocenters (sediment wedge) on the landward flank of salt (see Figure 5.4, Appendix B) as seen in pilot experiment 1 (Appendix B). The wedge shape salt basin allows an expulsion rollover and associated keystone grabens to form along a continually and slowly basinward migrating

salt massif. It is possible that the poorly imaged Mid – Late Jurassic strata beneath the shelf break and slope consist of a broad expulsion rollover with keystone grabens responsible for the efficient mobilization of salt from the autochthonous basin (Figure 6.3). Seismic reflectivity located at ~7.5 s at SP 2500 may indicate a remnant salt body left from previously inflated salt of a massif located at the distal autochthonous salt basin edge (Figure 6.2). Fault structures effecting Jurassic and Cretaceous strata imaged beneath the modern shelf break may additionally be associated with detachment on D or perhaps more likely a result of reactivation of keystone graben faults that formed in response to rolling strata of the expulsion rollover expelling salt from the basin (Figure 6.6).

6.5 Implications for the north central Scotian margin – Insights from co-studies

4-D analogue experiment and seismic interpretation results of the salt tectonics and basin history of the eastern Scotian margin concurrent with the 2 partner studies of the Abenaki and Sable Basin (salt Subprovince III: based on seismic interpretation of NovaSpan lines 1800 and 1600) demonstrate that the salt tectonic evolution of the north central Scotian Basin (Subprovinces III, IV, and V) is strongly linked in time and space.

A connection of salt tectonic elements across the margin can be made using paleogeograpical maps of the suspected major loci of sediment input (deltaic complexes) (East Coast Basin Atlas Series, 1991), depositional elements, timing and evolution of characteristic salt structures interpreted from regional seismic lines (NovaSpan,

publically available), and newly interpreted boundaries for the eastern autochthonous salt basin (Figure 6.7).

The timing and location of major sediment input, in particular the development of the big deltaic complexes, caused the diachronous salt mobilization along-strike of the rift basin. On the modern Scortian margin an overall trend of salt structures younging towards the southwest indicate that salt was to some extent mobilized from the northeast (Subprovinces IV, V?) and expelled to sub-basins of Subprovince III as major depocenters migrated. The development of characteristic salt features in the salt subprovinces is linked to the age and size of sediment pulses (Figure 6.5) and the salt basin architecture in the different sub-basins.

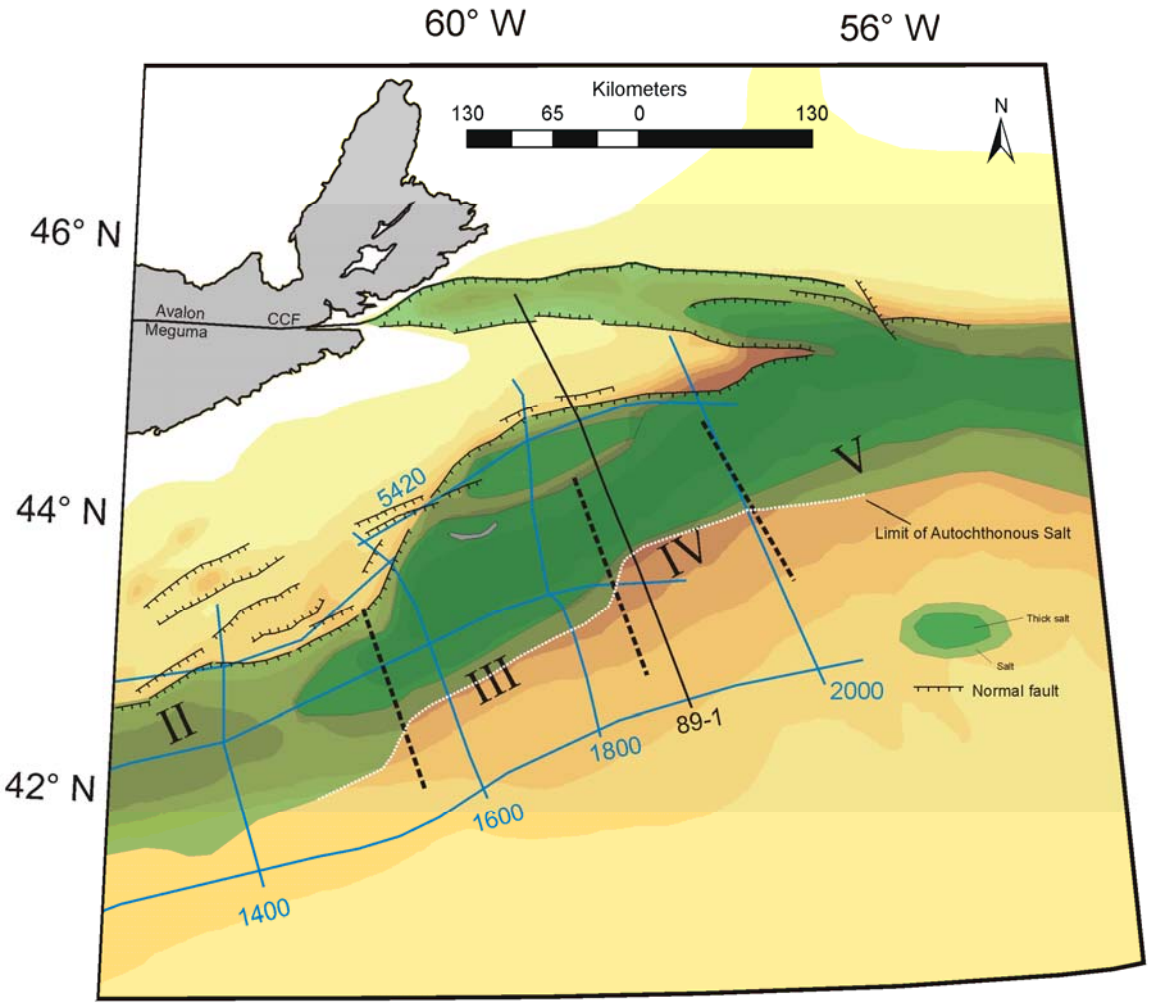

Figure 6.7. Early Jurassic location of the original salt basin of the Scotian margin redefined from the interpretation of regional seismic profiles (NovaSpan lines 1600, 1800, and 2000 – blue and GSC line 89-1 - black) (modified from Shimeld, 2004).

6.5.1 Diachronous evolution of the north central Scotian margin

The styles and timing of salt structures across the Scotian margin is very variable. The earliest indicators of allochthonous salt structures are small remnant salt bodies within the Banquereau Syn-kinematic Wedge (BSW) of Subprovince IV (and possibly V) and the comparable salt nappe system (BSW?) observed within NovaSpan line 2000 (Figure 6.2).

These structures formed already during the Late Jurassic and Early Cretaceous respectively.

To the southwest in Subprovince III, major allochthonous salt features are comprised of extensive (< 60 km) salt canopy systems near the basinward margin of the original salt basin (Figure 6.2). Here, salt canopies are characterized by near vertical feeders up to 8 km high, sourcing sub-horizontal canopies. The widespread canopies of the deepwater Sable area flowed passively on the sea floor during the early Late Cretaceous.

Average sedimentation rates for major depositional units of NovaSpan lines 2000, 1800, 1600 show the trend of sediment input through time within the different sub-basins of the eastern margin (Figure 6.5). Times of high sediment influx along the margin correlate with the major episodes of salt structure evolution in the individual salt subprovinces**.**

High approximated sedimentation rates during the Early through Late Jurassic Subprovince IV and possibly western V (NovaSpan Line 2000) have driven early salt mobilization in the autochthonous basin leading to the formation of an allochthonous salt nappe/detachment system. Major salt deformation ceased by the end of the Jurassic in the center of subprovince IV (line 89-1) and slightly later along the eastern edge of this region (NovaSpan line 2000) by the mid – Early Cretaceous (see Section 6.4).

In Subprovince III (NovaSpan Lines 1800 and 1600) high sedimentation rates were observed significantly later during the Late Jurassic and Early Cretaceous (Sable Delta)

(Figure 6.5). Due to low early sediment input and weak loading, salt remained mostly autochthonous through the Late Jurassic. Later (Early Cretaceous) high sediment input mobilized major salt walls at the autochthonous basin edge. Sedimentation kept pace with salt wall (feeder) vertical growth confining rising salt until the end of the Early Cretaceous when salt flowed passively in mostly a seaward direction.

6.5.2 Mobilization pattern of salt

The original salt basin of the north central Scotian margin covered most of the original rift basins from the rift hinge zone to basinward limit of autochthonous salt (Figure 6.7). The areas of thickest original salt deposits are located along the rift basin axis just seaward of the hinge zone (e.g. Laurentian and Sable Sub-basins) and in the smaller rift basins of the rift shoulder (e.g Abenaki sub-basin and Orpheus Graben).

New seismic interpretation results of NovaSpan Lines 1800 and 1600 of Subprovince III (Campbell, in press; MacDonald, in press) have shown that the seaward limit of the autochthonous salt basin is located slightly (~ 20 km) seaward compared to previous interpretations (Shimeld, 2004). In addition results (see section 6.4) of this study support a similar basinward adjustment for Subprovince IV.

Key factors determining the migration path and flow direction of salt throughout early margin evolution were paleo-sedimentation patterns and main depositional elements along the margin. In natural salt systems varying sedimentation patterns and basin

morphology cause complex 3-D flow patterns.

Middle Jurassic – Early salt withdrawal and basinward mobilization

The southwest direction of sedimentation input caused by the early Sable Delta suggests significant salt movement in Subprovince III by the Middle Jurassic (Figure 6.8). However, seismic interpretation results of NovaSpan Lines 1800 and 1600 suggest the absence of allochthonous salt by this time. Similarly, high Middle Jurassic sedimentation rates (NovaSpan line 2000) along the eastern margin suggest significant early salt mobilization in the eastern subprovinces (IV and V?). In the GSC line 89-1 stratigraphic indicators prove that salt was significantly mobilized basinward by the end of the Middle Jurassic.

In the center of Subprovince IV allochthonous salt was extruded by the Middle Jurassic. The main 3-D experiment demonstrated that major salt nappe formation is linked to sediment progradation on an inflated basinward salt massif and associated extruded salt (Figure 6.8). This early basinward salt massif is the source for the future development of the allochthonous BSW by the end of the Jurassic (Mic Mac). The eastern edge of Subprovince IV (Line 2000) also is characterized by high sediment input during the Early and Middle Jurassic; however stratigraphic control and modeling results (Figure 6.3) suggest that there was no major extrusion of allochthonous salt by the Middle Jurassic. However, no significant deltaic sources have been mapped seaward of the basement hinge within Subprovince IV at this time. The source of this significant sediment input is

still unknown, with an unmapped Sable Delta or early Laurentian Delta component a possibility.

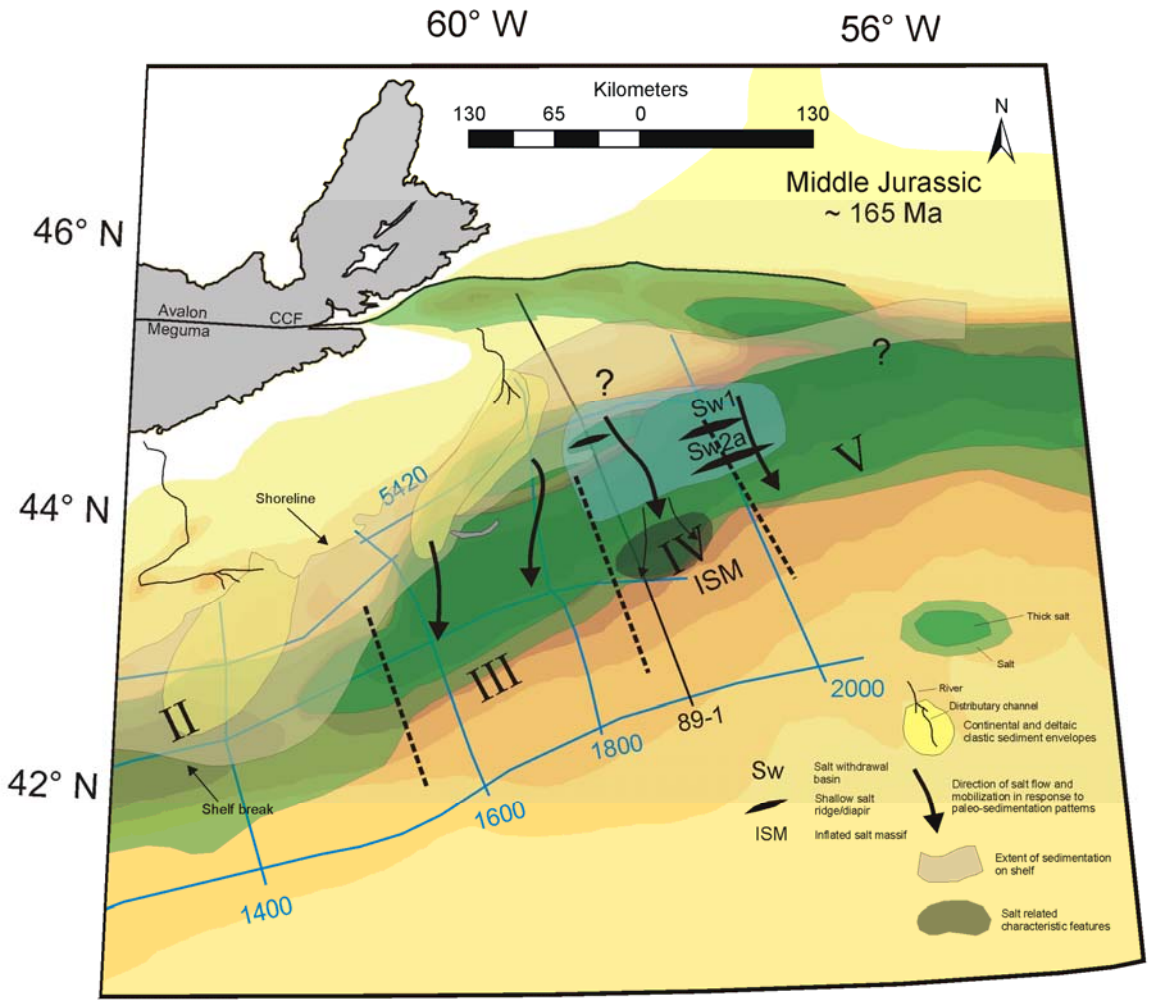

Figure 6.8. Paleogeography and sedimentation patterns of the Middle Jurassic (~165 Ma) (East Coast Basin Atlas, 1991). Blue transparent overlay - approximate limit of major Middle Jurassic (Scatarie/Mohican) deposition. Active salt withdrawal basins and salt structures derived from modeling results are labeled in proximity to line 2000. Characteristic salt features (grey overlay) and salt flow patterns (black arrows) are illustrated.

Overall the Early and Middle Jurassic were marked by the relatively gradual and uniform basinward mobilization of salt in the autochtoneous salt basin of the North Central Scotian margin. The only exception was the central Subprovince IV (Sable Sub-basin), where a major salt massif and possibly allochthonous salt glaciers developed in the distal

salt basin as consequence of efficient salt mobilization.

Late Jurassic – Early salt massif inflation and allochthonous extrusion

The Late Jurassic is marked by high sedimentation throughout the eastern margin as a result of the further development of the prominent Sable Delta and the initiation of the more easterly Laurentian Delta (Wade and MacLean, 1993) (Figure 6.9). The arcuate pattern of shallow salt within much of subprovince IV suggests that an overall radial pattern of salt withdrawal exists. Therefore salt was expelled from central subprovince IV and mobilized to both westerly and easterly adjacent regions as consequence of the formation of the allochthonous BSW.

To the east the Laurentian Delta was a major source of sediment input in Subprovince V. Paleogeographic reconstructions (Wade and MacLean, 1993) indicate an overall southwards sediment transport direction along the eastern Scotian margin. Thick Late Jurassic landward depocenters of the Scatarie/Mohican and Mic Mac Formations and deepwater equivalents on the eastern border of Subprovince IV (Line 2000) likely have been affected by the Laurentian Delta. Although this region experienced high amounts of sedimentation during the Late Jurassic, unlike most of subprovince IV, the eastern border did not fully form a nappe/detachment system. Instead model and seismic interpretation results imply that the high rates of Late Jurassic sedimentation and a seaward thinning ramp geometry of the second half graben wedge led to the basinward evacuation of salt and the development of an inflated salt massif (ISM) along the edge and outboard of the

autochthonous basin (Figures 6.9). To the west of this the BSW (salt detachment system) within central Subprovince IV has fully formed. Analogue modeling implies that early salt extrusion and inflation of a salt massif along the basinward margin followed by subsequent overriding Late Jurassic sedimentation mobilized allochthonous salt of the BSW while highly extending and rotating Late Jurassic strata.

The paleogeographic location of the Sable Delta during the Late Jurassic indicates that within Subprovince III salt was likely mobilized in a southwest direction. Implied radial salt flow patterns within subprovince IV show that originally autochthonous salt of this region may have been mobilized southwest to join autochthonous salt of Subprovince III (Figure 6.9). Seismic interpretation results of NovaSpan lines 1800 and 1600 in Subprovince III indicate that canopies were not formed at this time and that most salt remained autochthonous. Instead salt basinward mobilization due to saltwithdrawal beneath landward depocenters led to the gradual inflation of an autochthonous salt wall (ASW) within the basinward portion of the salt basin (Figure 6.9). Salt mobilization is delayed in Subprovince III when compared to the eastern margin most likely due to lower sediment input (Figure 6.5) on autochthonous salt and a wider initial salt basin within this region.

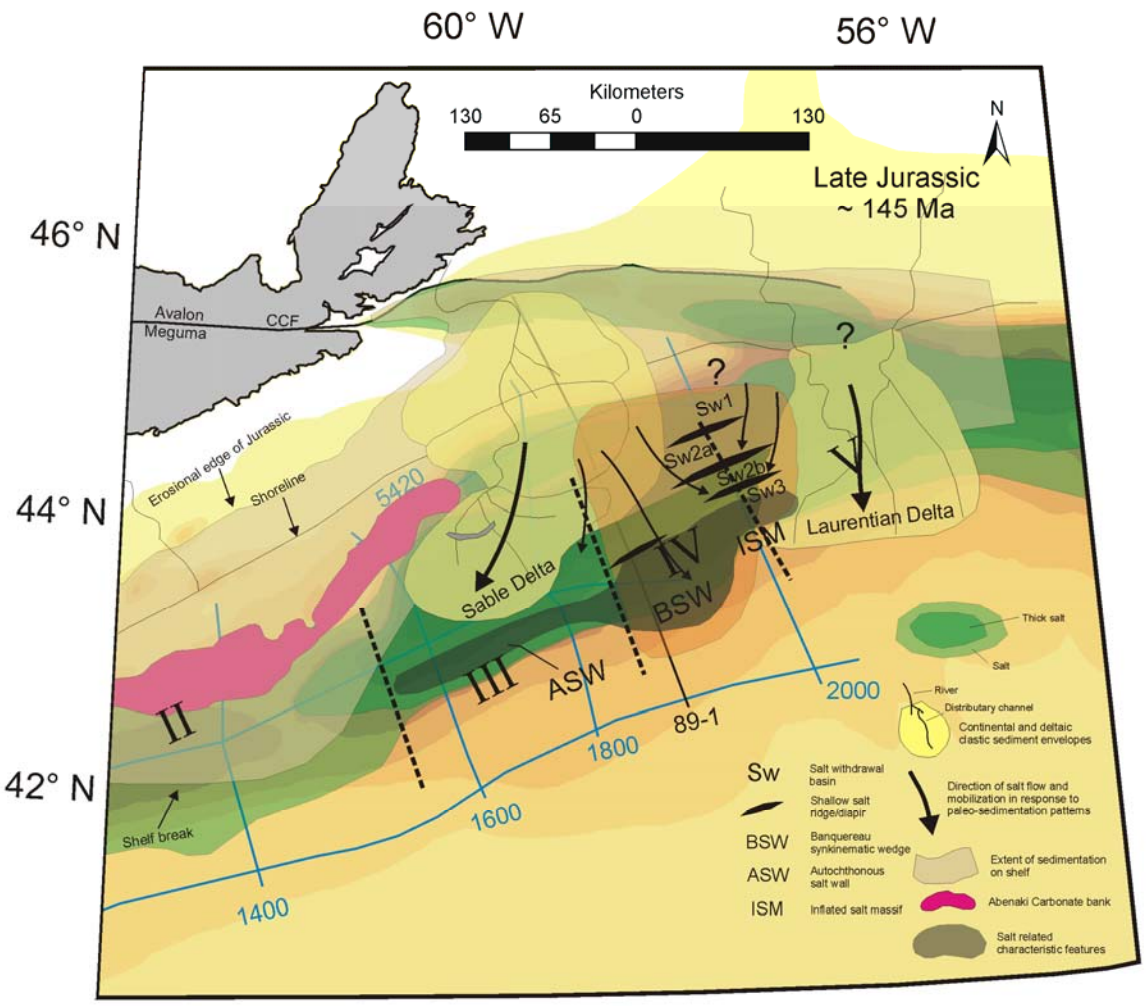

Figure 6.9. Paleogeography and sedimentation patterns of the Late Jurassic (~145 Ma) (East Coast Basin Atlas, 1991). Orange transparent overlay - approximate limit of major Late Jurassic (Mic Mac) deposition. Active salt withdrawal basins and salt structures derived from modeling results are labeled in proximity to line 2000. Characteristic salt features (grey overlay) and salt flow patterns (black arrows) are illustrated.

Early Cretaceous – Eastern salt nappe development

Salt tectonics in the eastern Scotian margin (Subprovince IV) was mostly shut down by the end of the Early Cretaceous. The majority of the BSW structure is composed of Late Jurassic strata. However, the eastern flank of this feature, as imaged by NovaSpan line 2000, suggests that deposition of Early Cretaceous sediments (Mississauga Formation

and deepwater equivalents) expelled salt seaward forming the extensive nappe system related to the BSW (Figure 6.10). The source of this sediment input is still unknown, however, remnant river systems and distributaries of the Laurentian Delta may be responsible.

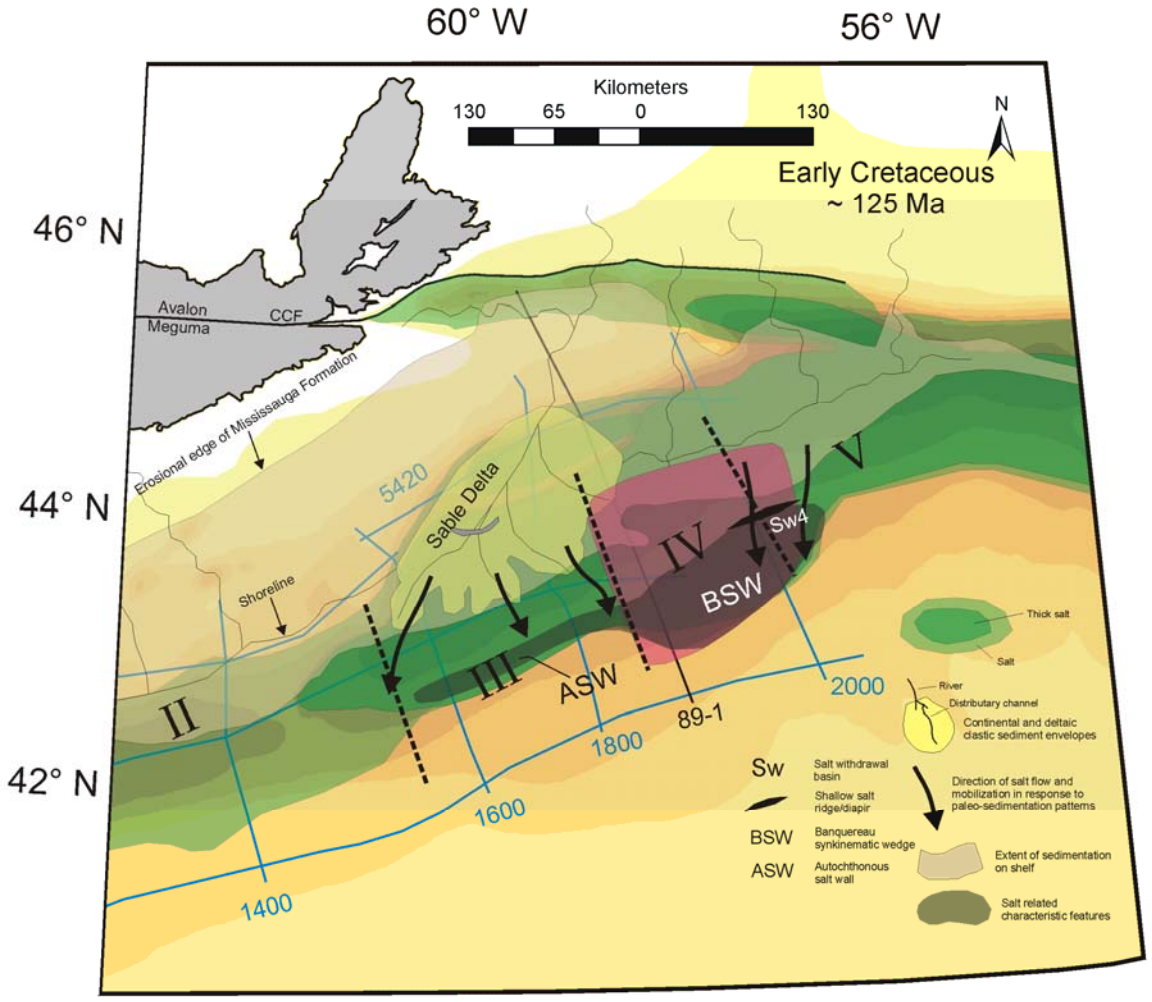

Figure 6.10. Paleogeography and sedimentation patterns of the Early Cretaceous (~125 Ma) (East Coast Basin Atlas, 1991). Magenta transparent overlay - approximate limit of major Early Cretaceous (Mississauga) deposition. Active salt withdrawal basins and salt structures derived from modeling results are labeled in proximity to line 2000. Characteristic salt features (grey overlay) and salt flow patterns (black arrows) are illustrated.

The majority of clastic input along the eastern margin at this time is due to the Sable Delta. Deltaic complexes have an overall southwest trend with a complex of distributary channels depositing sediment in both southwest and south orientations (Wade and MacLean, 1993) (Figure 6.10). Sediment loading led to the continued inflation of salt at the basinward portion of the autochthonous basin instead of leaving it (allochthonous salt). At this stage, the laterally continuous autochthonous salt wall (ASW) accumulated sediments on both landward and basinward flanks, obstructing seaward translation (Figure 6.10). The overall southwest direction of deltaic deposition during this period may have forced salt from the autochthonous basin of Subprovince III into adjacent western subprovinces (II and I).

mid – Early Cretaceous

The mid-Early Cretaceous to the Late Cretaceous is marked by the complex development of localized distributary channels in the North Central Scotian margin (Figure 6.11). Major salt mobilization along the eastern margin is limited to Subprovince III at approximately the onset of the Late Cretaceous. Here restricted sedimentation around inflated salt walls at the basinward margin of the initial salt basin has led to extensive salt canopies (up to 60 km in length). Canopies flowed in both seaward and landward directions, with seaward verging canopies being prominent (Figure 6.11).

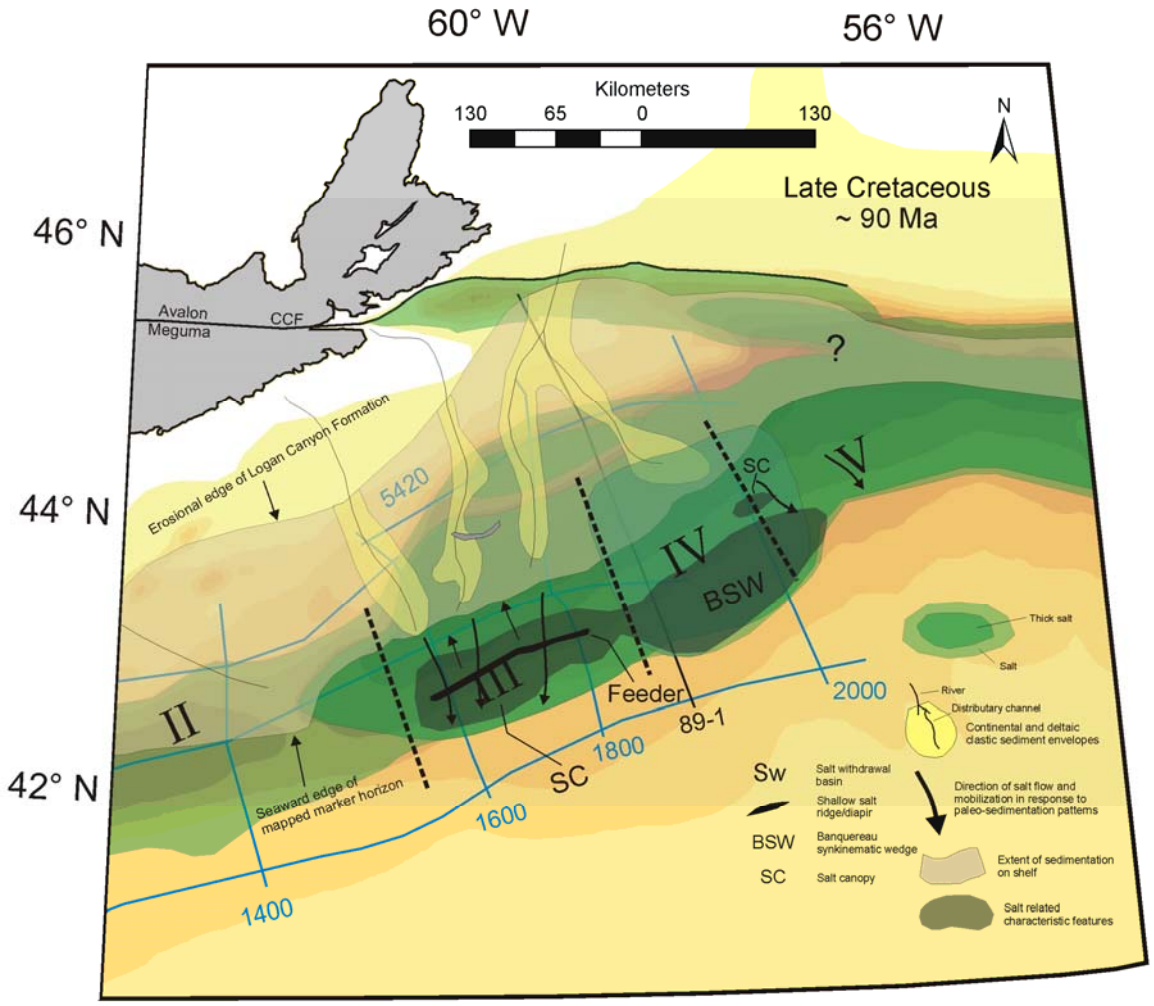

Figure 6.11. Paleogeography and sedimentation patterns of the Late Cretaceous (~90 Ma) (East Coast Basin Atlas, 1991). Green transparent overlay - approximate limit of major Early - Late Cretaceous (Logan Canyon) deposition. Active salt withdrawal basins and salt structures derived from modeling results are labeled in proximity to line 2000. Characteristic salt features (grey overlay) and salt flow patterns (black arrows) are illustrated.

Salt movement in the eastern subprovinces (IV, V) was restricted to late stage canopy formation as observed in NovaSpan line 2000 (Figures 6.1, 6.11). Canopies are likely sourced from diapirs located along the basinward margin of the autochthonus salt basin. With the formation and subsequent burial of extensive canopies within Subprovince III during the Late Cretaceous, all major salt tectonic elements of the eastern Scotian margin were in place. Small amounts of salt movement within existing structures continues

nearly to present day, however, the major location and style of salt structures characteristic to the eastern margin developed by the end of the Cretaceous.

6.6 4-D analogue modeling advances

Analogue “sand box” experiments have made big advances in the last two decades and have greatly improved our understanding of salt tectonic processes (Jackson, 1995; Jackson and Talbot, 1994). However, only very recently analogue experiments were used to analyze salt tectonic processes on sedimentary basin scale, from the landward extensional domain to the deep-basin contractional domain (Fort et al., 2004). Further development of analogue modeling techniques has led to the use of appropriate scaling factors and now the quantification of model surface deformation through the use of digital image correlation (DIC).

Scaled physical experiments based on NovaSpan line 2000 seismic interpretation have successfully simulated the first-order salt structures and timing of depositional systems of the eastern Scotian margin. Structural cross-sections of final experiment give insight into structures, their related depocenters, and implications for their development. However, new DIC techniques allow interval and finite values for 3-D strain. The temporal evolution and surface displacement patterns and rates in the experiment were monitored by DIC techniques throughout basin evolution. Structures that develop during the experiment were analyzed and strain measurements at the model surface give insights in the kinematics and mechanics of their structure development.

For instance, in the main 3-D experiment silicone inflation in the distal portion of the autochthonous basin was monitored from the onset of sedimentation through nearly half of the experiment. The large amount of landward extensional and basinward contractional deformation that was accommodated by this salt massif has major implications for the salt tectonics evolution and basin history. However, is very difficult to recognize this in the seismic data through the imaging of a modern day salt and sediment configuration that has been overprinted by subsidence and passive downbuilding. Mid-basin inflation prevalent throughout much of the early basin history would have major implications for reservoir characterization. Starved sedimentation as a result of inflation and a lack of early accommodation space may cause degraded reservoir quality in these early depocenters. Similarly, a lack of accommodation space above salt-cored anticlines will have the same effect. The crests of these structures, often with flanking rolling and growth strata, attract the interest of petroleum exploration due to their structural closure. However, flanking growth packages – forming stratigraphic traps, not the crestal closure, are more likely to accumulate better reservoir quality through high rates of subsidence, assuming that these structures are proximal to the shelf.

Strain monitoring (DIC) allows the accurate structural restorations available to model cross-sections. Due to the complexity and duration of analogue experiments, accurate structural restorations can be very difficult to produce, therefore missing valuable information regarding basin evolution. Without a scaled and precise profile of the model surface in conjunction with model strain data restorations would not have been possible. Strain data indicated huge amounts of early horizontal translation and extension within

the main 3-D model during a relatively short period (48 h). The extent of rafting depocenters can be seen from model sections, however the timing, rates and mechanisms of these structures is not possible without the input of DIC data. For instance, the early rafting of the sediment wedge (Middle Jurassic – Scatarie/Mohican) and passive flow of early diapir ridges indicated that the initiation of salt structures early in basin evolution in large dictate the final location of major salt features and therefore the basin evolution.

DIC monitoring indicated that seaward extrusion of salt from the basin during the Early Cretaceous (140 – 216h) led to welding of landward depocenters. The termination of subsidence within the landward salt basin reduced accommodation space and encouraged sediment bypass into the deeper basin where petroleum plays (rolling growth packages flanking salt) are very deep (> 8 km) and most likely beyond the oil and gas window. However, complex sediment fairways throughout the Cretaceous (168 – 288h) (Figure 5.9) were controlled primarily by the topography of allochthonous salt (nappe) and secondary canopy development at the salt basin edge. Here, localized sediment input (simulating turbidite channels) accumulate between passive salt features where subsidence is active. These small potentially sandy deposits are the most likely source for untapped reservoir accumulation across the eastern Scotian margin.

Chapter 7: Conclusions

The contributions of this study are grouped in three distinct categories:

1. Advances in regional seismic interpretation for the eastern Scotian margin;
2. Implications of analogue experiment results for salt tectonics and basin history of the eastern Scotian margin;
3. Application of regional study results for future industry projects.

7. 1 Advances in regional seismic interpretation for the eastern Scotian margin

- The eastern part of Subprovince IV, as imaged by NovaSpan Line 2000, is characterized by a series of broad (~ 10 km) triangular passive diapirs separated by very thick (> 4 km) mostly undeformed salt withdrawal basins. However, autochthonous salt structures of western-central Subprovince IV (line 89-1) are virtually absent.

- An extensive (~70 km long) climbing (1°) Late Jurassic – Early Cretaceous allochthonous salt nappe and associated small diapirs are imaged in the deepwater basin along NovaSpan profile 2000. This salt nappe is related to the Middle – Late Jurassic salt detachment (D) and roho-system associated with the BSW in the western-central Subprovince IV (Line 89-1).

- A Middle Jurassic through Early Cretaceous progradational trend of seaward migrating depocenters can be observed in line 2000. In contrast, the majority of progradational pulses imaged in line 89-1 are Jurassic.

- Approximated sedimentation rates suggest an overall trend of initial high sediment input (Jurassic) in the early post-rift stage that decreased throughout drift stage (Cretaceous). Peak sedimentation (~ 200m/Ma) occurred during the Late Jurassic (Mic Mac).

- Highest sediment input in NovaSpan Line 2000 resulted in thick (up to ~ 5km) Late Jurassic (Mic Mac) salt withdrawal basins within the basinward portion of the autochthonous salt basin. Early Cretaceous minibasins developed ontop of the allochthonous salt nappe, where the differential loading of overriding sediments is responsible for salt extrusion and nappe development.

- Rafting and basinward translation of depocenters is prevalent along line 2000 with Middle Jurassic early depocenters rafting within the autochthonous basin between diapirs and Late Jurassic – Early Cretaceous sediments rafting and translating along the salt nappe.

- Crustal velocity (Funck et al., 2004) and gravity models (Keen and Potter, 1995; Zheng and Arkani-Hamed, 2002) have been used to better constrain the salt basin morphology of GSC line 89-1. The salt basin floor forms an overall seaward

thinning wedge with the autochthonous terminus of the salt basin located significantly farther seaward (> 40 km) than previous interpretations, being more compatible with surrounding subprovinces (III and V).

7.2 Implications of analogue experiment results for salt tectonics and basin history of the central-eastern Scotian margin

The following is a summary of important derived geologic constraints and corresponding experiment results for the eastern Scotian margin as imaged by NovaSpan line 2000.

Thick (3 cm/km) maximum silicone (salt) thickness	Passive downbuilding of sediments achieved through mostly Poiselle flow of thick silicone in landward part of salt basin. This lead to the formation of thick salt withdrawal basins and efficient basinward inflation of silicone (salt).
2 rift half graben wedge salt basin geometry	Early inflation and extrusion of silicone (salt) from the landward graben into the basinward graben caused the spatial decoupling of depocenters. The basinward half graben favoured gradual inflation of a prominent salt massif at the seaward margin of the salt basin.
Variable sedimentation input during basin history	**Middle Jurassic** (Scatarie/Mohican) high sedimentation rates close to the continental rift margin caused the early and efficient basinward mobilization of silicone (salt). **Late Jurassic** (Mic Mac) peak sediment input efficiently evacuated silicone (salt) from the original basin while forming an inflated massif along its seaward margin. **Early Cretaceous** (Mississauga) sediments loaded on the salt massif led to the seaward extrusion and formation of the extensive salt nappe.

Table 7.1. Summary of important derived geologic constraints and corresponding experiment results.

Salt thickness

- Main 3-D experiment supports initially thick (~3 km) salt deposits within the autochthonous salt basin as interpreted from line 2000.

- Main 3-D experiment with thick (3 cm) silicone reproduced the characteristic depocenter pattern with thick undeformed salt withdrawal basins as depocenters translated basinward through passive downbuilding as opposed to basinward extension through widespread faulting (Table 7.1).

- Thick silicone effectively reduced the mechanical coupling between the ductile layer (silicone) and sedimentary overburden (Table 7.1). This low coupling favoured the passive downbuilding of sediments through mostly Poiselle (channel) flow as opposed to extension of overburden through Couette (shear) flow.

Salt basin geometry

- Pilot experiment 2 results support salt basin configuration as interpreted from profile 2000 and comprised of two proportional seaward thinning half graben wedges with filling late syn-rift salt.

- Extrusion of silicone from the landward rift graben into the seaward graben by sediment loading encouraged decoupling of depocenters along the boundary of the two grabens and subsequent basinward translation of depocenters (Table 7.1).

- Continual passive downbuilding of segmented depocenters and the efficient seaward extrusion of silicone dominated basin evolution within the eastern Subprovince IV (Line 2000).

- The basinward half graben wedge favoured gradual inflation and early development of a salt massif at the basinward limit of the salt basin (Table 7.1). The placement of this massif at the end of the Jurassic is crucial in the development of the extensive salt nappe characteristic identified in profile 2000.

- Mid-basin diapirs (D2 in profile 2000), although initiated landward of their modern positions often become arrested along basement highs (e.g. boundary between two half grabens). This occurs as a result of inflation of silicone at these topographic highs and the subsequent trapping of silicone (salt) through the ongoing development of basinward salt withdrawal basins.

Sedimentation and Depocenters

- Sediment input directly influences the timing of silicone / salt mobilization.

- A high amount of sediment input (100m/Ma) in the landward part of the salt basin in the early post-rift phase (0 – 96 hours, Middle Jurassic) was crucial in initiating significant basinward inflation of salt / silicone (Table 7.1).

- Early formation of passive diapir walls in the autochthonous salt basin determined the long-term location of major salt structures and adjacent depocenters. Although autochthonous diapirs translate basinward along with salt withdrawal basins through model and basin evolution, their approximate final configuration is determined early in basin evolution (96 hours, Late Jurassic). Therefore early post-rift basin evolution is key in understanding Scotian Basin salt tectonics, given that early basin evolution determines the structural style for the remaining basin development.

- Peak sediment input during intermediate model / basin evolution (96 – 144 h, Late Jurassic) facilitated the efficient basinward extrusion of silicone / salt leading to the formation of an inflated silicone / salt massif at the basinward edge of the autochthonous basin (Table 7.1).

- Later sedimentation (> 144 h, Early Cretaceous) through differential loading on the salt massif (as a result of landward welding) led to the development of the extensive allochthonous nappe. The nappe spread easily basinward due to an open toe with translating depocenters above it, instead of an extensive salt glacier loaded by sediments (Table 7.1).

- The salt detachment (D) of profile 89-1 formed in much the same way with a salt massif developing at the salt basin margin during the Middle Jurassic. Subsequent Late Jurassic sedimentation initated extrusion of allochthonous salt and subsequent sediment progradation caused roho-style deformation through the rotation of strata and the formation of the detachment.

Regional salt mobilization patterns

- Salt flowed from the central Subprovince IV salt basin in a radial pattern during the Early/Middle Jurassic (see Section 6.5.2).

- Easterly flowing salt from central Subprovince IV was mobilized to join autochthonous salt in the location of Line 2000. The addition of this extra salt allowed for the formation of broad autochthonous diapirs and the extensive formation of the allochthonous salt nappe with associated passive diapirs.

- Westerly flowing salt from Subprovince IV was mobilized into the wide autochthonous salt basin of Subprovince III (Sable Sub-basin) (see Section 6.5.2) Additional salt aided in the development of an extensive salt wall and later salt canopy spreading (latest Cretaceous) at the basinward edge of the original salt basin.

- Allochthonous salt canopies of Subprovince V and eastern Subprovince IV (Line 2000) are sourced from salt bodies along the seaward margin of the original salt basin, the remains of large inflated salt massifs related to nappe development.

7.3 Application of regional study results for future industry projects

- Mid-basin inflation of salt prevalent throughout much of the early basin history of the eastern Scotian margin led to a lack of early accommodation space and starved sedimentation. This would result in degraded reservoir quality for early depocenters

- Despite structural closure above salt-cored anticlines or along the crests of rollovers, a lack of significant accommodation space during the development of these structures makes for often poor reservoir quality.

- Growth packages flanking salt bodies – forming stratigraphic traps, are more likely to accumulate better reservoir quality through high amounts of subsidence and accommodation space, assuming that these structures are proximal to the shelf and are not deeply buried. However, many Early Cretaceous (Mississauga) structures above the continental shelf and basement hinge zone have already been explored.

- The seaward extrusion of salt from the basin during the Late Jurassic through Early Cretaceous led to welding of landward depocenters. The termination of subsidence within the landward salt basin reduced accommodation space and encouraged sediment bypass into the deeper basin where potential petroleum plays (rolling growth packages flanking salt) likely contain mostly fines and are very deep (> 8 km), being most likely beyond the oil and gas window.

- Complex sediment fairway patterns throughout the Cretaceous were controlled mostly by the topography of allochthonous salt (nappe) and secondary canopy (C) development at the salt basin edge. Here, it is likely that localized channels (turbidites) transporting sediments seaward form adjacent to salt canopies where subsidence is active. These small potentially sandy deposits beyond the slope of the eastern Scotian margin are the most likely source for untapped reservoir accumulation.

APPENDIX A: GLOSSARY OF SALT TECTONIC TERMINOLOGY

Diapir – the most recognizable and often most common of all salt structures. They are defined as a dome or anticlinal fold that formed as a result of rupturing overburden through squeezing out a plastic core material, usually salt or shale (Bates and Jackson, 1987). Jackson and Vendeville (1994), through A study of 18 major salt-diapir provinces and physical analogue modeling, suggest that salt upwelling and mobilization of salt into diapirs is closely linked in time and space to regional extension. Extension thins brittle overburden through the formation of grabens and half grabens above salt layers and locally reduces sediment load. These graben structures (1) cause differential loading of salt by their surface relief and (2) weaken the overburden strength by fracturing and thinning it. These models propose that diapirs follow three stages of evolution: reactive dipairism, active diapirism and passive diapirism (A-1).

During the reactive diapirism stage salt reacts to extension by passively filling in the space created by extending and shifting fault blocks within the grabens above salt, regardless of overburden thickness, density or lithology (Vendeville and Jackson, 1990). This results in a triangular diapir with flanking growth faults that young toward the diapir crest. This diapir can grow in size as extension continues as long as salt is still sourced from the initial salt layer. Only when the brittle sediment roof of the reactive diapir is thinned to a critical thickness can the diapir actively pierce through to the surface. This is known as active diapirism and occurs as a result of the salt pressure differential becoming great enough to pierce the thin overburden. This stage, once thought of as the dominant mechanism for diapiric formation, is only a brief transition period between reactive and passive diapirism.

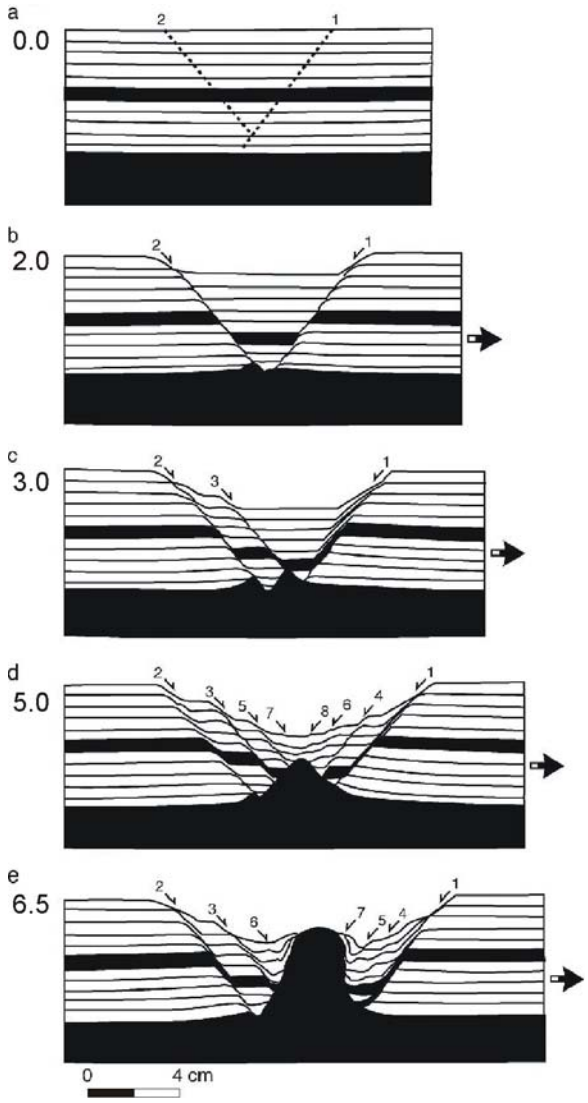

A1. Temporal evolution of diapirism development in analogue model comprised of stratified sediments and silicone putty (black) (modified from Jackson and Vendeville, 1994). a, b, c, d, and e show experiment after 0 cm, 2 cm, 3 cm, 5 cm, and 6.5 cm of total extension, respectively. a) Graben initiation. b, c, d) Reactive diapirism. e) Diapir is at the passive stage. The active stage is short lived and occurs just before e). Faults are numbered in sequence of formation.

As salt breaks through to the seafloor or ground it enters the passive diapirism stage. Salt will continue to grow at or very near to the seafloor or ground surface for as long as there is sufficient salt in the source layer. Continued growth of the diapir is attributed to passive downbuilding of sediments along diapir flanks. After the salt source layer is

depleted the diapir will cease to grow and be covered by subsequent sedimentation. This is a result of lost fluid pressure due to source layer depletion, despite the density contrast of salt and surrounding sedimentary strata. Passive diapirism is recognized as the dominant and longest -lived style of diapir growth in salt basins worldwide (Rowan, 2005).

Contractional diapir – occurs as a result of contraction initiated after a diapir is formed. Often as the weakest part of a basin system, salt will accommodate and localize contractional strain. The evidence for this is seen in surrounding strata. Buried diapirs often display narrowed salt bodies, concentric overburden folds cored by salt, crestal normal faulting and sharply bending sheathing/tangential strata along salt bodies also known as “j hooks.” (A-2). This process of buried salt passively responding to imposing contractional forces is referred to as diapir rejuvenation.

Salt withdrawal basin (minibasin) – forms as a result of salt mobilization away from an area of increased sediment load, termed the protobasin. Displaced salt from beneath the protobasin moves laterally into flanking areas resulting in bathymetric highs adjacent to the salt withdrawal basin. A positive feedback cycle is then initiated where the minibasin as an area of subsidence receives further sedimentation resulting in higher differential salt pressures and flow into flanking highs (A-3). Subsidence ends when the salt source layer is depleted and forms a salt weld. The term salt withdrawal basin is often generic and refers to any area of overburden subsidence displacing salt, including areas influenced by basement architecture. Minibasins are more specifically locations of overburden

subsidence unrelated to basement and often form on allochthonous salt.

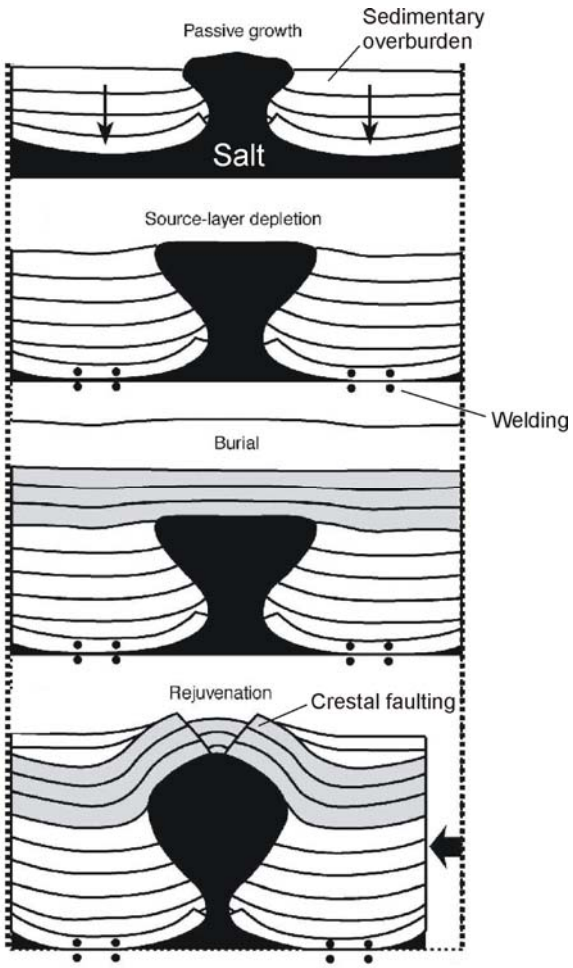

A2. Schematic illustrating the rejuvenation of a buried diapir due to late stage contraction. An existing passive diapir if firstly buried and subsequently squeezed as overlying sediments are folded and faulted until salt is forced up to fill accommodation space (Modified from Vendeville and Nilsen, 1995).

Salt weld – occurs as a result of complete withdrawal of salt from its source layer and is defined as the contact between overburden and sub-salt strata, where salt was previously emplaced (Rowan, 2005) (A-3, 4). Primary welds occur between overburden and sub-salt strata along the autochthonous or initial salt basin. Secondary welds are defined as welds

occurring along salt structures such as diapirs or stocks, and are often vertical or near vertical. These result from a lack of rejuvenation to salt structures from source layers and subsequent shut down of the structure. Tertiary welds form in much the same way as primary welds, with the exception that welding takes place at allochthonous salt bodies such as canopies or nappes.

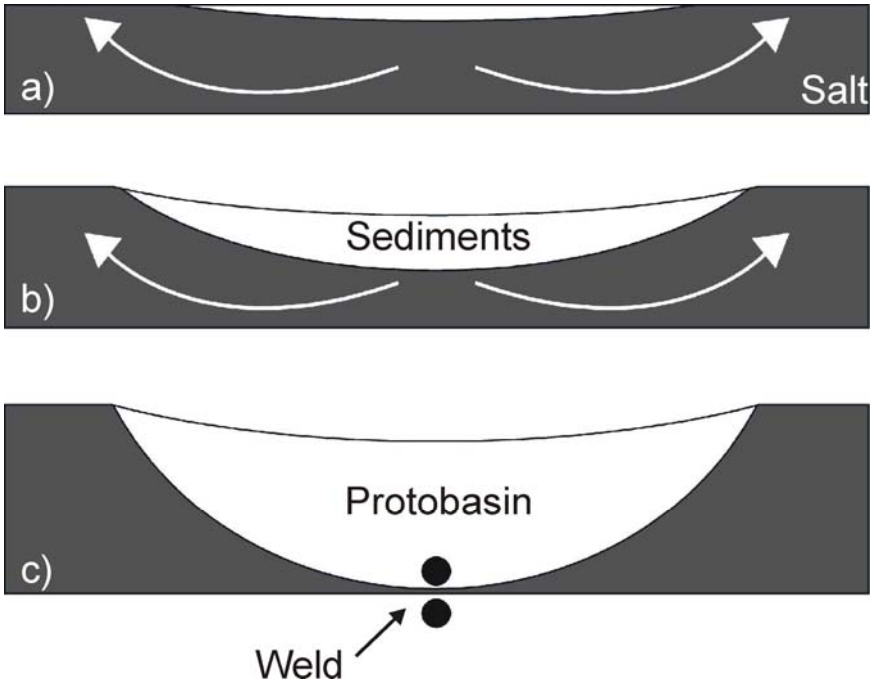

A3. Salt withdrawal basin illustrating the sediments of the protobasin and eventual welding occurring as a result of continued salt expulsion away from the main depocenter (white arrows). a) initiation of the withdrawal basin. b) differential loading drives subsidence of sediments and mobilization of salt. c) subsidence ends as salt is welded out. (Modified from Rowan, 2005).

Turtle structures – are a feature of some salt withdrawal basins. Although subsidence within the center of the salt withdrawal basin may have ceased due to welding, the flanks may also expel underlain salt and collapse. This occurrence causes flanks to become the new depocenters and an inversion of the old minibasin into an anticlinal turtle structure

(A-4).

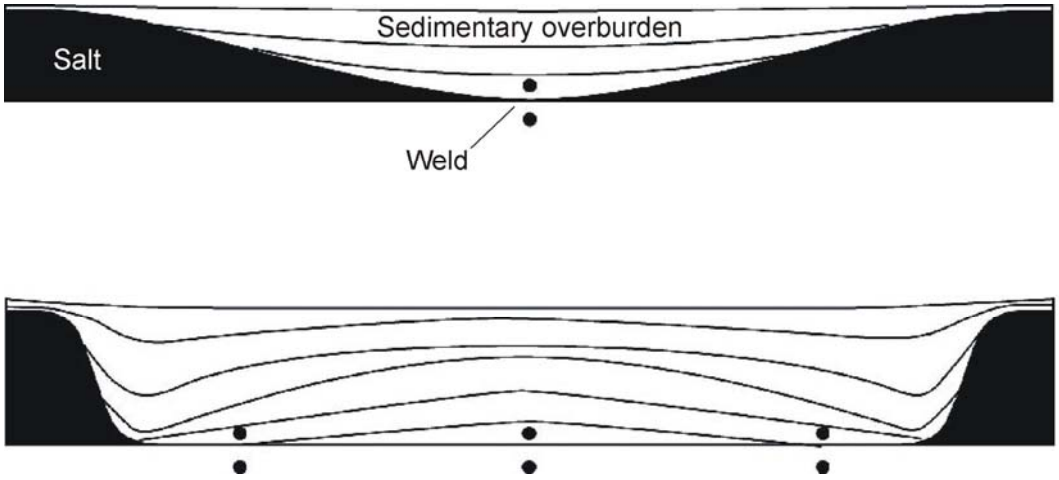

A4. Sequential formation of a turtle structure through flank collapse and inversion of salt withdrawal basin. Turtle structure formation begins with initial welding of the salt withdrawal basin (above) and is complete when welding of the flanks occurs (below). (Modified from Rowan, 2005).

Expulsion rollovers – are a common type of salt evacuation structure that develops as a response to diapirism. They form as a result of growth or "rolling" strata downbuilding on top of salt or along a salt body through asymmetric flank collapse (A-5). This process occurs during lateral salt withdrawal as strata downbuilds into or along adjacent salt. Strata eventually weld at the base of the source layer and are overridden by subsequent sediments. The rollover does not accommodate extension itself; instead the salt localizes the strain. This process causes depocenters to progressively shift in one direction, typically basinward through progradation. As the weld grows in length, salt is inflated and may form diapirs and eventually allochthonous salt bodies.

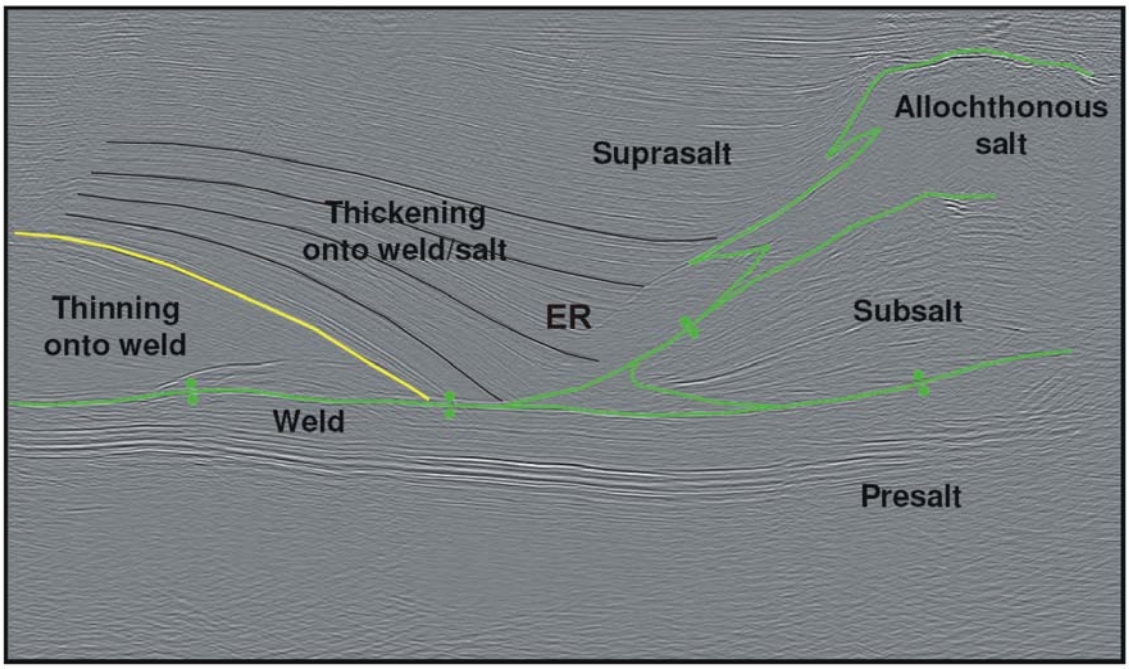

A5. Interpreted expulsion rollover structure (ER) from the Precaspian Basin illustrating a common transition from thinning of strata onto weld to thickening onto weld/salt (Modified from Rowan, 2005). This transition (yellow marker horizon) marks the time of initial welding of salt. Green marker horizons demonstrate the interpreted base and top of salt.

Growth fault rollover system – occurs as a result of strata thickening (growing) along a normal listric fault surface as sedimentation fills accommodation space created during extension. Strata appear to roll along the fault surface as it is displaced both vertically and laterally (A-6).

A6. Schematic of a growth fault rollover system with rotation of growing strata (coloured marker horizons) along normal fault indicated by red arrow. SR indicates a salt roller located below the growth fault rollover system. (Modified from MacDonald, 2007).

Salt rollers – are low-amplitude, sharp-crested, asymmetric reactive diapirs that are comprised of two flanks (A-6). One flank is gently dipping and conformable with overlying stratigraphy, while the other is more steeply dipping and is below the footwall of a normal often listric fault. The presence of these structures suggests extension within the system in the direction perpendicular to the rollers.

Salt canopies – are allochthonous salt systems that are comprised of three endmember components: salt tongues, bulb-shaped salt stocks, and salt nappes (A-7). Salt tongues are often asymmetric with basinward-leaning feeders and sub-horizontal tongues that are extruded basinward on stratigraphic higher levels often as a result of dipping sea floor or ground surface (Rowan, 2005). Salt stocks are more symmetrical in geometry and consist of a bulb-shaped salt body spreading from a nearly vertical feeder. Salt nappes, however are extruded basinward from the basinward edge of initial salt deposition as opposed to feeder systems. These structures often climb stratigraphically up-section over sediments as they are extruded seaward in a ramp-flat geometry. Nappe development is a result of three simultaneous processes: (1) depositional loading of the landward, deep source salt layer, (2) basinward translation of overburden on top of the source layer, and (3) basinward translation of the nappe (salt) itself due to continued landward depostional loading (Rowan, 2005).

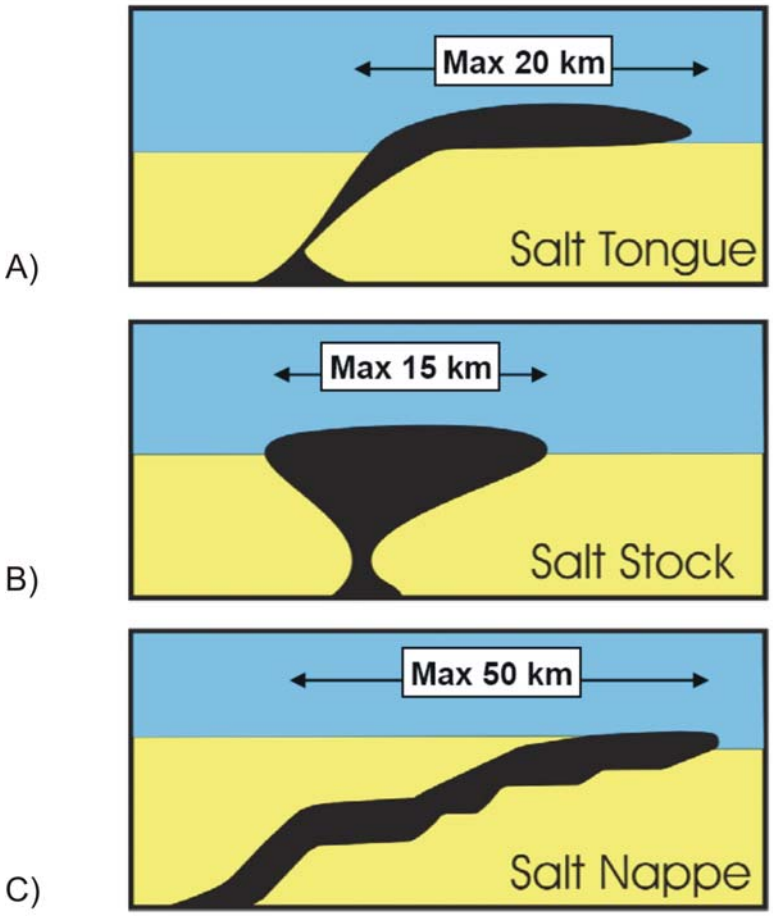

A7. Schematic of the three endmember components of passive salt canopies (modified from Rowan, 2005): a) Salt tongue; b) Salt stock; c) Salt nappe (Modified from Rowan, 2005). Yellow and blue indicate sedimentary overburden and sea water respectively. For discussion see text.

Roho systems – are a common evolutionary style of salt tongue or nappe development. These systems are dominated by extensional faults as salt accommodates basinward translation of overburden through gravity spreading of the slope (A-8).

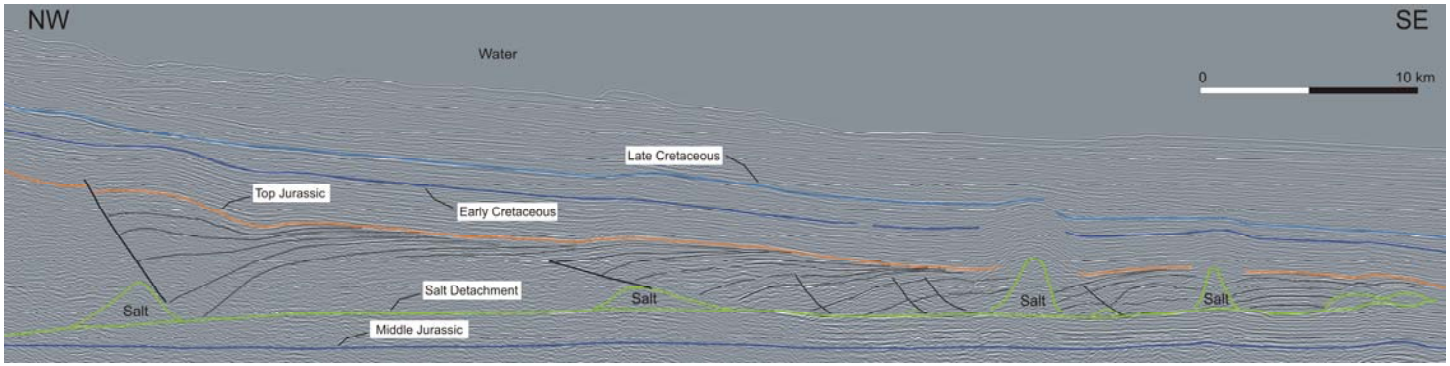

A8. Interpretation of the Banquereau Syn-kinematic Wedge (BSW) of the eastern Scotian Margin illustrating landward (NW) dipping strata rotated along southeast dipping faults above small salt diapirs and soling into the interpreted salt detachment (green marker horizon). The deposition of Jurassic sediments onto allochthonous salt has formed a roho structure as the extension of salt has been accommodated by the faulting and rotation of Jurassic strata along a salt detachment surface.

APPENDIX C: COMPLETE 2-D TIME SERIES DIC MODEL SURFACE IMAGES

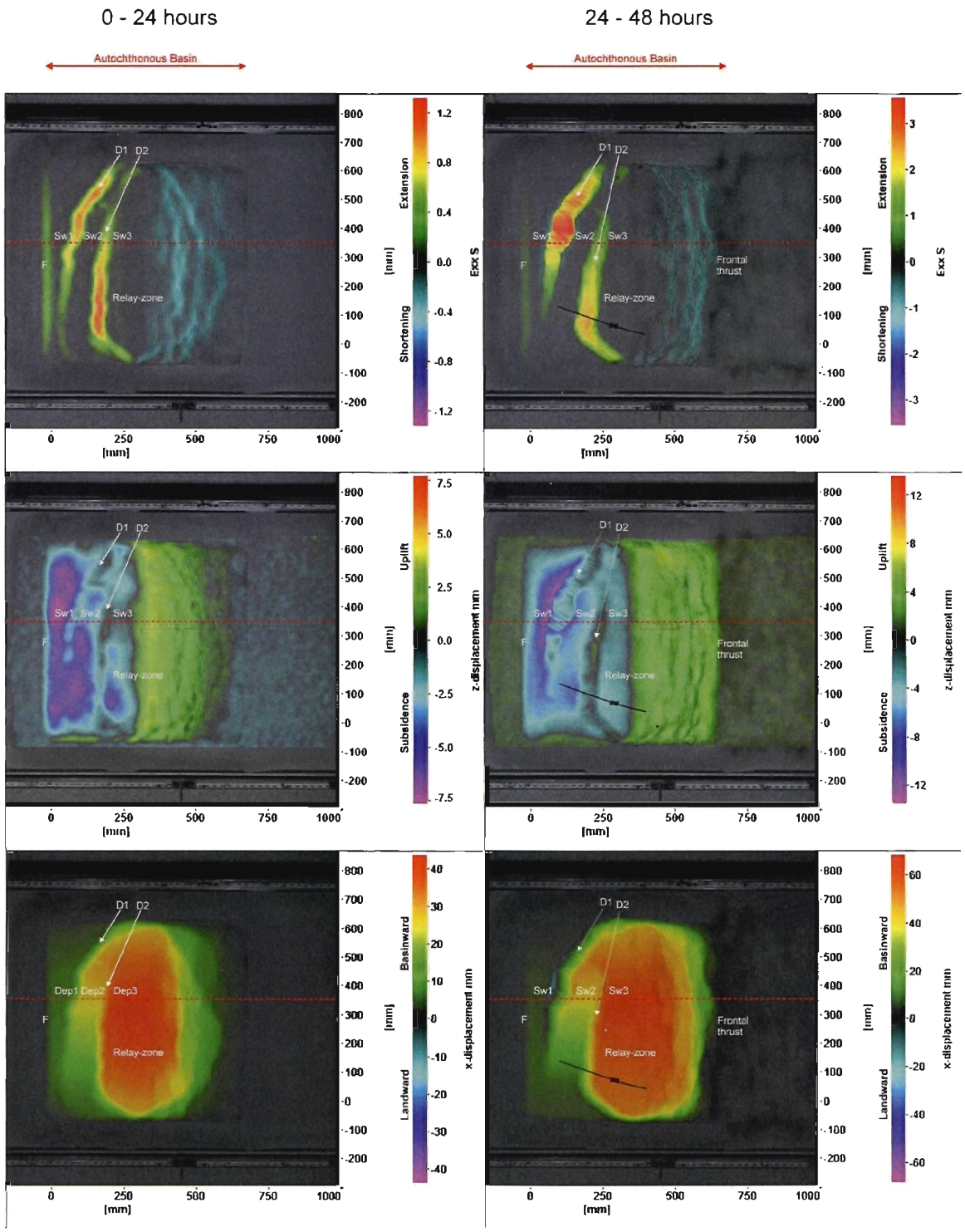

Figure C1. Temporal evolution of the 3D main analogue experiment simulating the eastern Scotian Margin salt basin evolution. Experiment evolution is visualized in 24 hour interval, through overlaying cumulative deformation (horizontal strain (Exx), horizontal displacement (Vx), vertical displacement (Vz)) on experiment surface images. Incremental strain and displacement components obtained by 3D DIC monitoring are summarized for the previous 24 hour interval and overlain on the ensuing model surface to visualize deformation trends for the individual intervals. Active silicone structures and salt withdrawal basins are illustrated. Red dashed line indicates location of 45 cm section used for structural restoration. See Chapter 5.8 for further discussion.

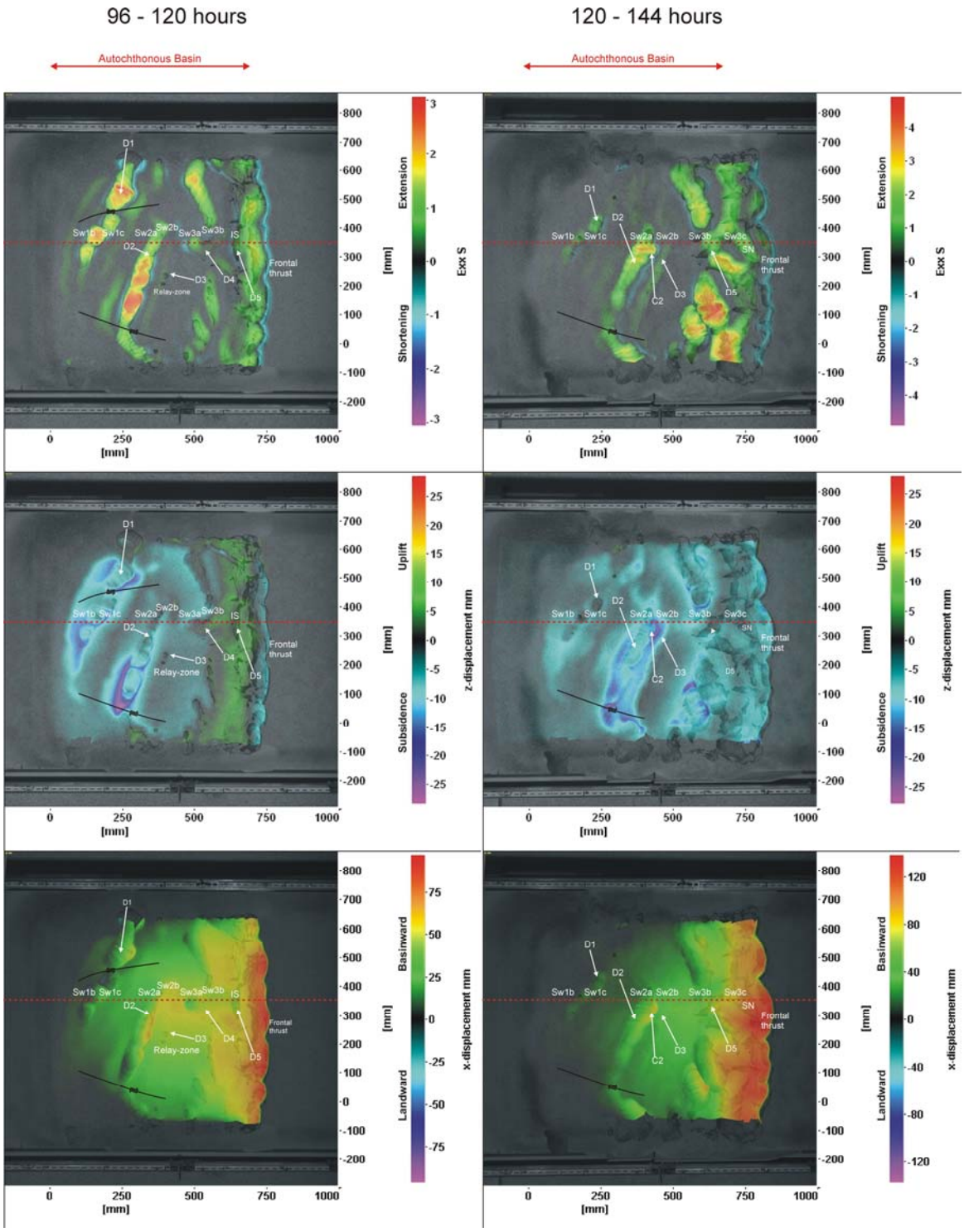
96 - 120 hours
120 - 144 hours
Autochthonous Basin
Autochthonous Basin
D1
D2
D3
D4
D5
C2
Sw1b
Sw1c
Sw2a
Sw2b
Sw3a
Sw3b
Sw3c
IS
SN
Relay-zone
Frontal thrust
Extension
Shortening
Exx S
Uplift
Subsidence
z-displacement mm
Basinward
Landward
x-displacement mm
[mm]

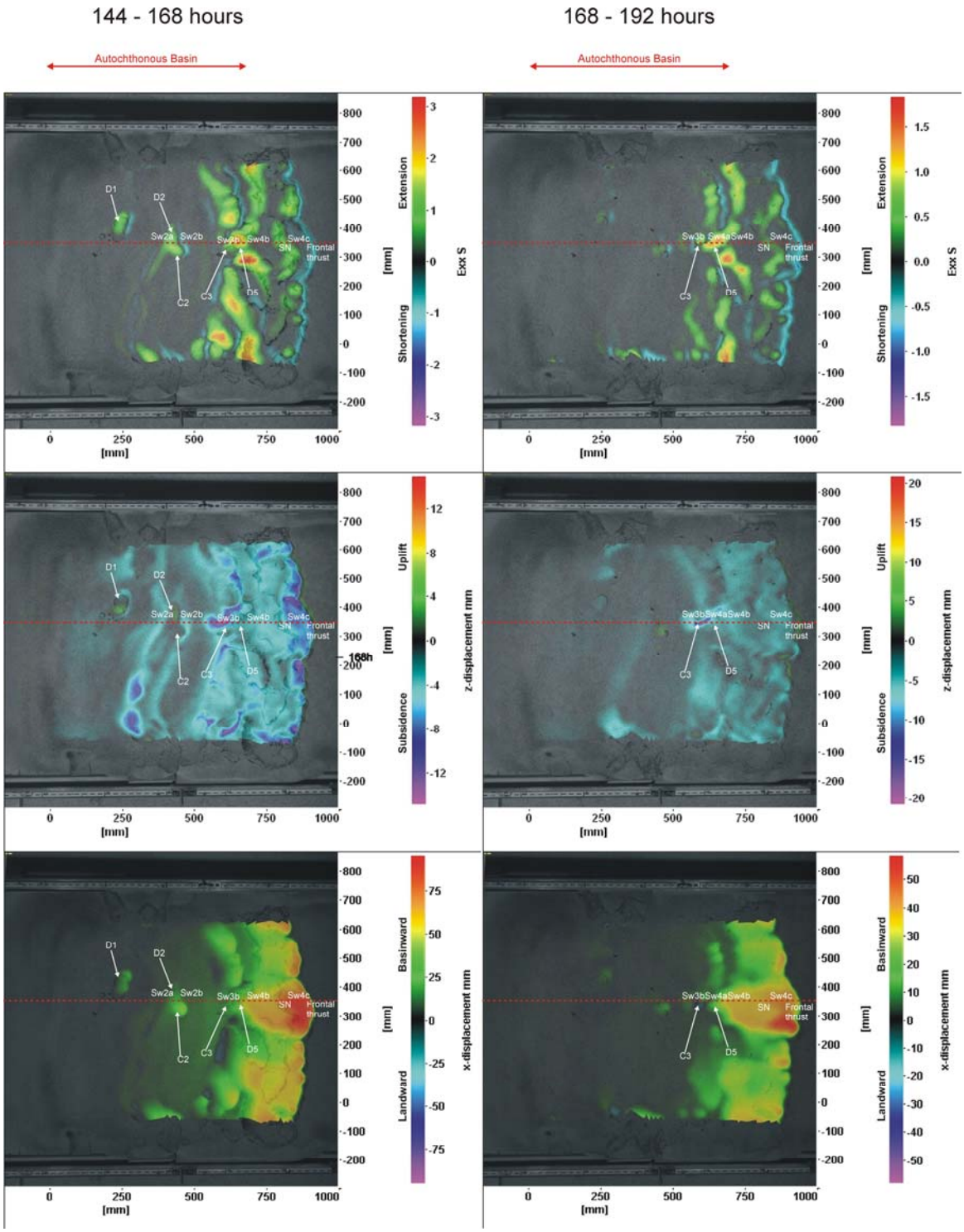
144 - 168 hours
168 - 192 hours
Autochthonous Basin
Autochthonous Basin
D1
D2
Sw2a
Sw2b
Sw3b
Sw4a
Sw4b
Sw4c
SN
Frontal thrust
C2
C3
D5
168h
[mm]
Extension
Shortening
Exx S
Uplift
Subsidence
z-displacement mm
Basinward
Landward
x-displacement mm

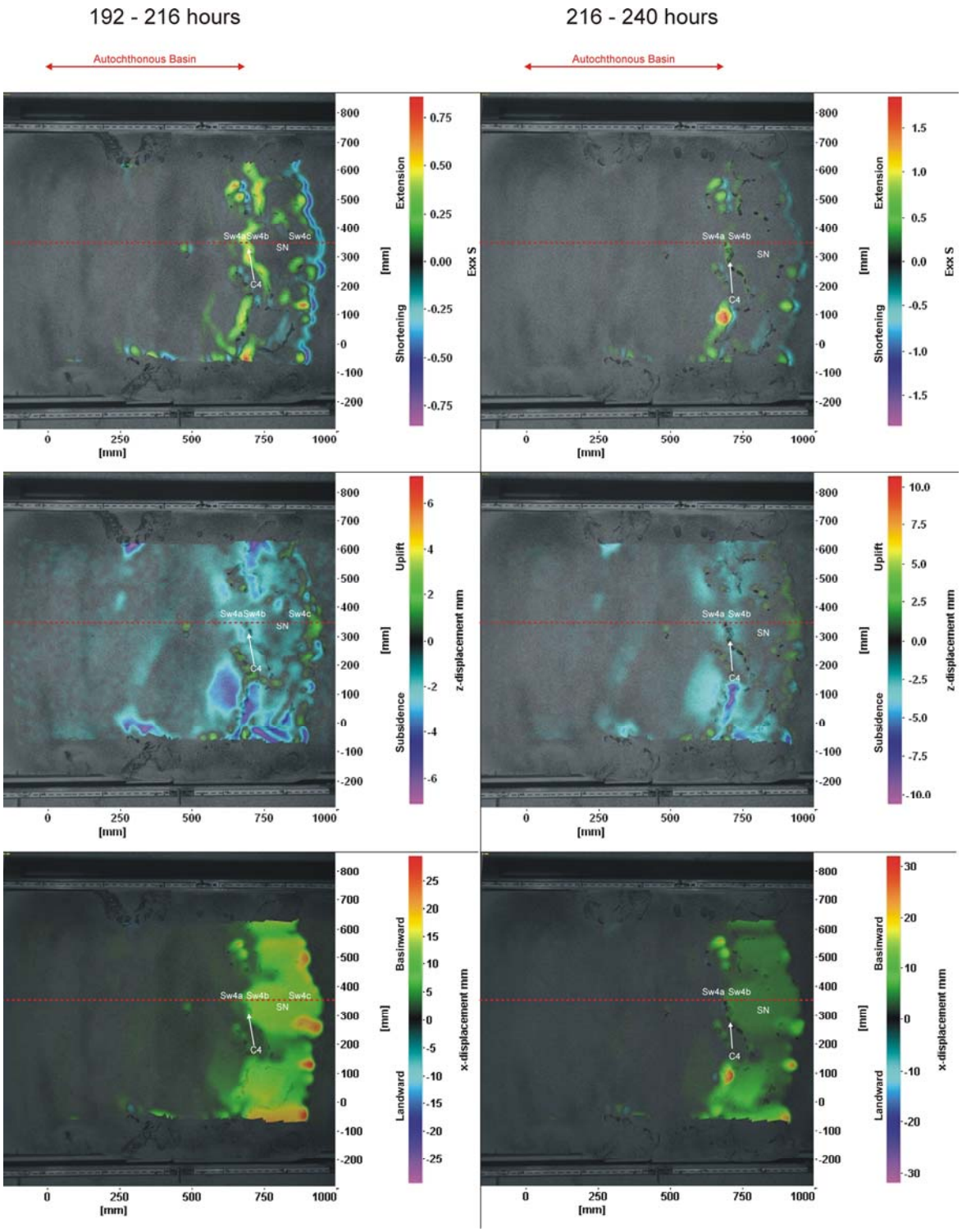
192 - 216 hours
216 - 240 hours
Autochthonous Basin
Autochthonous Basin
Sw4a Sw4b
Sw4c
SN
C4
Extension
Shortening
Exx S
Uplift
Subsidence
z-displacement mm
Basinward
Landward
x-displacement mm
[mm]
0
250
500
750
1000

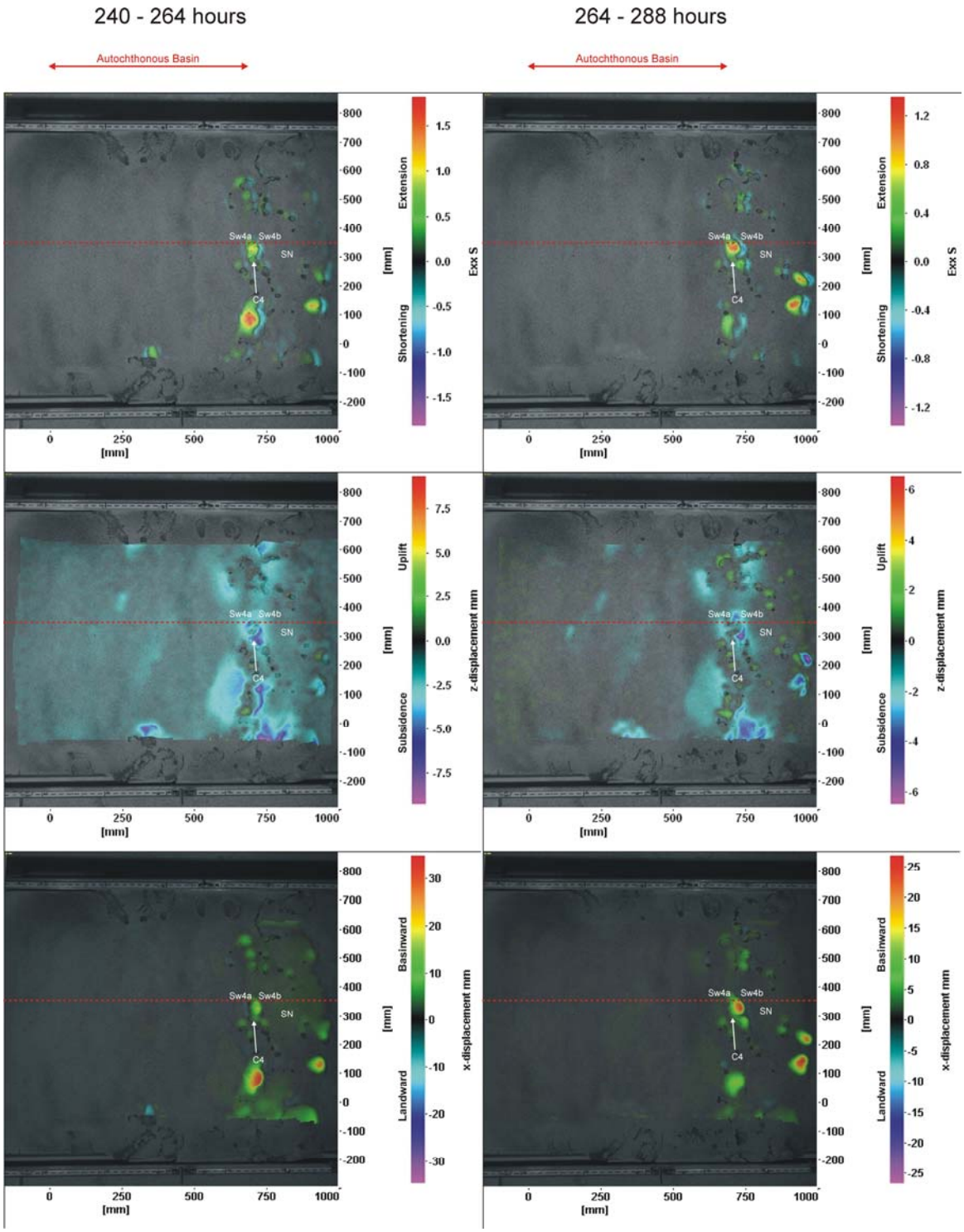
240 - 264 hours
264 - 288 hours
Autochthonous Basin
Autochthonous Basin
Sw4a
Sw4b
SN
C4
Extension
Shortening
Exx S
Uplift
Subsidence
z-displacement mm
Basinward
Landward
x-displacement mm
[mm]

REFERENCES

Adam, J., Krezsek, C., MacDonald, C., Campbell, C., Cribb, J., Nedimovic, M., Louden, K., and Grujic, D. 2008. Basin-Scale Salt Tectonic Processes and Sediment Progradation in the Slope and Deepwater Basin of the North-Central Scotian Margin, *In* Conjugate Margins Conference, Halifax, Nova Scotia, Canada.

Adam, J., Urai, J.L., Wieneke, B., Oncken, O., Pfeiffer, K., Kukowski, N., Lohrmann, J., Hoth, S., van der Zee, W. and Schmatz, J. 2005. Shear localization and strain distribution during tectonic faulting—new insights from granular-flow experiments and high-resolution optical image correlation techniques. Journal of Structural Geology, **27**, pp. 283–301.

Adams, R.L. 1989. Effects of inherited pre-Jurassic tectonics on the U.S. Gulf Coast: Transactions Gulf Coast Association of Geological Societies, pp. 1-10.

Bates, R.L. and Jackson, J.A. 1987. Glossary of Geology. (3rd ed.), American Geological Institute, Alexandria, VA.

Calassou, S., and Moretti, I. 2003. Sedimentary flattening and multiextensional deformation along the West African margin. Marine and Petroleum Geology, **21**, pp. 71–82.

Campbell, C. 2007. Physical modeling of the salt tectonics of allochthonous canopy and nappe systems at deepwater continental margins: Applications to the Abenaki and Sable sub-basins, Scotian Margin, BSc. Honours Dissertation, Dalhousie University, Halifax, NS.

Coffin, M.F., Gahagan, L.M., Lawver, L.A., Lee, T.Y., and Rosencrantz, E.1992. Atlas of Mesozoic/Cenozoic reconstructions (200 Ma to Present Day): PLATES Progress Report, No. 1-0192, Univ. of Texas Inst. For Geophys., Tech. Rept. no. 122, pp. 49.

Costa, E. and Vendeville, B. C. 2002. Experimental insights on the geometry and kinematics of fold-and thrust belts above weak, viscous evaporitic decollement. Journal of Structural Geology, **24**, pp. 1729-1739.

Doeven, P.H. 1983. Cretaceous nannofossil stratigraphy and paleoecology of the Canadian Atlantic Margin. *In* Geological Survey of Canada, Bulletin 356, pp. 70.

Durcanin, M.A., Withjack, M.O., and Schilsche, R.W. 2008. Postrift deformation on the passive margin of Nova Scotia, Canada: is it really passive? *In* Geological Society of America, 2008 annual meeting, Houston, TX, United States, Vol. 40, no. 6, pp. 311.

Ebinger, C.J. and Tucholke, B.E. 1988. Marine geology of Sohm Basin, Canadian Atlantic Margin. AAPG Bulletin, **72**, no. 12, pp. 1450-1468.

Ewing, J.I., and Rabinowitz, P.D. 1984. Eastern North American Continental Margin and Adjacent Ocean Floor, 34 to 41°N and 68 to 78°W; Ocean Margin Drilling Program, Atlas 4, Marine Science International, Woods Hole, Massachusetts.

Fort, X., Brun, J. P., and Chauvel, F. 2004. Salt tectonics on the Angolan margin, synsedimentary deformation processes. AAPG Bulletin, **88**, no. 11, pp. 1523-1544.

Funck, T., Jackson, H.R., Louden, K.E., Dehler, S.A. and Wu, Y. 2004. Crustal structure of the northern Nova Scotia rifted continental margin (Eastern Canada). J. Geophys. Res., Vol. 109, B09102, doi:10.1019/2004JB003008.

Ge, H., Jackson, M. P. A. and Vendeville, B.C. 1997. Kinematics and dynamics of salt tectonics driven by progradation. AAPG Bulletin, **81**, pp. 398-423.

Gemmer, L., Ings, S.J. , Medvedev, S. and Beaumont, C. 2004. Salt tectonics driven by differential sediment loading: stability analysis and finite-element experiments, Basin Research, **16**, pp. 199–218.

Gemmer, L., Beaumont, C. and Ings, S.J. 2005. Dynamic modelling of passive margin salt tectonics: effects of water loading, sediment properties and sedimentation patterns, Basin Research, **17**, pp. 383–402.

Hossack, J.R. 1995. Geometric rules of section balancing for salt structures. *In* Jackson, M.P.A., Roberts, D.G., & Snelson, S. (eds.) Salt Tectonics: a global perspective. Am. Ass. Petrol. Geol. Mem. 65, pp. 29-40.

Hubbert, M. K. 1937. Theory of scale models as applied to the study of geologic structures. Geological Society of America Bulletin, **48**, no. 10, pp. 1459-1519.

Ings, S.J. and Shimeld, J.W. 2006. A new conceptual model for the structural evolution of a regional salt detachment on the northeast Scotian margin, offshore eastern Canada. American Association of Petroleum Geologists Bulletin, **90**, pp. 1407-1423.

Jackson, M.P.A., 1995. Retrospective salt tectonics, *In* M.P.A. Jackson , D.G. Roberts, and S. Snelson, (eds.), Salt tectonics: a global perspective: AAPG Memoir 65.

Jackson, M. P. A. and Talbot, C. J. 1994. Advances in salt tectonics *In* P.L. Hancock, ed., Continental deformation: Oxford, U.K., Pergamon Press and International Union of Geological Sciences, pp. 159-180.

Jackson, M. P. A., and Vendeville, B. C. 1994. Initiation of salt diapirism by regional extension: global setting, structural style, and mechanical models: The University of Texas at Austin, Bureau of Economic Geology Report of Investigations No. 215, pp. 39.

Jackson, M. P. A. and Talbot, C. J. 1991. A glossary of salt tectonics: The University of Texas at Austin, Bureau of Economic Geology Geological Circular 91–4, pp. 44.

Jackson, M. P. A. and Talbot, C. J. 1989. Anatomy of mushroom shaped diapirs. Journal of Structural Geology, **11**, pp. 211-230.

Jackson, M.P.A. and Talbot, C.J. 1986. Stepwise centrifuge modeling of the effects of differential sediment loading on the formation of salt structures. *In* Lerche, I. & O'Brien, J. J. (eds.), Dynamical Geology of Salt and Related Structures. Academic Press, Orlando, Florida, pp. 163-259.

Jansa, L. F. and Wade, J. A. 1975. Geology of the continental margin off Nova Scotia and Newfoundland. Offshore geology of eastern Canada, Vol. 2. Regional geology. *In* W. M. Van der Linden and J. A. Wade (eds.), Geological Survey of Canada, Paper 74-30, pp. 51-105.

Keen, C.E. and Potter, D.P. 1995. The transition from a volcanic to a nonvolcanic rifted margin off eastern Canada: Tectonics, **14**, pp. 359–371.

Keen, C.E., MacLean, B.C., and Kay, W.A. 1991. A deep seismic reflection profile across the Nova Scotia continental margin, offshore eastern Canada. Canadian Journal of Earth Science, **28**, pp. 1112-1120.

Keen, C.E. and C. Beaumont. 1990. Geodynamics of rifted continental margins. Vol. I-1 of Decade of North America Geology. *In* M.J. Keen and G.L. Williams (eds.), Publication of Geological Survey of Canada and Geological Society of America, pp. 393-472.

Kent, D.V., Olsen, P.E., and Witte, W.K. 1995. Late Triassic-Early Jurassic geomagnetic polarity sequence and paleolatitudes from drill cores in the Newark rift basin, eastern North America. J. Geophys. Res., **100**(B8), pp. 14965–14998.

Keppie, J. D. 1989. Northern Appalachian terranes and their accretionary history. Terranes in the circum-Atlantic Paleozoic orogens. *In* R. D. Dallmeyer (ed.), Geological Society of America, Special Paper 230, pp. 159- 192.

Kligfield, R., Rowan, M.G., and Ratliff, R. 1989. Applications of computer-aided section construction, restoration, and balancing models to the petroleum industry. *In* Society of Exploration Geophysicists, 59th annual international meeting, Dallas, TX, United States, **59**, pp. 589.

Koyi, H., Talbot, C.J. and Torudbakken, B.O. 1995. Analogue models of salt diapirs and seismic interpretation in the Nordkapp Basin, Norway. Petroleum Geoscience, **1**, no. 2, pp. 185-192.

Krezsek, C., Adam, J., and Grujic, D. 2007. Mechanics of fault and expulsion rollover systems developed on passive margins detached on salt: insights from analogue modeling and optical strain monitoring *In*: S.J. Jolley, Barr, D., Walsh, J. J. & Kipe, R. J. (eds.), Structurally Complex Reservoirs. Geological Society, Special Publications, London, **292**, pp. 103-121.

Last, N.C. 1988. Deformation of a sedimentary overburden on a slowly creeping substratum. Numerical Methods in Geomechanics, **6**, pp. 577-585.

Lohrmann, J., Kukowski, N., Adam, J. and Oncken, O. 2003. The impact of analogue material parameters on the geometry, kinematics, and dynamics of convergent sand wedges. Journal of Structural Geology, **25**, no. 10, pp. 1691-1711.

Louden, K. 2002. Tectonic evolution of the east coast of Canada. CSEG Recorder, **27**, pp. 37-49.

MacDonald, C. 2007. Analogue modeling of the salt tectonics system, offshore Nova Scotia: Insights into initial salt mobilization and autochthonous salt structures, BSc. Honours Dissertation, Dalhousie University, Halifax, NS.

MacLean, B.C. and Wade, J.A. 1993. East coast basin atlas series: Seismic markers and stratigraphic picks in Scotian Basin wells. Atlantic Geoscience Centre, Geological Survey of Canada, pp. 276.

MacLean, B.C. and Wade, J.A. 1992. Petroleum geology of the continental margin south of the islands of St Pierre and Miquelon, offshore eastern Canada. Bulletin of Canadian Petroleum Geology, **40**, pp. 222–253.

Mauduit, T. and Brun, J.P. 1998. Growth fault/rollover systems: Birth, growth, and decay. Journal of Geophysical Research, **103**(B8), pp. 18119-18136.

Mauduit , T., Guerin, G., Brun, J.P. and Lecanu, H. 1997. Raft tectonics: The effect of basal slope value and sedimentation rate on progressive extension. Journal of Structural Geology, **19**, pp. 1219-1230.

Olsen, P.E. 1997. Stratigraphic record of the early Mesozoic breakup of pangea in the Laurasia-Gondwana rift system. Annual Review of Earth and Planetary Sciences, **25**, pp. 337-401.

Poliakov, A. N. B., van Balen, R., Podladchikov, Yu., Daudre, B, Cloetingh, S., and Talbot, C. 1993. Numerical Analysis of How Sedimentation and Redistribution of Surficial Sediments Affects Salt Diapirism. Tectonophysics , **226**, pp. 199–216.

Ratcliffe, N. M., Burton, W. C., D'Angelo, R.M., and Costain, J. K. 1986. Low-angle extensional faulting, reactivated mylonites, and seismic reflection geometry of the Newark basin margin in eastern Pennsylvania, Geology, **14**, pp. 766-770.

Ravenhurst, G.Li, C.E. and Zentilli, M. 1995. Implications of apatite fission track analysis for the thermal history of the Scotian Basin, offshore Nova Scotia. Bulletin of Canadian Petroleum Geology, **43**, no. 2., pp. 127 – 144.

Ross, D.I. (co-ord.), Lewis, C.F.M. (co-ord.), Howie, R.D. (asst. co-ord.), Cant, D.J. (sci. co-ord.), and Bates, J.L. (ed.). 1991. Scotian Shelf. Frontier Geoscience Program East Coast Basin Atlas Series. Atlantic Geoscience Centre, Geological Survey of Canada, Dartmouth, NS.

Rowan, M.G., 2005. Salt Tectonics and Sedimentation: A Structural and Sedimentary Framework for Petroleum Systems in Salt Basins.

Rowan, M. G., Peel, F. J., and Vendeville, B. C. 2004. Gravity-driven fold belts on passive margins, *In* K. R. McClay (ed.),Thrust tectonics and hydrocarbon systems: AAPG Memoir 82, pp 157-182.

Shimeld, J., 2004. A comparison of salt tectonic sub-provinces beneath the Scotian Slope and Laurentian Fan. P.J. Post, D.L. Olson, K.T. Lyons, S.L. Palmes, P.F. Harrison, N.C. Rosen (eds.): Salt-sediment interactions and hydrocarbon prospectivity: Concepts, applications and case studies for the 21st century, 24th Annual GCSSEPM Foundation Bob F. Perkins Research Conference proceedings, pp. 291-306.

Spiers, C.J., Urai, J.L., Lister, G.S., Boland, J.N., and Zwart, H.J., 1986. The infuence of fluid-rock interaction on the rheology of salt rock. European Communities Commission, Nuclear Science and Technology Series, EUR-10399.

Swift, S. A., Ebinger, C., and Tucholke, B. 1986. Seismic stratigraphic correlation across the New England Seamount Chain, western North Atlantic Ocean. Geology, **14**, pp. 346–349.

Talbot, C.J. 1992. Centrifuged models of Gulf of Mexico profiles. Marine and Petroleum Geology, **9**, no. 4, pp. 412-433.

Talwani, M. and Abreu, V. 2000. Inferences regarding initiation of oceanic crust from the U.S. east coast margin and conjugate South Atlantic Margins. *In* Atlantic Rifts and Continental margins Geophys. Monograph Series, **115**, pp. 211-233.

Urai, J.L., Spiers, C.J., Zwart, H.J., and Lister, G.S. 1986. Weakening of rock salt by water during long-term creep. Nature, **324**, pp. 554–557.

Urai, J.L., Spiers, C.J., Peach, C.J., Franssen, R.C.M.W., and Liezenberg, J.L. 1987. Deformation mechanisms operating in naturally deformed halite rocks as deduced from microstructural investigations. Geologie enMijnbouw, **66**, pp. 165–176.

Vendeville, B.C. 2005. Salt tectonics driven by sediment progradation: Part 1 – Mechanics and kinematics. AAPG Bulletin, **89** no. 8, pp. 1071-1079.

Vendeville, B. C., Jackson, M. P. A., and Weijermars, R. 1993. Rates of salt flow in passive diapirs and their source layers, *In* Armentrout, J. M., Bloch, Roger, Olson, H. C., and Perkins, B. F., (eds.), Rates of geologic processes: tectonics, sedimentation, eustasy and climate: implications for hydrocarbon exploration: Gulf Coast Section, Society of

Economic Paleontologists and Mineralogists Foundation, fourteenth annual research conference, program with papers, pp. 269–276.

Vendeville, B.C. and Jackson, M.P.A. 1992a. The fall of diapirs during thin-skinned extension. Marine and Petroleum Geology, **9**, no. 4, pp. 354-371.

Vendeville, B.C. and Jackson, M.P.A. 1992b. The rise of diapirs during thin-skinned extension. Marine and Petroleum Geology, **9**, no. 4, pp. 331-353.

Vendeville, B.C. and Jackson, M.P.A. 1990. Physical modeling of the growth of extentional and contractional salt tongues on continental slopes. AAPG Bulletin, **74**, pp. 784.

Wade, J. A. and MacLean, B. C. 1990. The geology of the southeastern margin: Aspects of the geology of the Scotian Basin from recent seismic and well data. *In* Geology of the continental margin of eastern Canada. M. J. Keen and G. L. Williams (eds.). Geological Survey of Canada, Geology of Canada No. 2, pp. 167-238.

Wade, J. A. 1981. Geology of the Canadian Atlantic margin from Georges Bank to the Grand Banks. *In* Geology of the North Atlantic Borderlines. J. W. Kerr and A. J. Ferguson (eds.). Canadian Society of Petroleum Geologists, Memoir 7, pp. 447460.

Wade, J.A. 1978. The Mesozoic-Cenozoic history of the northeastern margin of North America. *In* Offshore Technology Conference Proceedings, **3**, pp. 1849-1859.

Wawersik, W.R. and Zeuch, D.H. 1986. Modeling and mechanistic interpretation of creep of rock salt below 200 8°C. Tectonophysics, **121**, pp. 125–152.

Weijermars, R. 1993. Progressive deformation of single layers under constantly oriented boundary stresses. Journal of Structural Geology, **15**, pp. 911–922.

Weijermars, R., Jackson, M.P.A. and Vendeville, B. 1993. Rheological and tectonic modelling of salt provinces, Tectonophysics, **217**, pp. 143–174.

Williams, H. and Hatcher, R.D., Jr. 1983. Suspect terranes: A new look at the Appalachian orogen *In* Hatcher, R.D., Jr., Williams, H., and Zietz, I., (eds.). Contributions to the tectonics and geophysics of mountain chains: Geological Society of America Memoir, Vol. 158, pp. 33-54.

Wu, Y., Louden, K.E., Funck, T., Jackson, H.R., and Dehler, S.A. 2006. Crustal structure of the central Nova Scotia margin off Eastern Canada. Geophysical Journal International, **166**, pp. 878–906.

Zheng, Y. and Arkani-Hamed, J. 2002. The elastic properties of the lithosphere beneath Scotian basin, Tectonophysics, **344**, pp. 137-156.

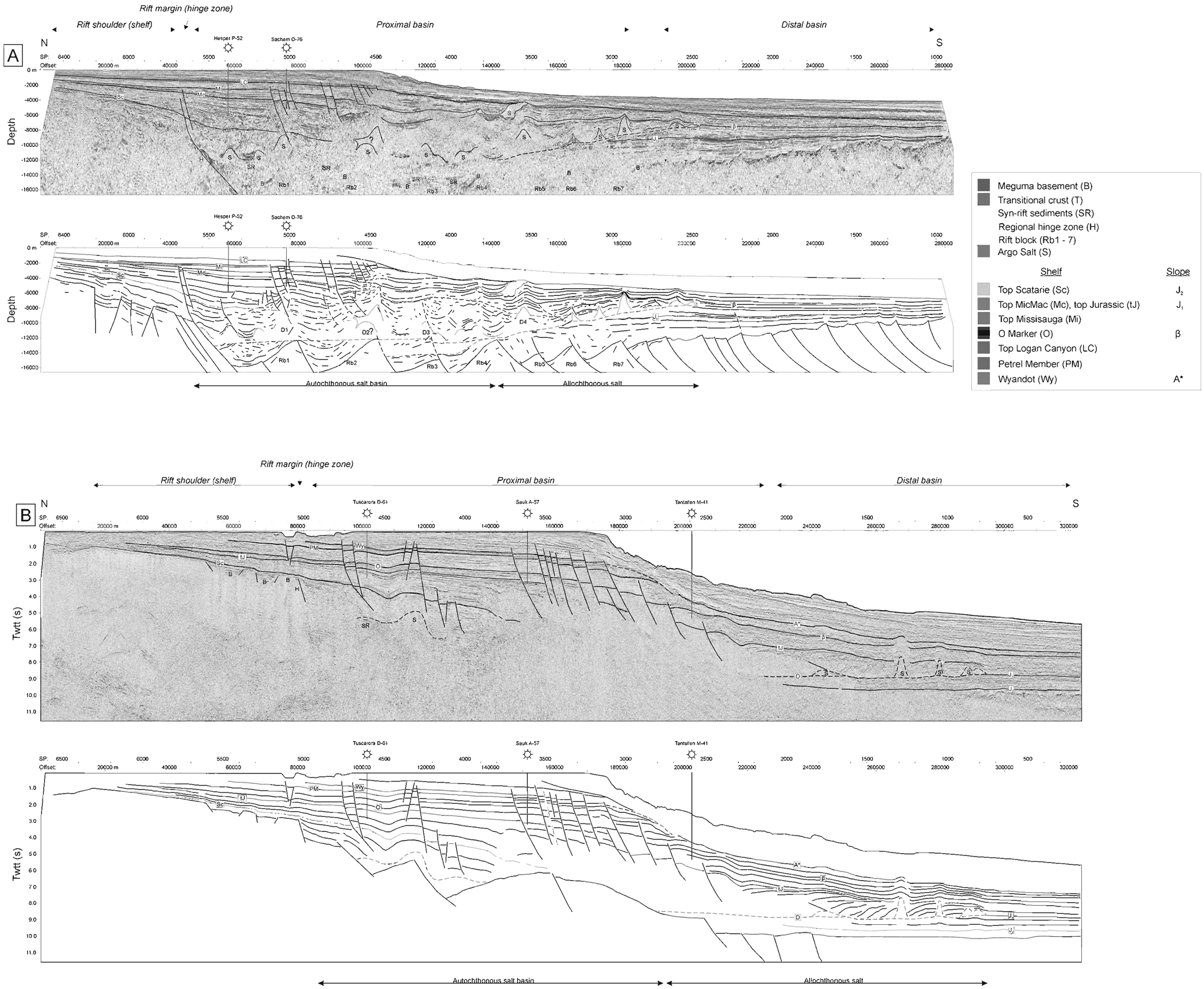

Figure 4.4 Reflection images and corresponding interpretations for two regional MCS profiles representing the key source of information for this thesis research. (A, upper panel) NovaSpan seismic profile 2000 with annotated interpretation of reflection horizons based on well data (Figure 4.2) and seismic signature indicating deep features such as salt structures, basement, and syn-rift sediments. (A, lower panel) Structural dip domain profile of line 2000 including extended interpretations and the limit of interpreted autochthonous and allochthonous salt. Major salt diapir structures are labelled D1 – 4.
(B, upper panel) GSC seismic profile 89-1 with annotated interpretation of reflection horizons based on well data (Figure 4.2) and seismic signature indicating deep features such as salt structures, basement, and syn-rift sediments. (B, lower panel) Structural dip domain profile of line 89-1 including extended interpretations (basement based on velocity model of Funck et al., 2004, Figure 4.5) and the limit of interpreted autochthonous and allochthonous salt. Refer to legend for annotations.

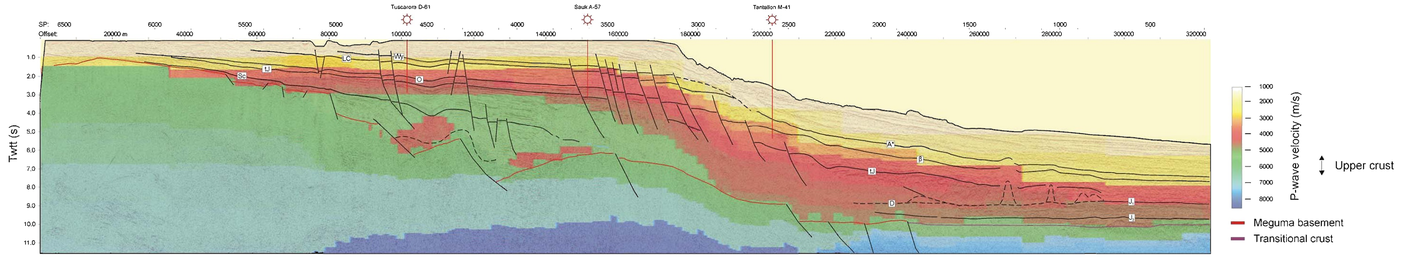

Figure 4.7 Seismic profile 89-1 overlain by a velocity model (Funck et al., 2004) and seismic interpretation. Velocity models were utilized to interpret basement features due to the poor quality of the seismic reflection image within the deep basin and deepwater. Although basement on the reflection image may be interpreted to show a high near SP 3500, wide-angle refraction velocity models in depth (Figure 4.5) suggest this to be incorrect. Instead basement forms a broad seaward climbing ramp outboard of SP 4500 to roughly SP 2500. Refer to the legend of Figure 4.4 for annotation of seismic horizons.

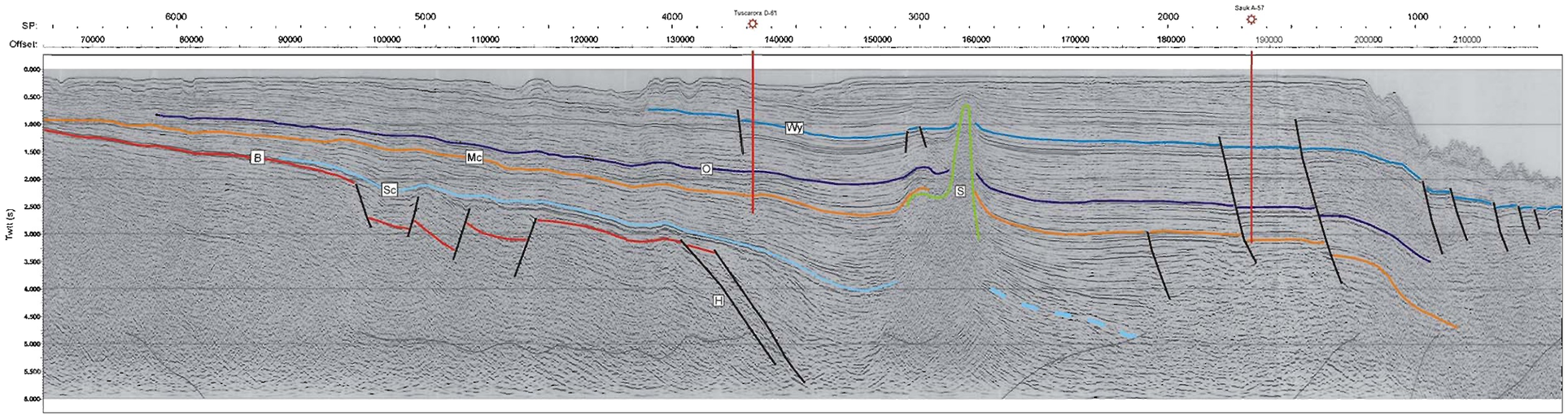

Figure 4.8. Seismic interpretation of a portion of line NS-6 (Figures 4.1, 4.5). Small grabens on the shelf and a distinctive hinge zone with synthetic normal faulting are similar to those of line 2000 (Figure 4.5). Salt diapir seaward of hinge zone exhibits a landward extension, similar to that interpreted for D2 of line 2000. (B – basement, H – Hinge, Sc – Scatarie Member, Mc – top Mic Mac, O – O Marker, Wy – Wyandot Formation, S – Argo Salt). Wells (Tuscadora D-61, Sauk A-57) used for stratigraphic correlation are illustrated with red lines.

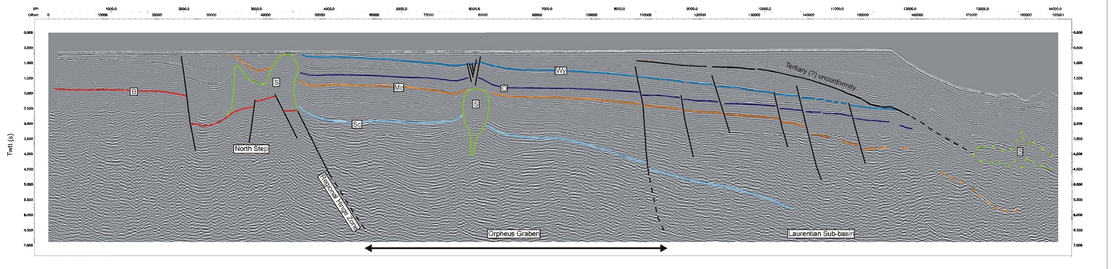

Figure 4.9. Seismic interpretation of line STP-3 (Figures 4.1, 4.5) imaging the transition from the Orpheus Graben to the Laurentian Sub-basin. The southern boundary of the small half graben North Step acts as the regional hinge zone. The Laurentian Sub-basin is located beyond the seaward edge of the Orpheus Graben (Canso Ridge). Salt diapirs within the Orpheus Graben have been greatly influenced by the confinement of the structure. Salt diapirs of the Orpheus Graben are narrow and subvertical with some experiencing squeezing. (B – basement, Sc – Scatarie Member, Mc – top Mic Mac, O – O Marker, Wy – Wyandot Formation, S – Argo Salt).

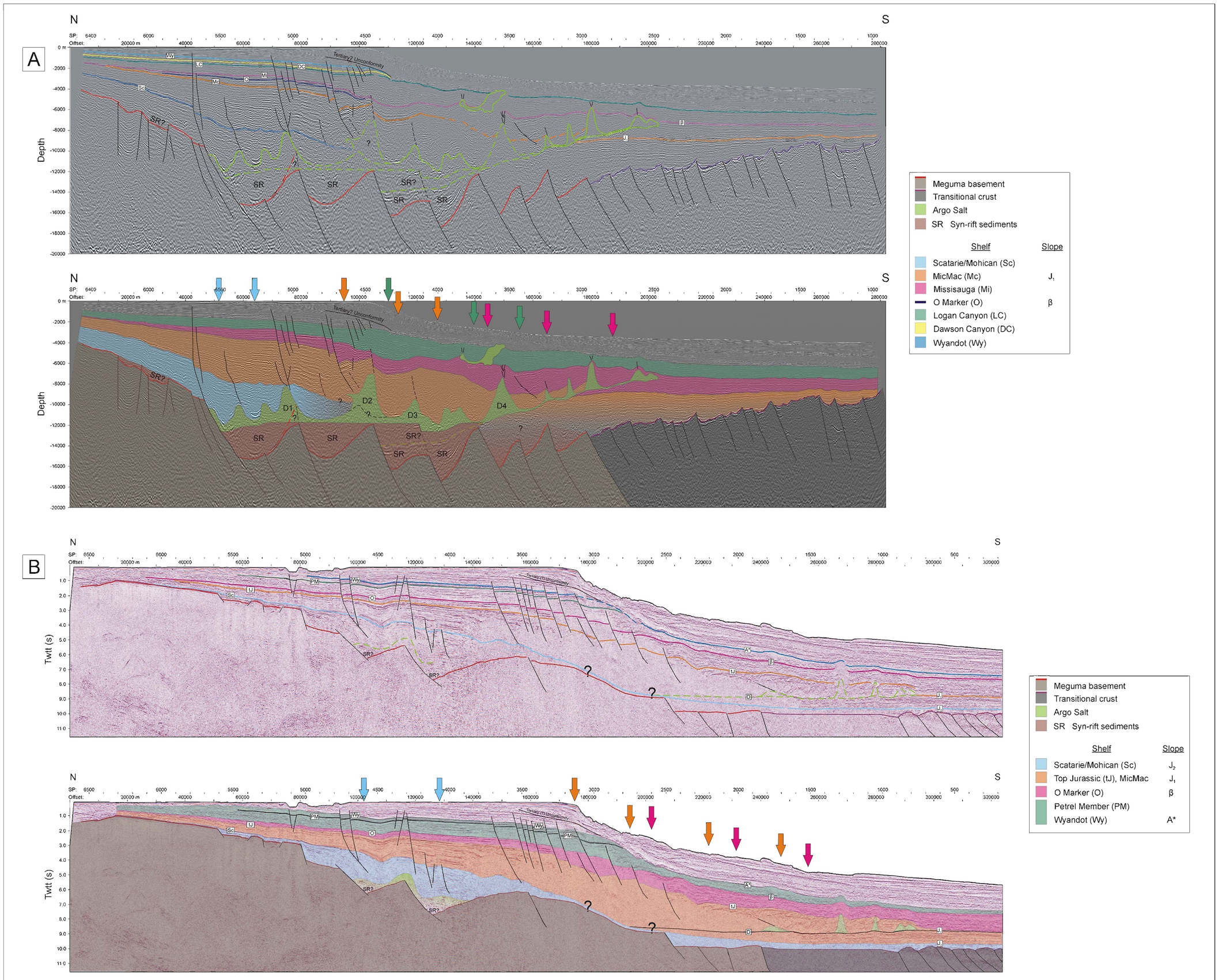

Figure 4.11 Major depositional units of the eastern Scotian margin (salt Subprovince IV) illustrating the seaward migration of major depocenters through the Jurassic and Early Cretaceous. (A, Upper panel) Seismic profile of NovaSpan line 2000 including interpretation of stratigraphic seismic horizons, syn-rift, salt and basement features. (A, Lower panel) Colour overlay indicating major depocenters (arrows) for indicated stratigraphic intervals. Major salt diapir structures are labelled D1 – 4. Interpretation indicates an overall seaward progradation of major depocenters (arrows) with the MicMac interval (orange) having the greatest sediment budget and rate within the basin. Major depocenters of the Scatarie/Mohican formations are comprised of a thick basinward thinning wedge along the hinge zone. Major depocenters of the Mississauga interval (magenta) appear to be thickest along the interpreted allochthonous salt nappe. (B, Upper panel) Seismic profile of GSC line 89-1 including interpretation of stratigraphic seismic horizons, syn-rift, salt and basement features. (B, Lower panel) Colour overlay indicating major depocenters (arrows) for indicated stratigraphic intervals. Interpretation indicates an overall seaward progradation of major depocenters with the MicMac interval (orange) having the greatest sediment budget and rate within the basin, constituting highly rotated strata (BSW) above the salt detachment (D) and small allochthonous salt structures.

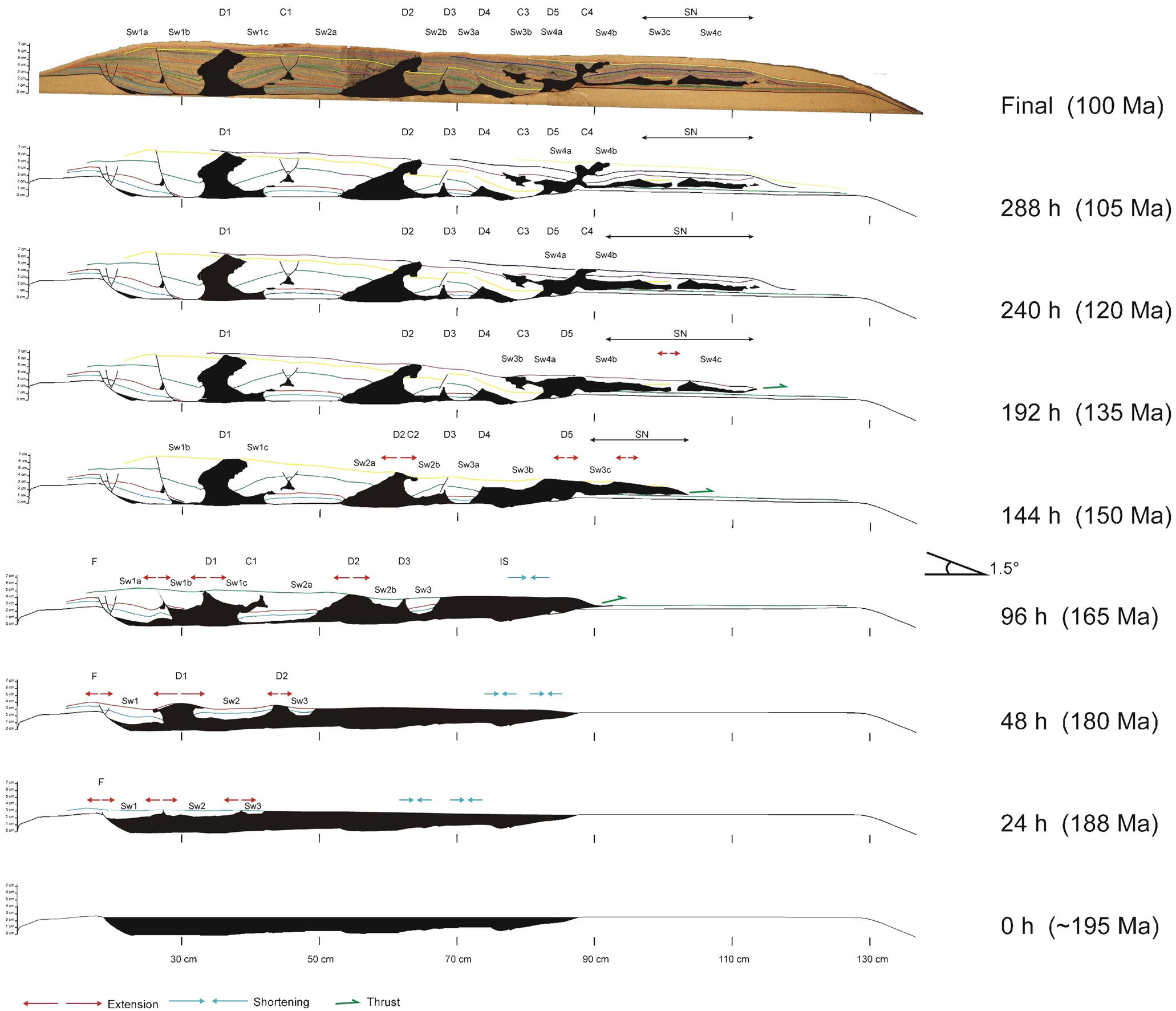

Figure 5.10 Sequential restoration of the central (45 cm) cross-section of the main 3-D experiment based on topographic profiles of model surface and incremental DIC strain and displacement data (Appendix C). Early model evolution is restored for 24 hour periods, while later model evolution restores horizons every 48 hours. Active and subsiding salt withdrawal basins are labelled. Silicone structures (black, diapirs-D, canopies-C, and salt nappe-SN). Active extension, contraction and active thrusting deduced from DIC strain analysis.

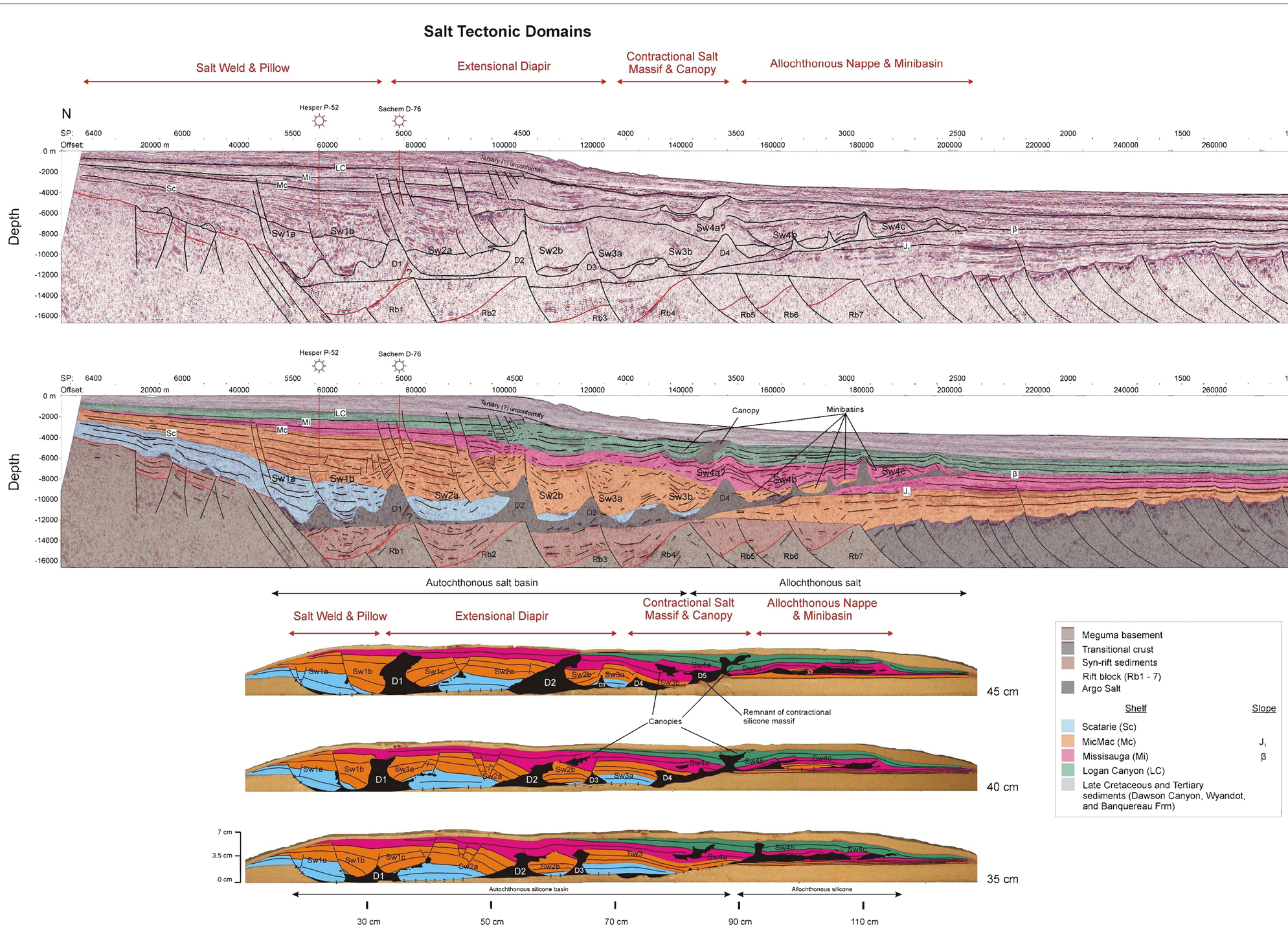

Figure 6.1 Comparison of extended interpretations of NovaSpan seismic profile 2000 (above) and main 3-D experiment sections (below) illustrating distinctive and similar salt tectonic domains. Colour overlays indicate key stratigraphic units in experiment and seismic section. Main depocenters (Sw – salt withdrawal basins) observed during experiment evolution are correlated with similar depocenters within profile 2000. D – salt/silicone diapirs.

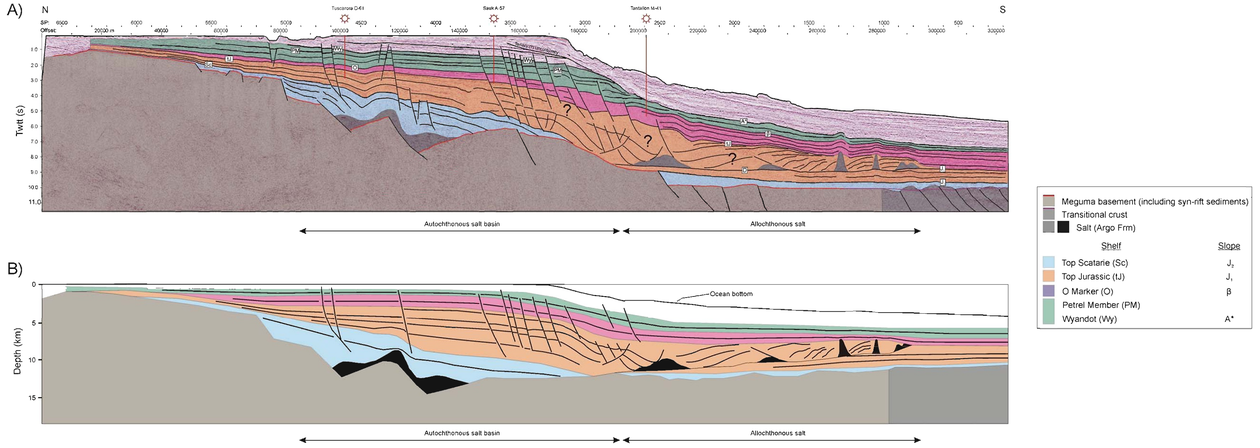

Figure 6.6. Schematic interpretation of GSC seismic profile 89-1 based on concepts derived from pilot experiment 1 (Appendix B). A) Time seismic section. B) Schematic depth converted drawing of line 89-1 illustrating the configuration of the autochthonous basin and climbing of Late Jurassic depocenters up the salt detachment system.

Pilot Experiment 1

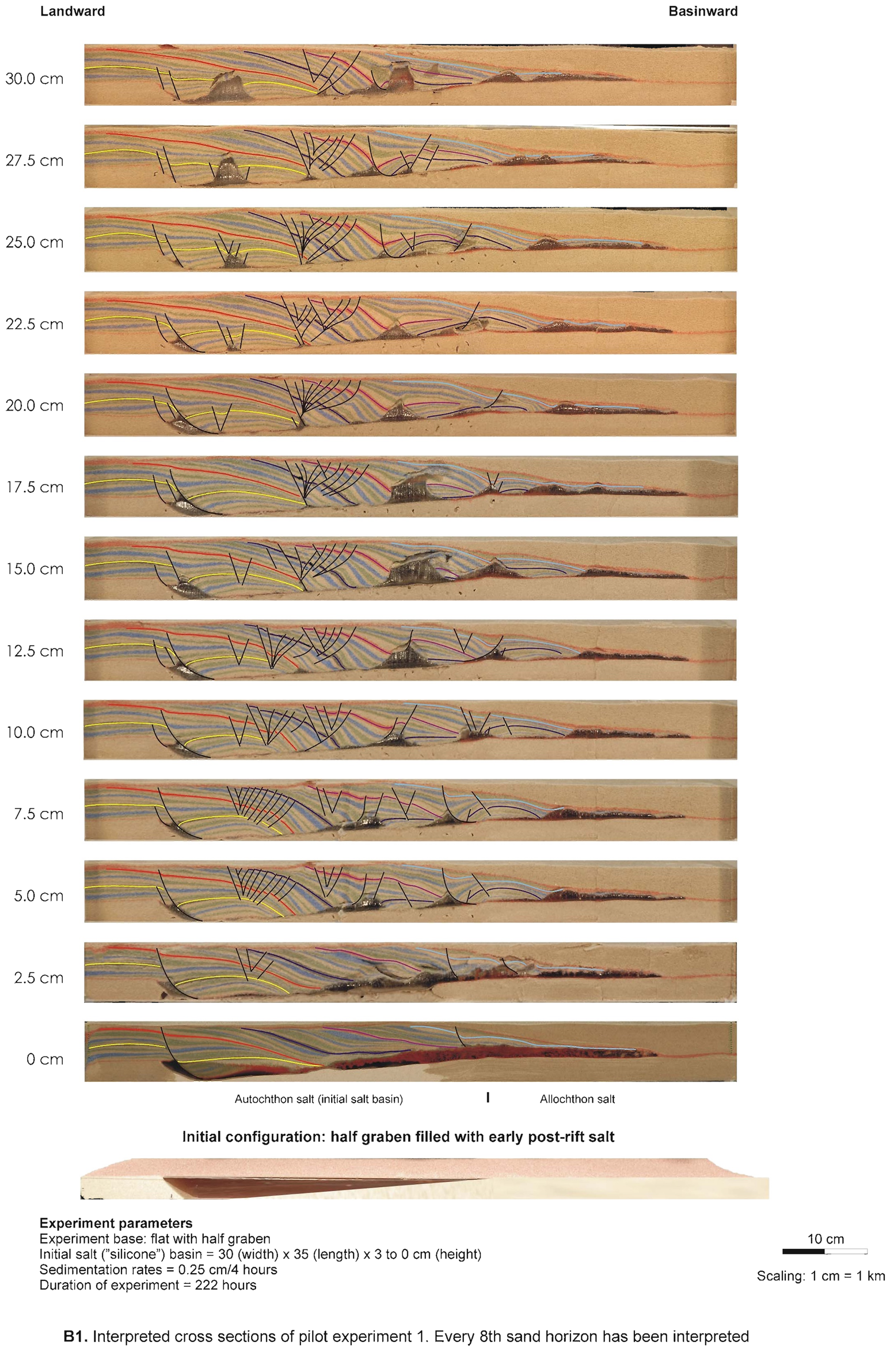

Initial configuration: half graben filled with early post-rift salt

Experiment parameters
Experiment base: flat with half graben
Initial salt ("silicone") basin = 30 (width) x 35 (length) x 3 to 0 cm (height)
Sedimentation rates = 0.25 cm/4 hours
Duration of experiment = 222 hours

10 cm

Scaling: 1 cm = 1 km

B1. Interpreted cross sections of pilot experiment 1. Every 8th sand horizon has been interpreted

Pilot Experiment 2

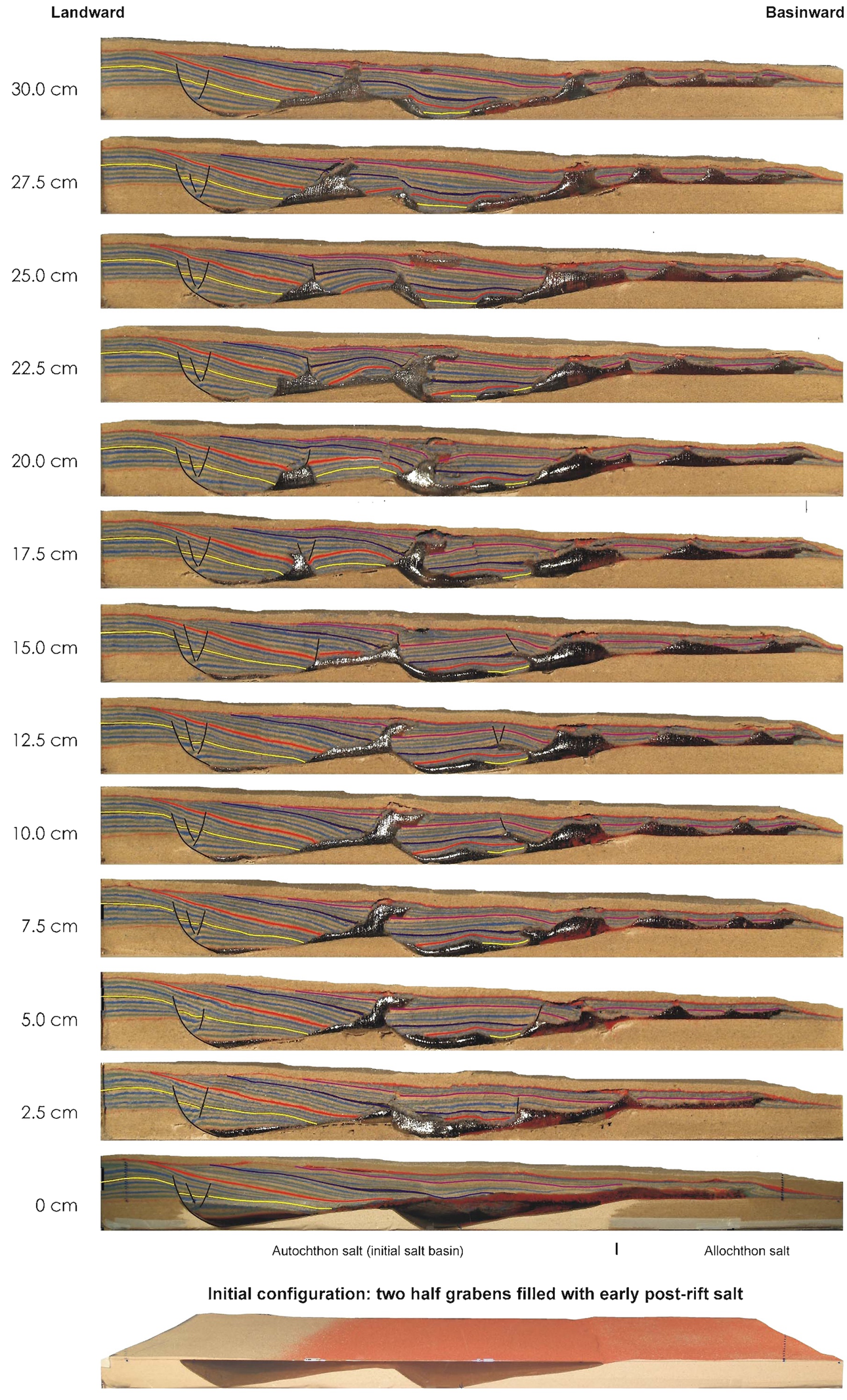

Experiment parameters
Experiment base: flat with two half grabens
Initial "salt" (silicone) basin = 30 (width) x 40 (length) x 3 to 0 cm (height) - [each half graben = 30 (width) x 20 (length) x 3 to 0 cm (height)]
Sedimentation rates = 0.25 cm/2 hours (day time/12 hours) and no sedimentation (night time/12 hours)
Duration of experiment = 170 hours

10 cm

Scaling: 1 cm = 1 km

B2. Interpreted cross sections of pilot experiment 2. Every 8th sand horizon has been interpreted

Main 3-D Experiment: Eastern Scotian Margin

Salt Tectonic Domains

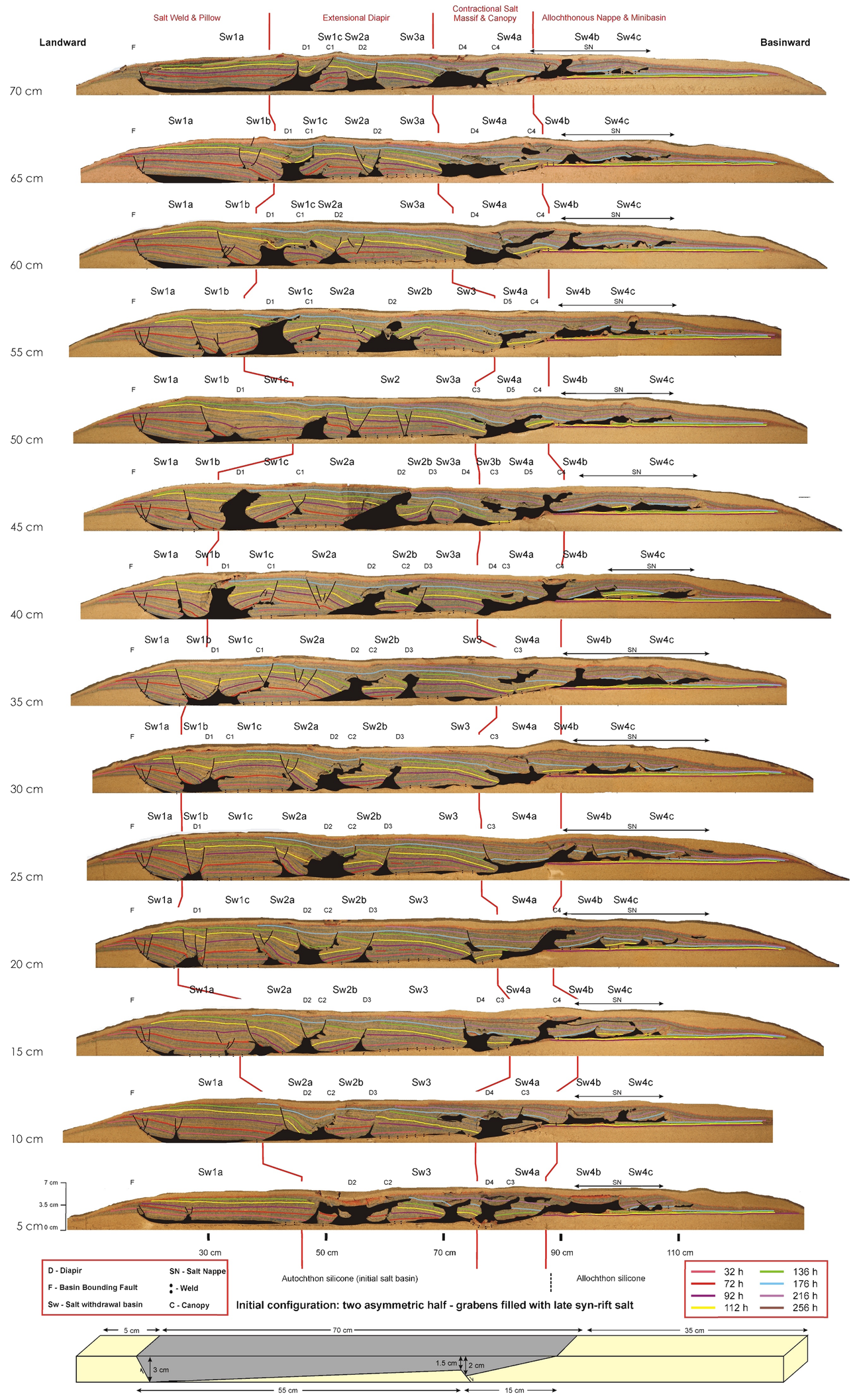

Experiment parameters
Experiment base: half graben wedge with small internal seaward wedge
Initial salt ("silicone") basin = 80 (width) x 70 (length) x 3 (height) cm
Sedimentation rates = (0 - 80h) - 0.25 cm/8 hours; (80 - 136h) - 0.25 cm/4 hours; (136 - 216h) - 0.17 cm/8 hours; (216 - 304h) - 0.15 cm/8 hours
Duration of experiment = 304 hours

10 cm

Scaling: 1 cm = 1 km

B3. Interpreted cross sections of main 3-D experiment (Eastern Scotian Margin). Correlatable silicone structures and "salt" withdrawal basins have been labelled.